UNIVERSITÀ DEGLI STUDI DELL'AQUILA
DIPARTIMENTO DI INGEGNERIA CIVILE, EDILE - ARCHITETTURA E AMBIENTALE

Dottorato di Ricerca in Ingegneria Civile, Edile-Architettura e Ambientale (Ph.D.ICEAA)

Curriculum in Ingegneria Civile e Ambientale

XXXVII ciclo

Titolo della tesi

"Non-Destructive Techniques for Infrastructure and Transportation Corridors Analysis: Comparison of Morphological and Learning-Based Approaches Using LiDAR and UAV Photogrammetry for Enhanced Crack Detection and Risk Assessment"

08/A4 – Geomatica (S.S.D. ICAR/06 Topografia e Cartografia)

Dottoranda

Ing. Nicole Pascucci 282581

Tutor

Prof.ssa Donatella Dominici

Co-Tutor

Prof. Ayman Habib

Coordinatore del corso

Prof. Federico De Matteis

a.a. 2023/2024





UNIVERSITÁ DEGLI STUDI
DELL'AQUILA
DEPARTMENT OF CIVIL,
CONSTRUCTION-ARCHITECTURAL AND
ENVIRONMENTAL ENGINEERING

Non-Destructive Techniques for Infrastructure and Transportation Corridors Analysis: Comparison of Morphological and Learning-Based Approaches Using LiDAR and UAV Photogrammetry for Enhanced Crack Detection and Risk Assessment

DOCTORAL THESIS

Nicole Pascucci
282581

Tutor (s)
Prof. Donatella Dominici

Reviewer (s)
Prof. Ayman Habib

The Coordinator of the PhD Program
Prof. Federico De Matteis

L'Aquila, 2025

XXXVII Cycle

To my family, always by my side
between here on Earth, and the other side.

Alla mia famiglia, sempre accanto a me
da qui, sulla Terra, e dall'altra parte.

"*Dilegua, o notte! Tramontate, stelle!*

Tramontate, stelle! All'alba vincerò! Vincerò! Vincerò"

Giacomo Puccini, “Nessun Dorma”, Turandot

ABSTRACT

This research focuses on the application of geomatic techniques, prioritizing non-destructive methodologies (NDT, Non-Destructive Techniques) to acquire high-precision data for assessing risks associated with infrastructures and transportation corridors. The study integrates LiDAR data collection through Mobile Mapping Systems (MMS) and Simultaneous Localization and Mapping (SLAM), along with UAV-based photogrammetry. These approaches allow detailed analysis of infrastructure problems, including occlusions in road markings, cracks in road pavement, and concrete infrastructure. The research is based on national and international case studies representing diverse and replicable contexts. Examples include the I-65 highway in the United States, connecting Lafayette to Indianapolis, where MMS was used to evaluate road sign visibility and pavement cracking;a viaduct located in L'Aquila, Italy, acquired with SLAM technology to analyze cracking; finally, a concrete specimen subjected to compression cycles to further investigate the replicability and applicability of the techniques to different infrastructures. In addition, the study includes a comparative evaluation of geomatic techniques, considering parameters such as precision and accuracy and practical applicability. Through the integration of machine learning and deep learning approaches, the research identifies effective methodologies for the detection and classification of infrastructure hazards.Another pivotal aspect of this research is the development of an open-source WebGIS

platform aimed at supporting the prevention, management, and maintenance of infrastructure. The platform was designed in accordance with the guidelines set forth by the Indiana Department of Transportation (INDOT) and the Ministry of Infrastructure and Transportation (MIT), ensuring full compliance with both national and international standards. This WebGIS offers practical and user-friendly tools for risk assessment and safety enhancement, while also guaranteeing universal accessibility and scalability for infrastructure operators and stakeholders. Ultimately, the research aspires to establish innovative and adaptable strategies for infrastructure maintenance and safety, contributing significantly to improved risk prevention and management practices.

SOMMARIO

Questa ricerca si concentra sull'applicazione di tecniche geomatiche, prediligendo metodologie non distruttive (NDT, Non-Destructive Techniques) per l'acquisizione di dati ad alta precisione, finalizzati alla valutazione dei rischi legati alle infrastrutture e ai corridoi di trasporto. Lo studio integra dati LiDAR raccolti tramite Mobile Mapping Systems (MMS) e Simultaneous Localization and Mapping (SLAM), oltre alla fotogrammetria basata su UAV. Questi approcci consentono di analizzare in dettaglio i problemi delle infrastrutture, tra cui le occlusioni della segnaletica orizzontale, le crepe nella pavimentazione stradale e nelle infrastrutture in calcestruzzo. La ricerca si basa su casi studio nazionali e internazionali, rappresentativi di contesti diversi e replicabili. Tra gli esempi, l'autostrada I-65 negli Stati Uniti, che collega Lafayette a Indianapolis, è stata analizzata con tecnologia MMS per valutare la visibilità della segnaletica stradale e le crepe nella pavimentazione; un viadotto situato a L'Aquila, in Italia, acuisito con la tecnologia SLAM per analizzare la fessurazione; infine, un provino di calcestruzzo sottoposto a cicli di compressione per approfondire la replicabilità e l'applicabilità delle tecniche a diverse infrastrutture. Inoltre, lo studio include una valutazione comparativa delle tecniche geomatiche, considerando parametri quali precisione e accuratezza e l'applicabilità pratica. Attraverso l'integrazione di approcci di machine learning e deep learning, la ricerca identifica metodologie efficaci per il rilevamento e la classificazione dei pericoli

infrastrutturali. Un ulteriore aspetto centrale della ricerca è lo sviluppo di un sistema WebGIS open-source, progettato per supportare la prevenzione, la gestione e la manutenzione delle infrastrutture. La piattaforma è stata sviluppata seguendo le linee guida dell'Indiana Department of Transportation (INDOT) e del Ministero delle Infrastrutture e dei Trasporti (MIT), garantendo la conformità agli standard nazionali e internazionali. Il WebGIS fornisce strumenti pratici per il controllo dei rischi e il miglioramento della sicurezza, assicurando al contempo accessibilità universale e scalabilità per operatori e gestori. In definitiva, il lavoro mira a sviluppare strategie innovative e scalabili per la manutenzione e la sicurezza delle infrastrutture, contribuendo a migliorare la gestione e prevenzione dei rischi.

CONTENTS

List of figures v

List of tables x

List of abbreviations xii

1. Infrastructure and Transport Corridors: Prevention, Safety and Maintenance - State of the art 1

1.1 Abstract 1

1.1.1 Introduction 2

1.2 Importance of Prevention and Maintenance of Infrastructure and Transportation Corridors 3

1.2.1 Guidelines in the United States: Focus on Indiana and INDOT 5

1.2.2 Guidelines in Europe: Focus on Italy and MIT 9

1.3 Best survey techniques for infrastructure inspection and crack detection 12

1.3.1 Advantages and applications of Non-Destructive Testing (NDT) 13

1.4 Research Questions & Goals 15

1.5 Thesis Outline 19

1.5.1 Chapter 1 – Introduction 19

1.5.2 Chapter 2 - Methodologies and advantages of geomatic techniques for acquiring detailed data in infrastructure 19

1.5.3 Chapter 3 - Statistical methods for performance evaluation and data analysis 20

1.5.4 First Case study: Traffic Sign Visibility and Occlusion in the USA 20

1.5.5 Chapter 5 - Second Case study: Detection of Road Surface Cracks in the USA 20

1.5.6 Third Case study: Crack Analysis on L'Aquila Viaduct, Italy 21

1.5.7 Chapter 7 - Fourth Case study: Concrete Specimen Crack Identification 21

1.5.8 Chapter 8 - Creation of 3D Models with integration of predictive analytics and maintenance suggestions 21

1.5.9 Chapter 9 - Conclusions 22

2. Methodologies and advantages of geomatic techniques for acquiring detailed data in infrastructure 23

2.1 Methodologies and advantages of geomatic techniques for acquiring detailed data in infrastructure 23

2.2 Analysis of commonly used survey techniques 24

2.2.1 Overview of Conventional and Contemporary Survey Techniques 25

2.3 Applications of LiDAR-Based MMS, SLAM, and UAV Photogrammetry in infrastructure maintenance 37

2.4 Morphological and learning-based approaches in risk detection 43

2.4.1 Filtering techniques for UAV photogrammetry: Enhanced Lee, Frost, and Median filters 46

2.4.2 LiDAR Data Filtering Method Based on Cloth Simulation 47

2.4.3 LiDAR Data enhancement with Normalized Intensity 50

2.4.4 Segmentation techniques for risk detection: MCSS and OBIA 53

2.4.5 Clustering-based approaches: DBSCAN 57

2.4.6 Machine learning for risk classification: Random Forest 59

2.4.7 Deep learning in point cloud data analysis: Super Point Graph (SPG) 61

2.5 Application of methodologies in case studies 64

3. Statistical methods for performance evaluation and data analysis 66

3.1 Introduction to Statistical Methods in Geomatic Studies 67

3.2 Evaluation metrics for classification performance 69

3.2.1 True Positive (TP), False Positive (FP), False Negative (FN), Recall and Precision, F1-Score 70

3.2.2 Jaccard Index 71

4. First Case study: Traffic Sign Visibility and Occlusion in the USA 73

4.1 Chapter Abstract 73

4.2 Introduction 74

4.3 Materials and Methods 78

4.3.1 Data Acquisition Systems 78

4.3.2 I-65 Highway Datasets 80

4.3.3 Summary of Methodology 81

4.4 Experimental results 82

4.4.1 Comparative Analysis of MCSS and SPG 82

4.5 Signage Visibility Analysis 90

4.6 Conclusion and Future Studies 93

5. Second Case study: Detection of Road Surface Cracks in the USA 95

5.1 Chapter Abstract 95

5.2 Introduction 96

5.3 Materials and Methods 99

5.3.1 Data Acquisition Systems 99

5.3.2 I-65 Highway Datasets 99

5.3.3 Summary of Methodology 101

5.4 Experimental results 103

5.4.1 Comparative Analysis of DBSCAN and Random Forest with and without Intensity Normalizzation 103

5.5 Analysis of Crack Detection in Point Cloud Data 109

5.6 Conclusion and Future Studies 113

6. Third Case study: Crack Analysis on L'Aquila Viaduct, Italy 115

6.1 Introduction 115

6.2 Materials and Methods 117

6.2.1 Data Acquisition Systems 117

6.2.2 Viaduct in Campo di PILE, L'Aquila (Italy) 118

6.2.3 Summary of Methodology 119

6.3 Experimental results 122

6.3.1 Comparative Analysis of DBSCAN and Random Forest with and without Intensity Normalization 122

6.4 Analysis of Crack Detection in Point Cloud Data 129

6.5 Conclusion and Future Studies 131

7. Fourth Case study: Concrete Specimen Crack Identification 133

7.1 Chapter Abstract 133

7.2 Introduction 134

7.3 Materials and Methods 139

7.3.1 Data Acquisition Systems 139

7.4 Case of study 140

7.4.1 Photogrammetric Processing 141

7.4.2 OBIA Classification 144

7.5 Experimental results 145

7.5.1 OBIA Classification + Filter Results on ROI 145

7.6 Discussion 147

7.7 Conclusion and Future Studies 154

8. Creation of 3D Models with Open Source Tools and WebGIS Integration for Maintenance Suggestions 156

8.1 Introduction to 3D Models in infrastructure analysis 158

8.2 Data Preparation for 3D Model Creation 159

8.2.1 Creation and Optimization of 3D Models Using Blender and the BlenderGIS Plugin 161

8.3 WebGIS database integration with QGIS and Lizma 165

8.4 Maintenance Recommendations Based on Database 177

9. Conclusions 179

9.1 Summary 179

9.2 Conclusions and Future Developments 181

Addendum A 186

Addendum B 188

Bibliography 193

Acknowledgements 234

Ringraziamenti 236

LIST OF FIGURES

Figure 1.1: The organization of the bridge and pavement team (data source: INDOT). 7

Figure 1.2: Flow of data governance model (bridges, large culverts, and structures (data source: INDOT). 9

Figure 1.3: Multilevel approaches and relationships between levels of analysis illustrates the different levels of analysis defined by the guidelines and their interrelationships. These levels enable a comprehensive and systematic approach to bridge assessment and maintenance (Data source: MIT 2020). 11

Figure 2.1: MMS LiDAR systems used in the study – PWMMS-HA (Top) and PWMMS-UHA (Bottom). 38

Figure 2.2:Leica BLK2GO used in the study. 40

Figure 2.3: GeoSLAM ZEB Horizon used in the study. 41

Figure 2.4: Leica GS15 GNSS Receiver used in the study. 42

Figure 2.5: UAV systems used in the study – DJI Matrice 200 V2 (Top) and Zenmus e X5S (Bottom). 43

Figure 2.6: Illustrates the relationship between AI, ML, and DL, demonstrating how these disciplines interconnect while maintaining distinct roles. AI serves as the overarching domain, with ML and DL representing specialized subsets that focus on algorithmic learning and feature extraction, respectively. 44

Figure 2.7:Overview of the cloth simulation algorithm (Zhang et al., 2016) illustrates the key steps of the process, including inversion of the point cloud, cloth initialization, and deformation, leading to the generation of the DTM 48

Figure 2.8: An example CS in a case of study. 49

Figure 2.9: Illustrates the general workflow of OBIA. 54

Figure 2.10: Illustration of MCSS dataset segmentation results, with planar regions depicted in green, pole-like regions in red, and rough regions in blue. 57

Figure 2.11: DBSCAN workflow for crack detection, including pre-processing, clustering, and evaluation of results. 59

Figure 2.12: A representation of a decision tree in a Random Forest model. For the study described in next Chapter, 100 trees were used, with a random seed set to 42 to ensure reproducibility in the classification process. 61

Figure 2.13: Illustration of geometric partitioning. On the left: an undirected graph representing the point cloud, with nodes color-coded based on geometric features. On the right: partitions displayed as piecewise constant approximations of these geometric features. SP1, SP2, and SP3 correspond to superpoint 1, superpoint 2, and superpoint 3, respectively. 62

Figure 2.14: Schematic representation of the superpoint embedding and contextual segmentation process. The model structure includes a superpoint graph, where each superpoint is processed through PointNet to generate an embedding vector. These superpoint embeddings, along with the superedges, are then input into a graph network composed of a series of GRU layers for further processing. 63

Figure 2.15: Summary of all approved case studies. 65

Figure 3.1: Published international contributions by country reporting Geomatics and Statistics (2010-2020).The data presented in Figure 3.1 were collected through a bibliometric analysis conducted manually using [Scopus/Web of Science/Google Scholar]. The search focused on research articles published between 2010 and 2020, using keywords such as geomatics, statistics, LiDAR, UAV photogrammetry, and machine learning applied to spatial data. To ensure the relevance of the results, only peer-reviewed journal articles were considered, while conference papers and non-peer-reviewed sources were excluded. The classification of articles was based on their explicit mention of statistical methodologies applied to geomatics.The final dataset consists of the number of publications per country, reflecting international contributions to the integration of statistical methods in geomatics research. 68

Figure 4.1: Illustration of a road sign (red circle) obscured by vegetation along the highway. 76

Figure 4.2: Proposed framework for comparative analysis of geometric/morphological and learning-based strategies for detecting signage occlusions. 78

Figure 4.3:MMS LiDAR systems used in the study – PWMMS-HA (Top) and PWMMS-UHA (Bottom). 79

Figure 4.4: Closer view of ROIs located along the I-65 state highway area (West Lafayette, Indiana, US). 80

Figure 4.5: Comparison of partitioning results derived from MCSS and SPG (left). Evaluation of prediction performance for MCSS, SPG before QC, and SPG after QC (right) using reference data (top right), for ROI 1 from PWMMS-HA. Misclassifications are highlighted by black dashed circles. 84

Figure 4.6: Comparison of partitioning results derived from MCSS and SPG (left). Evaluation of prediction performance for MCSS, SPG before QC, and SPG after QC (right) using reference data (top right), for ROI 1 from PWMMS-UHA. Misclassification is highlighted by black dashed circles. 87

Figure 4.7: Comparison of partitioning results derived from MCSS and SPG (left). Evaluation of prediction performance for MCSS, SPG before QC, and SPG after QC (right) using reference data (top right), for ROI 2 from PWMMS-HA. Misclassification is highlighted by black dashed circles. 89

Figure 4.8: Comparison of partitioning results derived from MCSS and SPG (left). Evaluation of prediction performance for MCSS, SPG before QC, and SPG after QC (right) using reference data (top right), for ROI 2 from PWMMS-UHA. Misclassification is highlighted by black dashed circles. 90

Figure 4.9: To determine whether the vegetation point is within the pyramid, the volume of the tetrahedron consisting of the pyramid ABCDE is used. If the vegetation point (V) is within the pyramid (ABCDE), the sum of six triangular volumes shall be the same. If not, that point is not considered to be an obscured point for signage. 91

Figure 4.10: Example of wheel-based MMS LiDAR data visualized with intensity coloring, illustrating the impact of driver-to-sign distance on signage visibility. 91

Figure 4.11: Comparison of occlusion rate based on the distance from the sign-to-driver's viewpoint for PWMMS-HA in red and PWMMS-UHA in blue. 93

Figure 4.12: Figure 10. Comparison of LiDAR point clouds between PWMMS-HA and PWMMS-UHA for the sample traffic sign in ROI 2. The sign, vegetation points, and natural terrain are shown in red, green, and blue, respectively. 93

Figure 5.1: Proposed framework for comparative analysis of clustering and machine learning-based classification for detecting cracks in road surface. 98

Figure 5.2: MMS LiDAR systems used in the study: the PWMMS-UHA. 99

Figure 5.3: Study site showing the data collection route and bridge locations along State Highway I-65, with an aerial view adopted from Google Earth imagery. The inset provides a detailed zoom of a road surface segment. 100

Figure 5.4: Visual inspection of all 27 studied segments along State Highway I-65, with each segment color-coded based on intensity thresholding. The image highlights the variation in surface features across the dataset, allowing for a comprehensive overview of the road surface conditions, including the detection of cracks. 101

Figure 5.5: An example of a tile illustrating the effectiveness of the proposed method in isolating the DTM, BE and AG. 102

Figure 5.6: On the left, the road segment near Bridge 17 is visualized with coloring based on intensity thresholds. The center image showcases the clustering results obtained using the DBSCAN algorithm, while the rightmost image presents the DBSCAN clusters with manual labeling applied for further classification and validation. 105

Figure 5.7: On the left, the road segment near bridge 17 is colored based on intensity thresholds, with intensity values previously normalized. In the center, from the normalized dataset, it is evident that lane marks become distinguishable from cracks based on the threshold. On the right, DBSCAN results are shown without and with manual labeling. . 107

Figure 5.8: On the left, the road surface without intensity normalization, and on the right, the road surface with intensity normalization, both classified using RF. 109

Figure 5.9: Quantitative estimation of crack surface area calculated using the Poisson algorithm in CloudCompare. The intervention threshold is defined as follows: Roads with minor cracks (0.5–2 m² of cracks per 100 meters of road); roads with obvious cracks (2–10 m² of cracks per 100 meters of road); highly damaged roads (more than 10 m² of cracks per 100 meters of road). Crack surface measurements have been rounded to two decimal places to enhance clarity and readability. 112

Figure 6.1: Study site showing viaduct locations along Via Campo di Pile, L'Aquila (Italy), with an aerial view adopted from Google Earth imagery. 115

Figure 6.2: From left to right: GeoSLAM ZEB Horizon, Leica BLK2GO, and GNSS receiver GS15. 118

Figure 6.3: Case of study from left to right: view adopted from Open Street Map and Viaduct's image. 118

Figure 6.4: Sample results of the CS process distinguishing BE and AG points. On the left, data collected using the GeoSLAM ZEB Horizon; on the right, data from the Leica BLK2GO. 119

Figure 6.5: Crack detection results based on intensity thresholding. At the top, the GeoSLAM ZEB HORIZON dataset shows distinguishable cracks with varying intensity thresholds. At the bottom, the Leica BLK2GO dataset, with a shorter range and lower resolution, fails to clearly identify cracks, highlighting the limitations of this system for crack detection. 121

Figure 6.6: Application of DBSCAN BE without normalised intensity on datasets from GeoSLAM ZEB HORIZON 123

Figure 6.7Application of DBSCAN AG without normalised intensity on datasets from GeoSLAM ZEB HORIZON. 124

Figure 6.8: Results of applying normalized intensity to the DBSCAN algorithm for BE datasets (top) and AG datasets (bottom). 125

Figure 6.9: Application of RF on the left without normalized intensity and on the right with normalized intensity on BE dataset from GeoSLAM ZEB HORIZON. 127

Figure 6.10: Application of RF on the left without normalized intensity and on the right with normalized intensity on AG dataset from GeoSLAM ZEB HORIZON. 128

Figure 6.11: Quantitative estimation of crack surface for BE. 130

Figure 6.12: Quantitative estimation of crack surface for AG. 130

Figure 7.1: Image and technical specifications of the UAV used in this work. 139

Figure 7.2: image and technical specifications of the Zenmuse X5S used in this work. ... 140

Figure 7.3: Reinforeced concrete specimen used for testing. 140

Figure 7.4: Workflow applied from the initial acquisition phase, through photogrammetric processing for orthophoto generation and the subsequent application of filters and OBIA classification, up to the final validation phase. 141

Figure 7.5: Orthomosaic of the entire site scene with the reinforced concrete specimen used for the test (processed with Agisoft Metashape Software). 141

Figure 7.6: Orthomosaic of the chosen ROI at the node of the reinforced concrete specimen used following the compression test, characterized by cracking (processed with Agisoft Metashape software). 142

Figure 7.7: Application of Median filter algorithm on the ROI (processed with ENVI software). 143

Figure 7.8: Application of Enhanced Lee filter algorithm on the ROI (processed with ENVI software). 143

Figure 7.9: Application of Enhanced Frost filter algorithm on the ROI (processed with ENVI software 143

Figure 7.10: OBIA classification on the unprocessed orthophoto. The red box represents a sample area where a crack can be identified. 146

Figure 7.11: OBIA classification on the orthophoto with Median filter. The red box represents a sample area where the improvement in crack identification can be observed. The crack is highlighted within the red box, demonstrating how the application of the Median filter has enhanced the ability to identify cracks in the ROI. 146

Figure 7.12: OBIA classification on the orthophoto with Enhanced Lee filter. The red box represents the same sample area considered where the identification of cracks can be observed with the application of the Enhanced Lee filter. 147

Figure 7.13: OBIA classification on the orthophoto with Enhanced Frost filter. The red box represents the same sample area considered where the identification of cracks can be observed with the application of the Enhanced Frost filter. 147

Figure 8.1: General workflow from case study to WebGIS creation. 156

Figure 8.2: An illustration of the general workflow, showcasing the transition from raw input data to processed models and their final visualization in a WebGIS platform. 161

Figure 8.3: An example from 3D Model creation to the rendering process in Blender. 163

Figure 8.4: Examples of different areas to get shapefiles using BlenderGIS plugin both for the United States (up) and Europe (bottom). 164

Figure 8.5: Conceptual Model. Representation of the relationship between geometric and alphanumeric entities. 167

Figure 8.6: Logical scheme that enables the project's procedural process. 171

Figure 8.7: Final physical model representation zooming in on an example of a road segment and related bridge with the different criticality, analysis and intervention types in the attribute table. 173

Figure 8.8: Defining layer settings in the Lizmap plugin. 175

Figure 8.9: Web-GIS Architecture adapted from Lizmap. 175

Figure 8.10: From the left the Layers panel with the type of interventions and on the right the Basemaps from OpenStreetMap (B&W/color). An example for the city of L'Aquila (up) and Lafatte to Indianapolis (Bottom). 177

LIST OF TABLES

Table 2.2.1: An overview of advantages and limitations of Geomatic Technologies. 36

Table 2.2: Details of the georeferencing and LiDAR sensors, along with the anticipated accuracy of the point cloud generated by Mobile LiDAR Mapping Systems. 39

Table 2.3: Technical characteristics of the Leica BLK2GO. 40

Table 2.4: Technical characteristics of the GeoSLAM Zeb Horizon system. 41

Table 2.5: Technical characteristics of the UAV systems. 43

Table 4.1: Description of the four datasets located in two different ROIs acquired by the Mobile Mapping Systems. 80

Table 4.2: Quantitative evaluation of MCSS classification results for ROI 1 from the PWMMS-HA. 85

Table 4.3: Quantitative evaluation of SPG classification results before QC for ROI 1 from the PWMMS-HA. 85

Table 4.4: Quantitative evaluation of SPG classification results after QC for ROI 1 from the PWMMS-HA. 85

Table 4.5: Quantitative evaluation of MCSS classification results for ROI 1 from the PWMMS-UHA. 87

Table 4.6: Quantitative evaluation of SPG classification results before QC for ROI 1 from the PWMMS-UHA. 88

Table 4.7: Quantitative evaluation of SPG classification results after QC for ROI 1 from the PWMMS-UHA. 88

Table 5.1: Validation results from the comparison between the DBSCAN point cloud without intensity normalization and the ground truth (GT). 105

Table 5.2: Validation results from the comparison between the DBSCAN point cloud with intensity normalization and the GT. 107

Table 5.3: Validations obtained by comparing the two point clouds from RF without normalized intensity and the GT and from RF with normalized intensity and the GT, respectively. 109

Table 5.4: Metrics obtained by comparing the two point clouds from DBSCAN with and without normalized intensity, RF with and without normalized intensity, and GT only for crack-related classes. 110

Table 6.1: Validation results from the comparison between the DBSCAN BE without intensity normalization and the ground truth (GT). 123

Table 6.2: Validation results from the comparison between the DBSCAN AG without intensity normalization and the ground truth (GT). 124

Table 6.3: Quantitative results of applying normalized intensity to the DBSCAN algorithm for BE and AG datasets. 126

Table 6.4: Validations obtained by comparing the two point clouds from BE RF without (top) and with (bottom) normalized intensity and the GT, respectively. 127

Table 6.5: Validations obtained by comparing the two point clouds from AG RF without (top) and with (bottom) normalized intensity and the GT, respectively. 128

Table 7.1: PERCENTAGE OF CRACKS OBTAINED AS A RESULT OF THE JACCARD SIMILARITY COEFFICIENT IDENTIFIED IN EACH CLASSIFICATION. 148

Table 7.2: AREAS OF EACH CRACK. 149

Table 7.3: DETECTION PERCENTAGE OF EACH CRACK 150

Table 7.4: OBIA classification with cracking on original ROI (a), on ROI with Enhanced Frost filter (b), on ROI with Enhanced Lee filter (c), and with Median filter (d). In the red rectangle the crack with ID 45 and in the blue rectangle the crack with ID 4. 152

Table 7.5: OBIA ID 45 crack classification on original ROI (a), on ROI with Enhanced Frost filter (b), on ROI with Enhanced Lee filter (c), and with Median filter (d); the black area below corresponds to Ground Truth crack. 152

Table 7.6: OBIA ID 4 crack classification on original ROI (a), on ROI with Enhanced Frost filter (b), on ROI with Enhanced Lee filter (c), and with Median filter (d); the black area below corresponds to Ground Truth crack. 153

LIST OF ABBREVIATIONS

AG: Above Ground

AI: Artificial Intelligence

BE: Bare Earth

CC: CloudeCompare

CNNs: Convolutional Neural Networks

CP: Check Point

CS: Cloth Simulation

CSF: Cloth Simulation Filtering

DBSCAN: Density-Based Spatial Clustering of Applications with Noise

DL: Deep Learning

DTM: Digital Terrain Model

EDM: Electronic Distance Measurement

FN: False Negative

FP: False Positive

FID: Feature ID number

GCPs: Ground Control Points

GNSS: Global Navigation Satellite System

GNNs: Graph Neural Networks

IMUs: Inertial Measurement Units

IN: Intensity Normalization

INDOT: Indiana Department of Transportation

INS: Inertial Navigation Systems

LiDAR: Light Detection and Ranging

LDP: Local Point Density

LPS: Local Point Spacing

LSA: Least Squares Adjustment

LUT: Look-Up Table

ML: Machine Learning

MCSS: Multi-Class Simultaneous Segmentation

MIT: Ministry of Infrastructure and Transportation

MMS: Mobile Mapping Systems

MLS: Mobile Laser Scanning

NDT: Non-Destructive Testing

OA: Overall Accuracy

OBIA: Object-Based Image Analysis

PCA: Principal Component Analysis

QC: Quality Control

RF: Random Forest

ROI: Region of Interest

SfM: Structure from Motion

SLAM: Simultaneous Localization And Mapping

SPG: SuperPoint Graph

TP: Truth Positive

UAV: Unmanned Aerial Vehicle

UGVs: Unmanned Ground Vehicles

Web GIS: Web Geographic Information Systems

1. INFRASTRUCTURE AND TRANSPORT CORRIDORS: PREVENTION, SAFETY AND MAINTENANCE - STATE OF THE ART

1.1 ABSTRACT

Infrastructure and transport corridors are critical components of modern society, ensuring the safe and efficient movement of people and goods. However, these structures are constantly subjected to various forms of degradation, including wear and tear from usage, environmental stressors such as temperature variations, and natural disasters. In recent years, the increasing frequency of extreme weather events, largely driven by climate change, has heightened the risks these systems face. The consequences of infrastructure failure can be catastrophic, impacting not only the economy but also public safety.

As a result, the need for systematic prevention, safety measures, and maintenance strategies has become paramount. Monitoring infrastructure health is a complex task that requires accurate and up-to-date data on structural conditions. Geomatic techniques, including LiDAR, Mobile Mapping Systems (MMS), Simultaneous localization and mapping (SLAM), and Unmanned Aerial Vehicle (UAV)-based photogrammetry, have proven to be powerful tools in the collection and analysis of such data. These

technologies allow for the detailed modeling and assessment of infrastructure, enabling more informed decision-making regarding repair and maintenance.

This chapter begins by exploring the necessity of regular inspection and maintenance of infrastructure, followed by an overview of the primary geomatic techniques used in the field. It concludes by examining how these methods contribute to improved safety and longevity of infrastructure systems, particularly in the face of evolving environmental challenges.

1.1.1 INTRODUCTION

Infrastructure forms the backbone of modern societies, playing a critical role in economic growth, public safety, and social well-being (Diane, 2024). The term "infrastructure" encompasses a wide range of essential systems, including transportation corridors, bridges, tunnels, and highways, all of which enable the movement of people, goods, and information (Levy, 1996). These systems are subject to continuous wear and tear due to both natural and human-induced factors. Transport infrastructure, in particular, is constantly exposed to environmental stressors, such as extreme weather events, temperature fluctuations, and seismic activity, as well as increasing traffic loads (Nemry et al., 2012; Hearn, 2016). These challenges not only degrade the physical structure of transportation networks but also heighten the risk of failure, which can have severe consequences for both economies and communities (Little 2002; Argyroudis et al., 2019). Maintaining and preserving the functionality of infrastructure is, therefore, a key concern for engineers, urban planners, and governments alike. The degradation of transport corridors poses a threat to public safety, national economies, and the continuity of services (Sinha, 2017). Factors such as climate change have exacerbated these issues by increasing the frequency and intensity of weather-related events. For instance, extreme temperatures, freeze-thaw cycles, and flooding can accelerate the deterioration of road surfaces, bridges, and other critical components of transport networks (Rattanachot et al. 2015; Li et al., 2022; Hosseini et al., 2024). Consequently, the need for

effective monitoring, maintenance, and preventive strategies has become a pressing issue. In this context, geomatics technologies have emerged as powerful tools for monitoring and assessing the condition of infrastructure. Techniques such as LiDAR, MMS, SLAM, and UAV-based photogrammetry allow for the collection of detailed and accurate spatial data, which is crucial for identifying vulnerabilities, planning maintenance, and ensuring the longevity of infrastructure systems (Agnisarman et al., 2019; Jiang et al., 2022; Kyriou et al., 2023). These technologies provide high-resolution, real-time data that enable a more precise understanding of the state of infrastructure, helping to prevent failures before they occur (Habib A. et al., 2005; Jordan S. et al., 2018; Sharifisoraki Z. et al., 2022). In the first part of this thesis, the state of the art in infrastructure monitoring will be explored, focusing on the key geomatic techniques used in this field. As infrastructure systems evolve and face new challenges, it is critical to adopt methodologies that are not only effective but also adaptable to changing conditions. The chapter will also examine the specific methods that are used to assess the condition of infrastructure, as well as the criteria for selecting the appropriate prevention techniques based on the characteristics of the infrastructure under study. The challenge lies in developing robust, repeatable, and cost-effective methods for assessing the condition of transport corridors, particularly as infrastructures age, experience natural wear, and face the impact of environmental and climatic changes. Geomatic techniques have proven invaluable in this regard, enabling for constant tracking and timely interventions. The goal is to ensure that infrastructure systems remain safe, reliable, and resilient, even in the face of growing pressures from both natural and anthropogenic forces.

1.2 Importance of Prevention and Maintenance of Infrastructure and Transportation Corridors

The prevention, safety, and maintenance of infrastructure and transportation corridors are crucial to ensuring the long-term viability and reliability of essential public assets (Priemus H. et al., 2003; Frangopol, D. M. et al., 2007; Gong J. et al., 2012; Blazey A. et al., 2020). Over the past decades, numerous countries, including those in Europe and North America, have faced growing concerns regarding the aging of critical infrastructure (Nagarajaiah S. et al., 2016; Gkoumas K. et al., 2019). As these structures reach or exceed their nominal design lifetimes, issues related to degradation become more pronounced. Therefore, addressing preservation and aging is fundamental. As infrastructure ages, proactive measures must be taken to prevent further deterioration, ensuring that maintenance activities are planned and executed in a timely manner (Yang D. Y. et al., 2019; Mitoulis S.,2020; Rodríguez M., 2024). Structural Health Monitoring (SHM) systems play a vital role in this process, as they continuously monitor the condition of infrastructure, detecting early signs of wear, cracking, or occlusions that could compromise structural integrity (Sohn H. et al., 2003; Farrar C. R. et al., 2007; Brownjohn J. M., 2007; Chiaia B. et al., 2020; He Z., 2022; De Flaviis A. et al., 2024).

The importance of infrastructure maintenance can be understood through four key aspects: preservation and aging, safety, maintenance management, and prevention (Frangopol D.M., 2014; Shapiro, V.B., 2015; Persia L., 2016; Xia Y., 2019). Each of these areas plays a critical role in ensuring that infrastructure remains functional, efficient, and safe over its lifespan.

- *Preservation & Aging*: Infrastructure requires regular maintenance to preserve its structural integrity and extend its lifespan. Proactive intervention, such as repairs or reinforcements, allows for early detection of vulnerabilities, reducing the likelihood of sudden failures or costly emergency repairs. These measures are crucial to avoid disruptions in transportation corridors, which play a critical role in economic connectivity and public safety.

- *Safety*: Maintaining the safety of infrastructure, especially in regions prone to natural disasters such as earthquakes, floods, or extreme weather

conditions, is paramount. A well-maintained structure is less likely to experience catastrophic failures, which could endanger lives and disrupt critical transport networks. Safety measures, combined with regular inspections and technological advancements in SHM, ensure that infrastructure remains resilient to both routine and extreme stressors.

- *Maintenance Management*: Efficient infrastructure management optimizes the use of available resources, ensuring that maintenance is both timely and cost-effective. By strategically planning maintenance activities, transportation authorities can minimize downtime and repair costs, thus ensuring operational efficiency. A well-managed infrastructure network is essential for reducing long-term degradation, allowing for smoother transportation of goods and people while minimizing the impact of aging infrastructure on public finances.

- *Prevention*: Preventative maintenance is one of the most important aspects of infrastructure management. Detecting the early signs of wear, such as cracks or stress points, allows for timely interventions, reducing the need for large-scale repairs. This proactive approach reduces not only the risk of failure but also long-term financial costs associated with extensive rehabilitation efforts. By investing in early detection technologies and maintenance strategies, governments and organizations can mitigate risks, ensuring infrastructure remains operational and safe for longer periods.

The challenges related to infrastructure maintenance, safety, and prevention are priorities shared globally. Regardless of geographic location, every nation recognizes the importance of effectively preserving and managing its transportation networks. Achieving these objectives, which are closely linked to infrastructure resilience, is essential for ensuring public safety and fostering economic growth. In this context, various countries have adopted specific guidelines to address these issues.

1.2.1 GUIDELINES IN THE UNITED STATES: FOCUS ON INDIANA AND INDOT

In the United States, transportation infrastructure management is guided by a combination of federal, state, and local agencies, each playing a crucial role in ensuring the safety and efficiency of the nation's road networks. This section focuses specifically on the role of the Indiana Department of Transportation (INDOT), which is responsible for the construction, maintenance, and operation of the state's extensive transportation network. The INDOT plays a pivotal role in ensuring the construction, maintenance, and operation of Indiana's extensive network, which includes federal interstates, U.S. highways, and state roads. This responsibility encompasses over 11,200 centerline miles (approximately 29,600 lane miles) of roadways and more than 5,700 bridges (https://www.in.gov/dot/div/contracts/standards/book/sep21/2022%20Standard%20Specificatins%20(w_changes).pdf, Indiana Department of Transportation, 2022). Guided by its mission to deliver a superior transportation system, INDOT prioritizes safety, mobility, and economic development while adhering to the principle of fiscal and operational accountability. INDOT's approach to infrastructure management is centered on preservation, following the guiding philosophy of "taking care of what we have"(https://www.in.gov/indot/about-indot/indot-mission-goals-and-values/). Preventive maintenance is a cornerstone of this strategy, encompassing activities such as resurfacing, crack sealing, chip sealing, and stormwater drainage management. Regular monitoring of road surfaces, which includes visual inspections and advanced tools, allows the early detection of issues like cracks and potholes (https://www.in.gov/indot/current-programs/pavement-preservation-program/). Such interventions help prioritize repairs or resurfacing in critical areas, ensuring cost-effectiveness and user safety. For instance, proactive treatments like chip and crack sealing not only delay structural deterioration but also reduce the financial burden of future repairs, exemplifying sustainable and responsible resource management (https://www.in.gov/indot/maintenance-operations/).

Bridge maintenance follows a similarly rigorous framework. INDOT conducts both visual and instrumented inspections to detect structural issues, such as fissures, joint deterioration, and corrosion of metallic elements. These evaluations are supplemented by innovative technologies like drones and laser scanners, which enable the creation of detailed 3D models of bridges to predict critical stress points and guide interventions. Regular deck overlays and structural reinforcements help mitigate deterioration and maintain safety standards. As a result of these efforts, the proportion of bridges rated as "fair or better" has consistently improved over recent years, reflecting the effectiveness of INDOT's management strategies (https://www.in.gov/indot/files/2022-TAMP.pdf). The figure below 1.1 the current composition of the teams dealing with bridges and pavements, respectively. The first illustrates how INDOT's bridges team is organized to ensure effective management and timely maintenance of the state's bridges, contributing to the safety and longevity of these critical infrastructure elements; the second provides an overview of INDOT's pavements team organization, which is essential to ensure efficient pavement management and timely maintenance activities throughout the state (https://www.fhwa.dot.gov/asset/pubs/hif23019.pdf).

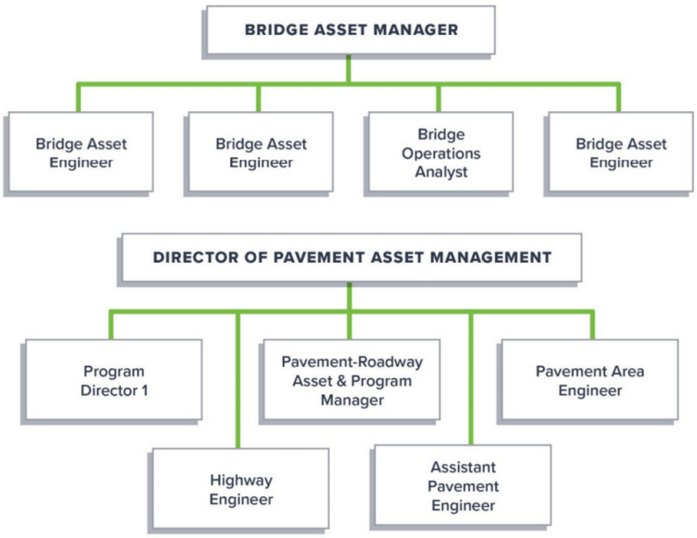


Figure 1.1: The organization of the bridge and pavement team (data source: INDOT).

Vegetation management along roadways is another critical focus, balancing safety, aesthetics, and ecological sustainability. To ensure clear visibility of traffic signals and road signs, INDOT performs routine mowing cycles, multiple times a year in urban areas and rural zones. This prevents obstruction while controlling the spread of invasive species. Furthermore, the integration of native plantings along roadsides reduces the need for frequent mowing and herbicide application, promoting ecological habitats and supporting biodiversity (https://www.in.gov/indot/current-programs/green-initiatives/roadside-management-program/mowing-and-vegetation-management/). These initiatives underscore INDOT's dual commitment to maintaining operational safety and fostering environmental stewardship.

In fact, INDOT operates through multiple district offices strategically distributed across the state, ensuring localized operations such as road construction, traffic signal management, and essential maintenance tasks like pothole repairs and snow removal. This decentralized framework enables a timely response to regional needs while maintaining consistency in statewide projects. Overall, INDOT exemplifies an integrated approach to infrastructure management, addressing both immediate operational demands and the long-term challenges of sustainability and growth. Figure 1.2 illustrates the flow of data governance related to bridges, large culverts, and other critical structures, highlighting how data is used to inform maintenance decisions and ensure consistency across projects.

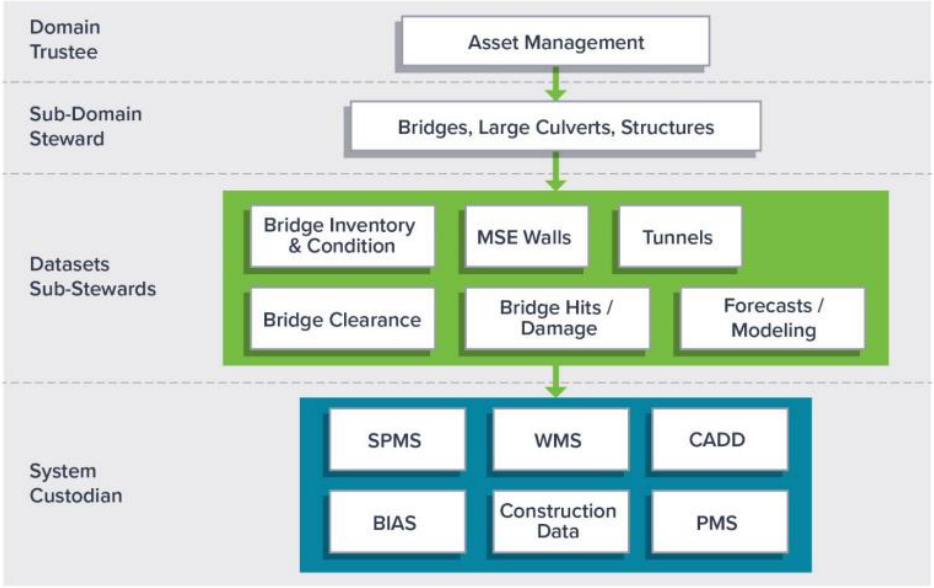


Figure 1.2: Flow of data governance model (bridges, large culverts, and structures (data source: INDOT).

1.2.2 GUIDELINES IN EUROPE: FOCUS ON ITALY AND MIT

In Europe, the maintenance and safety of transportation infrastructure, particularly bridges, have been increasingly emphasized in response to aging structures and catastrophic failures, such as the collapse of the Morandi Bridge in Genoa in 2018 (Alessandrini S., 2020). This event underscored the critical need for robust evaluation and maintenance frameworks, leading to significant policy updates across the continent. Italy, due to its orographic conformation, has one of the largest infrastructure assets in terms of bridges and viaducts in Europe. The heritage of works of art on the Italian territory counts about 63,575 bridges, of which: about 19,000 belong to the railway network managed by RFI, 14,575 are located on the road and highway network managed by ANAS, and about 30,000 are managed by Concessionary Companies, Regions, Provinces and Municipalities. These are infrastructures that have an average age of more than fifty years and that, although they have so far performed their function regularly, have nevertheless undergone continuous and constant degradation

related to the environment and operation, degradation that is often not counteracted with adequate maintenance by the owning or managing entities (Bellino 2019). As a result, recognizing the many problems associated with the natural aging of infrastructure, the need for ensuring their adequate performance over time has emerged, taking into account the specific needs and usage classes. Inevitably, in Italy, the Ministry of Infrastructure and Transportation (MIT) introduced comprehensive guidelines through Decree No. 578 on December 17, 2020 (https://www.mit.gov.it/ MIT 2020, MIT 2022). These guidelines establish a mandatory framework for the risk classification, safety assessment, and monitoring of existing bridges. Their objective is to prevent structural failures through systematic and scalable evaluations, incorporating six progressive levels of analysis (Levels 0 to 5). The approach begins with basic visual inspections and documentation at Level 0 and advances to detailed structural analysis and prioritization of interventions at higher levels. This methodology considers multiple risk factors, including structural, seismic, flooding, and geotechnical risks, while accounting for the aging and deterioration of materials over time (https://www.mit.gov.it/nfsmitgov/files/media/normativa/2020-12/1_Testo_Linee_Guida_ponti.pdf).

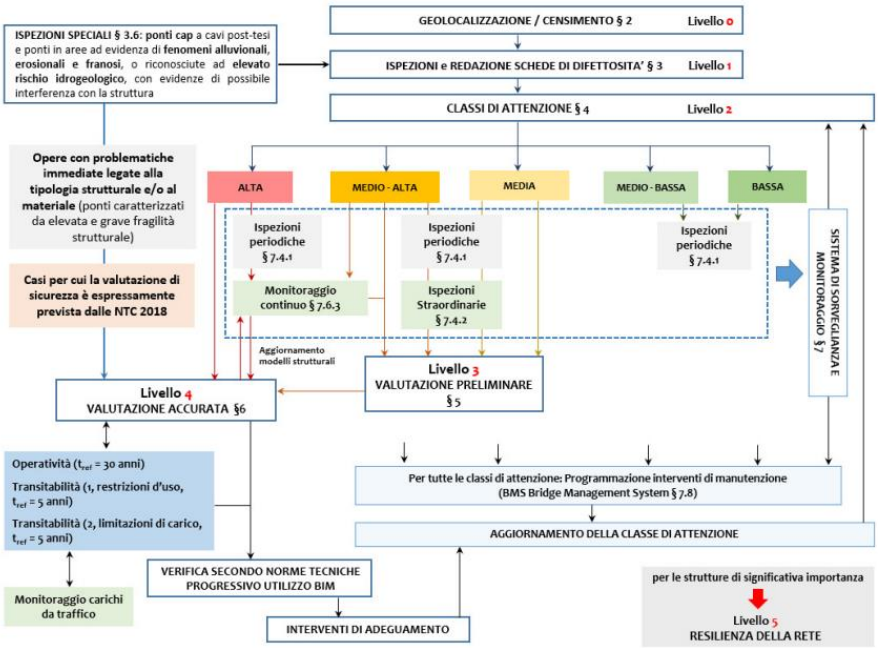


Figure 1.3: Multilevel approaches and relationships between levels of analysis illustrates the different levels of analysis defined by the guidelines and their interrelationships. These levels enable a comprehensive and systematic approach to bridge assessment and maintenance (Data source: MIT 2020).

One of the innovative aspects of the Italian guidelines is their focus on a "Class of Attention" (in Italian guidelines Classe di Attenzione (CdA) framework. This system assigns risk levels ranging from low to high based on the combined influence of material degradation, seismic vulnerability, and environmental risks. This classification helps allocate resources effectively, prioritizing critical bridges for maintenance or retrofitting. Furthermore, the guidelines align with the broader European standards, ensuring harmonization with risk assessment practices across the EU (https://eur-lex.europa.eu/legal-content/EN/TXT/PDF/?uri=CELEX:52015XC0808(01)). To address these challenges, the MIT has established comprehensive guidelines and operational frameworks for infrastructure monitoring and maintenance. These guidelines emphasize periodic inspections, risk assessments, and the integration of advanced technologies. For instance, MIT's "Linee guida per la classificazione e gestione del rischio, valutazione della sicurezza e monitoraggio dei ponti esistenti" provides a structured approach for assessing the condition of bridges based on parameters like structural health, material degradation, and seismic vulnerability. This framework prioritizes preventive maintenance, aiming to extend the lifecycle of aging structures while minimizing disruptions. The adoption of these guidelines is exemplified by projects such as the national database for bridge and viaduct monitoring, which collects data from inspections and integrates it into a centralized platform. This approach not only facilitates real-time decision-making but also enables more accurate risk classification, helping authorities allocate resources effectively. Through these measures, MIT's guidelines not only address the immediate needs of an aging transport network but also lay the groundwork for a sustainable and resilient infrastructure system capable of withstanding future challenges. Italy's proactive adoption of these guidelines not only addresses immediate risks

but also contributes to the development of a sustainable infrastructure maintenance strategy, reinforcing the resilience of its transportation networks. These efforts position Italy as a model for integrating innovative, risk-based approaches into national infrastructure policies.

1.3 BEST SURVEY TECHNIQUES FOR INFRASTRUCTURE INSPECTION AND CRACK DETECTION

The assessment of infrastructure integrity and the detection of structural anomalies, such as cracks, require advanced and reliable survey techniques. Modern methods combine traditional practices with innovative technologies to provide comprehensive and non-invasive solutions for infrastructure management. Among the key methods, Non-Destructive Testing (NDT) stands out for its ability to deliver precise assessments without causing damage to the structure (Teza G. et al., 2009; Riveiro B. et al., 2016; Le N.D. et al., 2024).

Other prominent technologies, such as LiDAR and photogrammetry from UAVs, complement NDT by enabling large-scale data acquisition and analysis. LiDAR offers high-resolution spatial data, while UAVs provide rapid and cost-effective visual inspections, especially in inaccessible areas (Haala N. et al., 2020; Gaspari F. et al., 2022). These techniques will be discussed in greater detail in Chapter 2 Methodologies and advantages of geomatic techniques for acquiring detailed data in infrastructure.

Incorporating these tools with Machine Learning (ML) models enhances their effectiveness, automating anomaly detection and reducing inspection times (Nassif A.B. et al., 2021; Selim G.E.I. et al., 2021). Together, these methods provide a robust framework for maintaining infrastructure safety and functionality.

1.3.1 ADVANTAGES AND APPLICATIONS OF NON-DESTRUCTIVE TESTING (NDT)

Traditionally, infrastructure inspection has relied on visual assessments conducted by experts, often supported by Non-Destructive Testing (NDT) methods to validate and enhance findings (Koch C. et al., 2015; Spencer Jr B.F. et al., 2019). Over time, NDT has become an indispensable component of modern maintenance strategies, providing precise, non-invasive evaluations of structural integrity while minimizing operational disruptions. These methods play a pivotal role in infrastructure inspection by offering insights into material properties, detecting surface defects, and enabling localized assessments to identify issues such as material degradation or hidden cracks with high precision (DwivediS. K. et al., 2018; Artagan, S.S. et al., 2020; El Masri, Y. et al., 2020; Kot P. et al., 2021).

NDT offers a unique capability to evaluate the condition of materials and structural components without causing physical alterations or damage. This characteristic is especially vital for essential infrastructure such as bridges, tunnels, and transportation corridors, where invasive testing could result in operational disruptions, safety risks, and significant economic impacts (Bertovic M., 2015; Gkoumas K. et al., 2024). By employing advanced diagnostic techniques, NDT can identify issues often imperceptible to visual inspections, enabling timely and targeted interventions to mitigate risks. Economically, NDT reduces the necessity for large-scale repairs through preventive maintenance, while the real-time data generated by certain methodologies enhances decision-making processes, ensuring informed responses to emerging challenges (Vyas V. 2020; Futai M. M. et al., 2022). Moreover, the non-invasive nature of NDT preserves the structural integrity of assets, extending their service life and avoiding the adverse effects associated with destructive testing methods. In the realm of infrastructure management, NDT has become a cornerstone for assessing the performance and safety of materials, including concrete, steel, and composites, particularly in aging structures (Zollini S. et al. 2020; Alicandro M. et al.

2023). Its primary applications include the detection of both surface and subsurface defects, such as cracks that could compromise the structural integrity of critical assets, and the monitoring of corrosion in reinforced concrete and steel components exposed to environmental stressors like moisture and chlorides, which accelerate material degradation (Verma S. K. et al., 2013; Rathod H. et al., 2019) . Beyond conventional applications, advancements in technology have significantly enhanced the scope of NDT methodologies by integrating innovative tools such as LiDAR, digital twin frameworks, and WebGIS platforms (Al-Sehrawy R. et al. 2021; Liang H. et al., 2023; Gao Y. et al., 2024). The incorporation of WebGIS allows for the visualization, analysis, and management of geospatial data related to infrastructure, facilitating a centralized repository for national and international case studies. This approach enables stakeholders to access real-time insights and monitor infrastructure conditions effectively, promoting collaborative and informed decision-making processes. Similarly, digital twin frameworks enhance predictive capabilities by simulating structural behavior under varying loads and stress conditions, complementing the diagnostic potential of NDT. The effectiveness and reliability of NDT are further supported by adherence to internationally recognized standards, which ensure consistency in methodologies and the accurate interpretation of results. Standards such as ANSI/ASNT CP-105, Recommended Practice No. SNT-TC-1A, ISO 9712, and EN 473 provide comprehensive guidelines for the qualification and certification of NDT personnel, as well as the application of techniques in diverse contexts. These standardized practices contribute to maintaining the applicability of NDT in critical infrastructure assessments. By integrating advanced methodologies such as WebGIS and digital twins with NDT processes, infrastructure management can benefit from enhanced safety measures, cost-optimized maintenance strategies, and improved operational reliability. This combined approach underscores the potential of non-invasive diagnostics to address emerging challenges in infrastructure preservation and sustainability, fostering resilience in both national and international contexts.

1.4 RESEARCH QUESTIONS & GOALS

The primary objective of this thesis is to develop semi-automated and automated methodologies to facilitate the inspection and maintenance of infrastructure. Central to this effort is the creation of a WebGIS platform that serves as a universal tool, accessible globally, to enable effective large-scale management strategies. This ambitious undertaking necessitates a critical evaluation of existing challenges in infrastructure monitoring and the formulation of innovative approaches to address them effectively. The research integrates advanced geomatic techniques, including LiDAR from MMS, SLAM-based technologies, and UAV photogrammetry, with Non-Destructive Testing (NDT) methods. These techniques, known for their ability to assess structural conditions without causing damage, will enhance the proposed framework's capacity to detect cracks, monitor corrosion, and evaluate structural integrity. The envisioned approach will leverage artificial intelligence (AI) to ensure a robust, stable, and user-friendly solution, adaptable to diverse infrastructural and geographic contexts. The integration of NDT techniques with AI-driven analytics aims to improve diagnostic precision and facilitate proactive maintenance strategies. By combining NDT methodologies, geomatic technologies within a WebGIS environment, the proposed solution aspires to provide a comprehensive, scalable, and practical tool for infrastructure management.

Taking the overarching objective into account, several interconnected and complex challenges have surfaced. A summary of the aims of this thesis is encapsulated in the following research questions:

Question 1. Why is the maintenance of infrastructure and transportation corridors crucial?

Question 2. What are the most suitable survey techniques for conducting infrastructure inspections effectively?

Question 3. Which methods are most effective for detecting cracks in road and concrete pavements and for analyzing potential hazards?

Question 4. How do different surveying technologies—such as LiDAR from mobile mapping, SLAM, and UAV

photogrammetry—impact the accuracy and precision of inspection results?

Question 5. Which analytical methodologies, including those leveraging e-learning and statistical approaches, are best suited for processing point clouds?

Specific research questions for each in-depth case study:

Question 6. How can classification methods improve the identification of signal occlusions?
Case Study: Signal occlusions caused by vegetation.
Technique: Multi-Class Simultaneous Segmentation (MCSS) and SuperPoint Graph (SPG) classification of point clouds from MMS.
Location: USA.

Question 7. What is the impact of incorporating intensity data on improving crack detection?
Case Study: Crack detection on road pavements of 27 bridges.
Technique: Point cloud analysis using Density-Based Spatial Clustering of Applications with Noise (DBSCAN) and Random Forest (RF), with and without intensity data from MMS.
Location: USA.

Question 8. How do results obtained using SLAM compare with those from mobile mapping systems in crack and degradation detection?
Case Study: Crack and degradation detection on a viaduct.
Technique: Point cloud analysis using SLAM with DBSCAN and Random Forest.
Location: Italy.

Question 9. How effective is Object-Based Image Analysis (OBIA) in detecting cracks on concrete compared to LiDAR-based techniques?
Case Study: Cracking detection on a concrete specimen.

Technique: Photogrammetry from UAV with classification and applying filters for OBIA.

Location: Italy (Replicable method anywhere and in any infrastructure).

Question 10. How can an open-source WebGIS platform enhance the accessibility and user-friendliness of infrastructure monitoring and maintenance tools?

To endeavor to address the aforementioned inquiries, the following objectives have been delineated:

Objective 1. To analyze the critical role of maintenance in preventing structural and functional risks, emphasizing its impact on public safety and infrastructure resilience. To evaluate the advantages of predictive maintenance over reactive approaches and identify global monitoring needs, proposing effective and scalable strategies for infrastructure management.

Objective 2. To compare advanced geomatic techniques, including LiDAR, SLAM, and UAV photogrammetry, based on their precision, cost-effectiveness, and applicability. To establish selection criteria for these technologies tailored to specific infrastructural contexts, while identifying current limitations and proposing improvements or integrations of multiple methods.

Objective 3. To evaluate the performance of various algorithms and crack detection techniques, as well as risk identification methods, in terms of accuracy and reliability. To adapt the most effective methodologies for detecting and classifying longitudinal and transverse cracks, and to analyze the potential implications of the collected data for safety and maintenance strategies.

Objective 4. To examine the impact of various geomatic techniques on quality metrics such as accuracy, precision, and spatial resolution. To identify the conditions and contexts in which each technology demonstrates optimal performance, and to provide practical guidelines for selecting the most appropriate technologies based on specific survey objectives.

Objective 5. To identify ML algorithms that enhance the quality of point cloud processing and incorporate advanced statistical

techniques. To evaluate the effectiveness of innovative approaches, such as Deep Learning (DL) and unsupervised clustering, in segmentation and classification tasks. To integrate advanced analytical methodologies to support data-driven decision-making processes.
DBSCA

To try to answer these questions, the following objectives were outlined for the individual case studies:

Objective 6. To study the effectiveness of MCSS and SPG methods in detecting signal occlusions caused by vegetation. To compare the performance of classification techniques on different types of occlusions. To propose solutions that enhance the management of signage in complex scenarios.

Objective 7. To evaluate the importance of intensity data in the accuracy and reliability of crack analysis. To compare the results obtained with and without intensity normalization in complex scenarios, such as the analysis of 27 bridges. To propose recommendations for the inclusion of intensity in detection processes.

Objective 8. To analyze SLAM's performance differences in accuracy, precision, and applicability. To study complex crack cases, such as the viaduct in Italy, to highlight the advantages and limitations of the SLAM approach. To define criteria for selecting the most suitable technology in specific infrastructural contexts.

Objective 9. To evaluate the effectiveness of UAV photogrammetry using OBIA in detecting and classifying cracks compared to LiDAR and other geomatic techniques. To analyze the impact of filters and classification techniques applied to UAV data. To demonstrate the replicability and adaptability of the OBIA approach to various types of infrastructures and geographic contexts.

Objective 10. To explore the potential of open-source WebGIS platforms in enhancing the accessibility and user-friendliness of infrastructure monitoring and maintenance tools. To assess the advantages of using open-source software in the development of a platform that can be universally applied for infrastructure management across diverse geographical and infrastructural contexts.

1.5 THESIS OUTLINE

The present thesis is organized as follows:

1.5.1 CHAPTER 1 – INTRODUCTION

In Chapter 1, the importance of infrastructure maintenance and the safety of transport corridors is emphasized, explaining how prevention plays a fundamental role in risk reduction and the durability of structures. The main guidelines for infrastructure maintenance are presented, with a comparative overview of practices in the United States (focused on Indiana and INDOT) and Europe (focused on Italy and MIT). Additionally, an overview of non-destructive testing (NDT) techniques and advanced geomatic technologies such as LiDAR and UAV photogrammetry is provided, highlighting their value for infrastructure safety and monitoring.

1.5.2 CHAPTER 2 - METHODOLOGIES AND ADVANTAGES OF GEOMATIC TECHNIQUES FOR ACQUIRING DETAILED DATA IN INFRASTRUCTURE

In Chapter 2, an analysis of the main geomatic techniques used to acquire detailed data in infrastructures and transport corridors is presented, comparing traditional and modern methods. The use of LiDAR and UAV photogrammetry for high-precision surveys is explored, with a focus on the applications of MMS, SLAM, and drone-based photogrammetry. The next section delves into geometric/morphological methodologies and machine learning-based approaches for risk detection, including data enhancement techniques such as normalized intensity and advanced filters (Lee, Frost, and Median). Finally, segmentation and clustering approaches (e.g., MCSS and DBSCAN), classification with RF, and DL (SPG) are illustrated through case studies, highlighting the effectiveness of each technique in managing and preventing infrastructure risks.

1.5.3 CHAPTER 3 - STATISTICAL METHODS FOR PERFORMANCE EVALUATION AND DATA ANALYSIS

Chapter 3 describes the statistical methods used to assess performance and analyze data in geomatics contexts. After a general introduction to statistical methods applicable in this field, it focuses on performance indicators for classifications, such as Truth Positive (TP), False Positive (FP), False Negative (FN), Recall, Precision, and F1-Score, as well as the Jaccard index to evaluate similarity between results.

1.5.4 FIRST CASE STUDY: TRAFFIC SIGN VISIBILITY AND OCCLUSION IN THE USA

In Chapter 4, the first case study is described, centered on the occlusion of road signs in the United States along Interstate 65 (I-65). The section introduces the topic and presents the data acquisition systems used, as well as data collected through MMS. Experimental results are discussed, with a comparative analysis of segmentation techniques such as MCSS and the DL approach SPG. Subsequently, an analysis of road sign visibility is conducted, highlighting issues and solutions to improve road visibility.

1.5.5 CHAPTER 5 - SECOND CASE STUDY: DETECTION OF ROAD SURFACE CRACKS IN THE USA

Chapter 5 illustrates the second case study, dedicated to crack detection on a road surface in the United States (Highway I-65). The initial section introduces the context of the case study and describes the data acquisition systems. In the experimental results, a comparative analysis is performed between the DBSCAN clustering method and RF classification for crack detection, with and without normalized intensity of the extracted data.

Subsequently, crack detection in point clouds is analyzed, discussing the results in terms of accuracy and the applicability of the methods.

1.5.6 Third Case study: Crack Analysis on L'Aquila Viaduct, Italy

Chapter 6 presents the third case study, focused on the Campo di Pile viaduct in L'Aquila, Italy. After a general introduction, the data acquisition systems are described, which are used for the survey by comparing the two SLAM technologies, GeoSLAM ZEB Horizon and BLK2GO with Leica GS15 GNSS Receiver. In the experimental results, a comparative analysis is conducted between DBSCAN and RF methods for crack detection, both with and without normalized intensity of the extracted surface data. The chapter continues with an analysis of crack detection in point clouds, illustrating the differences in methods applied to the viaduct context.

1.5.7 Chapter 7 - Fourth Case study: Concrete Specimen Crack Identification

Chapter 7 examines the fourth case study, focused on a concrete sample (a common type case anywhere). After a general introduction to the context of the analyzed sample and its characteristics, the data acquisition systems used are described, as well as the specific case study. The processing section explores the application of OBIA classification to enhance data quality. In the experimental results, the OBIA classification combined with the results of filters (Median, Enhanced Frost, Enhanced Lee) applied to the region of interest (ROI) is presented. The chapter concludes with a discussion on the extraction of each individual crack and a comparison of the area for each obtained result.

1.5.8 Chapter 8 - Creation of 3D Models with integration of predictive

ANALYTICS AND MAINTENANCE SUGGESTIONS

Chapter 8 discusses the creation of 3D models for infrastructure analysis, highlighting their role as essential tools for structural prevention and maintenance. The process is entirely open-source, ensuring accessibility and adaptability for researchers, professionals, and institutions worldwide. The chapter begins by emphasizing the importance of three-dimensional models in infrastructure management, continues with detailed guidelines on data preparation and the selection of suitable open-source software, and concludes with the integration of analytical results to predict potential issues and plan maintenance interventions. The integration leverages WebGIS platforms for interactive data visualization and efficient management in a web-based environment.

1.5.9 CHAPTER 9 - CONCLUSIONS

In the conclusions, the discussion revisits the initial research questions, providing a comprehensive analysis of the advantages and limitations of the various technologies employed. Maintenance recommendations, based on the results of the models created, are then presented. This highlights how these tools not only support informed decision making in infrastructure management, but also help advance communication and knowledge sharing within the industry. In addition, the study highlights the potential of these approaches to improve preventive planning, mitigate operational risks and optimize resource allocation for timely, safe and effective interventions.

2. METHODOLOGIES AND ADVANTAGES OF GEOMATIC TECHNIQUES FOR ACQUIRING DETAILED DATA IN INFRASTRUCTURE

2.1 METHODOLOGIES AND ADVANTAGES OF GEOMATIC TECHNIQUES FOR ACQUIRING DETAILED DATA IN INFRASTRUCTURE

In modern infrastructure management, the acquisition of precise and detailed data plays a crucial role in ensuring safety, functionality, and longevity (Brownjohn J.M.W., 2007; Plevris V. et al. 2024). This chapter explores the evolution of survey techniques, emphasizing the shift from traditional manual methods, which are often limited in scope and subject to human error, to innovative geomatic technologies that offer enhanced efficiency, accuracy, and safety. The analysis begins with a comparison of commonly used techniques, contrasting the labor-intensive and subjective nature of traditional visual inspections with the objectivity and automation of modern tools. Key technologies such as LiDAR (Light Detection and Ranging) and UAV photogrammetry are examined for their ability to provide high-precision datasets, particularly in challenging environments like tunnels, transportation corridors and elevated structures. Furthermore, the chapter delves into advanced methodologies for risk detection,

integrating geometric and morphological approaches with machine learning and deep learning techniques. These methods not only enhance data interpretation but also enable proactive decision-making in maintenance and prevention strategies. The case studies presented illustrate the practical applications and effectiveness of these methodologies in diverse scenarios, showcasing their transformative potential in infrastructure prevention, maintenance and, management.

2.2 ANALYSIS OF COMMONLY USED SURVEY TECHNIQUES

Surveying techniques form the backbone of infrastructure monitoring and management (Amin M., 2000). Over the years, these techniques have undergone significant advances, moving from traditional manual methods to automated systems that take advantage of cutting-edge technologies such as UAV photogrammetry and LiDAR (Greenwood W. W. et al., 2019; Rane N. et al., 2023). Each method has its strengths and limitations, and their applicability often depends on factors such as the complexity of the site, the level of accuracy required, and the resources available.

Conventional techniques are generally characterized by manual processes, such as visual inspections, use of total stations and levels. These methods, while reliable in certain contexts, can be laborious, time-consuming and, in some cases, unsafe for operators working in deteriorated or hazardous environments (Chin R.T. et al, 1982; Newman T. et al., 1995; Agnisarman S. et al., 2019). Contemporary techniques, on the other hand, integrate advanced sensors, machine learning algorithms, and automation, allowing for more efficient, detailed, and secure data collection, particularly for large-scale and inaccessible areas (H. Shakhatreh et al, 2019; Sun A. Y. et al., 2019; Wang H. et al. 2023). These advancements not only improve the quality of data collected but also address the challenges of working in complex and challenging environments, thereby enhancing the overall

safety and effectiveness of infrastructure surveys. The integration of modern survey techniques has therefore transformed the field, enabling a richer understanding of spatial phenomena and supporting data-driven decision-making processes (Pai S.G. et al., 2022; Kyriou A. et al., 2023).

2.2.1 Overview of Conventional and Contemporary Survey Techniques

Over the past decades, advancements in sensor technologies, mapping platforms, and data processing methodologies have revolutionized the field of remote sensing. These innovations have significantly broadened the scope of applications, particularly in infrastructure monitoring and maintenance. Modern MMSs now integrate a variety of platforms, such as UAVs, backpack systems, Unmanned Ground Vehicles (UGVs), and wheel-based systems, all equipped with advanced sensors capable of capturing data at high temporal and spatial resolutions. Additionally, the accessibility and cost reduction of direct georeferencing technologies—such as integrated Global Navigation Satellite Systems/Inertial Navigation Systems (GNSS/INS)—have enabled these systems to perform accurate, control-free mapping, making them highly efficient for large-scale surveys (Nex F. et al., 2014; Manish R. et al., 2021). Despite these advances, conventional surveying methods remain fundamental in many contexts due to their reliability, precision, and historical significance in geomatics. Traditional techniques, such as visual inspections, total stations, and leveling, have long served as the cornerstone of infrastructure monitoring (Agnisarman S. et al., 2019). Visual inspections, while inexpensive and intuitive, are often subjective and reliant on the surveyor's expertise (Spencer Jr B.F. et a. 2019; Zhou H. et al, 2022). These inspections are limited in their ability to provide detailed quantitative data and are best suited for preliminary evaluations or routine maintenance tasks. Total stations, on the other hand, deliver highly accurate point measurements and are essential for tasks requiring sub-millimeter precision, such as alignment checks or structural monitoring. However, they are limited in their spatial coverage and efficiency,

particularly over large areas, and require skilled operators and direct access to the surveyed area (Chekole S.D., 2014). Contemporary surveying methods integrate advanced technologies that offer enhanced safety, efficiency, and multi-dimensional datasets (Di Stefano F. et al., 2021). MMS, for instance, combine LiDAR sensors with GNSS and inertial systems to rapidly acquire high-density point clouds over extensive corridors (Sairam N. et al., 2016; Al-Bayari O., 2019). This technique is particularly effective for roadway and urban corridor surveys, offering high accuracy while minimizing disruptions. SLAM technologies, process data in real-time to generate maps with high adaptability. While SLAM offers unparalleled flexibility, its accuracy can be affected by sensor miscalibration or algorithmic drift (Chen W. et al., 2022). UAV photogrammetry, utilizing drones equipped with high-resolution cameras, is invaluable for surveying inaccessible or hazardous areas (Gomez C., et al., 2016). UAVs capture overlapping aerial images to generate orthophotos and 3D models with rich visual context, complementing LiDAR datasets and enhancing their geometric precision (Sharifisoraki Z. et al., 2023). The integration of contemporary surveying techniques has effectively addressed many limitations inherent in conventional methods by offering greater spatial coverage, improved efficiency, and enriched data context. Contemporary tools provide several critical advantages. For instance, remote sensing technologies enhance safety by reducing the need for personnel to operate in hazardous environments (Khan A. et al., 2020). Automation significantly accelerates data collection, making it feasible to survey large or complex areas efficiently. Moreover, advanced sensors yield dense datasets with high spatial and temporal resolution, enabling detailed analyses that were previously unattainable (Zhu X. et al., 2017; Zhang L. et al., 2022). Despite these advancements, conventional surveying methods remain valuable, particularly for tasks requiring meticulous accuracy or where resources for deploying contemporary systems are limited (Riveiro B. et al, 2016). For example, visual inspections, while simple and cost-effective, rely heavily on the expertise and subjective judgment of

inspectors, making them prone to bias and variability. Furthermore, their inability to capture detailed quantitative data restricts their use to preliminary evaluations or routine maintenance tasks. Similarly, tools such as total stations and leveling instruments provide unparalleled precision but are labor-intensive and less efficient over large-scale areas (Yang G. et al., 2022; Laflamme S. et al. 2023; Nahiyoon SA. et al., 2024). The transition from conventional to contemporary techniques reflects a fundamental shift in how data is conceptualized and utilized in infrastructure monitoring. While conventional methods excel in localized precision and well-defined tasks, contemporary tools prioritize large-scale efficiency, predictive modeling, and comprehensive spatial coverage (Rashidi M. et al, 2016; Sun Z. et al., 2024) . The interplay between these approaches highlights the importance of integration: combining the reliability and precision of conventional methods with the scalability and adaptability of contemporary technologies ensures comprehensive, reliable assessments (Chan B. et al., 2016; Wang X. et al, 2022). This balanced approach enables surveyors to address diverse project requirements effectively, meeting the challenges posed by contemporary infrastructure monitoring and maintenance. To address these limitations, more advanced tools, such as total stations have been introduced. Total stations represent a significant technological evolution, integrating an electronic theodolite and an electronic distance measurement (EDM) unit to measure horizontal and vertical angles as well as distances simultaneously (Corradeghini P., 2017). These instruments offer improved precision and versatility, making them indispensable in static surveys for civil engineering and cadastral applications (Lachat E. et al., 2017). They are particularly well suited for capturing small details and achieving high accuracy, with distance measurements approximately 1-2 mm and angular precision of approximately 0.1 mgon. However, these methods require skilled personnel, direct visibility between the instrument and target, and considerable time to acquire point-by-point data. Furthermore, their use in dynamic environments or real-time monitoring remains limited, which can hinder efficiency in large-scale infrastructure

assessments. In addition to conventional and contemporary survey techniques, satellite-based positioning systems like GNSS have emerged as critical tools for infrastructure monitoring. GNSS enables three-dimensional positioning [X,Y,Z] or o [ϕ, λ, h] of points in a geocentric reference system through the reception of radio signals transmitted by multiple satellite constellations orbiting the Earth (Cina A., 2014). Its applications extend across various fields, including transportation infrastructure assessment, where accurate positioning and georeferencing are essential.

The GNSS framework comprises several global positioning systems, including:

- NAVSTAR GPS: Developed by the United States Department of Defense, NAVSTAR GPS operates using the WGS84 geocentric datum and provides reliable positioning for static and dynamic environments.
- GLONASS: Russia's counterpart to GPS, based on the PZ90 datum, offering similar functionality with expanding satellite coverage.
- GALILEO: The European Union's satellite positioning system, under development, leveraging the GTRF datum.
- BeiDou, QZSS, and GAGAN: Regional systems developed by China, Japan, and India, respectively, which complement global capabilities through enhanced interoperability.

Furthermore, GNSS systems are characterized by three key components:

- Space Segment: The satellite constellations that transmit signals.
- Control Segment: Ground stations that manage and maintain the system.
- User Segment: Receivers equipped with antennas to capture satellite signals.

While GNSS offers millimeter- to centimeter-level accuracy, its performance can be affected by physical obstructions such as buildings, dense vegetation, or urban canyons, which may block or reflect signals. Moreover, GNSS is primarily used for discrete point measurements, making it most effective when integrated with other geomatic technologies. For instance, GNSS receivers are frequently employed for position control in

UAV-based photogrammetric and LiDAR surveys, providing georeferenced data critical for infrastructure assessments. Despite these limitations, GNSS remains a versatile and cost-effective option for many applications. The cost of GNSS receivers ranges from €2,000 to €12,000, depending on their specifications and intended use. A comparative table in the following section will detail the advantages, limitations, accuracy, and costs of GNSS and other survey methods, enabling a comprehensive evaluation of their suitability for infrastructure monitoring.

As geomatics technologies evolve, 3D laser scanning has emerged as a cornerstone for capturing highly detailed geometric data, complementing traditional and modern surveying methods. Laser scanners are advanced tools combining laser rangefinders with high-precision mechanical components to record the 3D position of a vast number of points with remarkable speed and accuracy. The resulting dataset, known as a "point cloud," provides an unparalleled representation of the surveyed environment, making this technology particularly well suited for infrastructure monitoring and documentation (Bornaz L., 2006). Laser scanners are active sensors that emit artificial laser light to directly capture the 3D geometric information of objects. Depending on the underlying measurement principle, these systems can acquire between 800 and over 12,500 points per second (Bartolucci D., 2009), enabling the rapid collection of millions of points. However, the dense and detailed point clouds they produce often necessitate significant post-processing efforts, including data cleaning, editing, and computationally intensive modeling. Despite these challenges, the precision of laser scanners—often achieving measurements within millimeter accuracy—makes them indispensable for tasks requiring high-resolution data. Modern laser scanners have expanded capabilities, now capturing additional attributes such as reflectance, color, and surface normals for each point, offering enriched datasets for advanced analyses. Laser scanners are widely employed for the 3D surveying of extensive surfaces such as bridges and viaducts, as well as smaller-scale objects. The high spatial resolution and density of the collected data allow

for detailed documentation and analysis of structural conditions, supporting preventive maintenance and safety assessments. This versatility has driven the adoption of laser scanning technology in the field of infrastructure investigations (Tang P. et al., 2007).

However, laser scanning is not without limitations:

• Line of sight dependency: Scanners require unobstructed views of the target, necessitating careful instrument placement or multiple scanning stations to ensure complete coverage.

• Handling complex surfaces: Glossy or transparent materials may introduce data gaps or distortions, requiring additional attention during acquisition and processing.

• Relatively slow data acquisition: For highly detailed surveys, static laser scanners can be slower than mobile or aerial systems, limiting their use in time-sensitive projects.

In conclusion, laser scanning is a transformative technology for infrastructure monitoring, balancing exceptional precision and data richness with challenges in acquisition and processing. The following sections will explore how laser scanning integrates with other geomatics techniques to address specific challenges in infrastructure assessment, particularly when combined with mobile and UAV-based systems.

In recent years, advancements in UAVs have revolutionized data acquisition techniques, particularly for surveying and inspection tasks (Everaerts J., 2008; Shakhatreh H. et al., 2019). UAV photogrammetry, an image-based surveying method, combines UAV platforms with high-resolution digital cameras to produce accurate 3D reconstructions of structures and terrains. This technique leverages principles of digital photogrammetry, which involve extracting geometric information from overlapping images, a method now enhanced by computer vision algorithms for faster and more precise processing. The use of UAV photogrammetry is especially valuable for infrastructure monitoring, offering efficient and safe data collection for objects that are difficult to access, such as bridges and viaducts. Its flexibility in capturing large datasets with high spatial resolution (1–5

cm/pixel) has made it an indispensable tool for applications ranging from architectural restoration to structural health monitoring. For example, UAV photogrammetry has been used for the detailed 3D modeling of complex structures like the Basento Bridge in Potenza, Italy (Marmo F. et al., et al., 2019). This study demonstrated the method's ability to accurately replicate the bridge's unique double-curvature geometry, enabling precise comparisons between as-built conditions and original design plans. Additionally, UAV photogrammetry has proven effective in assessing deformation and structural stability. Studies have demonstrated its application in real-time monitoring, such as the Second Bosphorus Bridge in Istanbul, where a fixed camera system was used to detect deformations with millimeter-level accuracy (Avsar Ö. et al., 2014). These insights can inform preventive maintenance strategies, reduce repair costs, and extend the lifespan of critical infrastructure. Despite its advantages, UAV photogrammetry has limitations. The method's accuracy can vary depending on the use of Ground Control Points (GCPs) and onboard GNSS/INS systems, with centimeter-level accuracy achievable under optimal conditions. Environmental factors like lighting, weather, and complex terrain can also influence data quality, requiring careful planning for effective deployment. Furthermore, while UAV photogrammetry is generally cost-effective compared to traditional surveying methods, the need for high-quality equipment and post-processing software can pose initial investment challenges. In summary, UAV photogrammetry is a transformative technology for infrastructure assessment and monitoring. Its ability to capture detailed and accurate 3D models, combined with the safety and efficiency of remote operations, makes it an invaluable tool in modern geomatics.

UAVs equipped with LiDAR sensors represent a transformative technology for detailed and efficient data acquisition in various applications, including infrastructure inspection, environmental monitoring, and forestry studies (Pádua L et al., 2017; Manfreda S. et al. 2018; Outay F., 2020). UAV LiDAR combines the mobility and flexibility of drones with the precision

and efficiency of LiDAR technology, offering unparalleled advantages for capturing high-resolution 3D data in complex or hard-to-reach environments. LiDAR works by emitting laser pulses and measuring their return times to generate accurate 3D point clouds of surveyed areas. When integrated with UAVs, this technology overcomes many of the limitations associated with traditional terrestrial or manned aerial platforms. UAV LiDAR systems enable the acquisition of high-density point clouds with centimeter-level accuracy, even in challenging conditions such as low-light environments or areas with dense vegetation (Guan S., 2022). A key advantage of UAV LiDAR is its ability to conduct surveys safely and efficiently in inaccessible locations, minimizing risks to operators. These systems are particularly valuable for applications where manual data collection is impractical, such as inspecting bridges, viaducts, or other infrastructure in remote regions. For example, in forested environments, UAV LiDAR can capture fine details of internal forest structures, including understory vegetation and tree canopies, with high spatial and temporal resolution (Zhou et al., 2022). From an economic perspective, UAV LiDAR systems have become more accessible due to advancements in sensor technology and reductions in costs. Mid-range UAV LiDAR systems typically cost between €1,500 and €15,000, with sensors priced from €1,000 to €5,000. This affordability, combined with their ease of deployment and rapid data acquisition, makes UAV LiDAR an attractive solution for researchers and practitioners alike. Despite its numerous advantages, UAV LiDAR has limitations that warrant consideration. For instance, while the technology is less sensitive to weather conditions than UAV photogrammetry, it may still be affected by factors such as heavy rain or dense clouds. Additionally, georeferencing the collected data often requires GCPs or onboard GNSS/INS systems to ensure positional accuracy. Point density and the presence of multiple returns are critical factors influencing the quality of the data, especially in areas with dense ground cover, in recent studies (Shokirov S. et al., 2021; Heinaro E. et al., 2023).

In the context of infrastructure monitoring, UAV LiDAR has demonstrated its potential for detailed inspections and deformation monitoring. High-resolution 3D point clouds generated by UAV LiDAR enable accurate modeling and analysis of structural elements, aiding in the early detection of damage, assessing structural integrity, and supporting maintenance planning. These capabilities make UAV LiDAR an indispensable tool for modern engineering applications, particularly in ensuring the safety and longevity of critical infrastructure.

SLAM has emerged as a critical technology for environments where traditional georeferencing methods reliant on GNSS/INS face limitations, such as under dense canopies or in GNSS-denied areas. Originally developed for robotics, SLAM enables devices to localize themselves while constructing detailed maps of their surroundings in real time. This dual capability has made SLAM-based systems indispensable for applications requiring high precision in complex or obstructed environments, such as forestry, infrastructure inspection, and indoor mapping (Xu L. et al., 2019; Jung S. et al., 2020). SLAM technology relies on integrating data from various onboard sensors, such as LiDAR, cameras, or IMUs (Inertial Measurement Units), to estimate position and build 3D point clouds. Unlike GNSS/INS-assisted systems, SLAM leverages local features—such as tree trunks, ground planes, or walls—for positioning, making it a robust solution in areas with intermittent or no GNSS signals (Lin Y. et al., 2010 ; Gupta et al., 2022). A key strength of SLAM lies in its adaptability to various platforms, such as handheld devices, UAVs, and backpack systems. Recent advancements have enabled the development of feature-based SLAM frameworks tailored for specific applications. For instance, forest inventory applications can benefit from SLAM frameworks that integrate semantic features like tree trunks and ground surfaces directly into the mapping process (Fan Y. et al., 2018; Zhou T. et al. 2024). This not only improves the geometric accuracy of the resulting point clouds but also streamlines data acquisition by embedding feature extraction into the SLAM workflow. In practice, SLAM-enabled backpack systems have demonstrated

impressive performance in generating highly accurate point clouds (Trybala P. et al., 2023). Studies comparing SLAM-based backpack systems with UAV LiDAR or commercial GNSS/INS-based solutions have shown that SLAM can achieve intra-dataset alignment quality in the range of 2–4 cm and positional accuracy of approximately 10 cm (Zhao C. et al., 2023). These results highlight SLAM's potential for producing reliable, georeferenced data even in challenging environments. However, SLAM systems are not without limitations. While they excel in accessibility and flexibility, they place physical demands on the operator, particularly in backpack-based setups, and are less suitable for dangerous or inaccessible locations. The accuracy of SLAM-generated maps also depends heavily on the quality and density of the sensor data, with systems ranging in cost from €300 for basic research tools to over €60,000 for professional-grade devices. In the context of infrastructure monitoring, SLAM provides a portable and cost-effective alternative for collecting detailed spatial data (Daneshgaran F. et al. 2021; Feng C.Q. et al., 2023). By enabling seamless transitions between indoor and outdoor environments, SLAM systems are particularly suited for inspecting complex infrastructure, such as tunnels, bridges, and building interiors. These capabilities make SLAM an essential component of modern geomatic workflows, complementing other technologies like UAV and mobile mapping systems.

MMS represent a significant advancement in geomatics, enabling the collection of high-resolution spatial data across large areas with unparalleled efficiency. These systems integrate advanced sensors such as LiDAR, GNSS, and cameras onto mobile platforms, including vehicles, trolleys, or other wheel-based carriers. Wheel-based MMS is particularly suited for applications requiring rapid data acquisition over extensive and linear areas, such as road networks, agricultural fields, and linear infrastructure like railways and pipelines. Wheel-based MMS platforms combine LiDAR and GNSS with additional sensors to acquire highly accurate georeferenced point clouds. These systems excel in collecting detailed measurements ranging from millimeters to centimeters in precision, depending on the

chosen configuration. The versatility of wheel-based MMSs makes them invaluable tools across a variety of fields, offering precise data acquisition and efficient workflows. In agriculture, these systems have been instrumental in advancing crop monitoring and phenotyping. For instance, utilized a 2D LiDAR mounted on a wheel-based platform to measure crop characteristics such as height, canopy cover, and plant volume in cotton fields (Sun S. et al., 2018). The use of multi-temporal LiDAR data facilitated the monitoring of growth patterns throughout the growing season, enabling the analysis of different cultivars' traits. In wheat cultivation, recent study developed a wheel-based MMS combining LiDAR and spectral reflectance sensors to estimate canopy height. Using odometry for geolocation, this system processed LiDAR point clouds to analyze canopy characteristics, demonstrating its effectiveness for field-based crop monitoring (Pérez-Ruiz M. et al., 2020). Beyond agriculture, wheel-based MMSs have proven essential in infrastructure assessment (Aldosari M. et al., 2020, Rashdi R. et al., 2024). Systems equipped with integrated GNSS and LiDAR are widely adopted for surveying roads, railways, and urban environments. These platforms enable continuous and high-speed data acquisition, allowing for precise 3D mapping and condition monitoring, which are critical for maintenance and planning. The advantages of wheel-based MMS are evident. Their mobility allows for rapid and extensive data collection, making them ideal for large-scale and linear applications. Depending on the system configuration, sub-centimeter accuracy can be achieved, while automated data acquisition significantly reduces the labor-intensive nature of traditional surveying. However, challenges persist. The reliance on GNSS for accurate georeferencing makes these systems vulnerable in areas with signal interruptions, such as urban canyons or dense forests (Javanmardi M. et al., 2017; Secco P., 2022). Furthermore, their cost remains a limiting factor, with configurations often exceeding €50,000, depending on sensor quality, system performance, and operational requirements. Despite these challenges, wheel-based MMS platforms are transforming modern geomatics by delivering comprehensive spatial

datasets with remarkable accuracy and efficiency. Their scalability and adaptability make them indispensable for diverse applications, ranging from precision agriculture to infrastructure maintenance and environmental monitoring. By seamlessly integrating robust GNSS and LiDAR technologies, these systems ensure reliable data collection while optimizing survey time and cost (Elhashash M. et al. 2022). As they continue to merge speed with high spatial resolution, wheel-based MMS platforms remain at the forefront of remote sensing and geospatial analysis.

The advantages, limitations, data resolution, accuracy, and costs of wheel-based MMSs MMS, along with other geomatic surveying tools, are summarized in the comparative table 2.1 below. This table provides a concise yet comprehensive overview of their suitability for various applications, ensuring a balanced perspective on their strengths and challenges in infrastructure monitoring and spatial data acquisition.

Table 2.2.1: An overview of advantages and limitations of Geomatic Technologies.

Technique	Advantages	Limitations	Data Resolution & Accuracy	Costs
Total Station 	- Ideal for static surveys and small details. - Suitable for measurements in controlled environments - Versatile: Due to the combination of angular and linear measurements, it is useful for various surveying applications.	-Measurements are slow compared to automated methods such as LiDAR or UAV. -Requires direct visibility between the instrument and the target. - Not suitable for capturing changes in real time.	Distances on the order of 1-2 mm. Angles on the order of 0.1 mgon	Instrument cost: € 5,000÷18,000
GNSS satellite positioning systems 	- Lightweight and portable instrumentation suitable for different types of surveying. - Direct measurements in a three-dimensional georeferenced system. - GNSS receivers can operate anywhere on the globe as long as there is visibility of satellites.	- operation affected by physical obstacles (such as buildings, dense trees, and urban canyons that may block or reflect satellite signals) - measurement of discrete points - often used in joint mode with other geomatics technologies (for example, these receivers are adopted for position control of UAVs used for photogrammetric and lidar surveys).	measurements ranging from the order of mm to the order of cm	Receivers cost: € 2,000÷12,000
Laser scanner 	- Designed for high-precision static surveying - ability to acquire extremely detailed data with a very high spatial resolution.	- For very detailed surveys, it can be relatively slow compared to mobile or aerial systems. - Line of sight is required: it is not possible to acquire points hidden by obstacles, which requires strategic positioning or the use of several scanning stations. - The handling and processing of point clouds requires advanced software and hardware. - Glossy or transparent surfaces can create gaps or distortions in the data.	measurements in the order of mm	Cost of laser scanner sensors: €5,000÷40,000
UAV Photogrammetry 	- Carry out surveys in inaccessible locations with remote control capability, while ensuring the safety of operators - High-resolution 2D images, 3D models reconstructed - Low-cost equipement - Easy deployment and minimal survey time	- Survey GCPs necessary for georeferencing if no GNSS/INS on board - Difficulty in matching features in scenery such as forests, woodlands, etc. - Sensitive (clouds, rain, illumination)	- Spatial resolution (GSD): 1-5 cm/pixel (depends on altitude and sensor) - Accuracy depends on whether relative or absolute and with or without GCP/RTK - Centimeter-level: 0.02-0.05 m	- Cost of mid-range digital cameras: €500÷3,000 - UAV cost for mid-range aerial photogrammetry: €1,500÷15,000
UAV LiDAR 	- Carry out surveys in inaccessible locations with remote control capability, while ensuring the safety of operators - 3D point cloud with precise distance information - Low-cost equipement - Easy deployment and minimal survey time - works even in low-light conditions	- Survey GCPs necessary for georeferencing if no GNSS/INS on board - Difficulty in matching features in scenery such as forests, woodlands, etc. - Minor Sensitive (clouds, rain)	- million points per second - Accuracy depends on whether relative or absolute and with or without GCP/RTK - Centimeter-level: 0.02-0.10 m	- Cost of mid-range sensor: €1000÷5,000 - UAV cost for mid-range : €1,500÷25,000
SLAM (Simultaneous Localization and Mapping) 	- Portable or backpack systems using SLAM for positioning. - ideal for outdoor and indoor environments and customized (backpack) systems for specialized applications.	Physical demands on the operator, not suitable for dangerous and inaccessible places.	measurements ranging from the order of mm to the order of cm depends on the sensors	Devices range from €300 for basic research tools to over €60,000 for high-end professional systems.
MMS wheel-based 	- Systems on vehicles (wheel-based) with GNSS and LiDAR for large areas (e.g. roads, linear infrastructure) -Speed, high spatial coverage	- Requires a stable GNSS, - overall expensive system	measurements ranging from the order of mm to the order of cm depends on the sensors	specific price depends on the system configuration excluding the type of vehicle and depending on the types of sensors chosen, the cost is over €50,000 - €100,000 and more.

These tools form the foundation of the methodologies applied in the case studies presented in later chapters, offering versatile solutions for infrastructure maintenance and analysis.

2.3 Applications of LiDAR-Based MMS, SLAM, and UAV Photogrammetry in Infrastructure Maintenance

Building upon the discussion of conventional and contemporary survey methods, this section focuses on the advanced tools employed in the context of infrastructure and transportation corridor maintenance, prevention, and inspection. These technologies, which include LiDAR-based MMS, SLAM-equipped platforms, GNSS receivers, and UAV photogrammetry, represent state-of-the-art solutions for acquiring detailed and accurate data. By leveraging their unique capabilities, these tools enable efficient and comprehensive monitoring of complex environments, addressing both localized precision and large-scale coverage requirements. Therefore, this section provides an in-depth discussion of the specific tools and platforms used in this research, highlighting their technical specifications, benefits, and relevance to geomatics applications. The data utilized in this study were collected using two custom-designed wheel-based mobile mapping systems developed by the research team: the Purdue Wheel-Based Mobile Mapping System for High Accuracy (PWMMS-HA) and the Purdue Wheel-Based Mobile Mapping System for Ultra-High Accuracy (PWMMS-UHA), as depicted in Figure 2.1. The PWMMS-HA is equipped with four Velodyne LiDAR sensors (three HDL-32E and one VLP-16 High Resolution) (Velodyne, 2024a; Velodyne, 2024b), three cameras, and a GNSS/INS unit to enable direct georeferencing (Applanix, 2024). In contrast, the PWMMS-UHA incorporates two high-precision 2D profiler LiDAR sensors (a Riegl VUX-1HA and a Z+F Profiler 9012) (Riegl, 2023; Z+F, 2024) two cameras, and a georeferencing system (Novatel, 2023). Table 2.2 provides the

technical specifications of the onboard LiDAR and georeferencing components. Both systems underwent in-situ calibration to ensure optimal accuracy, following a standardized calibration procedure (Ravi R. et al., 2018). Post-calibration analysis, conducted using a LiDAR Error Propagation Calculator, estimated the point cloud accuracy for each system at a sensor-to-object distance of 30 meters (Habib A. et al. Accessed 2024). The results indicated a precision range of ±2–3 cm for the PWMMS-HA and ±1–2 cm for the PWMMS-UHA.



Figure 2.1: MMS LiDAR systems used in the study – PWMMS-HA (Top) and PWMMS-UHA (Bottom).

Table 2.2: Details of the georeferencing and LiDAR sensors, along with the anticipated accuracy of the point cloud generated by Mobile LiDAR Mapping Systems.

	PWMMS-HA	PWMMS-UHA
GNSS/INS sensors	Applanix POS LV 220	NovAtel ProPak6; IMU-ISA-100C
Sensor weight	2.40 + 2.50kg	1.79+5.00kg
Positional accuracy	±2–5cm	±1–2cm
Attitude accuracy (roll/pitch)	0.015°	- 0.003°
Attitude accuracy (heading)	0.025°	- 0.004
LiDAR sensors	Velodyne VLP-16High-Res Velodyne HDL-32E	Riegl VUX1HA Z+F Profiler 9012
Sensor weight	0.830kg 1.0kg	3.5kg 13.5kg
No. of channels	16 32	1 1
Pulse repetition rate	~300,000 point/s (singlereturn) ~695,000point/s (singlereturn)	Upto1,000,000 point/s Upto1,000,000 point/s
Maximum range	100m 100m	135m 119m
Range accuracy	±3cm ±2 cm	±5mm ±2 mm

For the subsequent case studies described in the following chapters, additional tools were employed, focusing on SLAM-based systems. Among these, the Leica BLK2GO, introduced in 2019, served as a portable mobile mapping device capable of capturing 420,000 points per second with a reported accuracy of 10 mm in indoor environments (Figure 2.2 and Table 2.3) (Leica BLK2GO Geosystems, 2024). This system incorporates advanced features, such as the BLK2GO Live app, which enables real-time visualization of mapped areas and identifies regions requiring further data collection. This capability enhances operational efficiency and minimizes the need for extensive mission planning. BLK2GO relies on a class 1 LiDAR system, which captures a 360° horizontal and 270° vertical field of view, with an effective range from 0.5 m to 25 m. The LiDAR operates at a wavelength of 830 nm and maintains a noise range of approximately 3 mm. Additionally, the system is equipped with three cameras, each offering a resolution of 4.8 megapixels. These cameras generate panoramic images covering 300° horizontally and 135° vertically, which are used to identify

image correspondences and calculate the device's movement within the scanned environment.

Leica's Grand SLAM Technology addresses limitations traditionally encountered in SLAM systems, such as difficulties in accurately linking data from various locations without visual references. By integrating LiDAR data and panoramic imagery, the BLK2GO achieves precise mapping and real-time positioning, advancing the effectiveness of SLAM-based surveying in both indoor and outdoor environments (Bailey T et al., 2006; Dlesk A., et al. 2022; Gharineiat Z. et al., 2024)

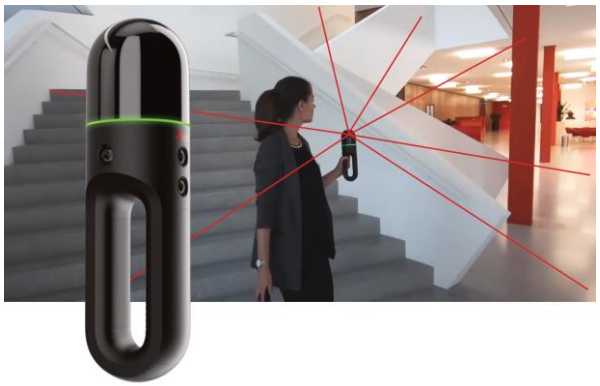


Figure 2.2:Leica BLK2GO used in the study.

Table 2.3: Technical characteristics of the Leica BLK2GO.

Range	0.5m+25m
Scan rate	420,000 pts/sec
Colour	yes
FOV	360° (horizontal)/270° (vertical)
Scan range noise	±3 mm
Relative accuracy	6-15mm

For the subsequent case studies outlined in this thesis, the GeoSLAM ZEB Horizon (figure 2.3 and table 2.4) scanner was employed for data acquisition (ZEB Horizon – GeoSLAM, 2024). This commercial, handheld mobile scanner is equipped with a compact VPL-16 LiDAR system and a MEMS-based inertial measurement unit (IMU), offering a robust and portable solution for diverse geomatic applications. The ZEB Horizon

supports a scanning range of up to 100 meters and collects approximately 300,000 points per second with an accuracy of 1–3 centimeters, making it suitable for both indoor and outdoor environments. It also features an optional accessory, the ZEB Cam, which integrates a Hawkeye Fire-246 fly 8SE action video camera. This enhancement allows for simultaneous image and point cloud data capture, providing contextual visual information alongside the 3D spatial dataset. Data acquisition with the ZEB Horizon is highly automated, relying on its internal SLAM (Simultaneous Localization and Mapping) algorithm. This algorithm processes raw laser data, aligning and co-registering it into a unified 3D point cloud. Additionally, the SLAM approach eliminates the need for external reference markers, streamlining the data collection process. The combined capabilities of the ZEB Horizon enable efficient, uninterrupted scanning, while the option to integrate imagery enhances its utility for applications requiring both spatial and contextual data (Gollob C. et al., 2020; Mikita T. et al., 2022; Di Stefano F. et al., 2023).



Figure 2.3: GeoSLAM ZEB Horizon used in the study.

Table 2.4: Technical characteristics of the GeoSLAM Zeb Horizon system.

Range	100m
Scan rate	300,000 pts/sec
Colour	yes
FOV	360° (horizontal)/270° (vertical)
Scan range noise	±30 mm
Relative accuracy	Up to 6mm

In the case studies presented in this thesis and detailed in the following chapters, precise georeferencing was supported by an RTK (Real-Time Kinematic) GNSS GS15 receiver, as shown in figure 2.4. (Leica Geosystems AG - Part of Hexagon, 2024). This system leveraged the Hexagon SmartNet network of permanent reference stations, enabling highly accurate positioning in real time (Chen Q. et al., 2018). The integration of this receiver ensured efficient, reliable, and non-invasive data acquisition, aligning with the objectives of the study to capture detailed spatial information with minimal disruption to the surveyed environment.



Figure 2.4: Leica GS15 GNSS Receiver used in the study.

To ensure rapid, safe, and non-destructive data acquisition, the study employed a DJI Matrice 200 UAV (DJI Matrice 200, 2024) equipped with a Zenmuse X5S gimbal and camera, as shown in figure 2.5 and table 2.5. This quadcopter platform provided an efficient solution for capturing high-resolution imagery and video data. The Zenmuse X5S camera, mounted on the UAV, offers video recording capabilities of up to 4096×2160 pixels at 30 frames per second, ensuring detailed and precise data collection (Zhang W. et al., 2020). This advanced setup was instrumental in meeting the study's objectives by delivering comprehensive aerial datasets while minimizing operational risks and time constraints.

Table 2.5: Technical characteristics of the UAV systems.



Model	DJI Matrice 200 V2
Tipology	Quadricopter
Weight at takeoff	734 g
Autonomy	27 min
Operating altitude	5000 m



Model	Zenmus e X5S
Focal lenght	15 mm
Photo size - Width	5280 px
Photo size - Height	3956 px
Sensor dimensions - Width	18 mm
Sensor dimensions - Height	13.5 mm
Weight	461 g

Figure 2.5: UAV systems used in the study – DJI Matrice 200 V2 (Top) and Zenmus e X5S (Bottom).

2.4 MORPHOLOGICAL AND LEARNING-BASED APPROACHES IN RISK DETECTION

The detection and assessment of risks in infrastructure demand a multidisciplinary approach, combining advanced geomatic techniques with computational methods. High-precision data acquired through LiDAR and UAV photogrammetry form the foundation for these analyses, enabling the identification of structural anomalies and other risks. This chapter provides an in-depth overview of methodologies, ranging from morphological enhancements to advanced machine learning (ML) and deep learning (DL) techniques (Samuel A., 1959; Dechter R., 1986). These approaches are designed to process and analyze complex datasets, often comprising millions of points or high-resolution imagery, with applications tailored to specific case studies. Depending on the scenario, methods are applied either directly to point clouds or to photogrammetric outputs, ensuring adaptability and robustness across diverse contexts. In recent years, global attention has increasingly focused on Artificial Intelligence (AI). AI, which first emerged in the late 1950s, began as an exploration of whether computers could simulate human thought. Over time, it has evolved into a multifaceted field encompassing various subdomains, among which ML and DL have become

central. These subfields have enabled AI to address intricate tasks, offering groundbreaking solutions in areas such as data processing, pattern recognition, and predictive modelling, as shown in Figure 2.6 (Skinner E.R., 2012).

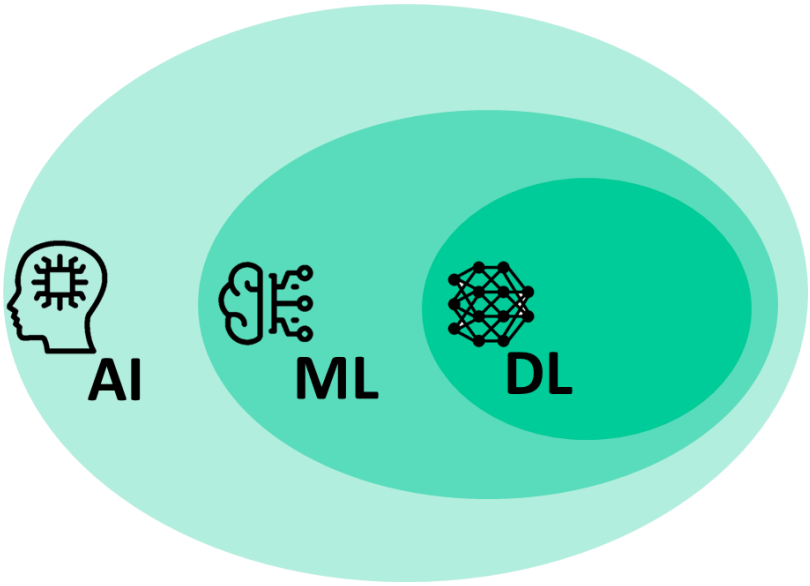


Figure 2.6: Illustrates the relationship between AI, ML, and DL, demonstrating how these disciplines interconnect while maintaining distinct roles. AI serves as the overarching domain, with ML and DL representing specialized subsets that focus on algorithmic learning and feature extraction, respectively.

By leveraging these advanced methodologies, this chapter explores how morphological and learning-based approaches enhance data quality, mitigate noise, and improve accuracy in risk detection processes. The synergy of traditional techniques and AI-driven methods provides a comprehensive framework for addressing modern challenges in data analysis and infrastructure monitoring (Khan M.W. et al., 2024). These approaches are tailored to process and analyze complex datasets, often characterized by millions of points or high-resolution imagery. Depending on the specific case study, the methods are applied either directly to point clouds or to photogrammetric outputs, ensuring flexibility and adaptability to different scenarios. The primary objective of these methodologies is to improve the quality of data, ensuring both accuracy and reliability in the detection of risks. These approaches address several key challenges. First, they tackle issues related to data noise and inconsistencies by employing filtering and

enhancement techniques that minimize errors arising during the data acquisition process. Additionally, advanced segmentation and classification algorithms play a crucial role in dividing the data into meaningful regions, facilitating more precise analysis. Lastly, the scalability of these methods, particularly those based on morphological and learning-based approaches, allows for the efficient handling of large and complex datasets, further enhancing their applicability to real-world scenarios.

To improve the quality of raw data and reduce noise and inconsistencies, specific pre-processing techniques were applied depending on the data source. For LiDAR data, intensity normalization was used to enhance the consistency of reflected intensity values, enabling more reliable downstream analysis. In contrast, advanced filtering techniques were employed for UAV photogrammetry data to minimize noise and enhance image quality. Although tailored to different types of data, both approaches share the common goal of ensuring cleaner and more accurate datasets for subsequent processing and analysis.

Segmentation and clustering techniques, including MCSS, OBIA, and DBSCAN, are instrumental in delineating regions of interest or detecting anomalies within the data. Furthermore, learning-based approaches, which encompass machine learning methods such as Random Forest and deep learning techniques like SPG, enable detailed classification and analysis. Each of these methodologies is tailored to meet the specific requirements of the datasets and objectives of the case studies examined. For instance, in the analysis of 3D point clouds, DBSCAN has been employed for clustering road cracks, while SPG, a deep learning technique, has been used to classify data and analyze signal occlusion caused by vegetation. Similarly, UAV photogrammetry outputs were analyzed using OBIA and filtering techniques to study cracks on the node of a concrete specimen subjected to compression and decompression cycles. These methods are replicable and adaptable for analyzing similar structural elements. The subsequent sections will elaborate on these methodologies, linking them directly to the case studies discussed in later chapters.

2.4.1 FILTERING TECHNIQUES FOR UAV PHOTOGRAMMETRY: ENHANCED LEE, FROST, AND MEDIAN FILTERS

Advanced filtering techniques are essential for reducing noise in photogrammetric data, thereby enhancing image quality and reliability for subsequent analysis. These techniques are particularly effective in highlighting critical features such as edges, which are fundamental for tasks like segmentation and classification. Convolution filters are often employed to adjust pixel brightness through weighted averaging of neighboring pixels, emphasizing structural boundaries and improving the accuracy of automated feature extraction.

Median Filter

The median filter is a spatial image processing method designed to enhance image uniformity while preserving edges larger than the kernel dimensions. It operates by replacing each pixel with the median value of its surrounding neighborhood, effectively removing speckling noise and mitigating the impact of outliers. Unlike mean filters, the median filter is less sensitive to extreme pixel values, making it particularly robust in maintaining structural details. This characteristic allows for efficient noise reduction without compromising the clarity of important features, such as linear discontinuities or edges (Huang T. et al., 1979; Rezaee A. et al. 2021) .

Enhanced Lee Filter

The Enhanced Lee filter is an adaptive technique developed to reduce speckle noise while preserving texture and detail in radar and other imaging data. It utilizes local statistics, specifically the coefficient of variation, within individual filter windows to classify pixels into three categories:

- Homogeneous Regions: Pixels in areas of uniform intensity are replaced with the mean of the filter window, effectively smoothing consistent regions and reducing noise.
- Heterogeneous Regions: In areas with varying intensity, a weighted averaging approach is applied to retain texture while minimizing noise.

- Point Targets: Pixels representing isolated features are preserved, ensuring that fine details remain intact.

This filter is particularly suited for applications requiring both noise suppression and the retention of structural texture, enabling accurate representation of complex surfaces (Lopes A., et al., 1990).

Enhanced Frost Filter

The Enhanced Frost filter is another adaptive filtering method designed to mitigate speckle noise while preserving the fidelity of texture in high-resolution data. Like the Enhanced Lee filter, it uses local statistics within filter windows to classify pixels into homogeneous, heterogeneous, and point target categories:

- Homogeneous Regions: Uniform areas are smoothed using a mean value, ensuring noise reduction in consistent regions.
- Heterogeneous Regions: For complex or textured areas, a convolution kernel is employed to calculate pixel values, maintaining intricate details without introducing artifacts.
- Point Targets: Isolated features are retained without modification to preserve critical details.

Both the Enhanced Lee and Frost filters are highly adaptable, making them valuable for improving data quality in scenarios where structural and textural integrity is paramount.

These filtering methods provide a robust foundation for subsequent segmentation and classification processes by ensuring that noise and inconsistencies are minimized while essential features are preserved (Lopes A., et al., 1990).

2.4.2 LiDAR Data Filtering Method Based on Cloth Simulation

Cloth Simulation (CS) has been widely employed as an effective technique for separating ground from non-ground features in LiDAR datasets. This method was particularly chosen for this study to isolate the road surface while distinguishing it from overlying structures such as bridges. Initially,

both automatic and semi-automatic recognition techniques were explored, but Cloth Simulation emerged as the most reliable and adaptable approach for this application. The Cloth Simulation Filtering (CSF) technique, introduced by Zhang W. et al. (2016) (figure 2.7), was implemented iteratively in this study.

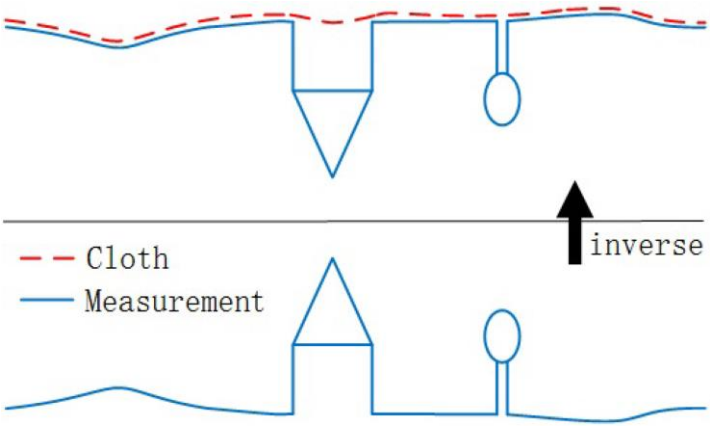


Figure 2.7:Overview of the cloth simulation algorithm (Zhang et al., 2016) illustrates the key steps of the process, including inversion of the point cloud, cloth initialization, and deformation, leading to the generation of the DTM

Various configurations of cloth rigidity, including uniform and adaptive rigidness, were applied to the point cloud to generate three distinct datasets (Figure 2.8):

- Bare Earth (BE): Points representing the ground surface.
- Digital Terrain Model (DTM): A smoothed representation of the ground surface.
- Above Ground (AG): Points corresponding to structures and vegetation above the ground.

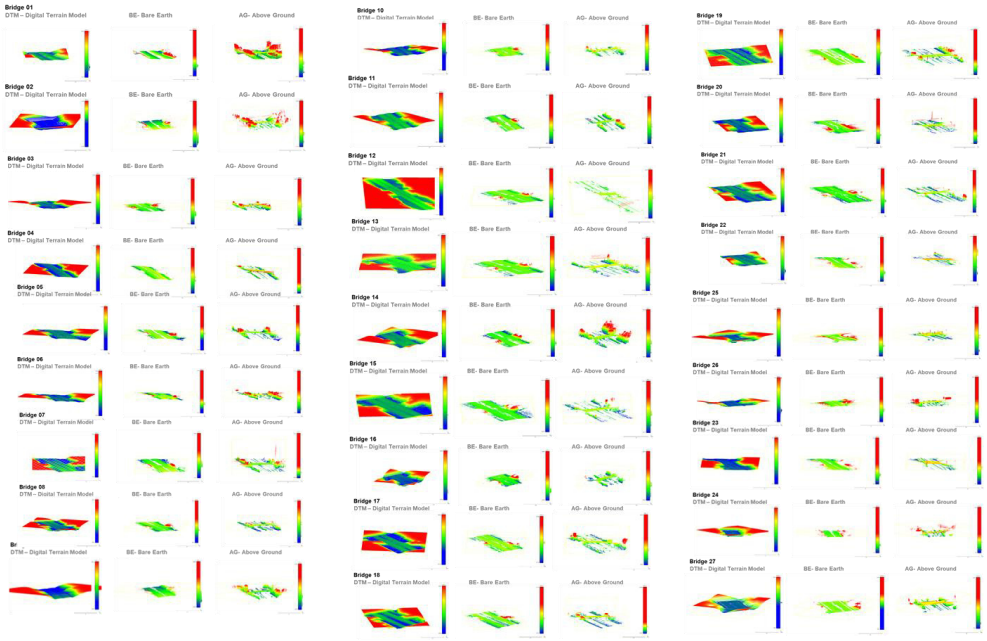


Figure 2.8: An example CS in a case of study.

In the CS method, originally proposed by Zhang et al. (2016), was implemented to extract a bare-earth point cloud from LiDAR data. This approach is conceptually straightforward and involves simulating a virtual cloth interacting with the terrain. The process begins by inverting the LiDAR point cloud, simulating an environment where a virtual cloth—composed of interconnected particles with defined rigidity—is positioned above the cloud. Under the influence of gravity, the cloth descends and deforms until it conforms to the underlying terrain. The final shape of the cloth represents the Digital Terrain Model (DTM), which is then used to separate ground points from above-ground features. An adaptive extension of this method, as introduced by Lin Y-C. et al., (2021), further refines the DTM generation by dynamically adjusting the rigidity of each particle based on the local point density. This adjustment enables the algorithm to produce reliable results even in areas with sparse bare-earth points. By modifying the cloth's rigidity according to point density, the adaptive approach ensures a high level of accuracy across diverse terrain conditions. Several modifications were necessary to tailor the cloth simulation method to LiDAR datasets. First, particle movement was constrained to vertical

displacements, simplifying collision detection with the terrain. Particles were classified as immovable once they reached the defined terrain height. The simulation proceeded iteratively until the maximum variation in particle height fell below a user-defined threshold or the maximum iteration count was reached. The overall process of applying cloth simulation to LiDAR data involves several key steps. Initially, outliers are removed using preprocessing tools such as CloudCompare. The LiDAR point cloud is then inverted, and a virtual grid representing the cloth is positioned above the highest point. Both the cloth particles and the LiDAR points are projected onto a common horizontal plane, with the nearest LiDAR point assigned to each particle. During the simulation, particles adjust iteratively based on their relative heights, and the cloth deforms until it stabilizes. Finally, distances between the cloth particles and the original LiDAR points are calculated to classify points as either bare earth or above-ground features. This method has proven to be highly effective in distinguishing ground points from non-ground points, providing a robust foundation for further analysis. By combining uniform and adaptive rigidity settings, the cloth simulation method ensures accurate differentiation between road surfaces and overlying structures, making it a critical tool for infrastructure monitoring and analysis. For this reason, this procedure was used to effectively separate ground points (BE) from non-ground points (AG), providing a solid foundation for subsequent analyses. By combining uniform and adaptive stiffness settings, the technique ensured accurate differentiation between road surfaces and overlying structures, a critical aspect for the case studies described in the following chapters.

2.4.3 LiDAR Data enhancement with Normalized Intensity

Intensity Normalization (IN) is a critical preprocessing step to improve the usability and consistency of LiDAR data (Parajuli A. et al., 2013; Teo T. A. et al., 2015; Yang B. et al., 2017; Holgado-Barco A et al., 2017). This process mitigates variability in raw intensity values caused by factors such

as scanning range, incidence angle, and surface reflectivity, thereby enhancing the quality of data analysis. Traditionally, intensity normalization has been extensively employed for applications such as lane marking detection (Cheng Y-T. et al., 2022). This research investigates its potential application in identifying pavement cracks, extending its use beyond conventional studies focused on asphalt and lane markings, as described by Cheng Y-T (2022). LiDAR intensity normalization is founded on the principle that observed intensity values should remain independent of external variables, such as the distance between the sensor and the target, the angle of incidence, or variations in beam properties. This standardization is particularly vital for ensuring data consistency across different systems and acquisition setups. The observed intensity, without normalization, is influenced by factors like range, reflectivity, and the angle at which the LiDAR beam interacts with the target surface. Normalization addresses these dependencies, enabling a more robust analysis of LiDAR data.

For multi-beam LiDAR systems, the normalized intensity I_{norm} is derived using mathematical corrections that account for these factors. The formulas presented here represent generalized approaches and may require further refinement and parameterization to address specific characteristics of different systems and datasets. This approach assumes that for a given surface or target, intensity values should exhibit consistency when corrected for beam-specific and system-level variations. In MMSs, intensity normalization typically involves two essential stages: intra-sensor correction and inter-sensor normalization. The intra-sensor correction focuses on removing dependencies on the scanning range. A polynomial function *f (r)* is fitted to intensity values corresponding to varying ranges within localized segments of the dataset, such as road sections spanning 50–100 meters. The corrected intensity I_{corr} is calculated as (Eq.2.1):

Equation 2.1

$$Icorr = \frac{Iobs}{f(r)}$$

Where I_{obs} represents the raw intensity, and *f (r)* is the fitted polynomial function for the given range *r*. Inter-sensor normalization, on the other hand, ensures consistency across multiple beams in a multi-beam LiDAR system. A look-up table (LUT) approach is frequently used to standardize the intensity values recorded by different beams. Each beam's unique properties are corrected to ensure that the normalized intensity is comparable across the entire system. For SLAM-based or backpack systems, where the LiDAR sensor operates at closer proximities to the target compared to MMS, normalization often incorporates the inverse-square law to correct for distance effects. The corrected intensity I*corr* can be expressed as (Eq. 2.2):

Equation 2.2

$$Icorr = Iobs\ x\ d^2$$

where *d* is the distance from the LiDAR sensor to the target. As with MMS systems, this formula is a general representation and may require adaptation to the specific dynamics of the SLAM or backpack LiDAR system in use. This correction ensures that intensity values are comparable across varying orientations and distances, which is particularly critical when mapping complex environments with these systems. In the context of this research, intensity normalization is applied through a specific MATLAB code, which processes the LiDAR data by first downsampling it into tiles to handle large datasets efficiently. These tiles, typically covering road segments of 50–100 meters, are then normalized using a polynomial function to remove scanning range dependencies. The code also ensures that intensity values across multiple LiDAR beams are consistent, facilitating reliable analysis of pavement cracks. The data are further processed and exported into LAS format for advanced analysis of pavement anomalies, including longitudinal and transverse cracks. Intensity normalization has found widespread application in enhancing lane marking detection on asphalt surfaces. Previous studies, such as those conducted by Cheng et al. (2022), demonstrated significant improvements in lane marking extraction when normalized intensity values were used, achieving F1-score enhancements of up to 86.2%. In the context of this research, intensity normalization is

applied to the detection of pavement cracks, including longitudinal and transverse fissures, using both MMS and SLAM systems. The findings presented in subsequent chapters will examine how intensity normalization contributes to data consistency and its potential applications across various domains. While intensity normalization has been shown to enhance lane marking extraction by reducing the influence of extrinsic factors, its role in detecting pavement anomalies and structural irregularities remains an area of interest. This process highlights the importance of careful calibration to address system-specific characteristics, allowing for broader analytical applications and contributing to a deeper understanding of LiDAR data utilization.

2.4.4 SEGMENTATION TECHNIQUES FOR RISK DETECTION: MCSS AND OBIA

Segmentation is a fundamental step in the risk detection process, as it enables the division of data into meaningful and analyzable regions. By isolating specific features or areas of interest, segmentation facilitates targeted analysis and enhances the accuracy of subsequent processing steps. This section discusses two prominent segmentation techniques: Object-Based Image Analysis (OBIA) and Multi-Class Simulations Segmentation (MCSS). Each method is suited to different data types and applications. OBIA, widely used in remote sensing, is particularly effective for high-resolution imagery and will be applied in this study to UAV photogrammetry datasets. Its capacity to integrate spectral, spatial, and contextual information makes it well-suited for detecting and characterizing surface irregularities such as cracks and other structural anomalies (Hay G.J., 2006; Blaschke T., 2010). On the other hand, MCSS, designed for point cloud data, is advantageous for mobile mapping systems (Habib A. et al., 2016). In this research, it will be utilized to address challenges such as sign occlusion and the segmentation of complex road features, providing a robust framework for interpreting LiDAR-derived data. Both approaches offer unique strengths and limitations, depending on the dataset and the

specific challenges encountered. Initial studies underscore their effectiveness in distinct domains, with OBIA excelling in applications requiring a detailed morphological understanding, and MCSS offering flexibility in handling 3D point cloud datasets. These methods form the basis for the case studies presented in subsequent chapters, where their practical implementation and results are analyzed in depth. OBIA is a two-step methodology that combines segmentation and classification to extract meaningful information from high-resolution spatial datasets, as illustrated in Figure 2.9.

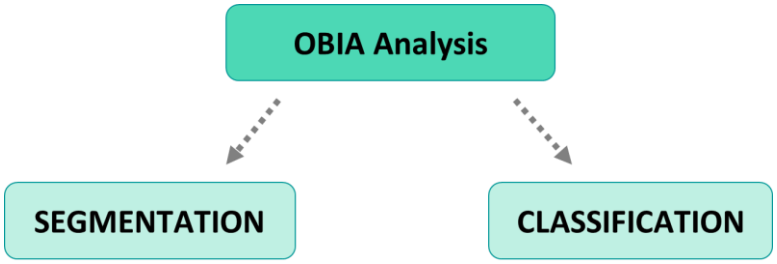


Figure 2.9: Illustrates the general workflow of OBIA.

During the segmentation phase, the dataset commonly an orthomosaic or high-resolution image is divided into discrete, coherent objects or segments. This process uses both spectral and spatial features, such as brightness, colour, texture, and topology, to group neighbouring pixels with similar characteristics. Unlike traditional pixel-based approaches, OBIA incorporates spatial information, including object dimensions, proximity relationships, and the number of pixels composing each segment, enhancing its ability to identify and delineate complex features. Following segmentation, the classification phase assigns semantic labels to the objects based on their extracted attributes. Supervised classification is a widely adopted approach, where an expert provides annotated training data to train the algorithm in recognizing specific classes, such as cracks, spalling areas, or undamaged surfaces. Advanced preprocessing techniques, such as contrast enhancement, edge detection, and noise reduction, are often applied to improve segmentation accuracy and ensure a robust classification process. OBIA offers several advantages over pixel-based approaches. By

reducing within-class spectral variability and incorporating spatial context, it produces more accurate thematic maps and detailed representations of surface conditions. For example, in the analysis of deteriorated infrastructure surfaces, OBIA has been shown to excel in distinguishing areas of damage, even in challenging scenarios such as mixed material compositions or shadowed regions (Zollini S. et al., 2020; Alicandro M. et al., 2023). However, certain challenges persist, particularly with large-scale datasets. The segmentation process can become computationally demanding, and the results are sometimes ambiguous when dealing with transitional or heterogeneous regions. Despite these limitations, OBIA is particularly effective in localized case studies where detailed analysis of specific areas, such as surface cracks or spalling on infrastructure, is required.

MCSS, on the other hand, is a geometric and morphological approach specifically designed for the segmentation of point cloud data. This technique excels in identifying geometric features, such as curvatures and discontinuities, and is particularly effective in applications related to infrastructure monitoring and risk detection. Its workflow integrates advanced mathematical and computational methods, ensuring precise segmentation and reliable results for subsequent analyses. The process begins with the structuring of the point cloud data using an octree, a hierarchical data structure that organizes points in three-dimensional space. This enables efficient data processing and supports the estimation of Local Point Density (LPD) or Local Point Spacing (LPS) within a user-defined neighborhood. The LPD or LPS values, estimated for a randomly selected subset of the point cloud, are extrapolated to represent the entire dataset (Habib et al., 2016). Following this, seed regions are generated by randomly selecting seed points across the dataset. These regions serve as the foundation for further classification, which is performed using Principal Component Analysis (PCA). PCA evaluates the local neighborhood of each seed region and classifies the points into three categories: planar, linear/cylindrical, and scattered.

The classification is based on eigenvalue analysis, where the eigenvalues (λ_1,λ_2,λ_3) are sorted in descending order ($\lambda_1 \geq \lambda_2 \geq \lambda_3$). Each point is evaluated to describe the local neighborhood by choosing the largest value in Equations 2.3 to 2.5 (Demantké J. et al., 2011).

Equation 2.3

Linearity: $$\frac{(\sqrt{\lambda_1}-\sqrt{\lambda_2})}{\sqrt{\lambda_1}}$$

Equation 2.4

Planarity: $$\frac{(\sqrt{\lambda_2}-\sqrt{\lambda_3})}{\sqrt{\lambda_1}}$$

Equation 2.5

Scattering: $$\frac{\sqrt{\lambda_3}}{\sqrt{\lambda_1}}$$

Once classified, a region-growing algorithm groups neighboring points that belong to the same feature type. For planar and pole-like features, this process is refined using Least Squares Adjustment (LSA) to fit geometric models, such as planes or cylinders, to the data. The quality of the model fitting is evaluated using the a-posteriori variance factor ($\hat{\sigma}^2$), which represents the normal distance between the points and the fitted model. Region-growing begins with the most accurate models, determined by the minimum a-posteriori variance factor, to ensure precision and reduce errors during segmentation. To further enhance the segmentation quality, outlier removal is performed iteratively during the region-growing process. Points that do not belong to any segment are reprocessed using a sequential region-growing approach. This ensures that even rough or irregular regions are classified effectively, as shown in Figure 2.10, which illustrates the segmentation results for planar, pole-like, and rough regions (depicted in green, red, and blue, respectively).

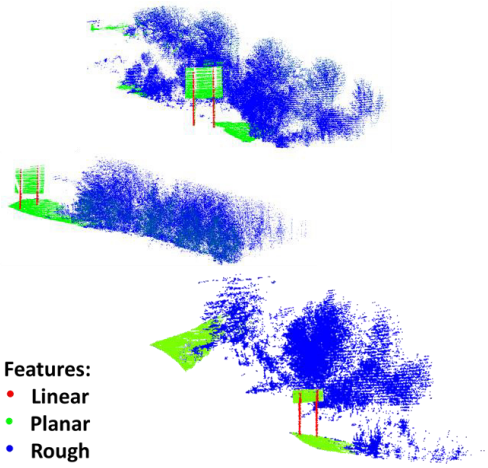


Figure 2.10: Illustration of MCSS dataset segmentation results, with planar regions depicted in green, pole-like regions in red, and rough regions in blue.

MCSS demonstrates significant advantages in identifying structural details across various scales, as will be shown in the case study on sign occlusion detection using mobile mapping systems. This application highlights the method's capability to accurately segment and classify complex geometric features critical for infrastructure monitoring. In summary, we will observe how both OBIA and MCSS demonstrate their potential in addressing the specific challenges of risk detection through their application in the case studies presented in the following chapters. These techniques provide valuable insights into segmentation's role in identifying critical regions for infrastructure assessment.

2.4.5 CLUSTERING-BASED APPROACHES: DBSCAN

The Density-Based Spatial Clustering of Applications with Noise (DBSCAN) is a clustering algorithm extensively applied in spatial data analysis. It is particularly advantageous for grouping data with arbitrary shapes and handling noise points without requiring a predetermined number of clusters (Ester M. et al., 1996). These attributes make DBSCAN an effective tool for analyzing datasets with varying densities and irregular geometries, such as those encountered in road infrastructure studies and crack detection (Taheri H. et al, 2022; Civera M. et al., 2023). DBSCAN is

recognized as a robust algorithm capable of clustering spatial data, with significant advantages over traditional techniques. Unlike k-means or hierarchical clustering, DBSCAN does not assume a predefined number of clusters, allowing it to adapt flexibly to the intrinsic structure of the data. Additionally, its ability to detect noise points is beneficial in scenarios involving noisy datasets, such as mobile mapping and pavement assessments. Previous studies have demonstrated the effectiveness of DBSCAN in clustering crack points and identifying surface anomalies in road infrastructure, leveraging its capability to discover clusters of arbitrary shapes and segment relevant data points (Shubert E. et al., 2017). In crack detection workflows, DBSCAN has been employed to group lane marking points into manageable segments, simplifying subsequent analysis. For instance, del Río-Barral et al. (2022) utilized DBSCAN on point cloud data generated by Mobile Laser Scanning (MLS) to identify pavement cracks. By applying intensity thresholding to detect candidate crack points, DBSCAN effectively clustered these points, providing a reliable methodology for crack analysis (del Río-Barral P. et al., 2023). For this reason, the refinement step starts with clustering crack regions using the DBSCAN algorithm. This algorithm requires two threshold values: a neighborhood distance threshold (ε) and a minimum number of neighboring points (*minPts*). The spread of a hypothesized cluster is defined by the maximum planimetric distance between two points in that cluster. All clusters with a spread less than a user-defined threshold (t_{Min_Length}) are eliminated. Selecting appropriate values for these parameters can be challenging and often requires an iterative process, as the optimal settings depend heavily on the characteristics of the dataset. Datasets with significantly varying densities may pose additional difficulties, as a single set of parameters may not perform consistently across the entire dataset (del Río-Barral P. et al., 2022). The workflow of DBSCAN applied in this case study is illustrated in Figure 2.11, which shows the various steps of the process, from data pre-processing to clustering and evaluation of results.

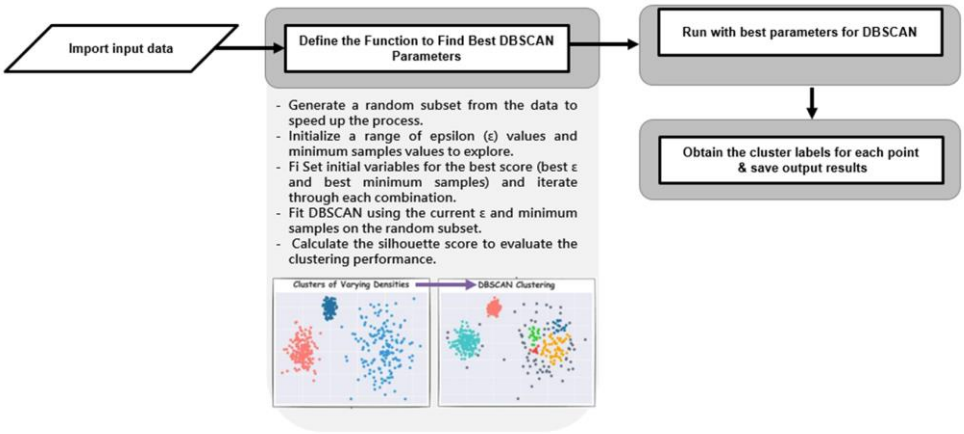


Figure 2.11: DBSCAN workflow for crack detection, including pre-processing, clustering, and evaluation of results.

In the subsequent chapters of this thesis, DBSCAN is applied to the road surface datasets, focusing on the extraction of cracks. The methodology involves identifying candidate crack points through intensity thresholding and employing DBSCAN to cluster these points. A comparison between the results of DBSCAN with and without normalized intensity is conducted against a ground truth dataset, evaluating the effectiveness of the algorithm using metrics such as true positives, recall, and precision.

2.4.6 Machine learning for risk classification: Random Forest

Random Forest (RF) is a widely used ensemble machine learning algorithm known for its effectiveness in classification and regression tasks. Introduced by Breiman L. (2001), RF constructs multiple decision trees during training using a bagging strategy, where random subsets of data and features are sampled for each tree (Figure 2.12). The final prediction is determined by a majority vote across all trees for classification tasks, while regression tasks are based on the mean prediction from individual trees. This approach enables RF to capture complex relationships within high-dimensional datasets, making it a powerful tool for handling non-linearities and datasets with numerous variables. One of the key strengths of RF is its ability to manage noisy, non-homogeneous data and its robustness in producing

accurate predictions even with imperfect or incomplete datasets (Ghose MK. et al., 2010). These features have made RF particularly popular in applications involving geomatic datasets, such as airborne, UAV, and terrestrial LiDAR data, where high-dimensional data and noisy measurements are common (Lopes Queiroz G. et al., 2019; Shokirov S. et al., 2021). In crack detection and risk classification workflows, RF has proven effective in differentiating between various crack types, such as longitudinal and transverse cracks, as well as intact road surfaces. The algorithm has been applied to dense point cloud data, such as those obtained from mobile mapping systems, where it has demonstrated its ability to handle large datasets efficiently. Grothum O. et al. (2023) highlighted RF's robustness when applied to such dense data, emphasizing its logarithmic time complexity, which facilitates processing large volumes of data quickly and accurately. Despite its many advantages, RF does have some limitations. Its performance is highly sensitive to the quality of the input data, including the accuracy of the ground truth. In particular, RF may face difficulties in detecting specific types of cracks, such as transverse cracks, due to the spacing between profile lines in point cloud data (Breiman L., 2001). Additionally, while RF is generally robust, it still requires careful tuning of parameters, such as the number of trees (N) and the number of features to consider for splitting at each node (m). The number of trees, for instance, is often recommended to be set at 500 to stabilize the model and reduce errors (Belgiu M. et al., 2016). Furthermore, although RF is designed to handle large and complex datasets, the quality of the data and ground truth can still impact its performance, and false positives can remain an issue, especially when expert assessments, such as those from road inspectors, are used for validation, potentially introducing subjectivity into the evaluation process. In the context of this thesis, RF is employed to classify risks associated with road surface cracks using point cloud data. The methodology involves training RF models on datasets with and without normalized intensity, followed by a comparison of the classification results against a ground truth dataset. The performance of the algorithm is assessed

using key metrics such as true positives, recall, and precision, which provide insight into the effectiveness of RF in accurately classifying points on road surfaces.

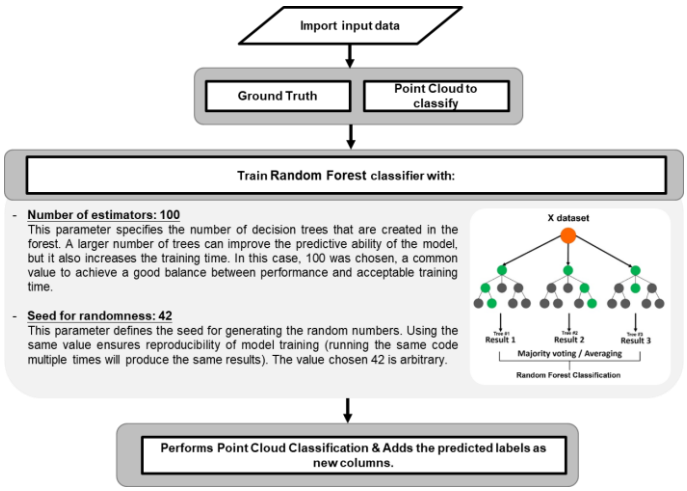


Figure 2.12: A representation of a decision tree in a Random Forest model. For the study described in next Chapter, 100 trees were used, with a random seed set to 42 to ensure reproducibility in the classification process.

2.4.7 DEEP LEARNING IN POINT CLOUD DATA ANALYSIS: SUPER POINT GRAPH (SPG)

The Super Point Graph (SPG) represents a state-of-the-art, learning-based approach for semantic segmentation of 3D point clouds. Originally proposed by Landrieu L. et al. (2018) and further refined by Lin Y. et al., (2022), SPG integrates geometric and contextual information to achieve high accuracy in classifying complex 3D data. This methodology is particularly effective in infrastructure related scenarios, as it combines computational efficiency with semantic precision. Assuming that semantic annotation is performed by categorizing the data into the following classes: (1) bridge deck, guardrails, and beams/girders; (2) bridge abutments and wing walls; (3) bridge piers; (4) man-made terrain; (5) natural terrain; (6) vegetation; (7) buildings; (8) scanning artifacts, such as moving vehicles and noise; and (9) other hardscape elements, including traffic signs, guardrails, and light poles. However, it should be noted that the testing datasets in this work do not include feature points from bridge components

or buildings. To enhance computational efficiency, a pruning process is applied. This involves voxelization, where the point cloud is divided into a grid, and each non-empty voxel is represented by a single point, resulting in a simplified yet representative dataset. The spatial structure of the point cloud is then modeled using an undirected graph, where nodes correspond to superpoints (clusters of points) and edges represent spatial relationships between these superpoints. The adjacency graph is constructed by identifying the k-nearest neighbors for each point using a KD-tree structure (figure 2.13).

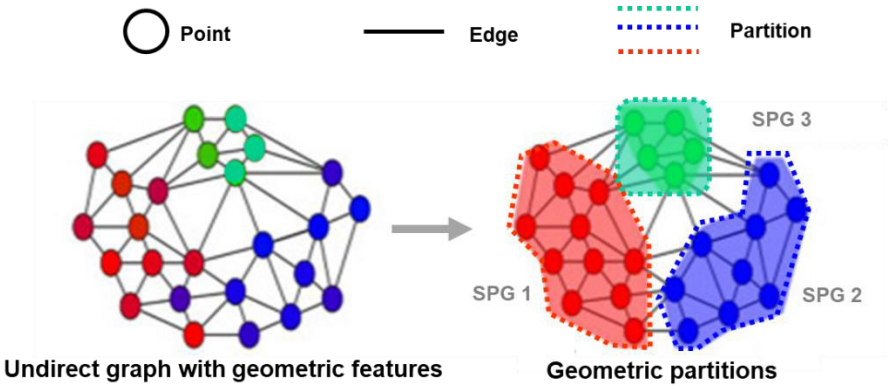


Figure 2.13: Illustration of geometric partitioning. On the left: an undirected graph representing the point cloud, with nodes color-coded based on geometric features. On the right: partitions displayed as piecewise constant approximations of these geometric features. SP1, SP2, and SP3 correspond to superpoint 1, superpoint 2, and superpoint 3, respectively.

This process determines the local neighborhood of each point and captures its spatial relationships. For each neighborhood, PCA is applied to derive geometric features, such as linearity, planarity, and sphericity, as described by specific mathematical equations (as mentioned in equation 2.3 to 2.5). Additionally, the verticality (equation 2.6) of the neighborhood is computed to assess the orientation of the local structure.

Equation 2.6

$$[\hat{u}]_i \propto \sum_{j=1}^{3} \lambda_j \left| [u_j]_i \right|, \text{ for } i = 1,\ 2,\ 3 \text{ and } \|\hat{u}\| = 1$$

The geometric properties of local neighborhoods are analyzed to segment the point cloud into distinct regions using the $l_{0\text{-cut}}$ pursuit algorithm

(Landrieu et al., 2017a; Landrieu et al., 2017b). Following this geometric segmentation, super points are defined to represent these geometrically uniform regions. To model the relationships between these super points, a Voronoi adjacency graph is constructed, capturing their spatial adjacency within the entire point cloud. Once the super point graph is established, descriptors for each super point are computed using PointNet (Qi et al., 2017), as show in figure 2.14.

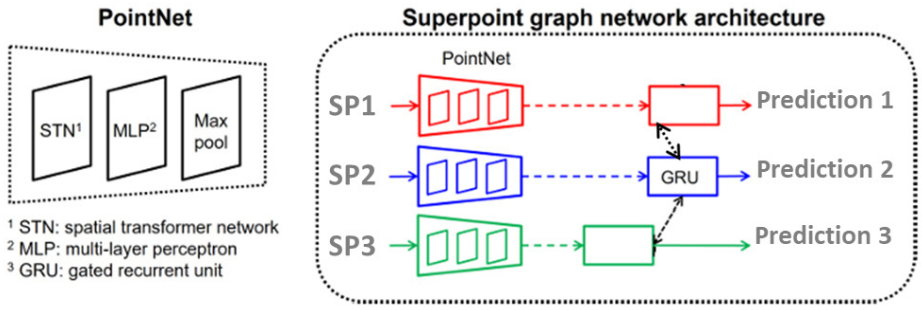


Figure 2.14: Schematic representation of the superpoint embedding and contextual segmentation process. The model structure includes a superpoint graph, where each superpoint is processed through PointNet to generate an embedding vector. These superpoint embeddings, along with the superedges, are then input into a graph network composed of a series of GRU layers for further processing.

This process incorporates handcrafted features, including: (1) geometric attributes such as linearity, planarity, scattering, and verticality, and (2) trajectory-based attributes such as the 2D distance to the trajectory and relative height to the ground. In the final phase, a graph convolutional approach is employed for contextual segmentation, enabling classification of each super point based on its embedding and its spatial context within the graph. Additionally, a quality control (QC) procedure, as proposed by Lin et al. (2022) for road infrastructure applications, is applied. This QC process uses trajectory data to refine predictions for man-made terrain and scanning artifacts. Any predictions with low confidence levels are flagged as "unclassified." The SPG framework demonstrates promise for achieving efficient and accurate semantic segmentation, especially in complex datasets involving bridge components and their surrounding environments. By prioritizing relevant information and disregarding less significant data, it

offers a compact representation. Its performance and suitability will be explored further in the sign occlusion case study .

2.5 APPLICATION OF METHODOLOGIES IN CASE STUDIES

The methodologies outlined in the previous sections were applied to four distinct case studies to evaluate their effectiveness in risk detection and their adaptability to different contexts. These case studies, conducted in the United States and Europe as shown in the figure 2.15, aimed to address specific challenges associated with infrastructure maintenance and inspection, leveraging both automatic and semi-automatic approaches. In Indiana, USA, the first case study focused on identifying signal occlusions caused by vegetation. This challenge was addressed using MCSS and SPG classification applied to point clouds generated by a wheel-based MMS. This approach aimed to explore how these classification methods could enhance the detection of occlusions and improve signal clarity. The second case study in Indiana examined crack detection on the road pavements of 27 bridges. Point cloud data collected via MMS was analysed using DBSCAN and RF clustering algorithms, with and without normalized intensity. This investigation sought to determine the role of intensity data in improving the detection accuracy of cracks on urban road surfaces. In Europe, specifically in Italy, the third case study focused on detecting cracks on a viaduct. The analysis relied on SLAM-derived point cloud data, processed with DBSCAN and Random Forest, to compare the effectiveness of SLAM for such applications. This comparison provided insights into the relative advantages and limitations of these technologies in infrastructure prevention. The fourth case study examined the cracking of a concrete specimen, using photogrammetry data acquired via UAV. Advanced filters and OBIA were employed to classify and analyse the data. This case study aimed to evaluate the effectiveness of OBIA in detecting concrete cracks compared to LiDAR-based techniques. These case studies collectively

aimed to experiment with automated and semi-automated reconnaissance methods, addressing both the research questions and objectives outlined in Chapter 1. In the following chapters, each case study will be examined in detail. The results will provide a deeper understanding of the potential and limitations of the methodologies applied for risk detection and inspection in infrastructure and transportation corridors.

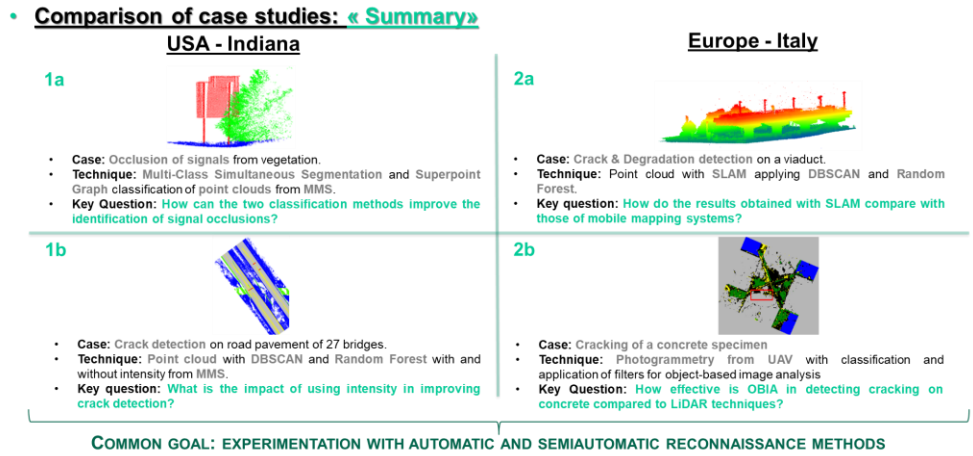


Figure 2.15: Summary of all approved case studies.

3. STATISTICAL METHODS FOR PERFORMANCE EVALUATION AND DATA ANALYSIS

Statistical methods form the backbone of modern data-driven research, providing robust frameworks for evaluating, comparing, and analyzing performance in various applications. In the field of geomatics, where the accuracy and reliability of spatial data directly influence decision-making processes, statistical techniques are indispensable to ensure the quality and consistency of results. (Smith L.I., 2002; Gomarasca M.A., 2009). Performance evaluation through statistical metrics allows researchers to validate algorithms, quantify classification outcomes, and assess the generalizability of predictive models (Steyerberg E. W.a et al., 2010; Ogundare J. O., 2018). Furthermore, these methods aid in identifying patterns, detecting anomalies, and drawing meaningful inferences from complex datasets, increasingly generated by advanced technologies such as LiDAR, UAV photogrammetry, and mobile mapping systems (Remondino F., 2011, Hassani S. et al. 2023). This chapter delves into the application of statistical methods in the context of geomatics, emphasizing their role in evaluating classification metrics, validating algorithms, and ensuring the reproducibility of results across case studies. By leveraging these techniques, geomaticians can enhance the precision of their analyses and foster innovation in applications related to infrastructure maintenance and transportation corridor assessments.

3.1 INTRODUCTION TO STATISTICAL METHODS IN GEOMATIC STUDIES

The field of geomatics has evolved significantly over recent decades, integrating advanced technologies such as UAV and terrestrial photogrammetry, LiDAR, SLAM, and MMS. This technological advancement has led to an unprecedented increase in the volume and complexity of spatial data, necessitating the application of rigorous statistical methods to ensure the accuracy, reliability, and interpretability of the results (Cressie N., 2015; Deibe D., 2020). Statistical methods in geomatic studies serve a dual purpose. First, they provide the means to evaluate the performance of algorithms and methodologies, ensuring their validity and robustness. This includes the assessment of classification accuracy, the detection of errors, and the identification of biases in predictive models (Di Stefano F. et al., 2021; Karasiak N. et al., 2022). Second, they enable data-driven insights by identifying spatial patterns, assessing correlations, and uncovering relationships within large and complex datasets (Li S. et al., 2016). To provide an overview of the international contributions to this field over the past decade, Figure 3.1 illustrates the number of research articles published globally, with a focus on studies integrating geomatic technologies and statistical methods. This highlights the significant role that statistical approaches play in advancing geomatic research.

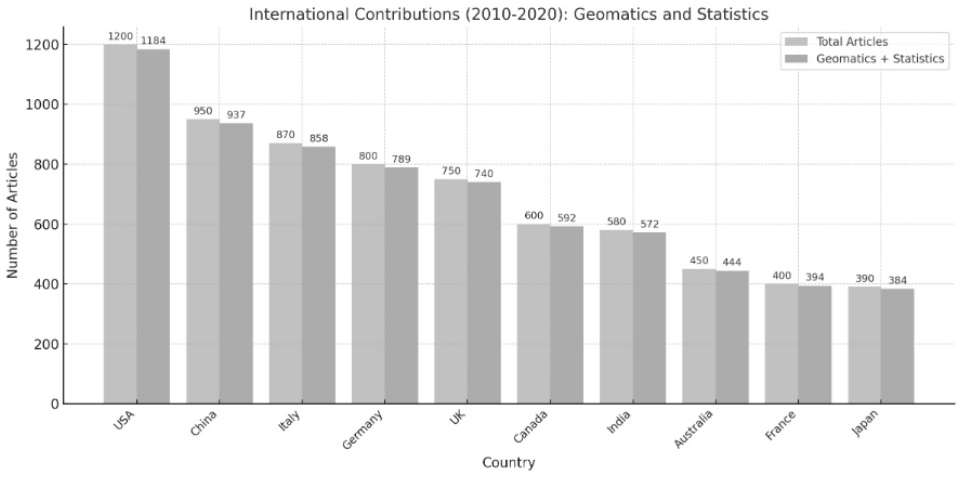


Figure 3.1: Published international contributions by country reporting Geomatics and Statistics (2010-2020).The data presented in Figure 3.1 were collected through a bibliometric analysis conducted manually using [Scopus/Web of Science/Google Scholar]. The search focused on research articles published between 2010 and 2020, using keywords such as geomatics, statistics, LiDAR, UAV photogrammetry, and machine learning applied to spatial data. To ensure the relevance of the results, only peer-reviewed journal articles were considered, while conference papers and non-peer-reviewed sources were excluded. The classification of articles was based on their explicit mention of statistical methodologies applied to geomatics.The final dataset consists of the number of publications per country, reflecting international contributions to the integration of statistical methods in geomatics research.

These capabilities are crucial in applications such as infrastructure monitoring, land-use analysis, and environmental management, where the quality of statistical analysis directly impacts decision-making processes (Kiker G.A. et al., 2005; Schwilch G. et al., 2011). Indeed, in the context of geomatics, statistical methods are often tailored to address specific challenges associated with spatial data, including its heterogeneity, autocorrelation, and scale-dependent characteristics. Techniques such as geostatistics, multivariate analysis, and machine learning have become integral to the discipline, offering tools to analyze and interpret spatial phenomena effectively (De Smith M. J. et al., 2007). The integration of statistical methods into geomatics not only enhances the precision and reliability of analyses but also fosters innovation in the design of novel algorithms and models. This chapter explores the key statistical techniques employed in geomatic studies, highlighting their applications in performance evaluation and classification accuracy.

3.2 EVALUATION METRICS FOR CLASSIFICATION PERFORMANCE

In geomatic studies, where classification tasks often involve large and heterogeneous datasets, evaluating the performance of algorithms is critical to achieving reliable and actionable results. Classification performance metrics provide quantitative tools to objectively measure the success of algorithms in identifying and categorizing data points into correct classes. These metrics are essential for comparing the effectiveness of different algorithms and for refining methodologies to optimize outcomes (Meng X. et al., 2010). The evaluation process typically relies on ground-truth data as a reference against which predictions are compared. The accuracy of a classification algorithm is not merely a measure of its overall correctness but also its ability to balance Precision, Recall (Sensitivity), and Overall Performance across different scenarios. Metrics such as True Positive (TP), False Positive (FP), False Negative (FN), Recall (Sensitivity), Precision, and the F1-Score are widely employed to capture the nuances of classification performance (Stehman S. V., 1997; Forman G., 2005; Powers D.M., 2008; Powers D.M., 2020). These measures provide insights into both the algorithm's sensitivity (ability to detect relevant instances) and specificity (ability to exclude irrelevant ones). Another important metric, the Jaccard Index, is particularly relevant in geomatics due to its capacity to quantify the similarity between predicted and actual classifications (Jaccard P., 1901; Jaccard P., 1912). This measure is often used in applications such as land cover mapping, infrastructure crack detection, and object-based analysis, where spatial overlap between predicted and actual categories is a key indicator of performance (Foody G. M. 2002; Sari I. L. et al., 2021; Alicandro M. et al., 2023; Pascucci N. et al., 2023; Zhao C et al., 2023; Pascucci N. et al. 2024; Shao J. et al., 2024). By using a combination of these metrics, a comprehensive understanding of the strengths and weaknesses of algorithms can be gained, enabling targeted improvements. The following subsections delve into the specific definitions, applications,

and interpretations of these metrics, highlighting their role in improving the reliability of geomatic analyses.

3.2.1 TRUE POSITIVE (TP), FALSE POSITIVE (FP), FALSE NEGATIVE (FN), RECALL AND PRECISION, F1-SCORE

As previously mentioned, in classification problems, especially within geomatics, the evaluation of algorithmic performance relies on fundamental metrics derived from a confusion matrix. These metrics - TP, FP, and FN - are critical for assessing the alignment between model predictions and the ground truth data, also referred to as reference data, were obtained through direct field measurements. The confusion matrix categorizes predictions into correct and incorrect classifications, serving as the foundation for higher-level evaluation metrics.

• *True Positives* (TP) represent instances that are correctly classified by the model as belonging to the positive class. In other words, these are cases where the predicted label aligns with the reference data for positive occurrences.

• *False Positives* (FP) refer to cases where the model incorrectly predicts an instance as belonging to the positive class, despite it being negative in the reference data. These errors can lead to overestimating the presence of a certain feature or phenomenon.

• *False Negatives* (FN) are instances where the model fails to classify a true positive correctly, mislabeling it as negative. This type of error can result in critical omissions of relevant features or events within the dataset.

From these foundational metrics, key measures such as Recall, Precision, and the F1-Score are derived:

- *Precision*, as shown in equation 3.1, evaluates the proportion of correctly identified positive instances among all instances predicted as positive. It is defined as the ratio of true positive observations to the total number of predicted positive observations.

Equation 3.1

Precision: $\frac{TP}{(TP+FP)}$

- *Recall (Sensitivity)*, as shown in equation 3.2, measures the proportion of actual positive instances in a dataset that are correctly identified by the model. It is defined as the ratio of true positive observations to the total number of positive instances in the dataset.

Equation 3.2

Recall: $\frac{TP}{(TP+FN)}$

- *F1-Score***,** as shown in equation 3.3, balances the trade-off between Recall and Precision. It is the harmonic mean of these two metrics, providing a single score that accounts for both false positives and false negatives. This makes it particularly useful in cases with imbalanced class distributions, where it is more informative than Accuracy.

Equation 3.3

F1-Score: $2 \times \frac{\text{Precision} \times \text{Recall}}{\text{Precision} + \text{Recall}}$

- *Overall Accuracy (OA)*, as given in equation 3.4, is a metric used to assess the overall performance of the classification. It is calculated as the ratio of TP observations to the total number of points in the dataset, multiplied by 100 to express the result as a percentage.

Equation 3.4

Overall Accuracy: $\frac{TP}{\text{Number of Points}} \times 100$

The discussed metrics provide a comprehensive framework for evaluating classification performance, particularly in high-dimensional and imbalanced datasets typical of geomatic applications. Their application ensures a systematic assessment of strengths and limitations, supporting the refinement of methodologies and their adaptation to practical scenarios. For example, in the context of infrastructure monitoring, balancing recall and precision is essential to minimize the risks of oversight while avoiding unnecessary interventions (Figueiredo E. et al., 2022). This approach enhances the reliability and efficiency of data-driven analyses in geomatics.

3.2.2 JACCARD INDEX

As stated earlier, the Jaccard Index, also known as the Jaccard Similarity Coefficient, is a widely recognized metric used to evaluate the similarity

and diversity between datasets, particularly in classification tasks. This index is defined as the ratio of the intersection to the union of two sets, making it particularly useful for assessing the overlap between predicted and actual classifications. Its mathematical formulation is expressed as eq. 3.5:

Equation 3.5

$$Jaccard\ Index = \frac{|A \cap B|}{|A \cup B|}$$

where A = GT's class
B = Predicted class for comparison

In this formulation, A represents the ground truth set, while B denotes the predicted set. The Jaccard Index is particularly useful for assessing the degree of overlap between predictions and the actual classifications in a dataset. In binary classification tasks, the Jaccard Index can be expressed in terms of the confusion matrix as follows in equation 3.6:

Equation 3.6

$$Jaccard\ Index = \frac{TP}{TP + FP + FN}$$

The Jaccard Index has been widely utilized in geomatics, particularly for spatial data analysis and segmentation tasks. It is frequently employed to evaluate the accuracy of classifications in applications such as land use mapping, feature extraction, and crack detection. By quantifying the agreement between predicted and actual datasets, the Jaccard Index provides a clear and interpretable metric that supports the validation and refinement of classification models (Kim Y.-M. et al. , 2012; Ouma Y.O. et al., 2017; Ray R. et al., 2023). This makes it an essential tool for ensuring the reliability and robustness of models in practical geomatic applications.

4. FIRST CASE STUDY: TRAFFIC SIGN VISIBILITY AND OCCLUSION IN THE USA

The following publication served as the source for the information in this chapter:

Pascucci, N., Shin, S.-Y., Hodaei, M., Dominici, D., and Habib, A.: COMPARATIVE ANALYSIS OF MORPHOLOGICAL (MCSS) AND LEARNING-BASED (SPG) STRATEGIES FOR DETECTING SIGNAGE OCCLUSIONS ALONG TRANSPORTATION CORRIDORS, Int. Arch. Photogramm. Remote Sens. Spatial Inf. Sci., XLVIII-1/W2-2023, 1651–1658, https://doi.org/10.5194/isprs-archives-XLVIII-1-W2-2023-1651-2023, 2023.

4.1 CHAPTER ABSTRACT

The visibility of signage along transportation corridors is a critical factor influencing road safety, traffic efficiency, and law enforcement. Ensuring that traffic signs are easily recognizable by both human drivers and autonomous vehicles is essential to prevent accidents and maintain safe driving conditions. In contemporary transportation studies, wheel-based MMS (as elaborated in Chapter 2) equipped with LiDAR technology have emerged as an effective tool for capturing detailed geospatial data. These systems allow for the scanning of road networks and their surrounding environments at standard driving speeds, offering a non-intrusive method to collect high-resolution 3D data. One of the key advantages of LiDAR-equipped MMS lies in its ability to detect and classify traffic signs, which

are characterized by distinct geometric features such as planar or linear structures. The 3D data acquired by MMS offers the precision needed to identify these features accurately, making it an invaluable resource for traffic sign recognition. Beyond sign detection, MMS LiDAR data facilitates the assessment of vegetation encroachment along the right-of-way, providing a comprehensive perspective on signage visibility. This capability is particularly relevant for evaluating potential obstructions caused by vegetation, which can compromise the visibility of critical traffic signs from a driver's viewpoint. This research presents an innovative framework leveraging MMS LiDAR data to detect traffic signs and vegetation, laying the groundwork for advanced signage visibility analysis. To achieve these objectives, two complementary methodologies are implemented:

- *Geometric/Morphological Approach*: This approach utilizes the Multi-Class Simultaneous Segmentation (MCSS) method (discussed in Chapter 2) to segment and classify LiDAR data based on geometric characteristics. This method is particularly effective in identifying well-defined shapes, such as those commonly associated with traffic signs.
- *Learning-Based Approach*: This study applies semantic segmentation techniques using the Super Point Graph (SPG) framework (explored in Chapter 2). This deep learning approach enables the classification of complex and diverse objects, enhancing the detection accuracy for both signage and vegetation.

The final stage of the framework focuses on signage visibility analysis. By calculating the occlusion rate of traffic signs from various driver viewpoints, the study evaluates the extent to which visibility is compromised under different scenarios.

4.2 INTRODUCTION

Recent research underscores the critical role of enhanced signage visibility in promoting driver awareness, reducing errors, and ensuring greater compliance with traffic regulations (Smith B.W., 2016; Oscar Oviedo-

Trespalacios O. et al., 2019). These findings reinforce the importance of adequate traffic sign visibility as a cornerstone of road infrastructure management and a key metric in safety assessments (Babić D. et al., 2022). Clear and recognizable signage not only supports human drivers by improving situational awareness but is also essential for the effective operation of autonomous vehicles, which rely on precise environmental cues to navigate safely. The growing demand for advanced tools in transportation infrastructure management has been met by the advent of Mobile Mapping Systems (MMS), equipped with cutting-edge LiDAR sensors. These systems have revolutionized the process of roadway analysis by enabling the rapid and efficient scanning of road networks and surrounding environments at standard driving speeds. One of the distinguishing features of MMS LiDAR technology is its ability to capture highly accurate 3D point cloud data, providing a rich source of information for infrastructure evaluation and maintenance. Traffic signs, characterized by their well-defined geometric properties, such as linear and planar features, are particularly well-suited for detection and analysis using MMS LiDAR data. This technology offers unparalleled precision in identifying these features, making it a reliable resource for evaluating both the presence and visibility of traffic signs within complex road environments (Zhang J. et al., 2019; Zhang S. et al., 2019; Hirt P.R. et al., 2022). Moreover, by leveraging this capability, transportation authorities can assess potential visibility obstructions and ensure that signs meet the required standards for effective communication with both human drivers and autonomous systems. As transportation networks continue to evolve, the integration of MMS LiDAR technology represents a significant advancement in road safety and infrastructure management. By combining speed, accuracy, and versatility, these systems provide a robust framework for identifying, analyzing, and improving signage visibility, thereby contributing to safer and more efficient roadway operations. In addition to its capacity for traffic sign detection, Mobile Mapping Systems (MMS) offer the capability to identify vegetation along road rights-of-way and evaluate its impact on signage visibility (Huang P. et al., 2017). Uncontrolled vegetation, as depicted in

Figure 4.1, can present significant safety hazards for a variety of reasons. Overgrown vegetation, including weeds, brush, and tree limbs, can obscure or obstruct a driver's view of critical elements such as the road ahead, traffic control devices, approaching vehicles, wildlife, pedestrians, bicycles, and other potential hazards (US Department of Transportation, 2008). These obstructions compromise both the safety and efficiency of roadways, making vegetation management a priority for infrastructure maintenance. Advancements in computer vision and machine learning techniques have revolutionized the analysis and improvement of signage visibility along transportation corridors. Semantic segmentation methods (Loce R. et al., 2013), combined with powerful deep learning algorithms (Abduljabbar R. et al., 2019), have significantly enhanced the ability to classify and analyze complex environments. These tools enable researchers and practitioners to assess visibility challenges more accurately and propose actionable solutions to mitigate the risks associated with vegetation-induced occlusion (Choi WC et al., 2022). Semantic segmentation has emerged as a critical tool in transportation corridor analysis. By classifying the various components of the road network into distinct object categories—such as road surfaces, traffic signs, vegetation, and barriers—these techniques facilitate a detailed understanding of the environment. This granular analysis provides invaluable insights for a range of applications, including road maintenance planning, support for autonomous driving systems, and comprehensive transportation safety evaluations (Balado J. et al., 2019).



Figure 4.1: Illustration of a road sign (red circle) obscured by vegetation along the highway.

The primary objective of this research is to leverage MMS LiDAR data for the detection of traffic signs and vegetation, establishing a critical foundation for conducting detailed signage visibility analysis. As depicted in Figure 4.2, the proposed methodology incorporates two distinct strategies: (1) a geometric/morphological approach and (2) a learning-based approach. These techniques enable a robust evaluation of how well different methods can identify and classify signage and vegetation points within transportation corridors. The first strategy focuses on a geometric/morphological approach, specifically employing Multi-Class Simultaneous Segmentation (MCSS) (Habib A. et al., 2016)(explored in Chapter 2). This technique is designed to segment components of transportation corridors based on their geometric features, such as planar surfaces and linear structures. By leveraging the inherent spatial characteristics of LiDAR data, MCSS provides a systematic method for isolating key elements within the road network, including traffic signs and vegetation. In contrast, the second strategy adopts a learning-based semantic segmentation method, utilizing the Super Point Graph (SPG) framework (Landrieu L. et al., 2018; Lin Y. et al., 2022) (discussed in Chapter 2). SPG is a state-of-the-art deep learning approach that excels in processing large-scale point cloud data by segmenting and classifying objects into semantically meaningful categories. This method provides greater flexibility in handling complex and heterogeneous environments, making it particularly valuable for analyzing diverse transportation settings. The comparative analysis of these two approaches forms a central focus of this study. By examining the effectiveness of geometric/morphological techniques alongside learning-based strategies, the research evaluates their respective capabilities in detecting signage and vegetation points. Furthermore, the performance of semantic segmentation is critically analyzed to determine its versatility in identifying a wide range of objects within the transportation environment. Ultimately, this study aims to provide a comprehensive assessment of the strengths and limitations of both morphological and learning-based methodologies. By doing so, it contributes to the development of more accurate and efficient tools for

infrastructure management, enhancing the understanding of object detection and classification in complex, real-world scenarios.

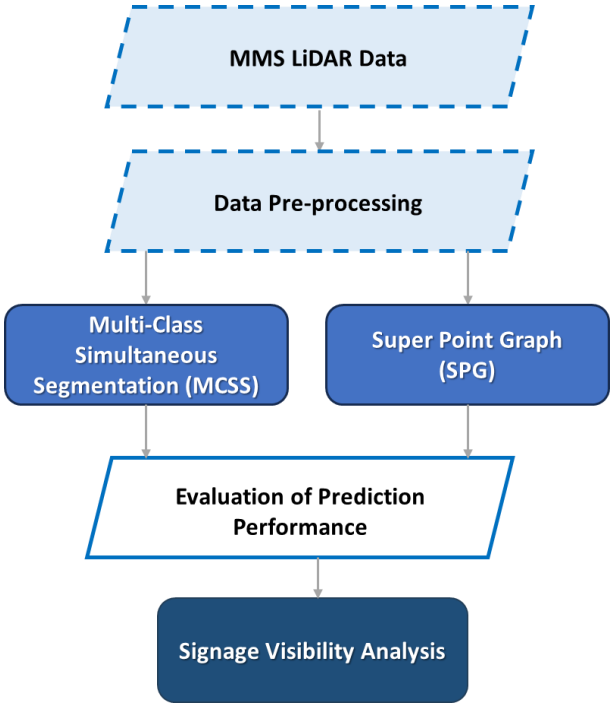


Figure 4.2: Proposed framework for comparative analysis of geometric/morphological and learning-based strategies for detecting signage occlusions.

4.3 Materials and Methods

In this study, four datasets were acquired along a highway using two wheel-based MMSs developed by the Digital Photogrammetry Research Group (DPRG) at Purdue University. The details of these systems, including their configurations and specifications, are thoroughly described in Chapter 2. Therefore, this section provides only a concise overview, supplemented with the relevant figures to contextualize the datasets.

4.3.1 Data Acquisition Systems

The MMS LiDAR datasets were collected using the Purdue Wheel-based Mobile Mapping System-High Accuracy (PWMMS-HA) and the Purdue Wheel-based Mobile Mapping System-Ultra High Accuracy (PWMMS-UHA). These systems are shown in Figure 4.3, which highlights the sensor configurations and technical components, illustrating the versatility and

accuracy of these systems, which enable the collection of high-quality LiDAR data for comprehensive highway analysis.

• PWMMS-HA: This system includes four LiDAR units (three Velodyne HDL-32E and one Velodyne VLP-16 High Resolution), three FLIR Grasshopper cameras, and an Applanix POS LV 220 unit for direct georeferencing. The system achieves a range accuracy of ±2 cm with the HDL-32E sensors and ±3 cm with the VLP-16 sensor. The GNSS/INS unit provides a positional accuracy of ±2 cm and an attitude accuracy of 0.020° for roll/pitch and 0.025° for heading.

• PWMMS-UHA: This system is equipped with two high-accuracy LiDAR units (Riegl VUX-1HA and Z+F Profiler 9012), two FLIR Flea2 FireWire cameras, and a NovAtel ProPak6 GNSS receiver. The range accuracy of the sensors is ±5 mm for the VUX-1HA and ±3 mm for the Profiler 9012, with the GNSS/INS unit achieving a positional accuracy of ±1–2 cm and an attitude accuracy of ±0.003° for roll/pitch and ±0.004° for heading.



Figure 4.3:MMS LiDAR systems used in the study – PWMMS-HA (Top) and PWMMS-UHA (Bottom).

4.3.2 I-65 HIGHWAY DATASETS

Four high-resolution LiDAR datasets were collected along the I-65 state highway located in West Lafayette, Indiana, USA. The data acquisition covered two distinct ROIs, as illustrated in Figure 4.4. These ROIs were strategically selected to represent varying environmental and seasonal conditions, ensuring a comprehensive analysis of traffic sign and vegetation detection under different scenarios.

- ROI 1: The first region was surveyed on February 23, 2021, during the leaf-off season. This period was chosen to minimize vegetation occlusion, providing clearer visibility of traffic signs and road infrastructure.
- ROI 2: The second region was surveyed on June 8, 2020, during the leaf-on season. This period captured dense vegetation coverage, offering a contrasting dataset for analyzing the impact of vegetation on signage visibility.

The combination of these datasets allows for a robust evaluation of the proposed methodologies under varying environmental contexts. Key parameters and acquisition details for these datasets are summarized in Table 4.1, provides a detailed overview of the datasets, including acquisition dates, environmental conditions, and key technical parameters.



Figure 4.4: Closer view of ROIs located along the I-65 state highway area (West Lafayette, Indiana, US).

Table 4.1: Description of the four datasets located in two different ROIs acquired by the Mobile Mapping Systems.

Platform	ROI ID	Collection Date	*Number of Points	Dimension
PWMMS-HA	ROI 1	February 23, 2021	1,341,784	58 m × 97 m
	ROI 2	June 8, 2020	3,805,240	56 m × 246 m
PWMMS-	ROI 1	February 23, 2021	663,275	58 m × 97 m

Platform	ROI ID	Collection Date	*Number of Points	Dimension
UHA	ROI 2	June 8, 2020	1,665,884	56 m × 246 m

*The number of points is after outlier removal and distance-based down-sampling of 5 cm.

4.3.3 SUMMARY OF METHODOLOGY

This section provides a summary of the methodology for signage visibility analysis using semantically segmented features derived from both geometric/morphological and learning-based approaches. The detailed theoretical and technical processes have already been described in Chapter 2. The analysis began with the preprocessing of MMS LiDAR data, which involved noise removal and a distance-based downsampling to a 5 cm resolution. These steps were implemented to enhance computational efficiency while maintaining the integrity of the data. For the segmentation process, two primary techniques were employed. The first was a geometric or morphological approach using MCSS. This method structured the point cloud using an octree framework and applied LPD and LPS metrics to classify features based on their geometric characteristics. Eigenvalues derived from a PCA were used to categorize regions as planar, linear, or scattered, followed by a region-growing process to group similar points. Additionally, LSA was used to refine the segmentation and ensure model-fitting accuracy. The second approach was based on machine learning, utilizing the SPG method for semantic segmentation. This technique began with voxelization to simplify the point cloud and create an adjacency graph using a k-nearest neighbors algorithm. Geometric features such as linearity, planarity, and verticality were extracted, while a graph convolution network classified each segment based on contextual relationships within the point cloud. This approach allowed for a detailed and structured analysis of the data. Semantic annotation was conducted using nine predefined classes, including features such as vegetation, traffic signs, scanning artifacts, and various structural components of the environment. To enhance the reliability of the results, a quality control refinement process was applied. This ensured

improved predictions for certain classes, such as man-made terrain, and flagged low-confidence predictions as “unclassified.”

4.4 EXPERIMENTAL RESULTS

This section provides a comprehensive overview of the experimental results obtained from the comparative evaluation of the MCSS and SPG methodologies. The analysis focuses on their respective performances in semantically segmenting and detecting specific features within the point cloud, particularly signage and vegetation points. By examining these two approaches, insights are gained into their capabilities, accuracy, and efficiency in processing complex datasets acquired through MMS. Following the segmentation analysis, a detailed examination of signage visibility is carried out for the two MMSs employed in this study: the Purdue Wheel-based Mobile Mapping System-High Accuracy (PWMMS-HA) and the Purdue Wheel-based Mobile Mapping System-Ultra High Accuracy (PWMMS-UHA). This visibility analysis aims to assess the effectiveness of these systems in capturing and representing signage features under varying conditions and configurations. The results presented in this section offer a critical comparison of the methodologies and systems, highlighting their respective strengths and limitations while providing valuable insights into their practical applications in road infrastructure analysis.

4.4.1 COMPARATIVE ANALYSIS OF MCSS AND SPG

This section presents a thorough comparative analysis of the prediction performance of the MCSS and SPG methods. For the SPG approach, the model was initially trained on datasets acquired from the PWMMS-UHA bridge surveys and later fine-tuned using datasets from the PWMMS-HA highway surveys, covering both driving directions. To establish a baseline for performance evaluation, reference data were generated through manual annotation of the point cloud. The evaluation process begins with a

qualitative assessment, where the predicted segmentation results are visually compared against the reference data. This assessment is conducted across the four distinct LiDAR datasets acquired in various ROIs by the PWMMS-HA and PWMMS-UHA systems. Subsequently, a quantitative analysis is performed to objectively measure the effectiveness of both methods. This analysis involves the computation of key performance metrics, derived using the reference data. These metrics are essential for evaluating the reliability and robustness of the segmentation approaches. The formulations for Precision, Recall, F1-Score, and Overall Accuracy were presented in Chapter 3. The integration of both qualitative and quantitative assessments provides a comprehensive framework for comparing the performance of MCSS and SPG in handling complex semantic segmentation tasks within LiDAR datasets.

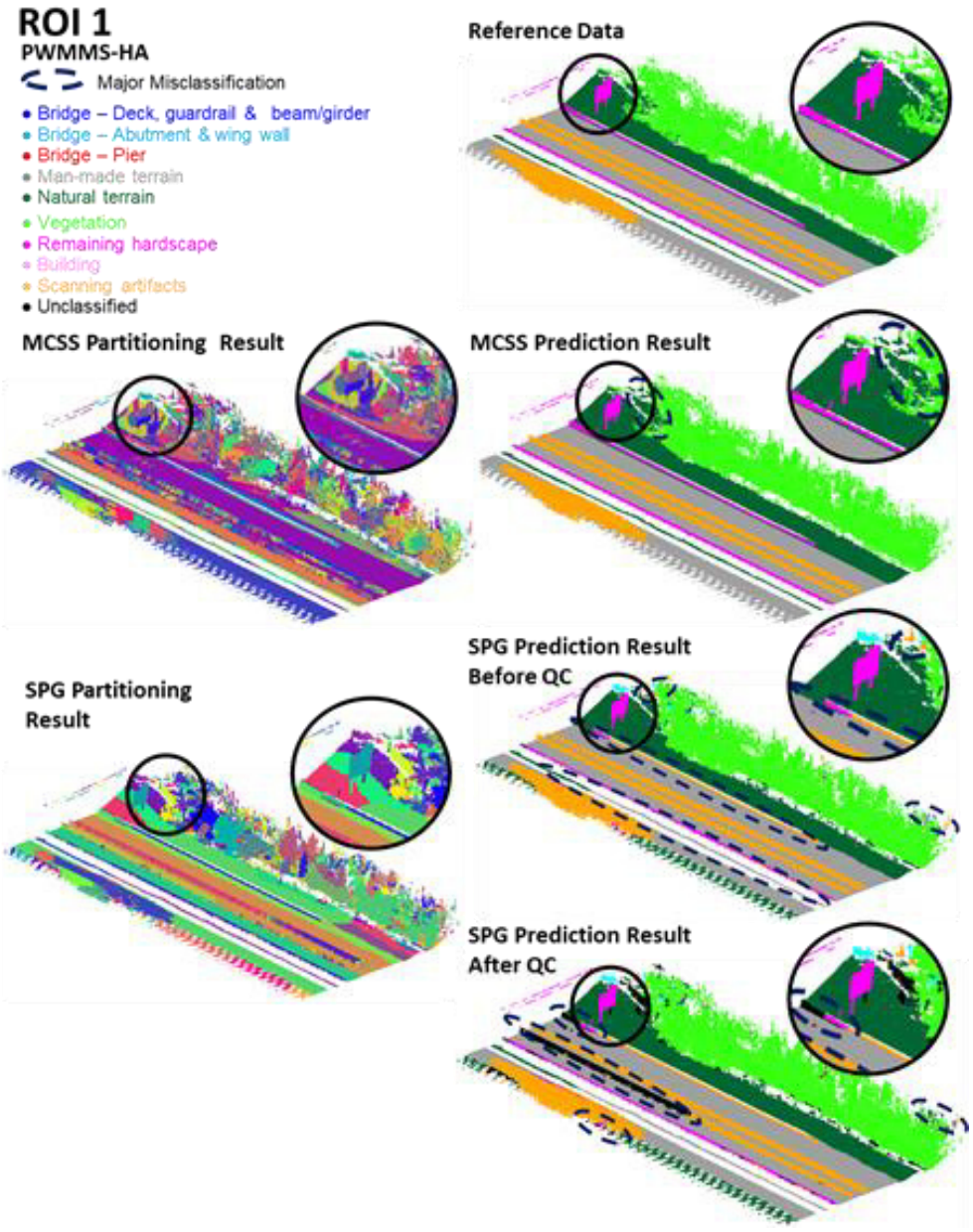


Figure 4.5: Comparison of partitioning results derived from MCSS and SPG (left). Evaluation of prediction performance for MCSS, SPG before QC, and SPG after QC (right) using reference data (top right), for ROI 1 from PWMMS-HA. Misclassifications are highlighted by black dashed circles.

Figure 4.5 presents the results of the qualitative evaluation for ROI 1 from the PWMMS-HA dataset. In the MCSS segmentation, several vegetation points were inaccurately classified as natural terrain. Similarly, in the SPG segmentation results prior to the QC process, vegetation points were misidentified as scanning artifacts, remaining hardscape, natural terrain, or bridge components. Additionally, certain points identified as remaining

hardscape were incorrectly classified as scanning artifacts or natural terrain. For natural terrain points, misclassifications included labeling them as man-made terrain or scanning artifacts. The quantitative assessment of ROI 1 for MCSS, as shown in Table 4.2, yielded an impressive overall accuracy of 99%. This suggests that the MCSS approach demonstrated a high degree of precision in correctly classifying point cloud data for this region. In contrast, the SPG approach exhibited a different performance trend. Tables 4.3 and 4.4 provide a comparative analysis of SPG's performance before and after applying QC. Prior to QC, the overall accuracy for SPG was recorded at 91%. After the application of QC procedures, the accuracy improved marginally to 92%. This indicates that although QC slightly enhanced the results, the overall impact on the SPG prediction accuracy was minimal.

Table 4.2: Quantitative evaluation of MCSS classification results for ROI 1 from the PWMMS-HA.

	TP	FP	FN	Precision	Recall	F1-score
Bridge – Deck	0.000	0.000	0.000	0.000	0.000	0.000
Bridge – Beam/girder	0.000	0.000	0.000	0.000	0.000	0.000
Bridge – Abutment & wing wall	0.000	0.000	0.000	0.000	0.000	0.000
Bridge – Pier	0.000	0.000	0.000	0.000	0.000	0.000
Man-made terrain	0.985	0.002	0.013	0.998	0.987	0.993
Natural terrain	0.941	0.045	0.013	0.954	0.986	0.970
Vegetation	0.982	0.005	0.013	0.994	0.987	0.991
Buildings	0.000	0.000	0.000	0.000	0.000	0.000
Remaining hardscape	0.942	0.041	0.016	0.958	0.983	0.970
Scanning artifacts	0.994	0.000	0.006	1.000	0.994	0.997
Overall accuracy	99%					

Table 4.3: Quantitative evaluation of SPG classification results before QC for ROI 1 from the PWMMS-HA.

	TP	FP	FN	Precision	Recall	F1-score
Bridge – Deck	0.000	1.000	0.000	0.000	0.000	0.000
Bridge – Beam/girder	0.000	0.000	0.000	0.000	0.000	0.000
Bridge – Abutment & wing wall	0.000	1.000	0.000	0.000	0.000	0.000
Bridge – Pier	0.000	1.000	0.000	0.000	0.000	0.000
Man-made terrain	0.841	0.122	0.037	0.874	0.958	0.914
Natural terrain	0.666	0.138	0.195	0.828	0.773	0.800
Vegetation	0.956	0.014	0.029	0.985	0.970	0.978
Buildings	0.000	0.000	0.000	0.000	0.000	0.000
Remaining hardscape	0.412	0.043	0.545	0.905	0.430	0.583
Scanning artifacts	0.861	0.119	0.020	0.878	0.977	0.925
Overall accuracy	91%					

Table 4.4: Quantitative evaluation of SPG classification results after QC for ROI 1 from the PWMMS-HA.

	TP	FP	FN	Precision	Recall	F1-score
Bridge – Deck	0.000	1.000	0.000	0.000	0.000	0.000
Bridge – Beam/girder	0.000	0.000	0.000	0.000	0.000	0.000
Bridge – Abutment & wing wall	0.000	1.000	0.000	0.000	0.000	0.000
Bridge – Pier	0.000	0.000	0.000	0.000	0.000	0.000
Man-made terrain	0.846	0.120	0.034	0.876	0.961	0.917
Natural terrain	0.679	0.123	0.198	0.847	0.774	0.809
Vegetation	0.962	0.013	0.024	0.987	0.975	0.981
Buildings	0.000	0.000	0.000	0.000	0.000	0.000
Remaining hardscape	0.428	0.040	0.533	0.915	0.445	0.599
Scanning artifacts	0.850	0.128	0.021	0.869	0.975	0.919
Overall accuracy	92%					

Figure 4.6 illustrates the qualitative evaluation for ROI 1 from the PWMMS-UHA dataset. In the MCSS segmentation results, several misclassifications were observed, notably where sections of natural terrain were incorrectly classified as vegetation, and vice versa. Similarly, the SPG segmentation results prior to the application of Quality Control (QC) revealed that natural terrain points were inaccurately labeled as scanning artifacts or man-made terrain. Additionally, points belonging to the remaining hardscape category were misclassified as scanning artifacts, natural terrain, or even bridge components. Following the QC process, several of these misclassifications were rectified, with the affected regions being reclassified as unclassified areas. Interestingly, after QC, a number of points that had previously been correctly classified were subsequently labeled as unclassified. Regarding the quantitative evaluation, the F1-Score for the remaining hardscape category, which includes traffic signage, was calculated at 86%. Table 4.5 shows that the MCSS approach achieved an overall accuracy of 98%, reflecting its high performance in classifying the point cloud data in ROI 1. On the other hand, the performance metrics for the SPG approach, before and after QC, are provided in Tables 4.6 and 4.7. For the remaining hardscape class, the F1-Score initially stood at 69%, but after QC, it experienced a slight decrease to 68%. Notably, there were no significant changes in the F1-Scores for man-made terrain, natural terrain, remaining hardscape, or scanning artifacts following the QC procedure.

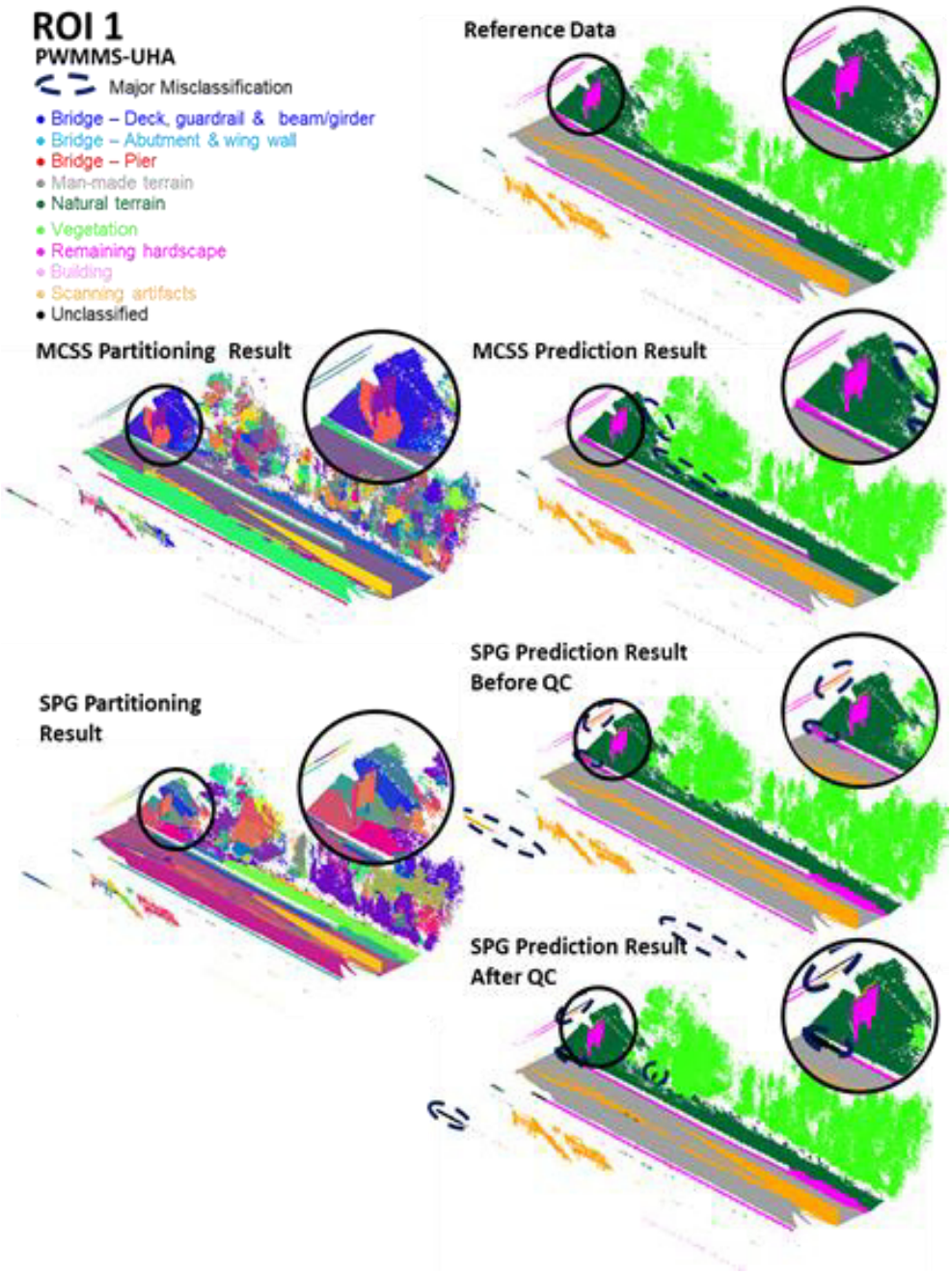


Figure 4.6: Comparison of partitioning results derived from MCSS and SPG (left). Evaluation of prediction performance for MCSS, SPG before QC, and SPG after QC (right) using reference data (top right), for ROI 1 from PWMMS-UHA. Misclassification is highlighted by black dashed circles.

Table 4.5: Quantitative evaluation of MCSS classification results for ROI 1 from the PWMMS-UHA.

	TP	FP	FN	Precision	Recall	F1-score
Bridge – Deck	0.000	0.000	0.000	0.000	0.000	0.000
Bridge – Beam/girder	0.000	0.000	0.000	0.000	0.000	0.000
Bridge – Abutment & wing wall	0.000	0.000	0.000	0.000	0.000	0.000
Bridge – Pier	0.000	0.000	0.000	0.000	0.000	0.000
Man-made terrain	0.978	0.000	0.021	0.999	0.979	0.989
Natural terrain	0.893	0.095	0.012	0.904	0.987	0.943
Vegetation	0.988	0.004	0.008	0.996	0.992	0.994
Buildings	0.000	0.000	0.000	0.000	0.000	0.000
Remaining hardscape	0.819	0.054	0.127	0.938	0.866	0.900
Scanning artifacts	0.996	0.000	0.003	0.999	0.997	0.998
Overall accuracy			98%			

Table 4.6: Quantitative evaluation of SPG classification results before QC for ROI 1 from the PWMMS-UHA.

	TP	FP	FN	Precision	Recall	F1-score
Bridge – Deck	0.000	1.000	0.000	0.000	0.000	0.000
Bridge – Beam/girder	0.000	0.000	0.000	0.000	0.000	0.000
Bridge – Abutment & wing wall	0.000	0.000	0.000	0.000	0.000	0.000
Bridge – Pier	0.000	1.000	0.000	0.000	0.000	0.000
Man-made terrain	0.942	0.037	0.020	0.962	0.979	0.970
Natural terrain	0.778	0.041	0.181	0.950	0.811	0.875
Vegetation	0.985	0.005	0.010	0.995	0.990	0.993
Buildings	0.000	0.000	0.000	0.000	0.000	0.000
Remaining hardscape	0.537	0.359	0.104	0.600	0.838	0.699
Scanning artifacts	0.913	0.074	0.013	0.925	0.985	0.954
Overall accuracy			96%			

Table 4.7: Quantitative evaluation of SPG classification results after QC for ROI 1 from the PWMMS-UHA.

	TP	FP	FN	Precision	Recall	F1-score
Bridge – Deck	0.000	1.000	0.000	0.000	0.000	0.000
Bridge – Beam/girder	0.000	0.000	0.000	0.000	0.000	0.000
Bridge – Abutment & wing wall	0.000	0.000	0.000	0.000	0.000	0.000
Bridge – Pier	0.000	0.000	0.000	0.000	0.000	0.000
Man-made terrain	0.943	0.036	0.021	0.963	0.978	0.971
Natural terrain	0.784	0.040	0.176	0.951	0.817	0.879
Vegetation	0.986	0.005	0.009	0.995	0.991	0.993
Buildings	0.000	0.000	0.000	0.000	0.000	0.000
Remaining hardscape	0.515	0.386	0.098	0.571	0.840	0.680
Scanning artifacts	0.929	0.060	0.012	0.940	0.988	0.963
Overall accuracy			96%			

A similar comparative analysis was performed for ROI 2, as depicted in Figure 4.7, which presents the qualitative evaluation for results obtained from the PWMMS-HA dataset. In the MCSS prediction output, certain vegetation points were incorrectly classified as natural terrain. Likewise, the SPG prediction results, prior to applying the QC process, displayed errors where scanning artifacts were misclassified as bridge components. Additionally, both vegetation and natural terrain points were reclassified as unclassified regions after QC. In terms of quantitative prediction performance, the MCSS approach achieved an overall accuracy of 90%. In contrast, the SPG approach exhibited a significantly lower overall accuracy

of 72%, with this result remaining consistent both before and after the application of QC. The qualitative analysis of the PWMMS-UHA dataset results is shown in Figure 4.8. In this case, the MCSS prediction output again displayed misclassifications, where some vegetation points were incorrectly identified as natural terrain. On the other hand, the SPG results before QC incorrectly labeled natural terrain points as scanning artifacts or man-made terrain. The same quantitative evaluation was applied to ROI 2 for the PWMMS-UHA dataset. The MCSS approach yielded an overall accuracy of 96%, reflecting a high level of precision in classifying the point cloud data. Meanwhile, the overall accuracy for the SPG approach after QC was 76%, showing a slight improvement from 74% before QC, indicating that the QC process had a minor but noticeable effect on enhancing the classification results. These results are shown in addendum A.

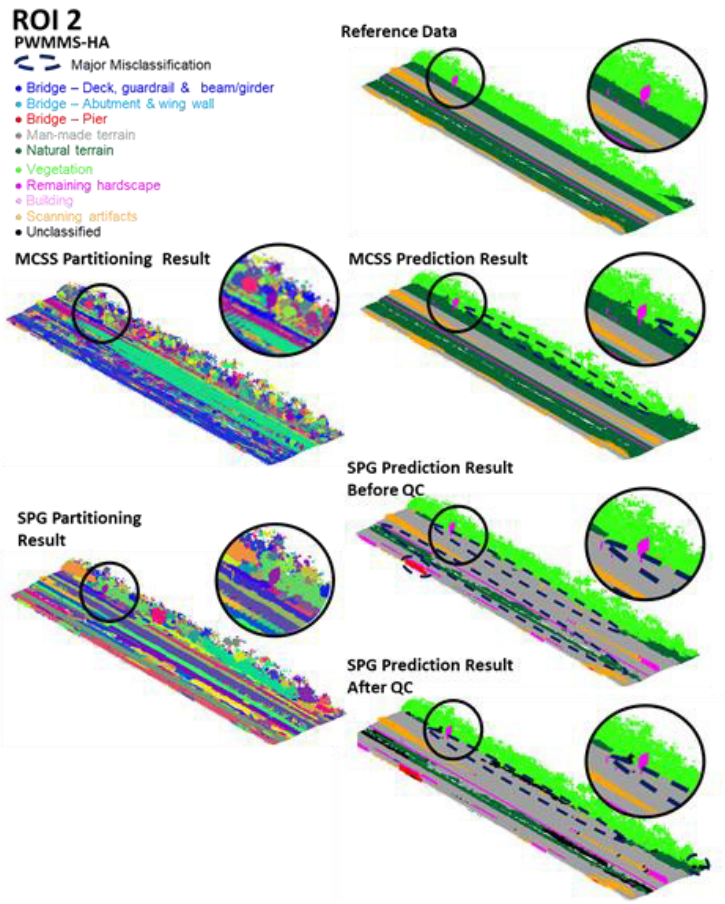


Figure 4.7: Comparison of partitioning results derived from MCSS and SPG (left). Evaluation of prediction performance for MCSS, SPG before QC, and SPG after QC (right) using reference data (top right), for ROI 2 from PWMMS-HA. Misclassification is highlighted by black dashed circles.

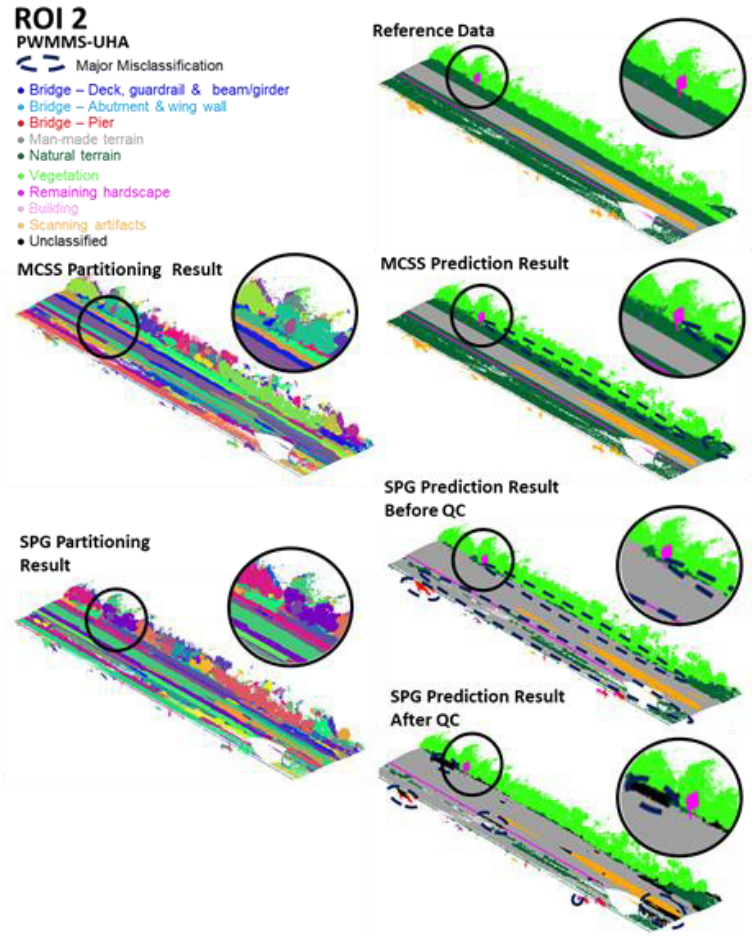


Figure 4.8: Comparison of partitioning results derived from MCSS and SPG (left). Evaluation of prediction performance for MCSS, SPG before QC, and SPG after QC (right) using reference data (top right), for ROI 2 from PWMMS-UHA. Misclassification is highlighted by black dashed circles.

4.5 Signage Visibility Analysis

In the signage visibility analysis, the occlusion rate is determined by constructing a pyramid, where the base of the pyramid is defined by the boundary points of the signage, and the trajectory point corresponds to the viewpoint of the driver (Figure 4.9 e 4.10).

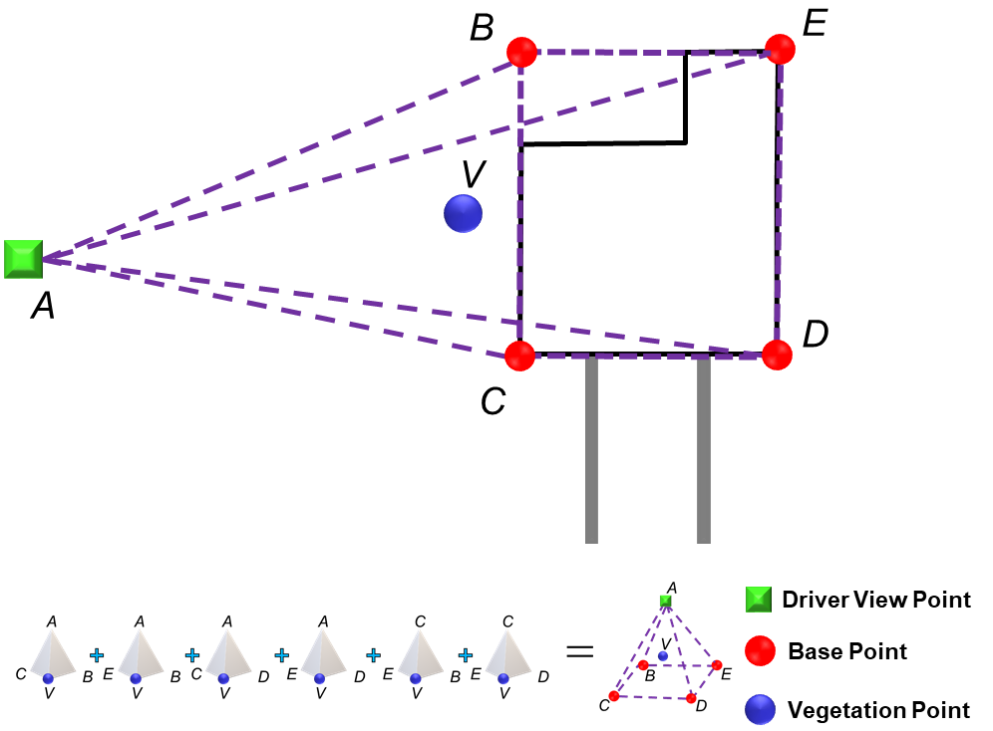


Figure 4.9: To determine whether the vegetation point is within the pyramid, the volume of the tetrahedron consisting of the pyramid ABCDE is used. If the vegetation point (V) is within the pyramid (ABCDE), the sum of six triangular volumes shall be the same. If not, that point is not considered to be an obscured point for signage.

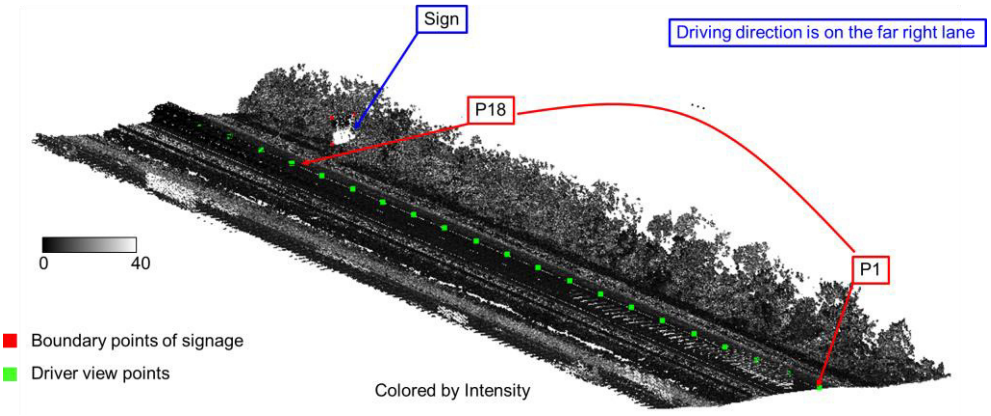


Figure 4.10: Example of wheel-based MMS LiDAR data visualized with intensity coloring, illustrating the impact of driver-to-sign distance on signage visibility.

In this context, vegetation points that intersect with the pyramid are considered as occluding elements. The computation of the occlusion rate, as detailed in Equation 4.1, begins by projecting these occluding points onto the surface of the sign. Subsequently, a 2D grid is overlaid within the boundary of the sign, with the grid's cell size being defined by the user. For this study, a cell size of 0.1 meters was chosen. The number of cells that are

occupied by occluding points is then tallied, and the occlusion rate is calculated by dividing the area of the occupied grid cells by the total bounding area of the sign, as shown in Equation 4.1. In this research, an occlusion rate below 10% is considered acceptable for maintaining clear visibility of the signage.

Equation 4.1

$$\text{Occlusion Rate} = \frac{\text{Area of Occupied Grid Cells}}{\text{Bounding Area of the Sign}}$$

In this research, the signage visibility analysis is performed based on ROI 2 , which was acquired during the leaf-on seasons, a period characterized by an increased likelihood of traffic signs being obscured by vegetation. A comparative analysis of the occlusion rates, considering the distance between the traffic sign and the driver's viewpoint, is conducted for both PWMMS-HA and PWMMS-UHA, as illustrated in Figure 4.11. The results indicate that for the PWMMS-HA dataset, the traffic sign becomes visible to the driver only within a distance of approximately 30 meters. Conversely, for the PWMMS-UHA dataset, the signage remains clearly visible up to a distance of 50 meters. The observed differences in the occlusion rates between the two systems are attributed to the distinct configurations of onboard LiDAR sensors and their respective scanning patterns. Specifically, the point cloud data from PWMMS-HA provides a more comprehensive representation of the vegetation, as shown in Figure 4.12, resulting in a higher and more accurate occlusion rate. According to the visibility standards outlined by the US Department of Transportation (2008), non-critical signs must be visible from a minimum distance of 91 meters for drivers traveling at a speed of 60 mph. Consequently, the results of the signage visibility analysis suggest that in the presented case, the vegetation obstructs the sign, thereby presenting potential safety risks for drivers.

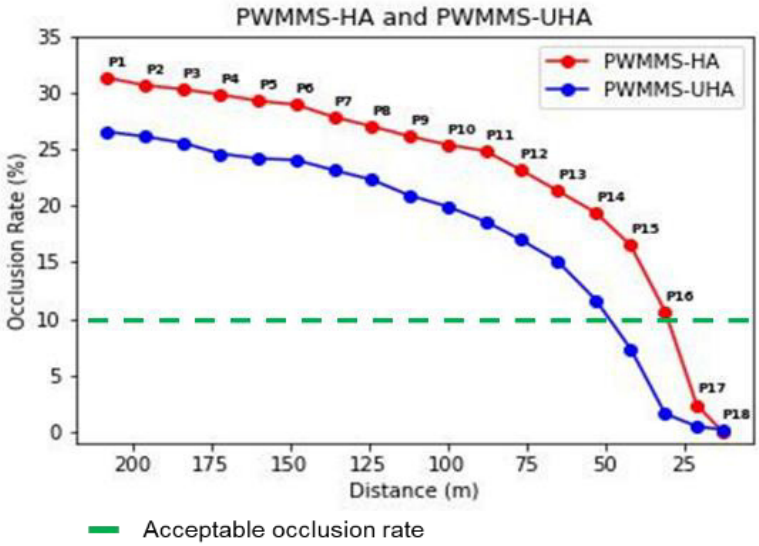


Figure 4.11: Comparison of occlusion rate based on the distance from the sign-to-driver's viewpoint for PWMMS-HA in red and PWMMS-UHA in blue.

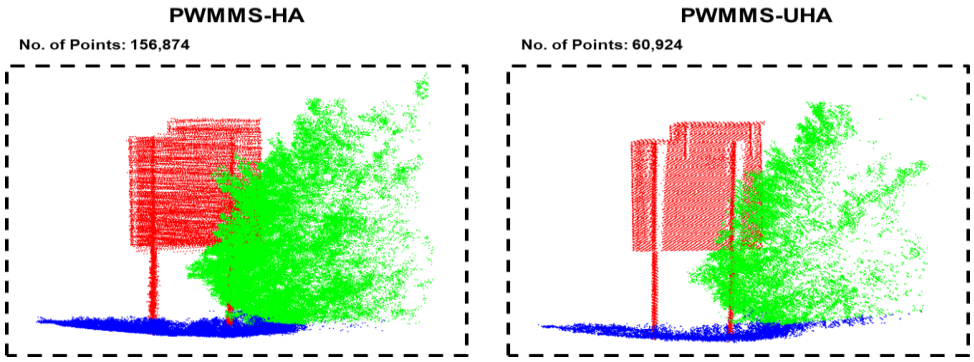


Figure 4.12: Figure 10. Comparison of LiDAR point clouds between PWMMS-HA and PWMMS-UHA for the sample traffic sign in ROI 2. The sign, vegetation points, and natural terrain are shown in red, green, and blue, respectively.

4.6 Conclusion and Future Studies

In terms of classification performance, the MCSS approach consistently outperformed the SPG technique across various datasets. However, it is important to highlight that the MCSS method relies on significant manual intervention during the classification process, which can limit its scalability. On the other hand, the SPG model, particularly before the QC process, demonstrated a limited capacity to accurately classify several categories, such as natural and man-made terrain. Moreover, the application of QC in the SPG method did not lead to a significant enhancement in classification

accuracy, indicating that the improvements from QC were minimal. Regarding the signage visibility analysis, distinct occlusion rates were observed for traffic signs, with notable differences between the two mobile mapping systems. In particular, the PWMMS-HA system produced a more reliable and comprehensive occlusion rate, thanks to its ability to capture a denser and more complete point cloud, facilitating a more accurate signage visibility assessment. In contrast, the PWMMS-UHA system showed relatively higher occlusion rates, although these results were not as robust due to the differences in point cloud density. Looking forward, future research will aim to enhance the accuracy of the deep learning-based segmentation approaches, with a particular focus on refining the QC process. Additionally, there will be efforts to improve the geometric partitioning in SPG by integrating MCSS's geometric segmentation into SPG's superpoint approach, which is expected to contribute to more precise segmentation outcomes. Another potential avenue for further investigation, as anticipated, is to explore the role of SPG in evaluating signage visibility, particularly in identifying areas where vegetation might obstruct traffic signs, thereby posing a potential hazard to driver safety.

5. SECOND CASE STUDY: DETECTION OF ROAD SURFACE CRACKS IN THE USA

5.1 CHAPTER ABSTRACT

This doctoral research focuses on the advanced analysis of road surface conditions using LiDAR datasets acquired with MMS. In the second U.S.-based case study, over 20 datasets were collected along a highway section using the Purdue Wheel-based Mobile Mapping System-Ultra High Accuracy (PWMMS-UHA), developed by the Digital Photogrammetry Research Group (DPRG) at Purdue University. The data, acquired on February 23, 2021, along Interstate I-65 in West Lafayette, Indiana, followed the guidelines of the Indiana Department of Transportation (INDOT). Preprocessing steps included noise removal and distance-based reduction to 2 cm resolution. Ground and non-ground separation was performed using the Cloth Simulation technique, generating Bare Earth (BE), Digital Terrain Model (DTM), and Above Ground (AG) point clouds. The BE layer was further optimized for intensity and color to enhance the detection of road cracks. A clustering-based approach, specifically the DBSCAN algorithm, was applied to identify cracks. Parameter optimization involved iterative tuning of epsilon (ε) and minimum sample size, with cluster performance assessed via the silhouette score. The clustering results were compared against manually labeled ground truth data, and metrics such as True Positives (TP), False Positives (FP), False Negatives (FN),

Precision, Recall, F1-Score, and Jaccard Index were calculated. Random Forest classification was also employed for comparison. Results highlighted that intensity normalization significantly impacted DBSCAN's performance, reducing its Jaccard Index for longitudinal and transverse cracks to 0%. In contrast, Random Forest demonstrated superior robustness, achieving Jaccard indices of 94% and 88% for longitudinal and transverse cracks, respectively, with minimal impact from normalization. Quantitative thresholds for intervention were established based on crack surface area, referencing standards from the Pavement Condition Index (PCI) and the Federal Highway Administration (FHWA). This study underscores the potential of integrating clustering and machine learning techniques for the automated assessment of road infrastructure, providing actionable insights for maintenance prioritization and planning.

5.2 INTRODUCTION

The deterioration of road infrastructure poses a significant challenge to transportation networks globally. Road cracks, which are among the earliest indicators of infrastructure degradation, jeopardize road safety, reduce driving comfort, and escalate maintenance costs if not addressed promptly (Schnebele E. et al.,2015; Merritt D.K. et al., 2015). The detection and assessment of road surface cracks have therefore become critical for transportation agencies, emphasizing the need for efficient and accurate methodologies to monitor and maintain road conditions (Ravi R. et al., 2020). While the importance of this issue is acknowledged universally, countries employ distinct approaches based on their unique infrastructural and climatic challenges. In the United States, state-level agencies such as the Indiana Department of Transportation (INDOT) face the demanding task of maintaining extensive transportation corridors. For instance, the Interstate I-65, connecting Lafayette and Indianapolis, endures significant wear and tear due to heavy vehicular traffic, requiring frequent maintenance. A primary contributor to road deterioration in regions like Indiana is the freeze-thaw cycle, where water infiltrates asphalt cracks, freezes, and

expands, exacerbating structural damage. This issue is further intensified by climate change, which introduces more extreme weather patterns and increases the frequency and severity of freeze-thaw events (Nakata T. et al., 2021; Cao H. et al., 2022, Zhang Y. et al., 2023). The advent of advanced geospatial technologies has revolutionized the field of infrastructure monitoring. Among these, Mobile Mapping Systems (MMS) equipped with LiDAR sensors and high-resolution imaging devices stand out as transformative tools (Zhou Y. et al., 2022). MMS enables the acquisition of high-precision 3D point cloud data at normal driving speeds, significantly reducing the time and labor traditionally required for manual inspections (Mei A. et al., 2022). These systems facilitate comprehensive road corridor analyses, from crack detection to the mapping of road features, signage, and vegetation. The use of machine learning algorithms, such as Density-Based Spatial Clustering of Applications with Noise (DBSCAN) and Random Forest (RF), further enhances the capability to process large datasets and accurately classify surface anomalies. The effectiveness of these methods for various geospatial applications, particularly in road surface analysis, has been demonstrated in previous studies (Dillon P. et al., 2021; Zhang Y. et al., 2019; Babić et al., 2022). While deep learning models applied to image-based crack detection have shown promising results, they often require extensive labeled datasets and high computation-al power. In the context of crack detection, both a morphological approach employing a clustering algorithm (DBSCAN) and a machine learning-based classification algorithm (RF) are utilized to compare their effectiveness in predicting and identifying cracks (longitudinal and transverse) in road pavement. Figure 5.1 illustrates the overall workflow adopted in this study, outlining the key steps for preprocessing, algorithm implementation, and performance evaluation.

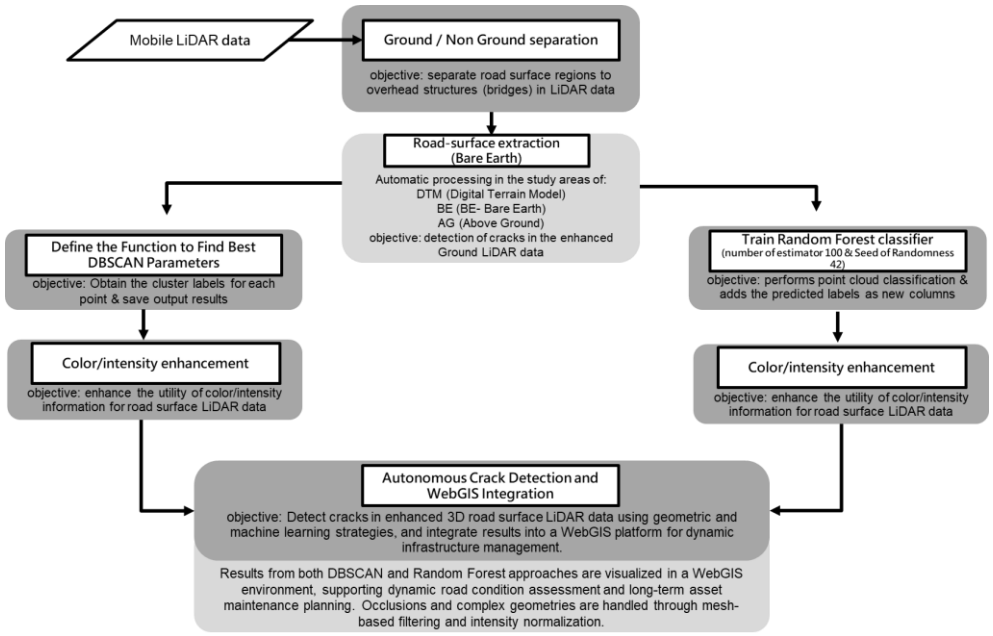


Figure 5.1: Proposed framework for comparative analysis of clustering and machine learning-based classification for detecting cracks in road surface.

This study contributes to the growing body of knowledge by focusing on the application of MMS technologies for autonomous crack detection and classification. Using data collected from the I-75 corridor in Indiana, the research employs a dual approach combining DBSCAN and Random Forest algorithms. DBSCAN, known for its robustness in identifying irregularly shaped clusters, is utilized for crack segmentation, while RF, a supervised learning method, is applied for crack classification. Both normalized and non-normalized intensity data are analyzed, allowing for a comparative evaluation of their effectiveness in enhancing detection accuracy (Cheng Y. et al., 2022). The choice of these methodologies is driven by their respective strengths: DBSCAN excels in processing spatially noisy datasets, making it suitable for segmenting cracks with varying geometries, whereas Random Forest is renowned for its ability to handle high-dimensional data and capture intricate relationships within the dataset (Tonhauser M., 2021; Cantisani G. et al., 2023). By integrating advanced MMS systems and machine learning techniques, this research aims to provide a scalable and efficient framework for the monitoring and maintenance of road infrastructure. This aligns with global efforts to mitigate the impacts of

climate change and ensure safer, more resilient transportation networks (European Commission, 2019).

5.3 Materials and Methods

In this study, a total of 27 datasets were collected along a highway using a wheel based MMS developed by the DPRG at Purdue University. Detailed information about the system's configuration and specifications is presented in Chapter. Consequently, this section offers only a brief summary, supported by relevant figures to provide context for the datasets.

5.3.1 Data Acquisition Systems

The MMS LiDAR datasets were acquired using the PWMMS-UHA. Figure 5.2 presents these systems, showcasing their sensor configurations and technical components. This highlights their precision and versatility, which facilitate the acquisition of high-quality LiDAR data essential for a detailed analysis of road surface extraction, focusing on crack detection.

- PWMMS-UHA: This system is equipped with two high-accuracy LiDAR units (Riegl VUX-1HA and Z+F Profiler 9012), two FLIR Flea2 FireWire cameras, and a NovAtel ProPak6 GNSS receiver. The range accuracy of the sensors is ±5 mm for the VUX-1HA and ±3 mm for the Profiler 9012, with the GNSS/INS unit achieving a positional accuracy of ±1–2 cm and an attitude accuracy of ±0.003° for roll/pitch and ±0.004° for heading.

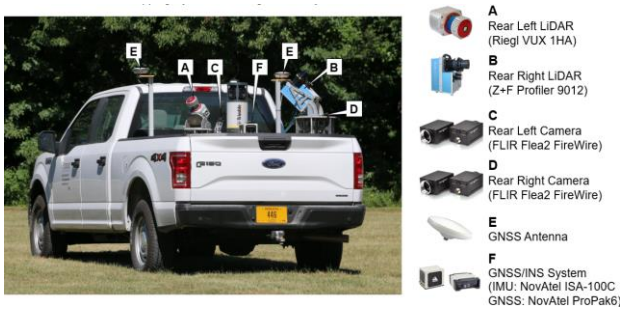


Figure 5.2: MMS LiDAR systems used in the study: the PWMMS-UHA.

5.3.2 I-65 Highway Datasets

This section focuses on the classification performance and the versatility of crack identification on a dataset acquired from two LiDAR sensors along State Highway I-65, located in West Lafayette, Indiana, U.S.A. The study area spans over 50 miles of highway and includes a total of 27 ROIs near bridges, providing a diverse set of surface conditions for analysis. The datasets were collected on February 23, 2021, under controlled conditions to ensure consistency and accuracy in the measurements. These ROIs were strategically selected to encompass various structural and environmental factors, such as bridge proximities, road surface materials, and traffic patterns, which are critical for evaluating the performance of the applied methodologies. Figures 5.3 and 5.4 illustrate the study area and highlight the spatial distribution of the 27 ROIs along the highway. These visualizations provide an overview of the dataset and contextualize the geospatial extent of the analysis. Using dual LiDAR systems for data acquisition ensures comprehensive coverage and high-resolution point cloud data, which are instrumental in accurately detecting and classifying road surface anomalies. By leveraging this dataset, the study aims to assess the effectiveness of the proposed methodologies in identifying and characterizing cracks (both longitudinal and transverse) across diverse road segments.

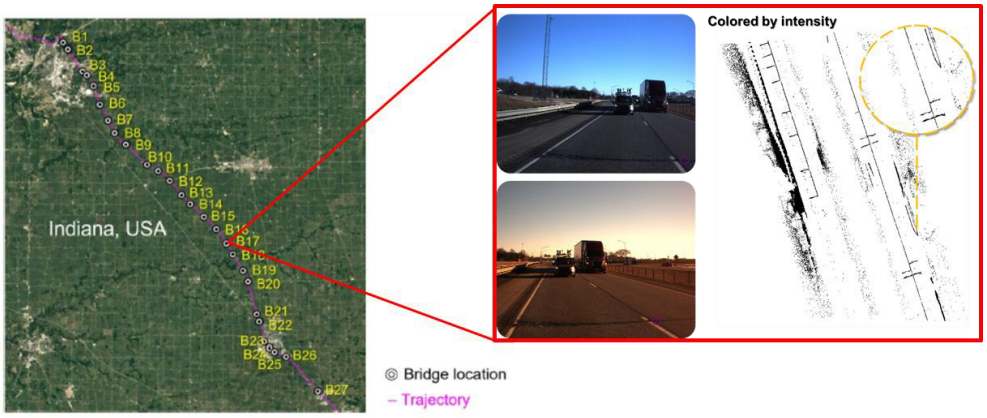


Figure 5.3: Study site showing the data collection route and bridge locations along State Highway I-65, with an aerial view adopted from Google Earth imagery. The inset provides a detailed zoom of a road surface segment.

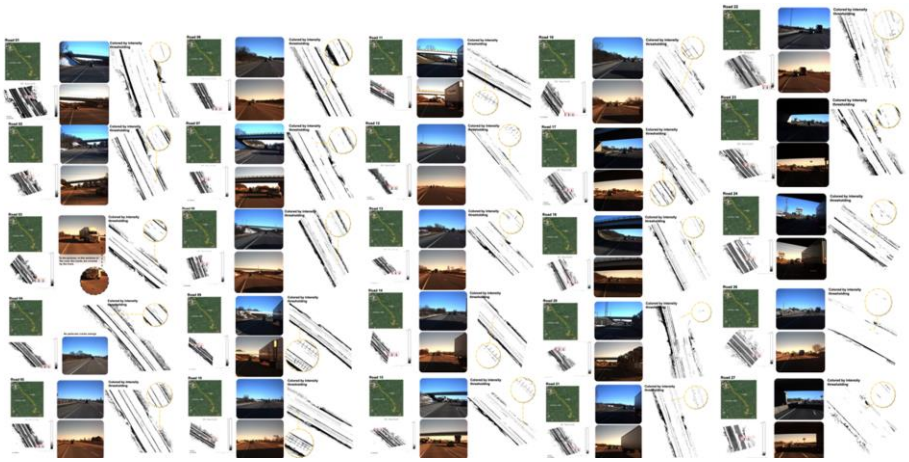


Figure 5.4: Visual inspection of all 27 studied segments along State Highway I-65, with each segment color-coded based on intensity thresholding. The image highlights the variation in surface features across the dataset, allowing for a comprehensive overview of the road surface conditions, including the detection of cracks.

5.3.3 Summary of Methodology

This section summarizes the methodology employed for the identification and classification of cracks on road surfaces using a comparative approach between a clustering method and a machine-learning-based classification algorithm. The detailed theoretical and technical aspects of these methods have been comprehensively described in Chapter 2. The analysis commenced with the preprocessing of MMS LiDAR data. This critical step involved the removal of noise and a distance-based downsampling of the point cloud to achieve a uniform resolution of 5 cm. By ensuring consistent data quality and reducing computational load, the preprocessing stage established a reliable foundation for subsequent analyses. Following this, the Cloth Simulation Code (CSC) was iteratively applied to the preprocessed point cloud. This algorithm, described in Chapter 2, incorporates uniform and adaptive stiffness parameters to simulate a cloth that is inverted and placed over the point cloud. Under the influence of gravity, the simulated cloth conforms to the underlying surface, enabling the generation of Bare Earth (BE) points, Digital Terrain Model (DTM) points and Above-Ground (AG) points. This approach ensures the objective separation of BE points from AG points, thereby facilitating a focused analysis of the road surface. The effectiveness of this method in isolating the

BE and AG points was demonstrated in multiple Regions of Interest (ROIs), with Figure 5.5 providing a representative example of a tile.

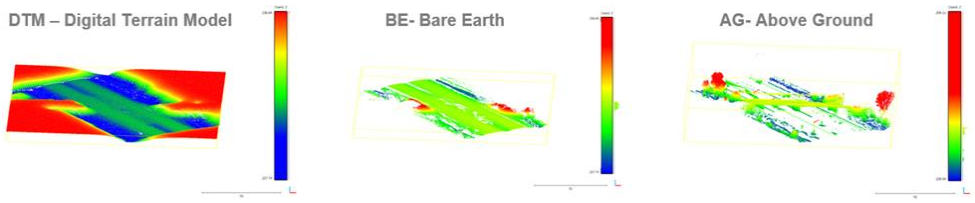


Figure 5.5: An example of a tile illustrating the effectiveness of the proposed method in isolating the DTM, BE and AG.

Subsequent to the pre-processing, candidate crack points were identified from individual scan lines of the point cloud. This step relied on intensity thresholds to distinguish potential crack points. To refine this identification process, the DBSCAN clustering algorithm was employed. As detailed in Chapter 2, DBSCAN was applied both with and without normalized intensity (IN), as explained in Chapter 2. The clustering phase facilitated the grouping of candidate crack points, enabling the differentiation between true crack points and noise. The algorithm's effectiveness was quantitatively assessed by comparing the resulting point cloud to the "Ground Truth" dataset, validated through visual inspection. Metrics such as precision, recall, F1-score, and others were computed to evaluate DBSCAN's performance in accurately labelling crack points. These metrics have been thoroughly detailed in Chapter 3, providing the necessary theoretical and methodological context for their application in this study. In addition to the morphological and clustering approaches, a Random Forest (RF) classification method was implemented. As discussed in Chapter 2, RF constructs an ensemble of decision trees during training. For each input, the classification output is determined either by the mode of classes (for classification tasks) or the mean prediction (for regression tasks) across all decision trees. The RF model was applied to the same dataset as the clustering algorithm, both with and without intensity normalization. The classified point clouds were then compared to the "Ground Truth" dataset to evaluate the performance of the RF classifier. Similar to DBSCAN, metrics such as precision, recall, F1-Score and so on were calculated to quantify the

effectiveness of the RF model in assigning labels to the points. Finally, a comparative analysis was conducted to evaluate the performance of DBSCAN and RF in crack detection and classification. This analysis highlighted the strengths and limitations of both approaches under varying conditions, including the presence or absence of intensity normalization. The results underscore the importance of selecting the appropriate method based on the specific characteristics of the dataset and the intended application. This methodology, encompassing pre-processing, clustering, and machine learning, provides a robust framework for automated crack detection and classification on road surfaces.

5.4 EXPERIMENTAL RESULTS

This section presents a comprehensive analysis comparing the performance of DBSCAN and Random Forest (RF) methods, both with and without intensity normalization, in detecting road surface cracks. By examining their application in processing LiDAR data, the analysis aims to identify the strengths and limitations of each methodology. A qualitative assessment was conducted by visually comparing the segmentation results from both methods to ground truth data across LiDAR datasets from various ROIs. This was followed by a quantitative evaluation using metrics such as Precision, Recall, F1-Score, and Overall Accuracy, as detailed in Chapter 3. The evaluation specifically emphasized the accurate labeling of transverse and longitudinal cracks, which are the primary focus of this study.

5.4.1 COMPARATIVE ANALYSIS OF DBSCAN AND RANDOM FOREST WITH AND WITHOUT INTENSITY NORMALIZZATION

In this section, a comparative analysis of DBSCAN and RF algorithms applied to LiDAR data for road surface crack detection, both with and without intensity normalization. The analysis considers all processing tiles, with detailed results and visual outputs included in the appendix for reference. This approach ensures transparency and provides a

comprehensive understanding of the methodology and results. Firstly, DBSCAN was applied to the dataset without performing intensity normalization. The analysis was carried out across all the tiles, which were carefully classified into distinct categories through manual labelling. These categories included:

- *Road*: Representing man-made terrain, primarily comprising the road surface itself;
- *Natural terrain and Vegetation*: Encompassing areas of natural land and vegetation, such as grass, soil, and trees;
- *Remaining hardscape, scanning artifacts, and bridge components*: Covering additional hard surfaces like sidewalks, curbs, bridge structures, and any scanning-related artifacts present in the data;
- *Longitudinal cracking*: Identifying cracks that run parallel to the road's direction;
- *Transverse cracking*: Capturing cracks oriented perpendicular to the road's direction.

Since DBSCAN is an unsupervised clustering method, manual interaction was required to assign meaningful labels to clusters, ensuring consistency with the ground truth. For example, in Tile 17, representing a region near a bridge (as shown in Figure 5.6), DBSCAN identified two distinct clusters corresponding to low and high vegetation. However, manual classification consolidated these into a single cluster under the “Natural terrain & Vegetation” class, as per the established labeling conventions. Moreover, transverse cracks in Tile 17 were distinguishable in the colour histogram and were identified by different shades, unlike longitudinal cracks, which appeared less distinct. In this case, DBSCAN initially recognized multiple clusters due to the presence of both Remaining hardscape & Scanning artifacts and Vegetation in the data. After manual labelling, transverse cracks misclassified as longitudinal cracks were re-labelled as longitudinal cracks to maintain consistency with DBSCAN’s automated outputs.

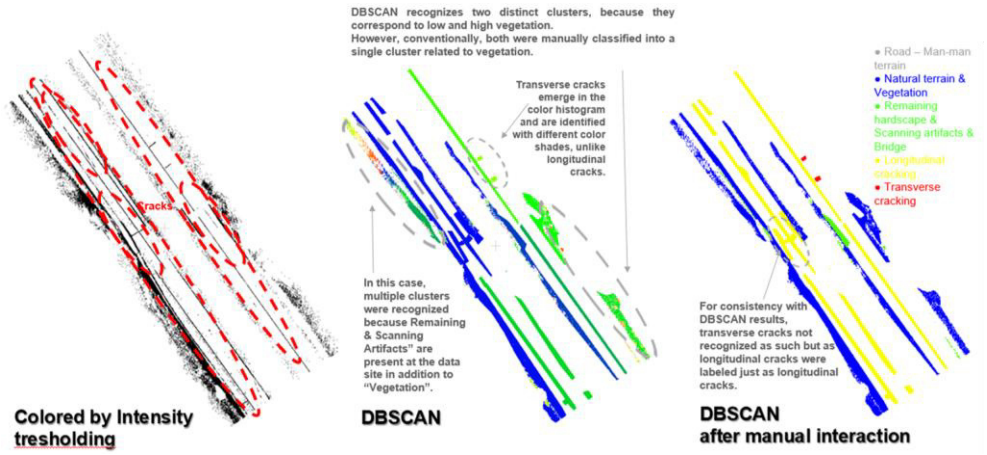


Figure 5.6: On the left, the road segment near Bridge 17 is visualized with coloring based on intensity thresholds. The center image showcases the clustering results obtained using the DBSCAN algorithm, while the rightmost image presents the DBSCAN clusters with manual labeling applied for further classification and validation.

The analysis of the results for Tile 17, as detailed in Table 5.1, provides valuable insights into the performance of the DBSCAN algorithm when applied without intensity normalization. Overall, the algorithm achieved an accuracy of 68%, reflecting moderate reliability in identifying the targeted features within this segment.

Table 5.1: Validation results from the comparison between the DBSCAN point cloud without intensity normalization and the ground truth (GT).

	TP	FP	FN	Precision	Recall	F1-Score
Mad Terrain & Road	0	0	2652	NaN	0.000	NaN
Natural terrain & Vegetation	1140	899	3847	0.559	0.228	0.324
Remaining hardscape & Scanning artifacts	58	135	324	0.300	0.151	0.0201
Longitudinal cracking	781	477	550	0.620	0.586	0.603
Transversal cracking	16	4	33	0.800	0.326	0.463
Overall accuracy	68%					

Focusing on the specific categories shown in the table above, it can be seen that DBSCAN, for longitudinal cracks, demonstrated a moderate ability to identify these features. The algorithm achieved a balance between precision and recall, with recall slightly lower than precision. This led to an F1-Score indicating a reasonable trade-off between correctly identified cracks and missed detections. However, a relatively high proportion of false positives and false negatives highlights the need for further improvement in accurately distinguishing these features. On the other hand, DBSCAN, for transverse cracks, exhibited stronger precision in identifying these features,

accurately classifying most of the detected instances as true positives. However, recall was notably lower, indicating that a significant number of transverse cracks were missed. The resulting F1-Score underscores the difficulty in achieving comprehensive detection for this type of crack, particularly when balancing precision and recall. These findings illustrate DBSCAN's limitations when applied without intensity normalization, especially for transverse cracks. The results suggest the need for manual refinement or complementary methods to address the algorithm's difficulty in achieving consistent accuracy across both longitudinal and transverse crack types.

The DBSCAN algorithm, applied to the dataset with intensity normalization, aimed to enhance the identification of features by leveraging normalized intensity values. The analysis was performed across all tiles, classified into the same distinct categories as in the non-normalized intensity approach: *Road; Natural terrain and Vegetation; Remaining hardscape, scanning artifacts, and bridge components; Longitudinal cracking; and Transverse cracking*.

Always considering tile 17 as an illustrative example (as shown in Figure 5.7). With intensity normalization, the algorithm demonstrated notable changes in the clustering behaviour. By adjusting the normalized intensity threshold, distinct features such as lane markings became more visible (center and top of Figure 5.7), while cracks appeared less pronounced (center and bottom of Figure 5.7). Despite this improvement in visibility for certain features, DBSCAN exhibited challenges in clustering point clouds with normalized intensities. The similarity in intensity values across adjacent regions often made it difficult to define clear boundaries between clusters. Manual intervention was necessary to refine the clustering results. For instance, parts of the "Bridge - shoulder and wing wall" category, which in the ground truth were labelled as "Remaining hardscape, Scanning artifacts, and Bridge," were reclassified as "Road - Man-made terrain" in the results. This adjustment was made to maintain consistency with the clustering outputs generated by DBSCAN, ensuring the labelled results aligned with the algorithm's grouping tendencies.

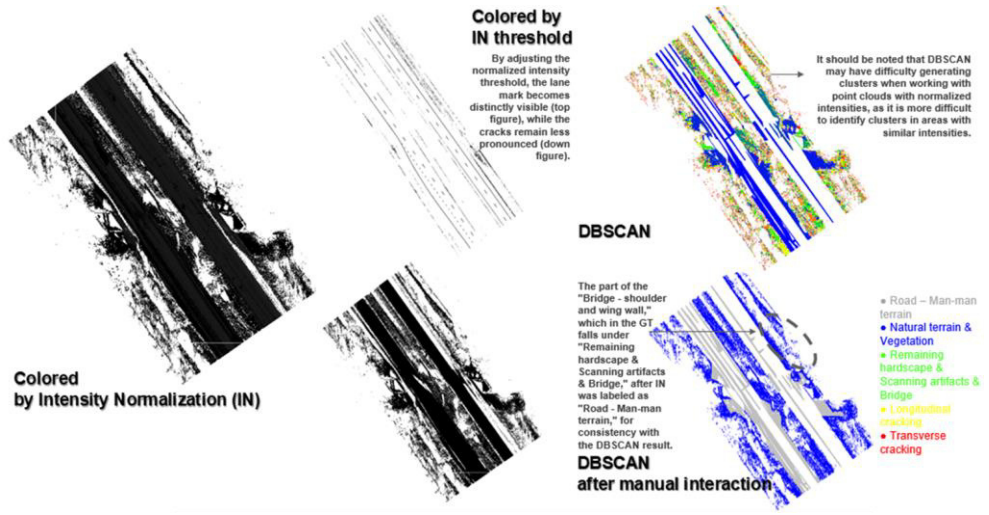


Figure 5.7: On the left, the road segment near bridge 17 is colored based on intensity thresholds, with intensity values previously normalized. In the center, from the normalized dataset, it is evident that lane marks become distinguishable from cracks based on the threshold. On the right, DBSCAN results are shown without and with manual labeling.

The analysis of the results for Tile 17, as detailed in Table 5.2, highlights the improved performance of the DBSCAN algorithm when applied with intensity normalization. The initial results demonstrate an increase in overall accuracy from 68% (achieved without intensity normalization) to 75%, reflecting enhanced reliability in identifying the targeted features within this segment.

Table 5.2: Validation results from the comparison between the DBSCAN point cloud with intensity normalization and the GT.

	TP	FP	FN	Precision	Recall	F1-Score
Mad Terrain & Road	859	2300	1796	0.271	0.323	0.295
Natural terrain & Vegetation	3315	3466	1635	0.488	0.669	0.565
Remaining hardscape & Scanning artifacts	0	0	398	NaN	0.000	NaN
Longitudinal cracking	0	0	1332	NaN	0.000	NaN
Transversal cracking	0	0	49	NaN	0.000	NaN
Overall accuracy	75%					

Focusing on the specific categories shown in the table above, it is evident that DBSCAN faced significant challenges in identifying both longitudinal and transverse cracks when applied with intensity normalization. The algorithm failed to produce any true positives for longitudinal cracks, resulting in a Precision, Recall, and F1-Score of zero. Similarly, no true positives were identified for transverse cracks, and the metrics - Precision, Recall, and F1-Score - also remained at zero. These outcomes suggest that

the intensity normalization process caused a redistribution of the true positive detections. An increase in true positives was observed in the "*Man-made terrain & Road*" and "*Natural terrain & Vegetation*" categories, indicating that the normalized intensity values may have caused the algorithm to prioritize these features over cracks. However, the lack of any true positives for both longitudinal and transverse cracks emphasizes the difficulty DBSCAN encountered in distinguishing these critical features when working with normalized intensity values. These findings illustrate the limitations of DBSCAN when applied to intensity-normalized datasets, particularly in the context of crack detection. While intensity normalization can enhance the identification of certain surface features, such as vegetation or road surfaces, it appears to compromise the algorithm's ability to detect finer details like cracks. This suggests the need for alternative clustering strategies, additional pre-processing steps, or manual refinement to address the shortcomings observed in the detection of longitudinal and transverse cracks under these conditions. However, the analysis reveals that the improvement in cluster generation remains limited. Given the challenges encountered, this can be attributed to DBSCAN's difficulty in effectively identifying clusters in areas with similar intensity values. To address this limitation, the application of machine learning classification was explored, specifically using the RF algorithm. This approach was pursued in line with the initial objective of experimenting with automatic and semi-automatic recognition methods, aiming to enhance the comparison process between point clouds. Special attention was given to evaluating the advantages and disadvantages of working with datasets both with and without intensity normalization. Subsequently, the two point clouds were compared: one derived from the GT and the other generated by applying the RF algorithm, both with and without intensity normalization. To assess the effectiveness of the RF algorithm in accurately assigning labels to the points, various performance metrics were calculated, as shown in Figure 5.8 and Table 5.3. These metrics provide a quantitative evaluation of the algorithm's classification capability. The results indicate that the overall accuracy of the RF model, when applied without intensity normalization, is 94%. In

contrast, when intensity normalization is applied, the accuracy slightly decreases to 93%. This minor drop suggests that while intensity normalization can enhance certain aspects of the dataset, its effect on the overall classification accuracy remains relatively small.

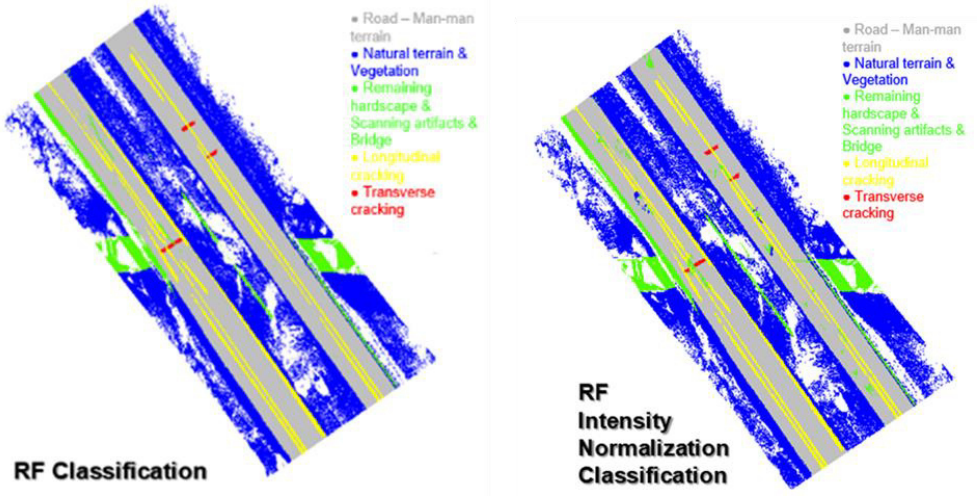


Figure 5.8: On the left, the road surface without intensity normalization, and on the right, the road surface with intensity normalization, both classified using RF.

Table 5.3: Validations obtained by comparing the two point clouds from RF without normalized intensity and the GT and from RF with normalized intensity and the GT, respectively.

RF No IN	TP	FP	FN	Precision	Recall	F1-Score
Mad Terrain & Road	1920	9	1418	0.995	0.720	0.836
Natural terrain & Vegetation	4590	600	376	0.884	0.924	0.903
Remaining hardscape & Scanning artifacts	352	480	33	0.423	0.914	0.578
Longitudinal cracking	1319	82	5	0.941	0.996	0.968
Transversal cracking	49	6	1	0.890	0.989	0.933
Overall accuracy	94%					

RF IN	TP	FP	FN	Precision	Recall	F1-Score
Mad Terrain & Road	1866	25	798	0.986	0.700	0.819
Natural terrain & Vegetation	4483	704	483	0.864	0.902	0.883
Remaining hardscape & Scanning artifacts	349	563	36	0.382	0.906	0.538
Longitudinal cracking	1318	92	6	0.934	0.995	0.964
Transversal cracking	49	6	1	0.890	0.980	0.933
Overall accuracy	93%					

5.5 Analysis of Crack Detection in Point Cloud Data

The detection and analysis of cracks in point cloud data play a crucial role in the assessment of road and infrastructure conditions. Point clouds, typically acquired through LiDAR or mobile mapping systems, offer high-resolution spatial data that can be used to identify structural damage, such as cracks, on roads and bridges. However, detecting cracks in point cloud data presents unique challenges due to the complexity and variability of the

surfaces, as well as the potential noise and incomplete data that may be present. In this section, we focus on the comparative analysis of two prominent crack detection methods: DBSCAN and RF. These methods were applied to the point cloud data to assess their effectiveness in identifying longitudinal and transverse cracks, both with and without intensity normalization. The comparison aims to evaluate the strengths and weaknesses of clustering versus classification algorithms for crack detection tasks and to explore how intensity normalization influences the performance of these methods. To ensure a thorough evaluation, various metrics were calculated to quantify the accuracy of each method. The Jaccard Index (previously described in Chapter 3), which measures the similarity between the predicted crack locations and the ground truth data, was chosen as the primary evaluation metric. In addition to the Jaccard, the surface area of the cracks was measured using the Poisson algorithm, which is known for providing accurate results for complex surfaces in point cloud data. This algorithm reconstructs a continuous surface from an unstructured point cloud by solving a Poisson equation, which fits an implicit function to the data based on normal vectors. The resulting mesh approximates the geometry of the cracks and allows for accurate surface area calculations. This method is particularly suitable for analyzing irregular and incomplete surfaces such as road cracks, as it handles noise and missing data robustly. By generating meshes of the segmented crack regions, it was possible to quantitatively compare the area of the detected cracks between different detection approaches. This measure allows for a quantitative comparison of the detected crack areas, further enhancing the evaluation of the methods' performance. However, Jaccard Index was calculated to evaluate the performance of the DBSCAN and RF methods in identifying longitudinal and transverse cracks, both with and without intensity normalization. As presented in Table 5.4, the results revealed significant differences in performance between the two methods under varying conditions.

Table 5.4: Metrics obtained by comparing the two point clouds from DBSCAN with and without normalized intensity, RF with and without normalized intensity, and GT only for crack-related classes.

		Type of cracking	TP	FP	FN	Precision	Recall	F1-Score	Jaccard Index
17	DBSCAN No IN	Longitudinal	781	477	550	0.620	0.586	0.603	43%
		Transversal	16	4	33	0.800	0.326	0.463	30%
	DBSCAN IN	Longitudinal	0	0	702	0.000	0.000	NaN	0%
		Transversal	0	0	169	0.000	0.000	NaN	0%
	RF No IN	Longitudinal	1319	82	5	0.941	0.996	0.968	94%
		Transversal	49	6	1	0.890	0.989	0.933	88%
	RF IN	Longitudinal	1318	92	6	0.934	0.995	0.964	93%
		Transversal	49	6	1	0.890	0.980	0.933	88%

DBSCAN, when applied without intensity normalization, achieved a Jaccard Index of 43% for longitudinal cracks and 30% for transverse cracks. These results suggest that while DBSCAN is able to identify some clusters corresponding to cracks, the overall effectiveness of the method is limited, particularly in identifying transverse cracks. However, when intensity normalization was applied, the Jaccard Index dropped drastically to 0% for both longitudinal and transverse cracks. This drastic reduction in performance indicates that DBSCAN, under these conditions, failed to effectively generate clusters, which could be attributed to the method's difficulty in handling intensity-normalized point clouds where the intensity values across clusters are uniform. In comparison, RF exhibited much higher performance. Without intensity normalization, the Jaccard Index for longitudinal cracks was 94%, and for transverse cracks, it was 88%. This indicates that RF was able to effectively differentiate and classify crack features with a high degree of accuracy. When intensity normalization was applied, the performance remained strong, with only a slight reduction in the Jaccard Index, decreasing to 93% for longitudinal cracks and 88% for transverse cracks. These results underscore the robustness of the RF algorithm in crack detection, even when intensity normalization is applied, and highlight its superiority over DBSCAN in this context.

In addition to the Jaccard Index analysis, the Measure Surface was calculated using the Poisson algorithm, which is known to deliver optimal results for complex surfaces in CloudCompare (Ghahremani K et al., 2018; Mohammadi M.E., 2019). This measure provides a quantitative estimate of the crack surface area in the dataset. As shown in Figure 5.9, the

intervention threshold was considered, based on crack surface area, with the following classifications, as outlined in the Pavement Condition Index (PCI) and Federal Highway Administration (FHWA) guidelines (Ong G. et al., 2010; Indiana LTAP, 2016; Gharaibeh N.G. et al., 2010; Holtz R. et al., 1998; Gagliardi, R.M.):

- *Roads with minor cracks*: 0.5-2 m² of cracks per 100 meters of road.
- *Roads with obvious cracks*: 2-10 m² per 100 meters.
- *Highly damaged roads*: More than 10 m² per 100 meters.

These classifications provide a structured approach for evaluating road deterioration and prioritizing maintenance interventions. In this study, the surface area of cracks was calculated using the mesh generated from the Poisson surface reconstruction algorithm in CloudCompare. This mesh allowed for an accurate estimation of the crack extent in square meters (m²). While crack length is commonly used in manual inspections, surface area provides a more comprehensive measure in 3D point cloud data, especially when cracks vary in width and shape. The use of area-based thresholds is consistent with the PCI and FHWA guidelines, which include surface damage classifications expressed in terms of affected area per unit length of road (e.g., m² per 100 meters). This approach enables a more robust and spatially explicit evaluation of road condition in LiDAR-based analysis.

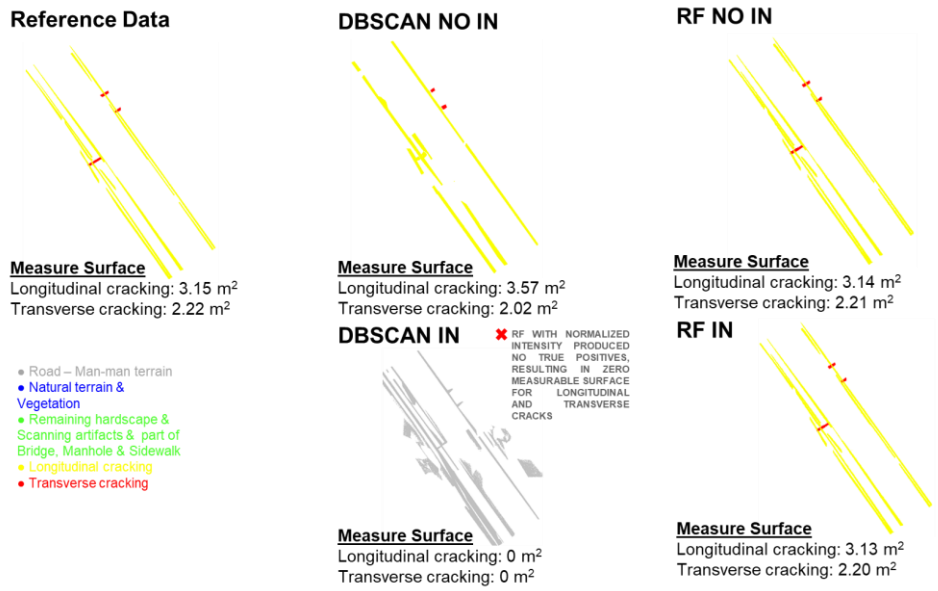


Figure 5.9: Quantitative estimation of crack surface area calculated using the Poisson algorithm in CloudCompare. The intervention threshold is defined as follows: Roads with minor cracks (0.5–2 m² of cracks per 100 meters of road); roads with obvious cracks (2–10 m² of cracks per 100 meters of road); highly damaged roads (more than 10 m² of cracks per

100 meters of road). Crack surface measurements have been rounded to two decimal places to enhance clarity and readability.

These results further support the observation that Random Forest consistently outperforms DBSCAN, with better overall surface area estimates for both longitudinal and transverse cracks. Notably, the performance of DBSCAN deteriorates when intensity normalization is applied, particularly in its inability to detect cracks accurately in the normalized data set. This highlights the importance of selecting appropriate algorithms and pre-processing techniques to optimize crack detection in point cloud data. These all results are shown in addendum B.

5.6 Conclusion and Future Studies

This study provides a detailed evaluation of two distinct methods—DBSCAN and Random Forest—for crack detection in point cloud data, with and without intensity normalization. The findings underscore the robustness of the Random Forest algorithm, which consistently demonstrated superior performance compared to DBSCAN in terms of accuracy, recall, and F1-score. Random Forest proved to be highly effective at detecting cracks, particularly longitudinal ones, achieving reliable results both with and without intensity normalization. In contrast, DBSCAN showed significant limitations, especially when intensity normalization was applied, rendering it ineffective in segmenting cracks. The clustering method's inability to handle intensity-normalized data and its tendency to produce high false negatives underscore its unsuitability for this specific application. These results reaffirm the importance of algorithm selection based on the characteristics of the data and the specific requirements of the task. A key observation is the difference in detection accuracy between longitudinal and transverse cracks. Longitudinal cracks, which are more continuous and well-defined, were identified with greater accuracy than transverse cracks, which are sporadic and less distinguishable. This emphasizes the need for targeted approaches when dealing with different crack types. The comparison also highlights the clear advantages of classification-based approaches like Random Forest over clustering methods like DBSCAN for crack detection

tasks. The ability of supervised models to leverage labelled training data enables them to make more accurate and generalized predictions, making them a reliable choice for analyzing complex features such as cracks in point cloud data. While this study has provided valuable insights into crack detection in point cloud data, there remain significant opportunities to advance the field. Future research could explore the integration of advanced machine learning and deep learning models, such as convolutional neural networks (CNNs) or graph neural networks (GNNs), which are well-suited for handling high-dimensional data and may enhance the detection of complex crack patterns, particularly transverse cracks. Combining clustering and classification techniques, such as employing DBSCAN for noise reduction followed by Random Forest for classification, could also be a promising avenue. Incorporating additional features, including surface roughness, curvature, and colour, beyond intensity, may improve accuracy by allowing algorithms to better differentiate cracks from other surface irregularities. Expanding validation efforts to include diverse datasets with varying road conditions, materials, and environmental factors would help ensure the generalizability of findings and address challenges related to dataset variability. Developing real-time crack detection systems, integrated into mobile mapping platforms or drones, could significantly enhance the efficiency of infrastructure monitoring and maintenance. Moreover, optimizing intervention thresholds based on metrics like crack severity and density, while integrating guidelines such as the Pavement Condition Index (PCI), could refine maintenance prioritization strategies. Automated or semi-automated methods for generating ground truth data would reduce reliance on manual annotation, saving time and improving consistency. Lastly, investigating the impact of environmental factors, such as lighting, weather, and wear over time, on detection performance could contribute to the development of more robust algorithms. Addressing these areas will not only build on the findings of this study but also enhance the accuracy, efficiency, and practical applicability of crack detection methods, ultimately improving infrastructure monitoring and maintenance practices.

6. THIRD CASE STUDY: CRACK ANALYSIS ON L'AQUILA VIADUCT, ITALY

6.1 INTRODUCTION

To comprehensively compare methodologies applied in international and national case studies, an additional European site was selected in Italy: a highway viaduct located in L'Aquila, as shown in Figure 6.1.

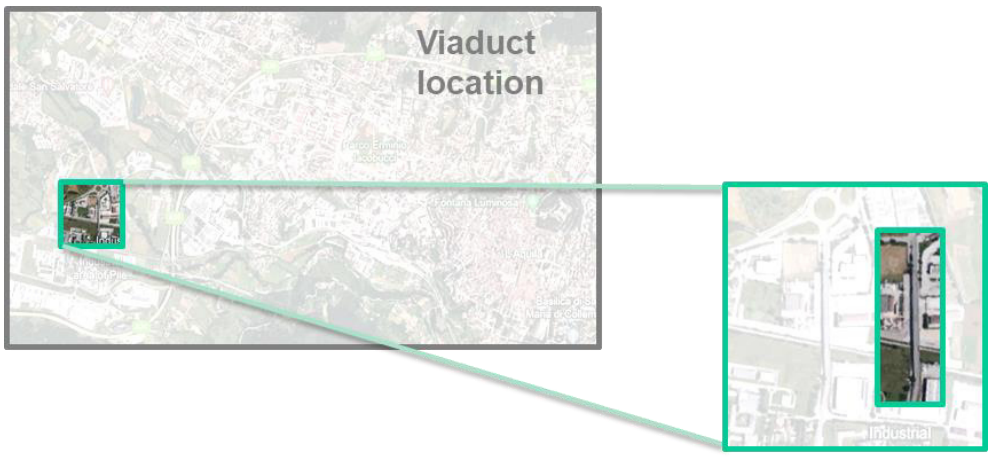


Figure 6.1: Study site showing viaduct locations along Via Campo di Pile, L'Aquila (Italy), with an aerial view adopted from Google Earth imagery.

This choice reflects the need to evaluate the adaptability of techniques across different geographic and structural contexts. Specifically, the study examines how advanced geomatic methods, particularly SLAM-based LiDAR data acquisition, can be effectively utilized to detect and analyze road surface conditions, including potential risks like cracks.

The selected site underwent surveys using two technologies:

- GeoSLAM ZEB HORIZON combined with a Leica G15 GNSS receiver on July 22, 2019.
- Leica BLK2GO integrated with a Leica G15 GNSS receiver on October 7, 2024.

These datasets enabled a detailed examination of the site's structural condition, aligning with European standards, such as those issued by the Italian Ministry of Infrastructure and Transport (MIT), which require systematic risk classification to prioritize maintenance and repair interventions (Ministry of Infrastructure and Transport - MIT, 2020.). Traditionally, risk assessments in Italy have relied on manual inspections and visual surveys, but these are gradually being replaced by automated approaches (Mei A. et al., 2022; Cantisani G. et al. 2023). Across Europe, similar efforts are underway to adopt advanced technologies that ensure road safety, though challenges remain in achieving a balance between accuracy, efficiency, and cost (Tonhauser M. et al., 2021; European Commission, 2019). To process the LiDAR datasets, a workflow similar to that used in the USA case study, previous chapter was implemented. The methodology included ground and non-ground separation through the Cloth Simulation. The BE layer was further optimized by enhancing intensity and color attributes to improve crack detection accuracy. Following this preprocessing stage, the DBSCAN algorithm was applied for clustering-based crack detection. Parameters such as epsilon (ε) and minimum sample size were iteratively fine-tuned, with clustering performance evaluated through metrics like the silhouette score. To ensure robust evaluation, the clustering results were compared with manually labeled ground truth data was generated through manual visual inspection of the LiDAR point clouds using CloudCompare and performance metrics were calculated. Additionally, a RF was employed to provide a comparative benchmark. The same workflow applied in the USA case study was adapted here to highlight the similarities and differences between MMS and SLAM-based approaches.

6.2 MATERIALS AND METHODS

This study focuses on the analysis of a highway viaduct located in L'Aquila, specifically in the area of Via Campo di Pile. Data acquisition for this site was conducted using two advanced SLAM-based systems. Detailed descriptions of the configurations and specifications of the employed systems are presented in Chapter 2, where their technical features and operational parameters are thoroughly outlined. In this section, only a concise summary is provided, accompanied by illustrative figures to contextualize the datasets and methodologies.

6.2.1 DATA ACQUISITION SYSTEMS

The SLAM datasets used in this study were collected utilizing two state-of-the-art technologies, each specifically chosen for their reliability, and suitability for infrastructure monitoring tasks. These systems enabled the acquisition of LiDAR data, providing a foundation for detailed analyses of road surfaces and crack detection. The first one , GeoSLAM ZEB Horizon (fig. 6.2), Paired with a Leica GS15 GNSS Receiver, this system was deployed to survey the site on July 22, 2019. The GeoSLAM is renowned for its lightweight design and ability to capture high-density point clouds, even in challenging environments. Its integration with the Leica GS15 ensures accurate georeferencing, enhancing the spatial precision of the acquired data. On the other hand, Leica BLK2GO (fig. 6.2) combined with a Leica GS15 GNSS Receiver, this advanced handheld system was utilized for a subsequent survey on October 7, 2024. The BLK2GO offers seamless data capture through its compact design and high-speed SLAM processing capabilities, making it ideal for dynamic environments like viaducts. Its compatibility with the Leica GS15 further ensures reliable positioning and georeferencing.



Figure 6.2: From left to right: GeoSLAM ZEB Horizon, Leica BLK2GO, and GNSS receiver GS15.

For a detailed overview of these systems, including sensor configurations, technical specifications and operational characteristics, please refer to Chapter 2. The comparative presentation of these tools highlights their respective strengths and versatility in acquiring high-quality datasets.

6.2.2 VIADUCT IN CAMPO DI PILE, L'AQUILA (ITALY)

This study investigates the performance of crack identification algorithms using LiDAR datasets collected from a viaduct located in L'Aquila, Italy, within the broader context of European infrastructure monitoring. The test site, a viaduct along Via Campo di Pile, spans approximately 330 meters and consists of 9 piers, as illustrated in Figure 6.3.



Figure 6.3: Case of study from left to right: view adopted from Open Street Map and Viaduct's image.

The viaduct represents a critical transportation link within the region, making it an ideal case study for the application of advanced geomatic techniques. Its structural complexity, combined with varying environmental conditions, offers a robust testing ground for analyzing both transversal and longitudinal cracks. The datasets acquired for this analysis enable a detailed examination of road surface conditions, investigating the versatility of LiDAR-based approaches in capturing structural anomalies.

6.2.3 Summary of Methodology

This section outlines the methodological approach adopted for the detection and classification of road surface cracks, leveraging a comparative framework between clustering-based and machine-learning-based classification algorithms. The detailed theoretical background and technical implementation of these methods are thoroughly discussed in Chapter 2. Here, the focus is on the application of these methodologies to the test site, using datasets acquired through SLAM-based systems. The analysis began with the pre-processing of the SLAM-acquired point clouds, ensuring the data's accuracy and suitability for subsequent workflows. Pre-processing steps included noise reduction and coordinate transformation to align the datasets with the test site's geospatial framework. Following the pre-processing stage, the Cloth Simulation Code (CSC) was systematically applied to the point cloud data. As detailed in Chapter 2, this algorithm simulates an inverted virtual cloth that drapes over the point cloud under gravitational influence. By adjusting both uniform and adaptive stiffness parameters, the CSC effectively separates Bare Earth (BE) points from Above-Ground (AG) points. These ROIs allowed for a robust evaluation of the CSC's performance in distinguishing BE and AG points. For a visual representation, Figure 6.4 showcases a sample result of this process applied to datasets collected from both SLAM systems.

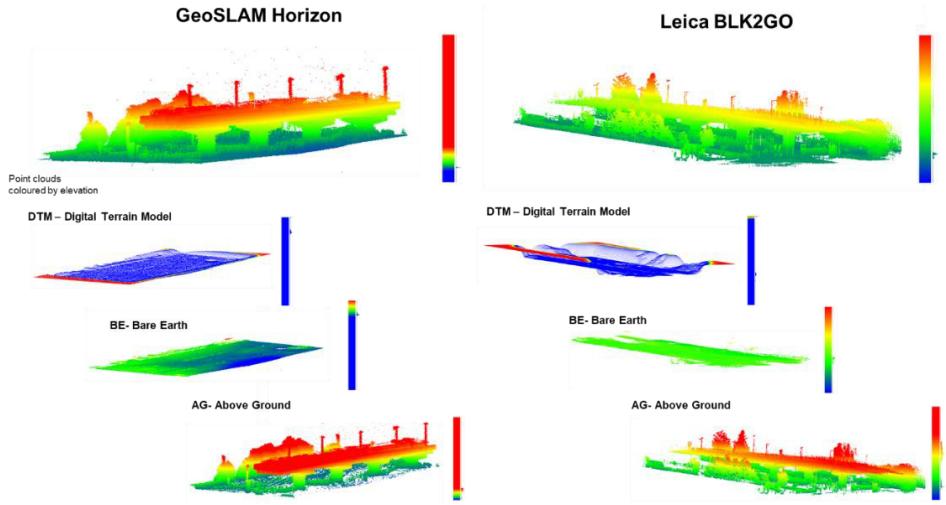


Figure 6.4: Sample results of the CS process distinguishing BE and AG points. On the left, data collected using the GeoSLAM ZEB Horizon; on the right, data from the Leica BLK2GO.

This approach to pre-processing and point cloud segmentation lays the foundation for road surface analysis by isolating the BE points. This method allows for targeted crack detection and classification, facilitating a detailed comparison of clustering algorithms and machine-learning models. Following the pre-processing of the collected data, both the DBSCAN and RF methods were applied in two versions: with and without intensity normalization (as outlined in Chapter 2). To adapt the code previously developed for mobile mapping technology, the inverse square formula was used for intensity normalization, as described in Chapter 2. Intensity normalization was calculated by comparing the measured intensity at a distance d from the source to the intensity at a reference distance (d*refe*) of one meter, as show in equation 6.1.

Equazione 6.1

$$Inorm = (\frac{d}{drefe})\text{^}2 \times Id$$

However, the issue of intensity thresholding (not normalization) was found to have a significant impact on the ability to distinguish cracks. This was particularly evident in the comparison of results between different SLAM technologies. The results of the two methods are presented in Figure 6.5.

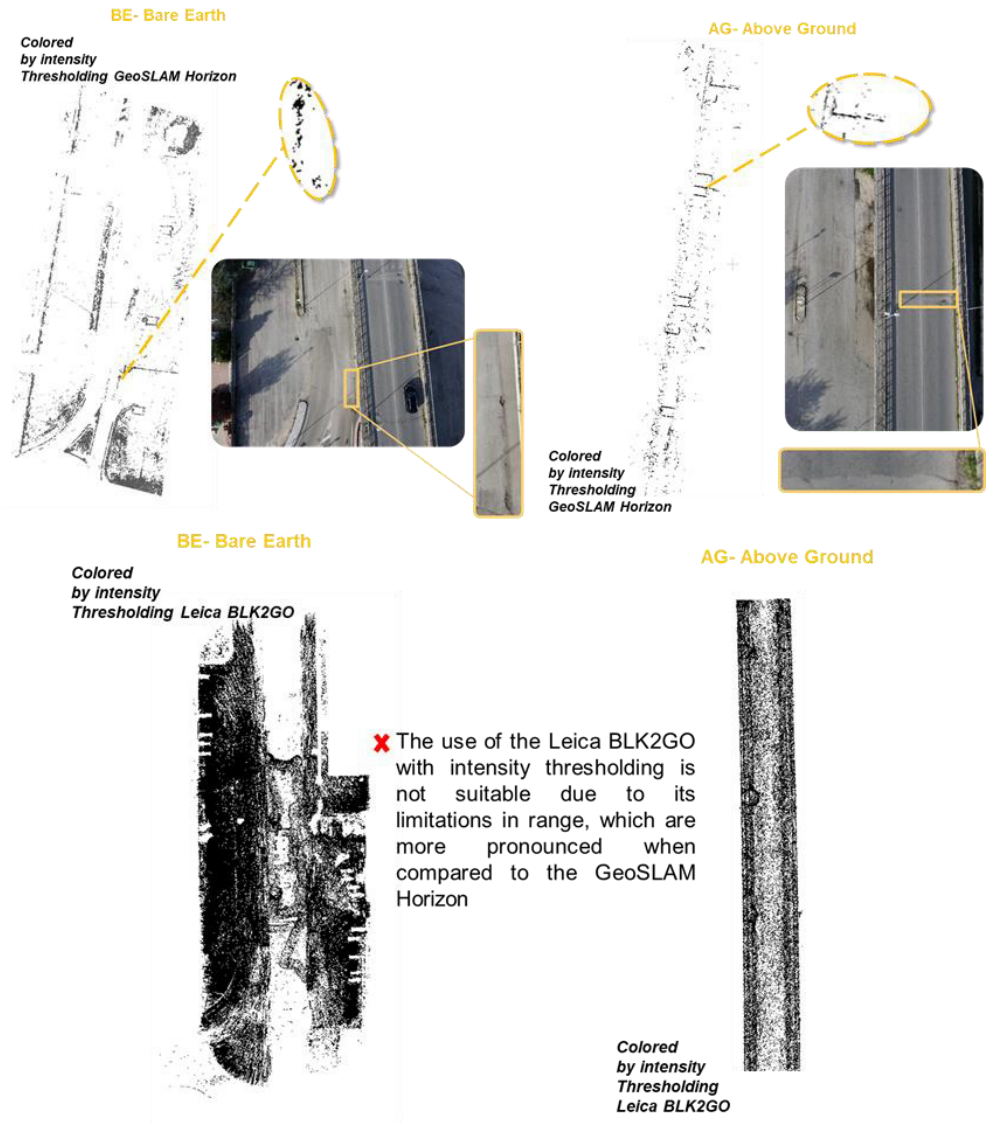


Figure 6.5: Crack detection results based on intensity thresholding. At the top, the GeoSLAM ZEB HORIZON dataset shows distinguishable cracks with varying intensity thresholds. At the bottom, the Leica BLK2GO dataset, with a shorter range and lower resolution, fails to clearly identify cracks, highlighting the limitations of this system for crack detection.

The analysis reveals differences in performance between the two SLAM systems. Specifically, for the GeoSLAM ZEB HORIZON survey, which has a range of 100 meters, crack detection was possible with both intensity normalization and intensity thresholding. The ability to distinguish cracks was influenced by the thresholding values applied, as seen in the figure. On the other hand, for the Leica BLK2GO, which has a more limited range of 25 meters, crack detection was not feasible due to the reduced scanning range and resolution, which limited the data clarity. As a result, DBSCAN

and RF methods were applied exclusively to the GeoSLAM ZEB HORIZON dataset, as it offered better conditions for crack detection in this specific case, due to its longer range and more suitable point cloud density.

6.3 EXPERIMENTAL RESULTS

This section provides an in-depth comparison of the DBSCAN and RF methods for detecting road surface cracks, considering both normalized and non-normalized intensity data. The analysis focuses on assessing the performance of these techniques when applied to LiDAR data, with the goal of highlighting the strengths and limitations of each method. A qualitative evaluation was performed by visually comparing the results of both algorithms against ground truth data. This was complemented by a quantitative analysis using key metrics such as Precision, Recall, F1-Score, and Overall Accuracy, as outlined in Chapter 3. The evaluation prioritized the accurate classification of both transverse and longitudinal cracks, which are central to the study's objectives.

6.3.1 COMPARATIVE ANALYSIS OF DBSCAN AND RANDOM FOREST WITH AND WITHOUT INTENSITY NORMALIZATION

This section presents a comparative analysis of DBSCAN and RF algorithms applied to LiDAR data for road surface crack detection, both with and without intensity normalization. This approach ensures clarity and comprehensively understands the methods and their results. Initially, DBSCAN was applied to the dataset without intensity normalization. The analysis was conducted for the case study, with careful classification into distinct categories through manual labelling. These categories include road surfaces, natural terrain and vegetation, other hardscapes, scanning artifacts, bridge components, and cracks (both longitudinal and transverse). The detailed classification and the legend remain consistent with the earlier description. As shown in the figure 6.6, the application of DBSCAN to the bare earth dataset of the viaduct identifies two distinct clusters, which

correspond to low and high vegetation. However, for consistency with conventional labelling, both clusters were manually classified into a single category labelled as vegetation. Transverse cracks are clearly visible in the colour histogram and are distinguished by different colour shades from longitudinal cracks. After manual iteration, DBSCAN's results were adjusted to maintain consistency. Specifically, transverse cracks that were misclassified as longitudinal cracks were relabelled as longitudinal, and this approach was similarly applied to the other identified classes. This ensures that the labelling is consistent throughout the analysis.

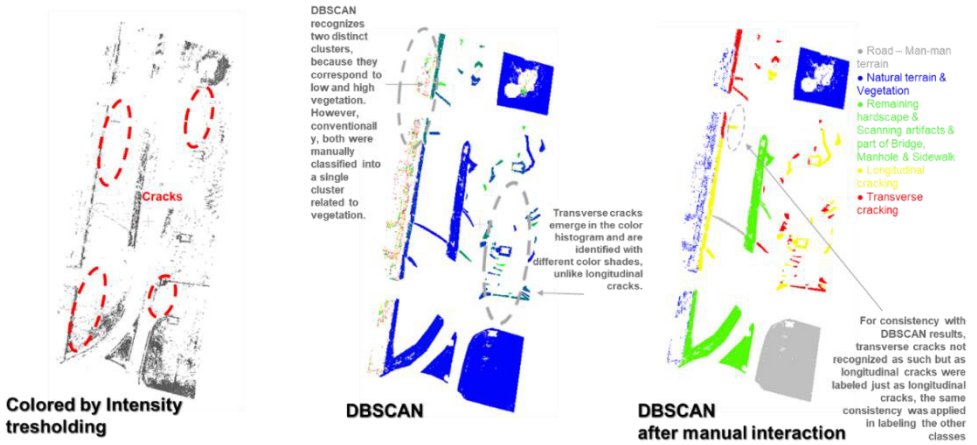


Figure 6.6: Application of DBSCAN BE without normalised intensity on datasets from GeoSLAM ZEB HORIZON

The analysis of the results for DBSCAN without intensity normalization in the BE dataset, as detailed in Table 6.1, provides valuable insights into the algorithm's performance.

Table 6.1: Validation results from the comparison between the DBSCAN BE without intensity normalization and the ground truth (GT).

	TP	FP	FN	Precision	Recall	F1-Score
Mad Terrain & Road	272	154	2620	0.638	0.094	0.163
Natural terrain & Vegetation	479	110	96	0.813	0.833	0.823
Remaining hardscape & Scanning artifacts	213	166	346	0.562	0.381	0.454
Longitudinal cracking	11	228	264	0.046	0.040	0.042
Transversal cracking	28	165	173	0.145	0.139	0.142
Overall accuracy	43%					

Overall, DBSCAN achieved an accuracy of 43%. However, a significant number of false positives were observed in the crack class, and the

Precision, Recall, and F1-Score metrics were insufficient, with values approaching zero. This indicates the need for further refinement and adjustment in the algorithm's parameters for more accurate detection of road surface cracks. As shown in Figure 6.7 and detailed in Table 6.2, the analysis of the DBSCAN results applied to the Above Ground road surface reveals that the algorithm primarily classified most of the dataset as "Road," with very few cracks identified. Transverse cracks are noticeable in the colour histogram and are distinguished by different colour shades from longitudinal cracks. After manual interaction, for consistency with the DBSCAN results, the few transverse cracks that were misclassified as longitudinal cracks were relabelled as longitudinal cracks. This consistency was applied to the other identified classes as well.

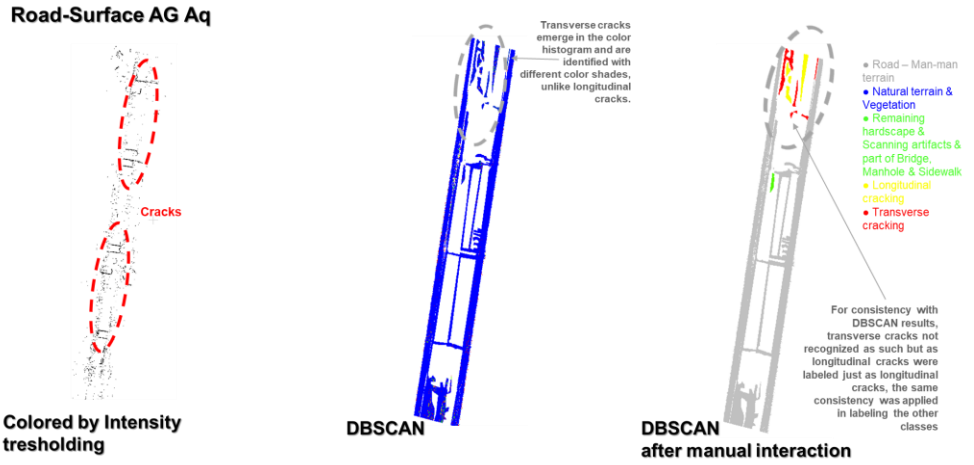


Figure 6.7Application of DBSCAN AG without normalised intensity on datasets from GeoSLAM ZEB HORIZON.

Table 6.2: Validation results from the comparison between the DBSCAN AG without intensity normalization and the ground truth (GT).

	TP	FP	FN	Precision	Recall	F1-Score
Mad Terrain & Road	8	866	7	0.009	0.533	0.017
Natural terrain & Vegetation	10	0	1130	0.998	0.008	0.017
Remaining hardscape & Scanning artifacts	12	33	140	0.266	0.078	0.121
Longitudinal cracking	4	44	105	0.083	0.036	0.050
Transversal cracking	-	-	-	-	-	-
Overall accuracy	71%					

Regarding the overall performance, the DBSCAN algorithm achieved an accuracy of 71%. However, there were a significant number of false positives, especially in the crack class, and many false negatives were

classified as vegetation. The misclassification of cracks as vegetation, despite the absence of actual vegetation in the dataset, suggests potential issues with the algorithm's sensitivity to small features or noise within the data. These points to the need for further refinement and adjustment of the algorithm's parameters to enhance classification accuracy.

Normalized intensity was applied to the DBSCAN algorithm for both the BE and AG datasets, as shown in Figure 6.8 (Top for BE and Bottom for AG). Visually, it is worth noting that DBSCAN may face challenges in generating clusters when working with point clouds that have normalized intensity. In particular, it becomes more difficult for DBSCAN to identify distinct clusters in areas where the intensities are similar.

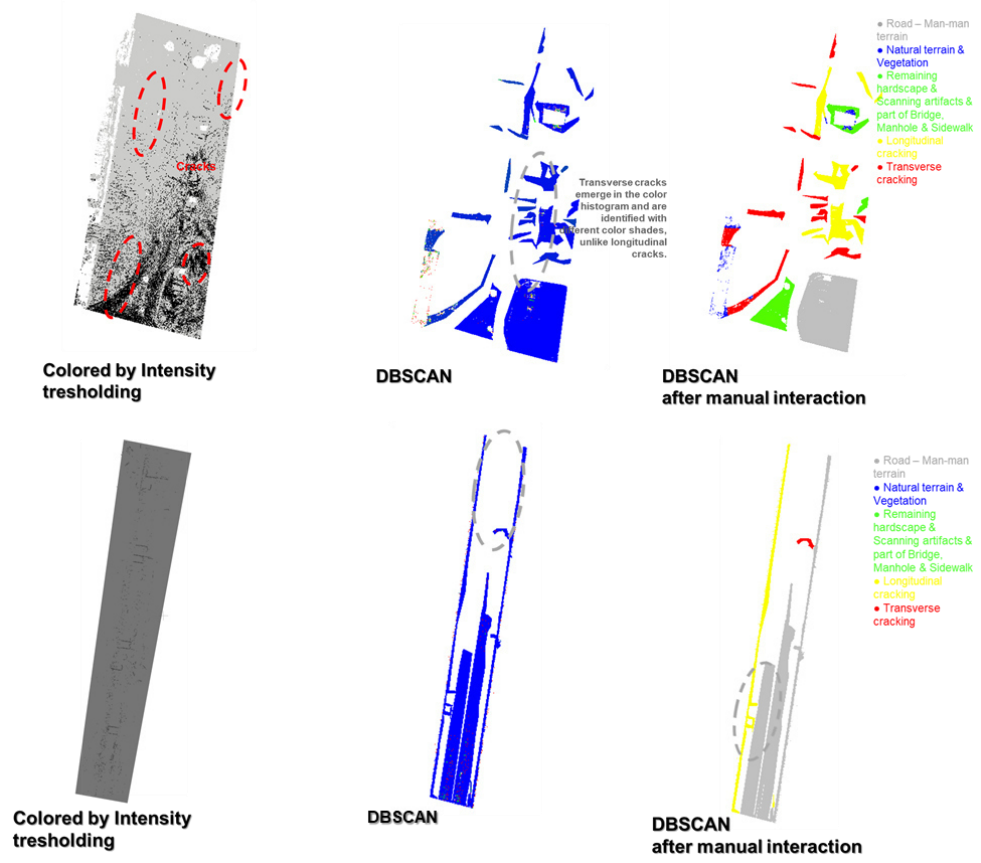


Figure 6.8: Results of applying normalized intensity to the DBSCAN algorithm for BE datasets (top) and AG datasets (bottom).

As observed in the colour histogram, transverse cracks emerge and are identified by distinct coloUr shades, unlike longitudinal cracks. After manual interaction, for consistency with the DBSCAN results, the few transverse cracks that were misclassified as longitudinal cracks were

relabelled as longitudinal cracks. This approach was consistently applied to the labelling of other classes as well.

Table 6.3: Quantitative results of applying normalized intensity to the DBSCAN algorithm for BE and AG datasets.

	TP	FP	FN	Precision	Recall	F1-Score
Mad Terrain & Road	254	151	2440	0.627	0.094	0.163
Natural terrain & Vegetation	53	30	411	0.638	0.114	0.193
Remaining hardscape & Scanning artifacts	63	156	479	0.287	0.116	0.165
Longitudinal cracking	30	249	227	0.107	0.116	0.111
Transversal cracking	4	306	191	0.012	0.020	0.015
Overall accuracy			30%			

	TP	FP	FN	Precision	Recall	F1-Score
Mad Terrain & Road	4	620	9	0.006	0.307	0.012
Natural terrain & Vegetation	0	0	1147	NaN	0.000	NaN
Remaining hardscape & Scanning artifacts	0	205	154	0.000	0.000	NaN
Longitudinal cracking	0	12	109	0.000	0.000	NaN
Transversal cracking	-	-	-	-	-	-
Overall accuracy			42%			

As detailed in Tables 6.3, DBSCAN applied to the BE dataset achieved an overall accuracy of 30%, while DBSCAN applied to the AG dataset achieved an accuracy of 42%. In both cases, no transverse cracks were identified, and a high number of false positives and false negatives again characterized the results. Additionally, RF was applied to the Bare Earth dataset, resulting in an improvement in overall accuracy compared to DBSCAN. In addition, the analysis of data collected using the GeoSLAM ZEB HORIZON revealed significant differences in the performance of the RF method. Without intensity normalization, the overall accuracy reached 98%, whereas with intensity normalization, the accuracy decreased slightly to 95%.Despite the high overall accuracy, the Random Forest model was unable to identify labels related to longitudinal and transverse cracks accurately. Both crack types exhibited 0 false positives, indicating a lack of precision in distinguishing and classifying these specific features. These results are illustrated in Figure 6.9 and detailed in Table 6.4.

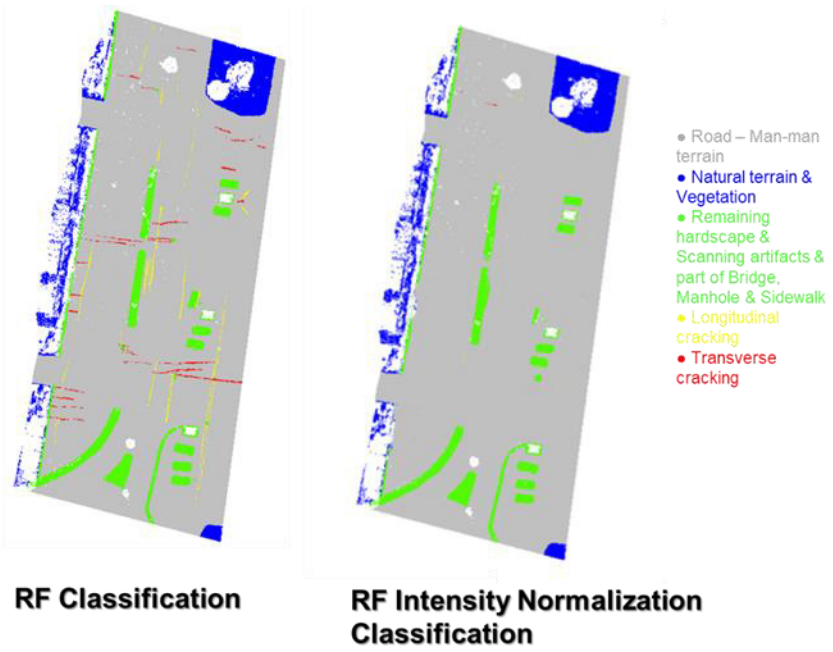


Figure 6.9: Application of RF on the left without normalized intensity and on the right with normalized intensity on BE dataset from GeoSLAM ZEB HORIZON.

Table 6.4: Validations obtained by comparing the two point clouds from BE RF without (top) and with (bottom) normalized intensity and the GT, respectively.

	TP	FP	FN	Precision	Recall	F1-Score
Mad Terrain & Road	2902	6	0	0.997	1.000	0.998
Natural terrain & Vegetation	584	0	0	1.000	1.000	1.000
Remaining hardscape & Scanning artifacts	514	0	36	1.000	0.934	0.966
Longitudinal cracking	279	17	0	0.942	1.000	0.970
Transversal cracking	220	19	0	0.920	1.000	0.958
Overall accuracy	99%					

	TP	FP	FN	Precision	Recall	F1-Score
Mad Terrain & Road	2902	1042	0	0.735	1.000	0.847
Natural terrain & Vegetation	511	30	73	0.944	0.875	0.908
Remaining hardscape & Scanning artifacts	55	0	495	1.000	0.100	0.181
Longitudinal cracking	0	0	279	NaN	0.000	NaN
Transversal cracking	1	0	219	1.000	0.004	0.009
Overall accuracy	95%					

Finally, RF method was also applied to the AG dataset, demonstrating high overall accuracy. Without intensity normalization, the model achieved an overall accuracy of 99%, while with intensity normalization, the accuracy decreased to 95%. However, despite the high overall accuracy, a notable

observation is the misclassification of cracking classes. Specifically, true positives for cracks without intensity normalization were classified as false negatives when intensity normalization was applied. This discrepancy could potentially be attributed to the impact of normalization on the distribution of intensity values, which might obscure subtle differences that are critical for distinguishing crack-related features from other classes. These findings highlight the sensitivity of the RF model to the input feature set and underscore the need for careful consideration of preprocessing steps, particularly when dealing with normalized intensity values. The results are visualized in Figure 6.10 and summarized in Table 6.5.

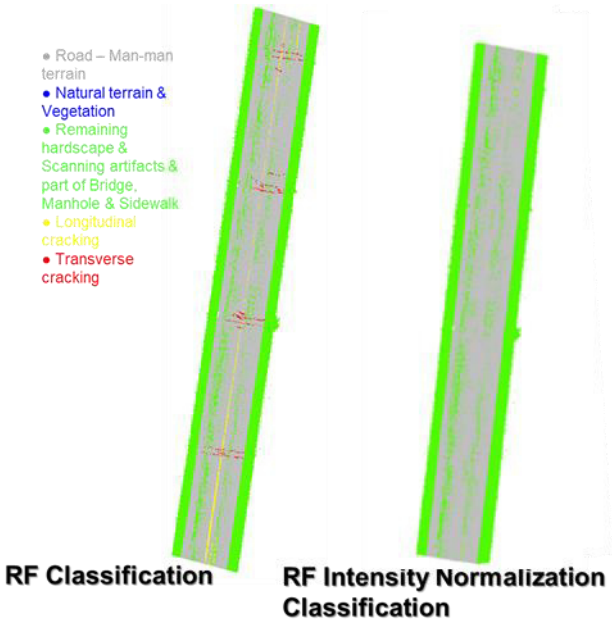


Figure 6.10: Application of RF on the left without normalized intensity and on the right with normalized intensity on AG dataset from GeoSLAM ZEB HORIZON.

Table 6.5: Validations obtained by comparing the two point clouds from AG RF without (top) and with (bottom) normalized intensity and the GT, respectively.

	TP	FP	FN	Precision	Recall	F1-Score
Mad Terrain & Road	14	92	0	0.132	1.000	0.233
Natural terrain & Vegetation	-	-	-	-	-	-
Remaining hardscape & Scanning artifacts	1054	28	95	0.974	0.917	0.944
Longitudinal cracking	154	0	0	1.000	1.000	1.000
Transversal cracking	109	0	0	1.000	1.000	1.000
Overall accuracy	99%					

	TP	FP	FN	Precision	Recall	F1-Score
Mad Terrain & Road	14	1045	0	0.013	1.000	0.026
Natural terrain & Vegetation	-	-	-	-	-	-
Remaining hardscape & Scanning artifacts	363	29	786	0.926	0.315	0.471
Longitudinal cracking	0	0	154	NaN	0.000	NaN
Transversal cracking	0	0	109	NaN	0.000	NaN
Overall accuracy	95%					

6.4 Analysis of Crack Detection in Point Cloud Data

In view of the results obtained, the detection of cracks in point cloud data is a critical task for assessing the condition of roads and infrastructure. Point cloud datasets, typically acquired through LiDAR or mobile mapping systems, provide high-resolution spatial information, enabling detailed analysis of structural surfaces. However, accurately identifying cracks in such datasets poses significant challenges due to surface complexity, noise, and data gaps. Both DBSCAN and RF were applied to datasets representing BE and AG surfaces. The results demonstrate the effectiveness and limitations of the approaches, particularly when intensity normalization is applied.For the BE dataset (Figure 6.11), Random Forest without intensity normalization achieved excellent performance. For longitudinal cracks, the model detected most cracks with high precision, recall, and F1-score. Similarly, transverse cracks were detected with high precision, recall, and F1-score. The Poisson method in CloudCompare was used to calculate the surface area, with the results closely matching the ground truth values for both longitudinal and transverse cracks. Despite a small number of false positives in both cases, the visual representation shows well-defined cracks, closely aligned with the ground truth.Conversely, Random Forest with intensity normalization was ineffective in detecting cracks in the BE dataset. For longitudinal cracks, the model failed to identify any true positives, while for transverse cracks, only one crack was detected, resulting in high precision but low recall. Visually, the results were sparse or empty, with only one transverse crack visible.

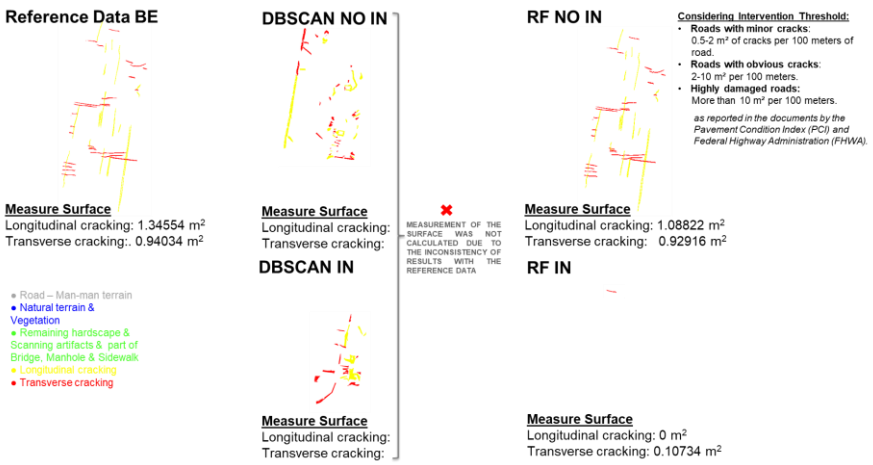


Figure 6.11: Quantitative estimation of crack surface for BE.

For the AG dataset (Figure 6.12), Random Forest without intensity normalization performed perfectly, accurately identifying all longitudinal and transverse cracks with excellent precision and recall. The measured surface areas closely matched the ground truth values. The visual representation showed precise crack detection with no false positives. In contrast, when intensity normalization was applied, Random Forest failed to detect any cracks. For both crack types, no true positives were identified, and the visual representation showed no cracks.

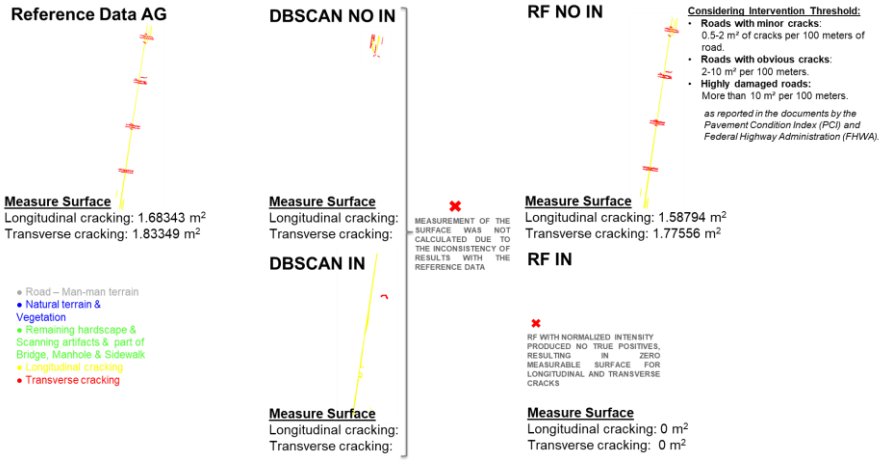


Figure 6.12: Quantitative estimation of crack surface for AG.

On the other hand, for DBSCAN, the results were less consistent across both BE and AG datasets. The clustering algorithm showed sensitivity to intensity variations, especially when normalized datasets were used, leading

to unreliable identification of cracks. As a result, the measurement of the surface was not calculated due to the inconsistency of results with the Reference Data. These results highlight the sensitivity of RF to intensity normalization, where normalization can negatively impact performance in certain datasets. On the other hand, RF without intensity normalization demonstrated robust and reliable crack detection across both BE and AG surfaces, achieving high precision and recall.

6.5 Conclusion and Future Studies

This study underscores both the potential and challenges associated with SLAM-based systems such as the GeoSLAM ZEB HORIZON and the Leica BLK2GO. While SLAM is invaluable for detailed three-dimensional reconstruction of infrastructure, certain limitations emerged in the context of crack detection. Specifically, the Leica BLK2GO was not explored in depth due to its shorter range compared to the GeoSLAM ZEB HORIZON, which proved more suitable for infrastructure-scale datasets. The GeoSLAM ZEB HORIZON delivered the best results when paired with Random Forest without intensity normalization, achieving higher Precision and Recall for crack detection. However, the same method performed poorly or even failed entirely with intensity normalization, reflecting the sensitivity of the algorithm to preprocessing inconsistencies. Similarly, DBSCAN struggled with the GeoSLAM data, yielding unreliable results for crack detection. These findings highlight the importance of refining preprocessing techniques, such as improving intensity normalization to ensure data consistency, and exploring alternative algorithms tailored to the unique characteristics of SLAM-based datasets. Challenges encountered during this study, such as noise and data completeness issues inherent to GeoSLAM data, restricted the scope of advanced analyses, including the calculation of crack surface areas. Addressing these challenges requires targeted noise reduction strategies and preprocessing pipelines optimized for SLAM-derived point clouds. Future research should investigate innovations in ML and DL, leveraging advanced models to enhance crack detection and

classification in noisy or incomplete datasets. Improved methodologies are expected to extend crack characterization capabilities, enabling accurate surface area calculation, depth estimation, and the analysis of additional parameters for a comprehensive evaluation. Furthermore, this study demonstrates the utility of RF and DBSCAN for crack detection while emphasizing the need to adapt these methods to better suit SLAM-acquired point cloud data. The insights gained lay a foundation for refining existing methodologies, overcoming observed limitations, and ultimately advancing the accuracy and reliability of crack detection in diverse applications.

7. FOURTH CASE STUDY: CONCRETE SPECIMEN CRACK IDENTIFICATION

The following publication served as the source for the information in this chapter:

Pascucci, N., Alicandro, M., Zollini, S., Dominici, D. (2024). Improving Infrastructure Monitoring: UAV-Based Photogrammetry for Crack Pattern Inspection. In: Arai, K. (eds) Proceedings of the Future Technologies Conference (FTC) 2024, Volume 1. FTC 2024. Lecture Notes in Networks and Systems, vol 1154. Springer, Cham. https://doi.org/10.1007/978-3-031-73110-5_24

7.1 CHAPTER ABSTRACT

Infrastructure degradation, manifested in forms such as cracking and occlusions, represents a critical challenge to the structural integrity of various constructions. Effective monitoring and timely interventions are essential to mitigate the risks associated with these degradations. Geomatic techniques, particularly those based on UAV photogrammetry, present innovative solutions for the inspection of crack patterns and the assessment of structural health. This research seeks to develop a comprehensive, rapid, and replicable methodology for the inspection of crack patterns that can be applied across different materials and structural types. The initial focus of this study is on reinforced concrete, a widely used material in construction, due to its susceptibility to various forms of degradation, including cracking. The aim is to optimize the inspection process by leveraging automatic and

semi-automatic methods, reducing manual effort while ensuring high accuracy in crack detection. UAV-based photogrammetry plays a crucial role in this methodology, as it provides detailed, high-resolution, and panoramic imagery that can be used to identify cracks and assess the overall health of structures. The proposed methodology involves several steps: the photogrammetric reconstruction of structural specimens, followed by the extraction of orthophotos for further analysis. Edge enhancement filtering techniques are applied to improve the visibility of cracks, facilitating more detection that is accurate. Additionally, Object-Based Image Analysis (OBIA) is employed for the automatic classification and extraction of cracks, streamlining the analysis process. The effectiveness of specific filters, such as Enhanced Frost and Median filters, is critically evaluated within the context of improving crack detection. Preliminary results suggest that these filters contribute positively to refining the identification of cracks, although further refinement of the methodology and additional testing are required to fully optimize the process. Ultimately, the proposed methodology has the potential to establish a rapid, efficient, and easily replicable system for monitoring the condition of infrastructures, with significant implications for improving safety, enhancing sustainability, and ensuring the longevity of critical structures. The integration of UAV photogrammetry, advanced image processing, and automated analysis techniques presents a promising direction for future advancements in infrastructure monitoring.

7.2 INTRODUCTION

Infrastructure is a critical element that supports various human activities, serving as the backbone for urban development, transportation, and essential services. However, over time, infrastructure is subjected to a range of degradation factors that can undermine its structural integrity and functionality. Among the most pressing risks associated with the deterioration of infrastructure, cracking and occlusions stand out as major concerns. These issues can compromise the safety and usability of

structures, highlighting the need for effective monitoring and timely interventions to prevent further damage and ensure long-term stability (Detchev, I. et al. 2012; Pascucci N. et al. 2023). The need for efficient methodologies that enable rapid, accurate, and detailed inspection of crack patterns in structural elements is increasingly evident within the realm of civil engineering. Such methodologies are essential for guaranteeing the safety and durability of buildings and infrastructures, which are not only vital for the functioning of modern society but also, contribute to the sustainability of urban environments and the well-being of citizens (Mishra M. et al., 2022). In this context, geomatic techniques, particularly those leveraging UAV photogrammetry, have emerged as promising tools for the development of efficient and reproducible investigation methodologies. These advanced techniques offer significant advantages due to their flexibility and wide applicability, making them ideal for monitoring various types of materials and structural forms. By facilitating the collection of high quality, detailed imagery, UAV photogrammetry offers innovative and highly effective solutions for ongoing infrastructure assessment and maintenance (Jofré-Briceño C et al., 2021; Albeaino G et al., 2019). Previous studies have demonstrated the potential of digital image processing in crack detection, as it mimics human visual capabilities while providing a level of precision and scalability that manual inspections cannot achieve. Among the commonly employed techniques for identifying crack boundaries in digital images, edge detection is a widely recognized method. This technique highlights the contrast between cracks and the surrounding homogeneous background, making it a crucial step for the accurate identification of crack patterns in RGB images (Yamaguchi T. et al., 2008). Recent research has extensively examined various image processing techniques for crack detection, underscoring the significant advancements brought about by the integration of both terrestrial and UAV photogrammetry with computer vision technologies. These combined methodologies have opened up new possibilities for rapid, efficient, and safe infrastructure inspections. The resulting high-quality imagery facilitates the creation of precise 3D models, mesh models, and orthophotos, which

can be used for detailed analysis and monitoring of the observed structures (Greenwood, W.W et al., 2019; Angeli S. et al., 2019; Berrett B.E., 2021; Alicadro M. et al., 2023). A range of image processing algorithms has been explored for crack detection, each with distinct strengths and limitations. Among these, CNNs have gained considerable attention due to their ability to classify images and detect cracks effectively. While CNNs have proven to be highly effective in detecting and categorizing structural degradation, their performance is heavily reliant on the availability of large datasets for training, which can be a time-consuming and resource-intensive process (Kim H. et al., 2019; Dung C.V. et al., 2019; Dais D. et al., 2021). OBIA techniques, on the other hand, focus on segmenting and analyzing images at the object level, providing a powerful alternative for crack detection. OBIA has shown promise in enhancing the precision of crack identification by considering the spatial relationships and context of image elements, allowing for more robust segmentation and classification of cracks (Fernandez Galarreta J., 2015; Rau J.Y., 2017) . Edge detection algorithms, which have long been utilized for crack detection, remain one of the most widely applied methods. These algorithms are particularly useful for highlighting the boundaries and edges of cracks in images, making them an essential tool for identifying and delineating cracks in both simple and complex structural conditions (Abdel-Qader I., et. Al., 2003; Cha Y.J., 2017). By comparing these different approaches, it is possible to assess the advantages and disadvantages of each algorithm. For example, studies utilizing Convolutional Neural Networks (CNNs) have demonstrated their effectiveness in classifying images and detecting cracks, but they require thorough training, which can be resource-intensive (Cha Y.J. et al., 2017; Kim B. et al., 2021). On the other hand, Object-Based Image Analysis (OBIA) techniques have shown promise in segmenting and analyzing images based on object-level information, offering an alternative that takes spatial context into account (Li X. et al., 2014; Gui R., 2019). Additionally, edge detection algorithms have been widely employed for crack detection due to their ability to highlight boundaries and edges in images, making them an essential tool for visualizing crack patterns (Zou Q., et al., 2012;

Dorafshan S. et al. 2018). The objective of this research is to provide an objective and in-depth analysis of the risks associated with the structural degradation of infrastructure, with a particular focus on the study of cracks. Cracks, which are a common phenomenon in concrete structures and various forms of civil infrastructure, can arise due to a range of factors, including excessive loads, ground movement, environmental conditions, and construction defects. When left unaddressed or inadequately repaired, these cracks can have severe consequences, including a reduction in the load-bearing capacity of the structure, the progressive spread of structural damage, and, in extreme cases, the potential collapse of the infrastructure. Effective crack monitoring is crucial for identifying the onset of damage at an early stage, enabling a timely assessment of its progression over time. Such monitoring allows for the implementation of appropriate corrective actions, thereby preventing further deterioration and more serious structural failures. The present study aims to develop a rapid, efficient, and reproducible methodology for inspecting crack patterns, with the goal of creating a system that can be applied across a wide variety of materials and structural types. The research begins with a preliminary analysis of reinforced concrete, a material widely used in infrastructure, as a case study. This provides a foundation for understanding the characteristics and behaviors of cracks in concrete structures. The overarching aim of the research is to consolidate and optimize the crack inspection process by prioritizing automatic or semi-automatic techniques. This will enhance the efficiency and accuracy of the methodology, and the findings will be further extended and refined to ensure the applicability of the system to other materials and structural conditions. This approach not only aims to refine the methodology for crack detection but also seeks to adapt it to the specific requirements and challenges posed by different types of infrastructure and materials. By developing a versatile and scalable system, the research aims to contribute to the broader field of infrastructure monitoring, with significant implications for the safety, durability, and sustainability of critical built environments. The overarching goal of this research is to develop a rapid, efficient, and easily replicable infrastructure monitoring

system that can significantly enhance the safety and sustainability of our building heritage. To achieve this, UAV-based photogrammetry emerges as a highly suitable survey methodology for inspecting crack patterns in various structures. By utilizing drones equipped with high-resolution cameras and sensors, it is possible to capture detailed and panoramic images of the area of interest. These images enable the swift identification of cracks and provide valuable insights into the overall health and stability of the structure. The use of UAV-based photogrammetry for crack pattern inspection offers several distinct advantages over traditional inspection methods. One of the primary benefits is that it enables non-invasive inspection, which not only minimizes the risk of causing any further structural damage but also ensures the safety of operators, as drones can operate from a distance without the need for direct physical interaction with the structure (Alotaibi M. et al., 2021). Furthermore, the rapid data acquisition facilitated by UAV photogrammetry allows for the collection of detailed information in much shorter timeframes compared to conventional techniques. This expedites the identification of potential issues and provides a clear foundation for timely interventions. Such efficiency is particularly valuable in the scheduling of maintenance and repair activities, enabling more effective resource allocation and prioritization of structural repairs, ultimately contributing to the preservation and longevity of infrastructure (Nooralishahi P. et al. 2021). For these reasons, UAV-based photogrammetry, due to its inherent flexibility and adaptability to a wide range of environmental conditions and structural types, proves to be a versatile and highly effective solution for inspecting crack patterns. Its ability to adapt to different settings makes it an invaluable tool for comprehensive infrastructure monitoring, thereby significantly contributing to the maintenance of safety, durability, and long-term sustainability of critical infrastructure (Plevris V. et al., 2024). In light of the considerations outlined above, this paper proposes a structured framework that encompasses the entire process, from the investigation of a specific case study to the final processing and extraction of the detected cracks. This comprehensive approach aims to provide a reliable, repeatable methodology

for crack detection that can be applied across various types of infrastructure, ensuring that the inspection process is both effective and scalable.

7.3 MATERIALS AND METHODS

A survey was conducted on a specially prepared concrete sample using a UAV system. The following subsections provide details on the specifications of the UAV system used, the dataset acquired, and the study site.

7.3.1 DATA ACQUISITION SYSTEMS

Given the imperative for the study to acquire data swiftly, and safely, and employing non-destructive techniques, the data acquisition activities were executed utilizing a UAV DJI Matrice 200 (Figure 7.1) equipped with a Zenmuse X5S camera (Figure 7.2), the specifications of which are delineated in Figure 1. The survey was meticulously planned, with a flight altitude set at 5 meters and an 80% image overlap. A total of 32 images were acquired during the survey process. Furthermore, to augment the precision of the data acquisition, 15 points were demarcated with targets and captured using an RTK (Real Time Kinematic) GNSS GS15 receiver, harnessing the Hexagon Smartnet network of Permanent Stations. This comprehensive approach ensured the expeditious, secure, and non-destructive acquisition of data essential for the study's objectives.



Model	DJI Matrice 200 V2
Tipology	Quadricopter
Weight at takeoff	734 g
Autonomy	27 min
Operating altitude	5000 m

Figure 7.1: Image and technical specifications of the UAV used in this work.



Model	Zenmus e X5S
Focal lenght	15 mm
Photo size - Width	5280 px
Photo size - Height	3956 px
Sensor dimensions - Width	18 mm
Sensor dimensions - Height	13.5 mm
Weight	461 g

Figure 7.2: image and technical specifications of the Zenmuse X5S used in this work.

7.4 CASE OF STUDY

Experiments on crack analysis and crack detection were conducted with a case study at a construction site in L'Aquila, Italy, using reinforced concrete specimens specially created by a construction company, as shown in Figure 7.3.



Figure 7.3: Reinforeced concrete specimen used for testing.

The methodology employed in this study begins with the photogrammetric reconstruction of the specimen using images acquired from a UAV, employing a photogrammetric approach based on Structure from Motion algorithms. Following the generation of the 3D model, the orthophoto of the area of interest is extracted and subjected to a filtering process aimed at enhancing the definition of crack edges. Subsequently, considering insights from previous studies on identifying degradation patterns in reinforced concrete pillars (Zollini S. et al., 2020), the OBIA classification is utilized in this initial phase for the automatic extraction of the crack framework, as illustrated in the workflow outlined in Figure 7.4.

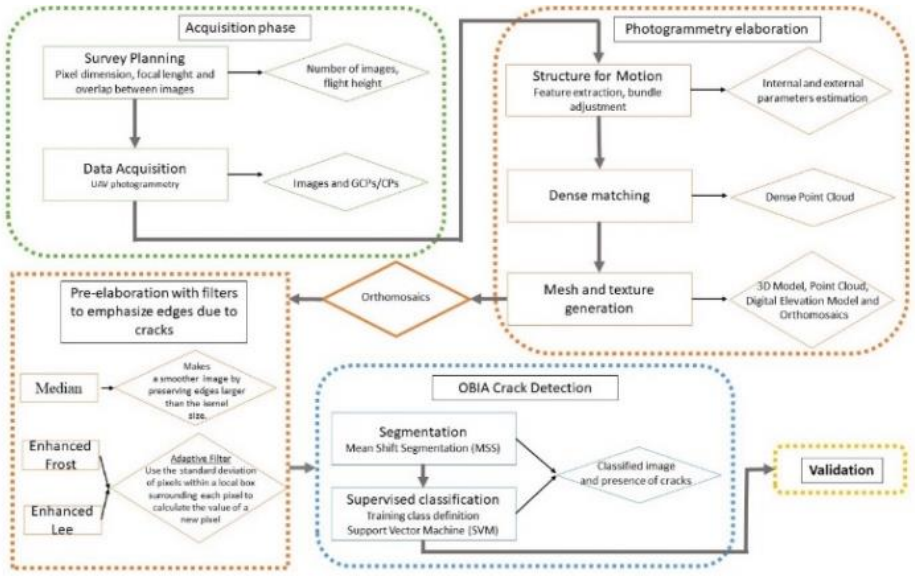


Figure 7.4: Workflow applied from the initial acquisition phase, through photogrammetric processing for orthophoto generation and the subsequent application of filters and OBIA classification, up to the final validation phase.

7.4.1 PHOTOGRAMMETRIC PROCESSING

In the initial phase of the study, acquired images underwent photogrammetric processing utilizing Agisoft Metashape software. Initially, automatic image alignment was performed, followed by the import of Ground Control Points (GCPs) and Check Points (CPs) strategically positioned within the construction area, as depicted in Figure 7.5.

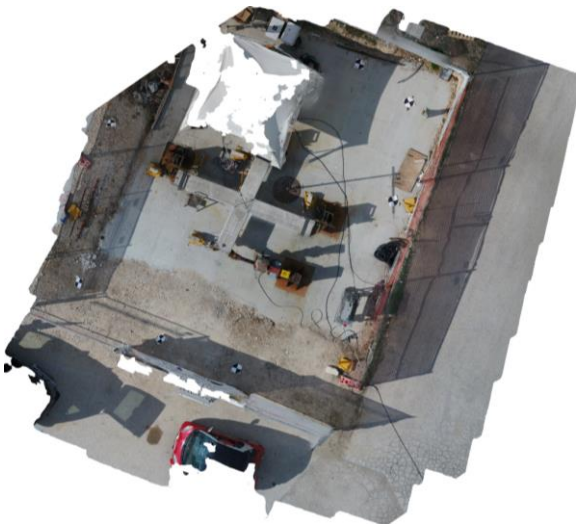


Figure 7.5: Orthomosaic of the entire site scene with the reinforced concrete specimen used for the test (processed with Agisoft Metashape Software).

Subsequently, a final bundle adjustment was executed to obtain the ultimate estimation of internal and external orientation parameters. Upon completion of this process, the sparse point cloud was densified using Dense Matching procedures, and the final model was generated through textured mesh creation. From this 3D model, an orthophoto was extracted specifically focusing on the central node of the specimen (ROI), where the majority of cracks were observed (refer to Figure 7.6).



Figure 7.6: Orthomosaic of the chosen ROI at the node of the reinforced concrete specimen used following the compression test, characterized by cracking (processed with Agisoft Metashape software).

To improve the automatic extraction of cracks for subsequent classification, filters were applied to the orthophoto to accentuate the edges of the cracks, which are the focus of this study. The filters are *Enhanced Lee*, *Enhanced Frost* and *Median* already described in Chapter 2.

The application of these filters yielded the following results:

- *Median*, the filter makes an image smoother, as shown in Fig. 7.7;
- *Enhanced Lee*, Adaptive filter using enhanced Lee filters, in Fig. 7.8;
- *Enhanced Frost* uses adaptive Frost filters, a result in Fig. 7.9.



Figure 7.7: Application of Median filter algorithm on the ROI (processed with ENVI software).



Figure 7.8: Application of Enhanced Lee filter algorithm on the ROI (processed with ENVI software).



Figure 7.9: Application of Enhanced Frost filter algorithm on the ROI (processed with ENVI software

7.4.2 OBIA CLASSIFICATION

Subsequently, following the application of filters to emphasize the cracks, the Object-Based Image Analysis (OBIA) technique was employed. OBIA is a supervised classification method that allows for the analysis and classification of images by leveraging not only the radiometric information of individual pixels, as is the case with pixel-based approaches, but also considers the spatial (dimensions, mutual distances, number of pixels per object, etc.) and topological information of the objects to be classified (Blaschke T., 2010). This approach facilitates a more comprehensive understanding and classification of features within the image dataset, particularly beneficial for delineating and characterizing complex features such as cracks. The OBIA analysis comprises two stages: segmentation and classification (Reddy G.O. et al., 2018). During segmentation, vector objects are created, consisting of groups of neighbouring pixels that share similar characteristics (such as brightness, colour, and texture). This process occurs from bottom to top: starting from individual pixels, similar pixels are grouped to form objects until predefined homogeneity criteria are met (Jin X., 2012). This systematic segmentation process allows for the creation of meaningful and homogeneous objects from the image data, laying the foundation for subsequent classification tasks. Once the vectors composed of pixels with similar characteristics are defined, they undergo supervised classification, where the operator defines training classes. Both the original orthophoto and the orthophotos processed with filters underwent OBIA classification, implemented using Envi software. The segmentation phase is based on the "watershed transform" approach, a principle derived from the concept of hydrological basins (Roerdink J.B.T.M. et al., 2000). The result is an image divided into various segments, with each region identified by the algorithm assigned the average spectral values of all pixels within that region. Subsequently, these segments underwent supervised classification, initially creating training classes and defining the classification algorithm. The various segments were subsequently subjected to supervised classification, initially creating training classes and defining the

classification algorithm. Considering the presence of other elements in the study area (e.g., transducers, shadow zones, etc.), five training classes were defined: concrete, cracks, transducers, areas external to the specimen, and others (shadows and various types of noise). Among the different classification algorithms, based on previous tests conducted in another study (Alicandro M. et al., 2023), the Support Vector Machine (SVM) was chosen over the K Nearest Neighbor and Principal Component Analysis (PCA). This decision was made because the other algorithms showed a greater tendency to generate noise in classification and to cause confusion, especially in crack detection. Conversely, SVM is a supervised classification method derived from statistical learning theory, which separates classes with a decision surface that maximizes the margin between classes. This surface is often referred to as the optimal hyperplane, and the data points closest to the hyperplane are called support vectors (Chang C.-C. et al., 2011). This selection of SVM ensures robust classification performance and minimizes the risk of misclassification, which is particularly crucial for the accurate identification of cracks among other elements in the image dataset.

7.5 EXPERIMENTAL RESULTS

In this section, the results obtained are presented from OBIA classification on untreated and filter-treated ROIs are discussed in detail.

7.5.1 OBIA CLASSIFICATION + FILTER RESULTS ON ROI

The results of the OBIA classifications conducted on the original orthophoto and the orthophoto processed with the Median, Enhanced Lee, and Enhanced Frost filters are presented in Figures 7.10, 7.11, 7.12 and 7.13, respectively. These figures provide a comparative analysis of the results, showing the effectiveness of each filter in delineating the features of interest, particularly cracks, within the image set. Further examination of

these results sheds light on the performance and suitability of each filter in improving feature detection and classification accuracy.

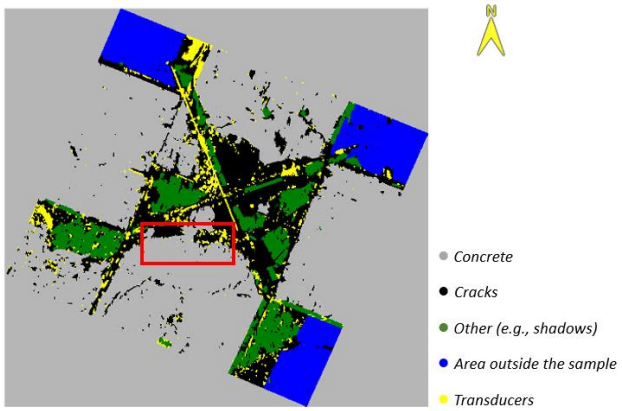


Figure 7.10: OBIA classification on the unprocessed orthophoto. The red box represents a sample area where a crack can be identified.

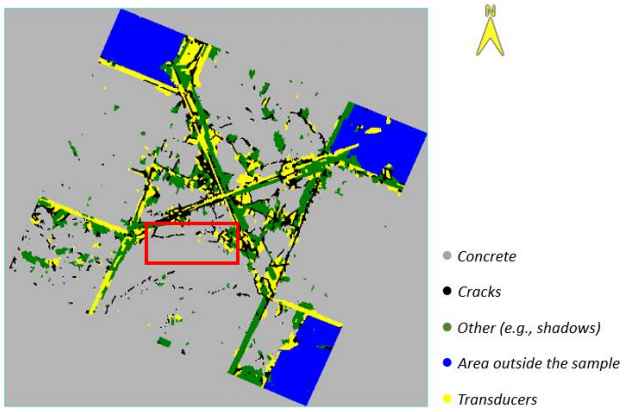


Figure 7.11: OBIA classification on the orthophoto with Median filter. The red box represents a sample area where the improvement in crack identification can be observed. The crack is highlighted within the red box, demonstrating how the application of the Median filter has enhanced the ability to identify cracks in the ROI.

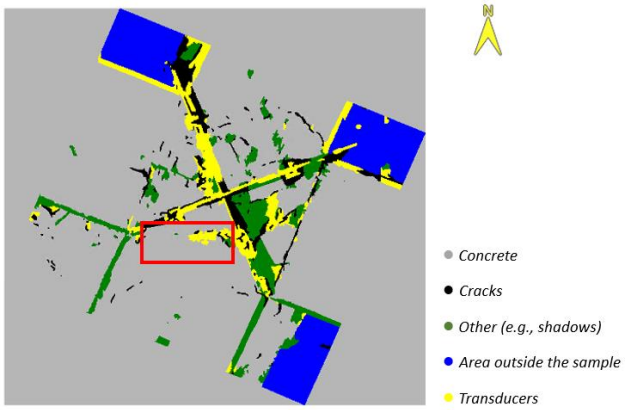


Figure 7.12: OBIA classification on the orthophoto with Enhanced Lee filter. The red box represents the same sample area considered where the identification of cracks can be observed with the application of the Enhanced Lee filter.

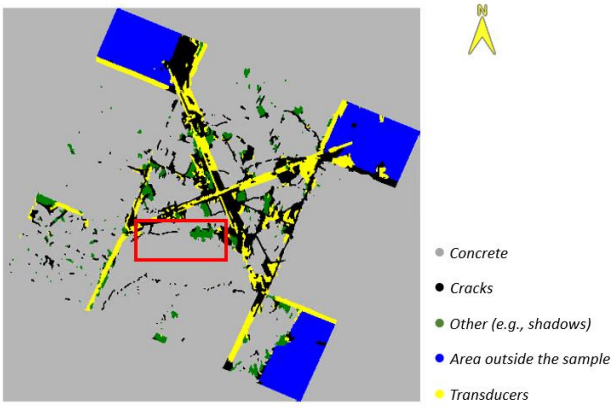


Figure 7.13: OBIA classification on the orthophoto with Enhanced Frost filter. The red box represents the same sample area considered where the identification of cracks can be observed with the application of the Enhanced Frost filter.

Despite the noise in the image, mainly caused by the transducers and the shaded areas in the central part, the initial visual estimation reveals an improvement in the detection of cracks within the highlighted region (enclosed by the red box) with the application of the Median and Enhanced Frost filters compared to the use of the Enhanced Lee filter and the untreated orthophoto. The results of the tests conducted thus visually demonstrated the ability of some filters to detect cracks and facilitated an improvement in the OBIA classification stage. In addition, to validate the result obtained, comparisons were made between the classifications obtained from the various orthophotos and the Ground Truth (GT) based on visual inspections performed on-site.

7.6 DISCUSSION

This section presents the validation of the obtained results through comparisons with the GT, obtained via visual extraction by the concrete expert, both qualitatively, as discussed in the first part, and quantitatively, as described in the second part. Through this comprehensive validation process, the reliability and accuracy of the classification outcomes are thoroughly assessed, ensuring robustness in the identification and characterization of cracks within the imagery dataset. As mentioned earlier,

the objective of this study was to evaluate the applicability of specific filters using the OBIA method on a metric orthophoto to extract and analyse the cracks induced on the concrete specimen. To achieve this goal, the focus was initially on isolating crack data to ensure a match between reference data and obtained results. As demonstrated in various studies (Kalfarisi R. et al., 2020; Sheng G.W. et al., 2023), the Jaccard similarity coefficient (Jaccard P., 1901, Jaccard P., 1912) was applied initially to provide an initial assessment of the results obtained regarding crack identification. The Jaccard index facilitates the comparison of the intersection between the classified cack areas and the GT crack areas with the union of these areas, thus quantifying the degree of overlap or agreement between them. This quantitative evaluation method offers valuable insights into the accuracy and reliability of the crack identification process conducted through the OBIA classification. The formula for the applied Jaccard similarity coefficient has already been described in Chapter 3 and is defined as the size of the intersection divided by the size of the union of the sample sets. Jaccard's index revealed that for the cracks, of which 65 were detected, the classifications with the Median and Enhanced Frost filters yielded superior results compared with the use of the Enhanced Lee filter and the untreated orthophoto, as shown in Table 7.1.

Table 7.1: PERCENTAGE OF CRACKS OBTAINED AS A RESULT OF THE JACCARD SIMILARITY COEFFICIENT IDENTIFIED IN EACH CLASSIFICATION.

	GT	ROI	Enhanced LEE	Enhanced FROST	MEDIAN
Number of cracks	65	24	32	61	52
Match after Jaccard Index		37%	49%	94%	80%

Following this, a final analysis was conducted on the 65 cracks filtered from the results and individually extracted to calculate the percentage area of each recognized crack from the classification on each filter and the unprocessed ROI, as shown in Table 7.2, depicting the areas of each crack and Table 7.3 the detection percentage, respectively. The not processed ROI

produced lower recognition values than the filters, while the Frost filter achieved higher crack detection percentages. This observation highlights the effectiveness of the Frost filter in improving crack detection and classification results in the study area.

Table 7.2: AREAS OF EACH CRACK.

ID Crack	***GT Area***	***ROI Area***	***Enhanced LEE Area***	***Enhanced Frost Area***	***MEDIAN Area***
1	0.209	0.027	NULL	NULL	0.052
2	5.58	2.093	0.616	1.755	0.492
3	5.178	2.823	1.666	3.04	2.150
4	1.344	0.066	NULL	NULL	0.345
5	9.291	0.017	NULL	2.454	2.112
6	3.826	0.427	NULL	0.14	1.042
7	3.953	NULL	2.3	3.568	3.277
8	0.757	0.122	NULL	NULL	NULL
9	0.565	NULL	NULL	0.29	NULL
10	0.696	NULL	NULL	0.673	NULL
11	4.952	NULL	1.383	1.543	1.205
12	0.741	NULL	NULL	0.353	0.14
13	1.675	NULL	1.069	1.624	NULL
14	13.429	NULL	7.6	10.686	0.616
15	3.974	NULL	0.96	2.441	NULL
16	1.507	NULL	0.175	0.66	0.076
17	10.957	2.316	1.211	4.059	1.711
18	0.388	0.122	NULL	0.08	0.017
19	0.448	0.222	NULL	0.298	0.152
20	2.619	NULL	NULL	1.798	NULL
21	4.959	NULL	2.729	2.035	NULL
22	4.393	NULL	1.001	2.451	0.348
23	1.055	NULL	NULL	0.316	0.684
24	1.57	NULL	0.155	1.318	1.322
25	2.804	NULL	2.285	2.733	2.653
26	2.004	NULL	0.486	1.199	0.742
27	0.676	0.493	NULL	0.658	0.649
28	0.836	0.433	NULL	0.452	0.275
29	0.771	0.421	NULL	0.326	0.116
30	1.653	1.144	NULL	1.647	1.207
31	0.959	0.279	NULL	0.129	0.19
32	1.012	NULL	0.082	0.426	0.557
33	2.607	NULL	1.711	2.307	2.409
34	0.969	NULL	NULL	0.638	0.452
35	1.191	NULL	NULL	1.123	1.058
36	1.772	NULL	1.181	1.289	1.092
37	1.56	NULL	NULL	0.559	0.539
38	0.329	NULL	NULL	0.052	0.052
39	0.535	NULL	NULL	0.026	0.186
40	2.256	NULL	2.025	1.069	1.841
41	1.086	0.343	NULL	0.523	0.603
42	1.101	0.107	NULL	0.574	0.761
43	0.779	0.051	NULL	0.241	0.423
44	4.497	NULL	1.263	1.666	2.182
45	1.688	1.632	0.996	1.479	1.33
46	2.034	NULL	NULL	1.008	1.194
47	0.284	NULL	NULL	0.229	0.269
48	1.114	NULL	0.139	0.649	0.639
49	1.096	NULL	NULL	1.058	1.023
50	2.476	NULL	0.158	1.072	1.384
51	3.208	NULL	NULL	1.661	1.432
52	2.034	NULL	0.297	1.945	NULL
53	9.85	NULL	1.423	4.335	1.883
54	0.375	NULL	0.02	0.196	NULL
55	1.827	NULL	NULL	1.481	0.623
56	0.19	NULL	NULL	NULL	0.182
57	5.748	NULL	1.432	4.802	NULL
58	4.981	0.095	1.334	1.892	2.819
59	1.807	NULL	0.836	1.309	NULL

ID Crack	***GT Area***	***ROI Area***	***Enhanced LEE Area***	***Enhanced Frost Area***	***MEDIAN Area***
60	2.306	1.176	0.641	1.093	1.116
61	0.81	0.042	NULL	0.399	NULL
62	1.064	NULL	NULL	0.107	0.107
63	0.744	0.032	0.105	0.105	NULL
64	0.496	NULL	0.076	0.378	0.424
65	0.575	NULL	0.19	0.36	0.249

Table 7.3: DETECTION PERCENTAGE OF EACH CRACK

ID Crack	***ROI %***	***Enhanced LEE %***	***Enhanced Frost %***	***MEDIAN %***
1	12.9 %	NULL	NULL	24.8 %
2	37.5 %	11.0 %	31.4 %	8.8 %
3	54.5 %	32.1 %	58.6 %	41.5 %
4	4.9 %	NULL	NULL	25.6 %
5	0.1 %	NULL	26.4 %	22.7 %
6	11.1 %	NULL	3.6 %	27.2 %
7	NULL	58.1 %	90.2 %	82.8 %
8	16.1 %	NULL	NULL	NULL
9	NULL	NULL	51.3 %	NULL
10	NULL	NULL	96.6 %	NULL
11	NULL	27.9 %	31.1 %	24.3 %
12	NULL	NULL	47.6 %	18.8%
13	NULL	63.8 %	96.9 %	NULL
14	NULL	56.5 %	79.5 %	4.5 %
15	NULL	24.1 %	61.4 %	NULL
16	NULL	11.6 %	43.7 %	5.0 %
17	21.1 %	11.0 %	37.0 %	15.6 %
18	31.4 %	NULL	20.6 %	4.3 %
19	49.5 %	NULL	66.5 %	33.9 %
20	NULL	NULL	68.6 %	NULL
21	NULL	55.0 %	41.0 %	NULL
22	NULL	22.7 %	55.8 %	79..2 %
23	NULL	NULL	29.9 %	64.8 %
24	NULL	9.8 %	83.9 %	84.2 %
25	NULL	81.4 %	97.4 %	94.6 %
26	NULL	24.2 %	59.8 %	37.0 %
27	72.9 %	NULL	97.3 %	96.0 %
28	51.7 %	NULL	54.0 %	32.8 %
29	54.6 %	NULL	42.2 %	15.0 %
30	69.2 %	NULL	99.6 %	73.0 %
31	29.0 %	NULL	13.4 %	19.8 %
32	NULL	8.1 %	42.0 %	55.0 %
33	NULL	65.6 %	88.4 %	92.4 %
34	NULL	NULL	65.8 %	46.6 %
35	NULL	NULL	94.2 %	88.8 %
36	NULL	66.6 %	72.7 %	61.6 %
37	NULL	NULL	35.8 %	34.5 %
38	NULL	NULL	15.8 %	15.8 %
39	NULL	NULL	4.8 %	34.7%
40	NULL	89.7%	47.3 %	81.6 %
41	31.5 %	NULL	48.1 %	55.5 %
42	9.7 %	NULL	52.1 %	69.1 %
43	6.5 %	NULL	30.9 %	54.3 %
44	NULL	28.0 %	37.0 %	48.5 %
45	96.6 %	59.0 %	87.6 %	78.7 %
46	NULL	NULL	49.5 %	58.7 %
47	NULL	NULL	80.6 %	94.7 %
48	NULL	12.4 %	58.2 %	57.3 %
49	NULL	NULL	96.5 %	93.3 %
50	NULL	6.3 %	43.3 %	55.9 %
51	NULL	NULL	51.7 %	44.6 %
52	NULL	14.6 %	95.6 %	NULL
53	NULL	14.5 %	44.0 %	19.1 %
54	NULL	5.3 %	52.2 %	NULL
55	NULL	NULL	81.0 %	34.0 %
56	NULL	NULL	NULL	95.7 %
57	NULL	24.9 %	83.5 %	NULL
58	1.9 %	26.7 %	37.9 %	56.5 %

ID Crack	***ROI %***	***Enhanced LEE %***	***Enhanced Frost %***	***MEDIAN %***
59	NULL	46.2 %	72.4 %	NULL
60	50.9 %	27.7%	47.3 %	48.3 %
61	5.1 %	NULL	49.2 %	NULL
62	NULL	NULL	10.0 %	10.0 %
63	4.3 %	14.1 %	14.1 %	NULL
64	NULL	15.3 %	76.2 %	85.4 %
65	NULL	33.0 %	62.6 %	43.3 %

The results show that the *Enhanced Fr*ost filter consistently outperforms both the *Enhanced Lee* and *Median* filters in the detection of cracks with different crack IDs. This suggests that the Enhanced Frost filter is particularly effective in improving the identification of cracks within the concrete specimen, however, it should be noted that some cracks have zero or missing values in all filters, which indicates difficulty in detecting cracks in certain areas or conditions one of the main causes could be the various interferences at the node (such as transducers and their shadows) occluding the cracks. Despite this, the comparison of the results with the untreated ROI reveals the improvement in crack detection achieved by applying the filters. This underlines the importance of pre-processing techniques, such as the application of filters, to improve the accuracy of crack detection through OBIA classification. Although the improvement achieved with filters was particularly notable in the case of the Frost filter as illustrated in the comparison depicted in Figure 7.4, the study proceeded to isolate and examine two individual cracks.

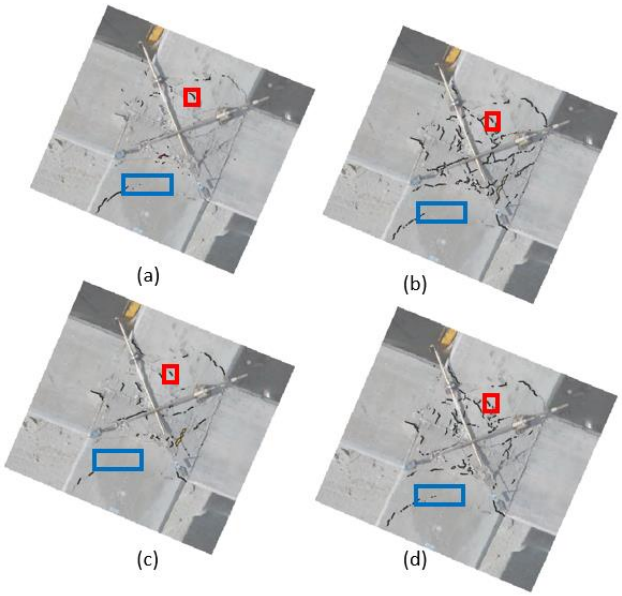


Table 7.4: OBIA classification with cracking on original ROI (a), on ROI with Enhanced Frost filter (b), on ROI with Enhanced Lee filter (c), and with Median filter (d). In the red rectangle the crack with ID 45 and in the blue rectangle the crack with ID 4.

The first crack, as illustrated in ID 45 in Table 7.2 e 7.3, identified a capillary phase progression with a width of 4mm, where the amplitude was beginning to increase, indicating almost complete detachment and hence loss of surface continuity (Fig. 7.5).

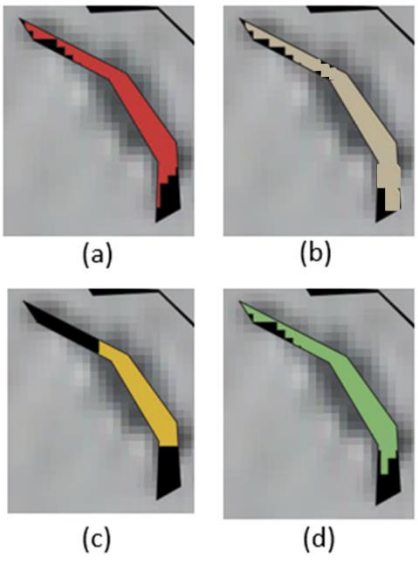


Table 7.5: OBIA ID 45 crack classification on original ROI (a), on ROI with Enhanced Frost filter (b), on ROI with Enhanced Lee filter (c), and with Median filter (d); the black area below corresponds to Ground Truth crack.

The second crack with ID 4, as shown in Figure 7.6, measuring 1mm in width, represented a capillary crack.

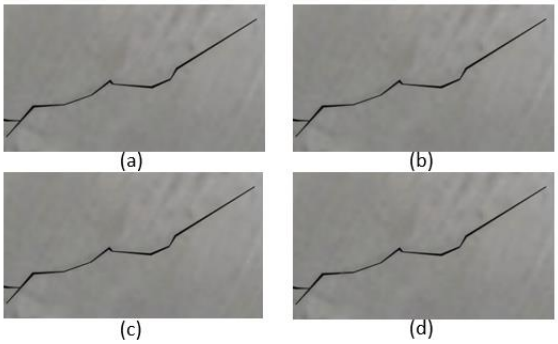


Table 7.6: OBIA ID 4 crack classification on original ROI (a), on ROI with Enhanced Frost filter (b), on ROI with Enhanced Lee filter (c), and with Median filter (d); the black area below corresponds to Ground Truth crack.

From the obtained percentages, it was found that while the classification successfully recognized the first crack (ID 45), it failed to identify the second one (ID 4). Consequently, the proposed method proves to be robust in the first case, while requiring further investigation in the second. Furthermore, an investigation was performed to establish a probable threshold size for cracks that might be consistently discovered using filters before utilizing the OBIA approach. The use of edge detection methods revealed that a minimum crack size of 6 mm might be accurately recognized before OBIA. Subsequent investigations found that Enhanced Frost increased crack detecting performance up to 3 mm, whereas cracks smaller than 2 mm required additional implementation. It should be highlighted that these findings are specific to the experimental conditions, and future research could look at applying similar criteria to other current samples or structures. However, analysis of individual crack IDs can provide information on the performance of each filter in detecting specific types of cracks or under different conditions. Overall, the results demonstrate the effectiveness of the Enhanced Frost filter in crack detection and highlight the importance of careful filter selection and evaluation to improve the accuracy of OBIA classification in identifying cracks in concrete specimens.

7.7 CONCLUSION AND FUTURE STUDIES

In conclusion, the objective of this work was to test the OBIA technique with the addition of specific filters on the orthophoto obtained from the photogrammetric process applied to a concrete specimen, to define the edges and distinguish the noise and salient shapes within the image to analyze the crack pattern of the concrete specimen. The main purpose of this work was, precisely, to extract cracks with a fast and automatic methodology useful for continuous monitoring of structures and infrastructure. Although the analysis needs further study and improvement, the first approach provided promising results. It has been shown that final rates improve most using filters, particularly the Enhanced Frost and Median. This study confirmed several advantages of using UAV-based photogrammetry and OBIA over traditional methods. Firstly, UAV-based photogrammetry offers a non-invasive inspection method, reducing the risk of structural damage and ensuring operator safety. Traditional methods, which often require physical access to structures, can pose significant risks and are time-consuming. Secondly, the integration of photogrammetry with SfM algorithms allows for the rapid creation of detailed 3D models and orthophotos, which facilitates swift identification and analysis of cracks. Compared to manual inspection methods, this approach significantly reduces inspection time and enables more frequent monitoring. Thirdly, the application of OBIA enhances the accuracy of crack detection by effectively differentiating between crack patterns and noise, which is a notable improvement over basic edge detection techniques used in conventional image processing. Moreover, the methodology is objective and replicable, unlike what happens with visual inspection. However, the study is not without its limitations. The initial results, even if promising, indicate the need for further testing and refinement of the methodology. Future work will focus on testing additional filters and new classification ML algorithms to improve the automatic extraction of cracks and minimize noise. These future improvements aim to make the methodology more robust and adaptable to various types of materials and structural conditions. Future

research will address several remaining questions and potential limitations. Key areas for improvement include enhancing the accuracy and reliability of crack detection algorithms, optimizing the processing time for large datasets, and extending the methodology to other types of materials and structural scenarios. Additionally, integrating advanced Machine Learning techniques such as CNNs for automated feature extraction and classification will be explored. Further testing on different structural types, including wood and masonry, will be conducted to validate the generalizability of the proposed methodology. By continuing to refine these methods and incorporating advanced technologies, the goal is to develop a rapid, effective, and easily replicable infrastructure monitoring system. Such a system will significantly contribute to the safety and sustainability of our building heritage, ensuring timely maintenance and reducing the risk of structural failures. In summary, while the current study lays a solid foundation for UAV-based photogrammetry and OBIA in crack detection, there remains significant potential for further enhancement and application across a broader range of infrastructure types.

8. CREATION OF 3D MODELS WITH OPEN SOURCE TOOLS AND WEBGIS INTEGRATION FOR MAINTENANCE SUGGESTIONS

After completing the validation of individual case studies, defined through specific evaluation metrics and independent test set validations, and conducting a thorough statistical comparison of model performance across diverse datasets and conditions, the next step involves the creation of a 3D model and a WebGIS platform, as shown in figure 8.1.

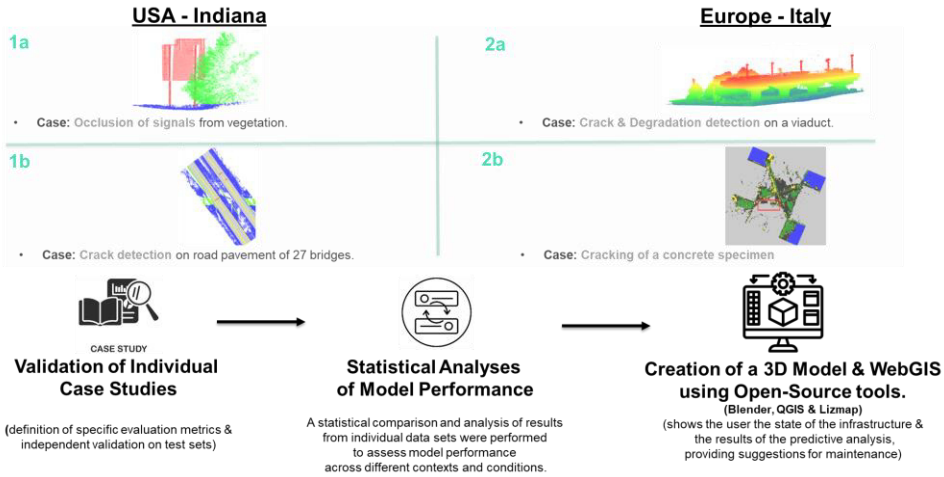


Figure 8.1: General workflow from case study to WebGIS creation.

This phase, carried out using open-source tools such as Blender, QGIS, and Lizmap, serves to visualize the state of the infrastructure while integrating predictive analytics and providing actionable suggestions for maintenance,

thereby offering a robust framework for informed decision-making in infrastructure management. Furthermore, the availability and organization of geospatial databases, comprising a wide range of data from public and private sources, represent essential resources for Geographic Information Analysis (GIS), visualization, and research. These databases are regulated by well-defined standards and protocols that facilitate data management and exchange through interoperable formats and services, addressing transparency and scientific sharing needs. In this research, the substantial volume of collected data required structured organization and careful optimization of datasets to highlight their main features. Consistent with the principles of data sharing promoted by European regulations such as EU Regulation 2019/1024 the idea of making the acquired data accessible through a Web GIS platform emerged. This platform was designed to visualize and share the collected datasets on a georeferenced map, with the ultimate goal of creating an integrated, corrected, and ready-to-use data infrastructure. Web GIS serves as an effective and intuitive means for disseminating geospatial data, thanks to its user-friendly interface and interactive navigation tools, such as zooming, panning, scale adjustments, and other essential functionalities that ensure accessibility to a wide range of users (Duarte L. et al., 2021). For the creation of this platform, the Lizmap plugin, integrated into the open-source QGIS software, was employed, showcasing how open-source technologies can provide a valid and sustainable alternative to proprietary solutions. Furthermore, the growing adoption of European strategies, such as the "Open Source Software Strategy 2020–2023," highlights the relevance of open-source technologies within the public sector (Coetzee et al., 2020; Mobasheri et al., 2020). In the geospatial field, the use of free and open-source software is continuously increasing, supported by governments and institutions worldwide. These solutions, now mature, offer capabilities equivalent to proprietary products and allow the development of customized Web GIS applications for various purposes (Singh and Gambhir, 2014). Web GIS platforms are widely used in numerous fields, including urban planning (Ostadabbas et al., 2021; Bendib

et al., 2016), meteorology (Stefanov, 2021), water and coastal management (Arias Munoz et al., 2017; Randazzo et al., 2021), tourism and cultural heritage management (Oxoli et al., 2019; Vacca et al., 2017), and health applications (Mushonga et al., 2017; Tiwari and Jain, 2013). Within this context, the present research integrates 3D models and predictive analytics into a Web GIS environment, providing recommendations for infrastructure maintenance and aiming to improve monitoring, management, and planning of maintenance activities.

8.1 Introduction to 3D Models in Infrastructure Analysis

In recent decades, the digital transformation of the construction and urban planning sectors has been driven by the adoption of Building Information Modeling (BIM) and City Information Modeling (CIM) (Volk R. et al., 2014; Domicini D. et al., 2022). These methodologies facilitate the integration of geometric, semantic, and updated data into 3D models, enabling more effective planning, design, construction, and maintenance processes (D'Uva D. et al., 2021; Eugeni F. et al., 2024)). BIM, in particular, has revolutionized the construction industry by providing a structured and collaborative approach to manage building life cycles, while CIM extends this concept to urban environments, integrating geospatial and infrastructure data to support decision-making processes for city-scale applications (Pascucci N. et al., 2024). Despite these advances, infrastructure-specific modeling and analysis remain less standardized compared to BIM and CIM. Critical infrastructures such as roads, bridges, and tunnels are subject to unique challenges, including exposure to dynamic environmental conditions, aging materials, and increasing demands for monitoring and maintenance (Bittencourt T.N et al., 2016; Argyroudis S.A. et al., 2019). Unlike buildings, which benefit from well-established BIM workflows, infrastructure elements often require tailored methodologies that incorporate geospatial, structural, and environmental data in an integrated

and scalable framework (Hakimi O. et al., 2023). The development of 3D models for infrastructure analysis aims to fill this gap by combining the precision of geomatics techniques, such as LiDAR and photogrammetry, with advanced predictive analytics and maintenance strategies. These models not only provide a detailed representation of infrastructure geometry but also integrate functional attributes, degradation patterns, and risk indicators, offering a comprehensive tool for monitoring, analysis, and decision-making (Kaartinen E. et al., 2022; Malihi S. et al., 2024). Moreover, the integration of infrastructure models into Web GIS platforms enhances their accessibility and usability, enabling stakeholders to interact with real-time georeferenced data for effective infrastructure management (Gaspari F. et al., 2023). By adopting open-source tools and protocols, this approach supports transparency, collaboration, and scalability, aligning with global trends toward open data and open-source solutions (Coetzee S. et al., 2024; Johnson E. et al., 2024). In this chapter, the creation of 3D models is explored as a foundational element for infrastructure analysis, emphasizing their integration with predictive analytics and maintenance planning. This framework not only supports the digitalization of infrastructure management but also aligns with the broader objectives of sustainability, resilience, and efficiency in addressing the challenges posed by aging infrastructure and increasing urbanization.

8.2 Data Preparation for 3D Model Creation

The preparation of data is a critical step in the development of 3D models for infrastructure maintenance. This process ensures that the final models are accurate, reliable, and capable of supporting both predictive analysis and maintenance planning. In this context, the integration of diverse geospatial and geometric datasets is essential, combining data from LiDAR, photogrammetry, and other geomatics techniques to produce a detailed

representation of the infrastructure. The 3D data model designed for infrastructure maintenance must meet three main requirements:

• *Centralized Management*: The Web-GIS platform must enable the management of public infrastructure within a single, shared geospatial database. This allows for comprehensive evaluation and assessment across various assets (Daud M et al., 2024).

• *Lifecycle Support*: The system must facilitate the management and maintenance of public infrastructure throughout their entire lifecycle, from construction to decommissioning (Guo H.L. et. Al., 2010).

• *Transparency and Accessibility*: The platform must provide a mechanism to share infrastructure-related information with relevant authorities and the general public, ensuring transparency and accessibility of data (Mendoza R.U. et al., 2020; Chang C.M. et al., 2023).

Developed in an open-source environment, this model leverages tools such as Blender, BlenderGIS, QGIS, and Lizmap to process and visualize data. The resulting framework supports stakeholders in identifying areas requiring maintenance and assessing the current state of infrastructure. By adopting open-source solutions, the model ensures accessibility, scalability, and cost-efficiency, making it an ideal choice for public infrastructure projects. The general workflow for creating 3D models for infrastructure analysis is divided into three main phases (Figure 8.2):

• *Input Data Acquisition*: High-resolution geospatial datasets are collected using technologies such as LiDAR from MMS and SLAM, and UAV photogrammetry. These datasets provide the geometric and semantic information necessary for model development.

• *Data Processing*: Data processing involves the integration and refinement of raw datasets. Tools such as Blender and BlenderGIS are used to clean and simplify 3D meshes, while QGIS is employed for georeferencing and spatial analysis. The combination of these tools ensures the models are both geometrically accurate and geospatially consistent.

• *Final Data Visualization*: Once processed, the models are integrated into Lizmap, an open-source Web-GIS platform that allows for real-time

visualization and interaction with 3D models. This step ensures that stakeholders can easily access and interpret the data, supporting decision-making processes.

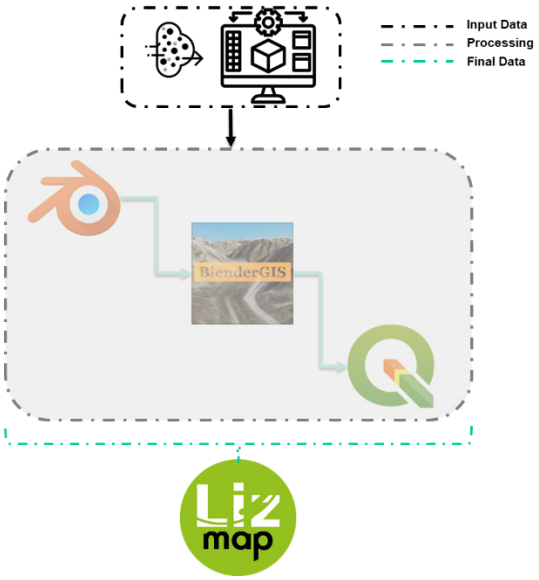


Figure 8.2: An illustration of the general workflow, showcasing the transition from raw input data to processed models and their final visualization in a WebGIS platform.

By combining cutting-edge geomatics tools and open-source technologies, this approach enables the creation of comprehensive 3D models that serve as the foundation for predictive analysis and maintenance planning. These models not only represent the current state of the infrastructure but also provide actionable insights, empowering authorities to prioritize interventions and ensure long-term sustainability.

8.2.1 Creation and Optimization of 3D Models Using Blender and the BlenderGIS Plugin

The creation and optimization of 3D models is a cornerstone of infrastructure analysis, enabling detailed representations of complex geometries and integration into Geographic Information Systems (GIS). Blender, a versatile open-source 3D modeling software, combined with the BlenderGIS plugin, offers a robust workflow for constructing, optimizing, and preparing 3D models for geospatial applications (Župan R et. al., 2023).

The process begins with the importation of point cloud data, which are typically exported from CloudCompare in FBX format. These point clouds represent the spatial geometry of the infrastructure and are processed in CC using Delaunay triangulation to generate a mesh. This triangulation ensures the accurate reconstruction of surfaces while maintaining computational efficiency, a critical factor for large-scale infrastructure projects. Once the 3D geometry is generated, additional refinements, such as noise reduction and mesh simplification, are applied to optimize the model for visualization and analysis in Blender. These refinements improve the computational performance while preserving essential details required for infrastructure assessment. After constructing the base geometry, the next step involves assigning realistic materials and textures to the 3D model. In this phase, Blender's advanced material system is used to apply surface textures (e.g., asphalt for roads, concrete for bridges). Texture mapping not only enhances the visual appeal of the models but also adds realism, aiding stakeholders in understanding the physical condition of the infrastructure. The textures are UV-mapped onto the geometry, ensuring proper alignment and minimizing distortion. This step is essential for achieving high-fidelity representations that can be used for both technical evaluations and public presentations. The final step within Blender involves rendering the 3D model to produce high-quality visual outputs (Figure 8.3). Blender’s rendering engine (e.g., Cycles or Eevee) is employed to generate photorealistic images and animations, which are then, integrated into WebGIS platforms. These visualizations provide users with an intuitive way to assess the infrastructure's current state and identify critical maintenance needs.

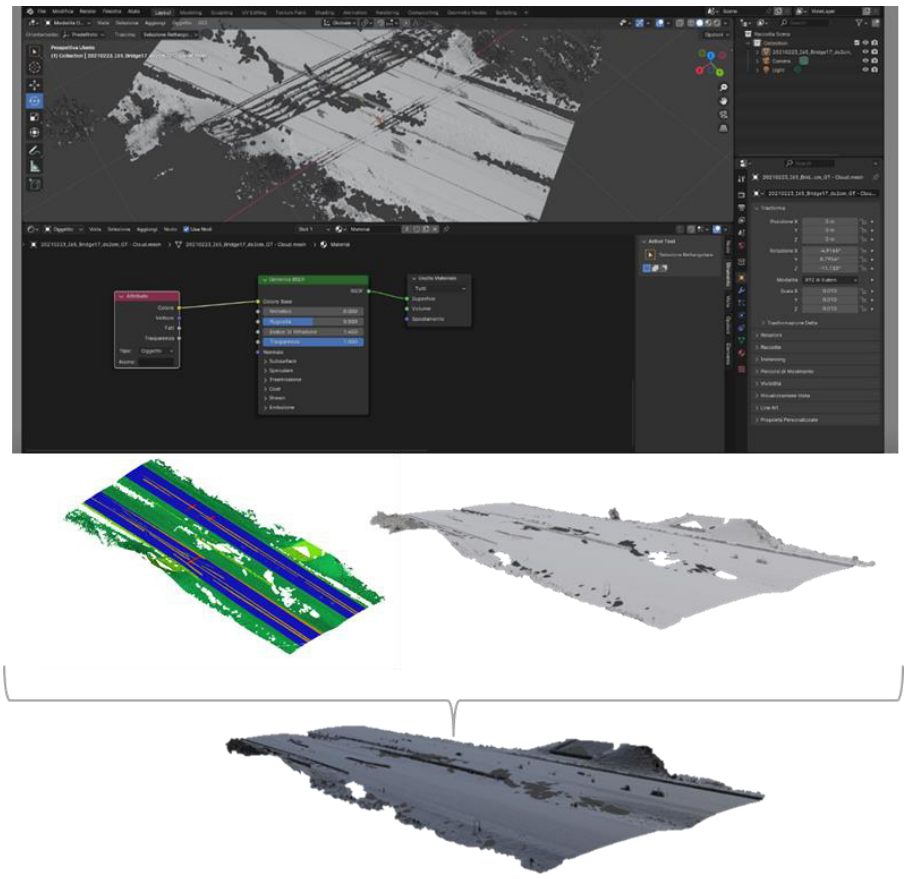


Figure 8.3: An example from 3D Model creation to the rendering process in Blender.

To facilitate geospatial integration, BlenderGIS, a plugin for Blender, is utilized for data preparation. BlenderGIS bridges the gap between 3D modeling and GIS by enabling the extraction and conversion of 3D spatial data into GIS-compatible formats (figure 8.4).

• *Importing 3D Models into QGIS*: Using BlenderGIS, spatial data are exported from Blender and imported into QGIS for further analysis. This includes the creation of vector layers that accurately represent infrastructure elements such as roads and bridges within a GIS environment.

• *Creation of Shapefiles*: The plugin allows for the direct conversion of 3D models into georeferenced shapefiles. These shapefiles are georeferenced using the WGS84 coordinate system, ensuring compatibility with global applications. This capability is especially important for projects spanning different regions, such as the United States and Europe.

• *Regional Applications*: The georeferenced shapefiles enable cross-regional integration of 3D models, supporting projects that require consistency across diverse geographical areas.

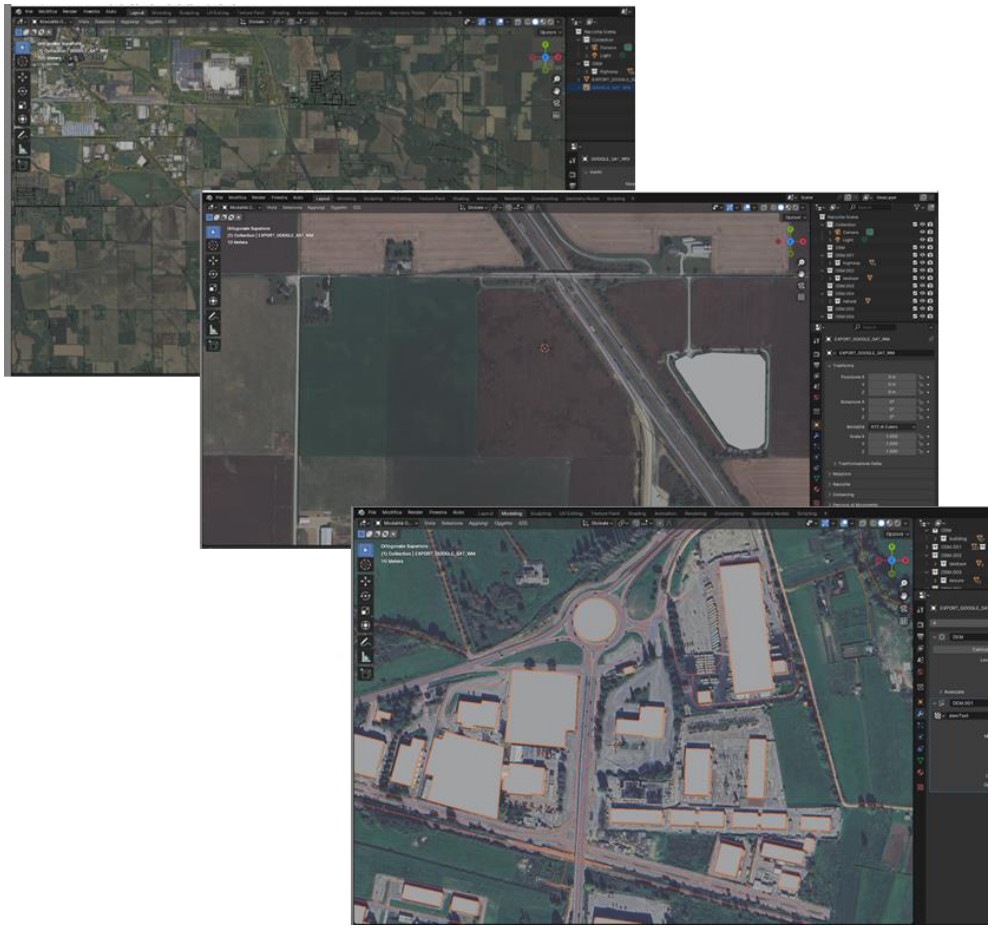


Figure 8.4: Examples of different areas to get shapefiles using BlenderGIS plugin both for the United States (up) and Europe (bottom).

Geospatial data prepared with BlenderGIS will be further integrated into WebGIS open source platforms such as Lizmap, as presented in the next section. This integration ensures that stakeholders can visualize the processed 3D models in a geospatial context, improving decision-making processes. By providing an intuitive interface for navigating and interacting with models, WebGIS open source platforms support collaborative infrastructure management, for any nation on any continent.

8.3 WEBGIS DATABASE INTEGRATION WITH QGIS AND LIZMA

The integration of spatial data with predictive analysis into a WebGIS environment is a critical step for facilitating interactive visualization and decision-making in infrastructure management. This process involves leveraging QGIS for spatial data preparation and attribute enrichment, followed by the deployment of the data on a WebGIS platform using Lizmap. The workflow begins with the systematic organization of spatial data in QGIS, adhering to conceptual, logical, and physical data modelling paradigms. This ensures consistency across datasets and promotes standardization for various case studies. The data model forms the basis of a set of rules that GIS software follows to digitally represent geographic reality. One of the fundamental purposes of a GIS system is to replicate the real world through data, models, and tools that not only govern the representation of spatial elements but also ensure the accurate positioning and relationships of objects within that reality (Bonham-Carter G., 1994; Bernhardsen T., 2002). To achieve this, it is necessary to identify and structure diverse data types that are compatible with the digital environment of the GIS software. The GIS data model systematically organizes all the information required to represent spatial and territorial features. This representation is shaped by rules imposed by projection and reference systems, ensuring geographic accuracy. Once these systems are defined, the actual storage of data within GIS is carried out using one or both primary formats: the vector model, which emphasizes discrete spatial features, and the raster model, which focuses on continuous surface representations (Burrough P.A. et al., 2015). Before the construction of a GIS system can begin, a detailed process of creating the data model must be undertaken. This ensures the system aligns with the intended objectives and can address specific spatial queries. The data modelling process consists of three key stages:

• The ***Conceptual Model***, as show in figure 8.5, represents a high-level abstraction of the real world, identifying the primary entities (e.g., road segments, bridges, and vegetation) and the relationships between them. It serves as the foundation for the GIS project, outlining the specific outcomes to be delivered and the essential, necessary, and optional data required to achieve the intended goals. This phase is crucial for defining the scope and focus of the GIS application, as it determines both the graphical and alphanumeric data of interest, ensuring their relevance to the project objectives. The process of developing a conceptual model begins with a comprehensive collection and analysis of all necessary documentation and available data. Based on this foundation, one or more Entity-Relationship (E-R) schemas are created. These schemas serve as a structured representation of the entities that constitute the graphical base of the dataset, along with the attributes required to describe them. The E-R model also establishes the logical and physical correlations among the various entities, forming a cohesive structure for subsequent stages of GIS development. To elaborate a conceptual model effectively, it is imperative to have a clear understanding of the project's objectives, the requirements of stakeholders, and the available resources. For instance, in the context of this research project, the goal is to develop a georeferenced platform that operates using the WGS 84 coordinate reference system. This platform, accessible online, is intended to enable efficient and comprehensive monitoring of public works while supporting improvements in the future design process for infrastructure. The platform aims to be user-friendly and accessible to a wide range of stakeholders, from field engineers to interested citizens. It must balance graphical and logical simplicity with the ability to provide detailed and actionable information. Consequently, the conceptual model is tailored to reflect these considerations, guiding the identification of entities to be represented geographically and the definition of descriptive attributes for each entity. Entities within the conceptual model are both geometric and alphanumeric in nature. These entities can be grouped into categories such as roads, bridges, vegetation, sign, guardrails, point features, and a central

Information Sheet entity. The Information Sheet acts as the logical nexus of the system, linking all geometric entities and providing detailed metadata. Each geometric entity (e.g., a road segment or bridge) is directly associated with an Information Sheet, which contains attributes that characterize and describe it. By structuring the conceptual model in this way, the GIS platform is designed to accommodate a diverse range of use cases. It ensures that all necessary information is organized efficiently, enabling both technical and non-technical users to interact with the system effectively and derive meaningful insights from its data.

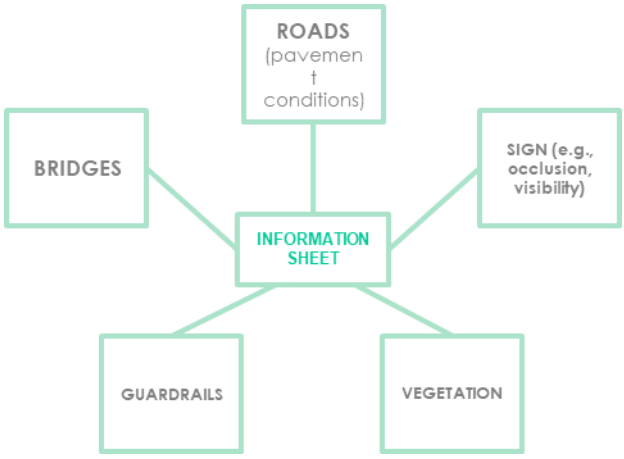


Figure 8.5: Conceptual Model. Representation of the relationship between geometric and alphanumeric entities.

The Information Sheet entity is a pivotal component of the GIS structure, as it consolidates all the critical technical and descriptive attributes required to accurately represent geometric entities. These attributes not only define the entities themselves but also serve as a foundation for ensuring consistency and usability across different levels of interaction, from technical professionals to private users. The essential fields included in the Information Sheet are:

- *Subject*: Specifies the primary category of the entity (e.g., road, bridge, vegetation, sign occlusion, guardrails).
- *Date of Data Collection*: Indicates when the data was acquired, ensuring temporal relevance.

- *Method*: Describes the technique or algorithm used for data analysis, such as DBSCAN, Random Forest (RF), or Superpoint Graph (SPG).
- *TP, FP, FN, Recall, Precision, and F1-Score*: Performance metrics to evaluate the reliability of feature detection and classification.
- *Type of Crack* (Bare Earth & Above Ground): Identifies the type of crack, such as longitudinal or transversal, observed on exposed surfaces.
- *Type of Vegetation*: Provides details about vegetation characteristics in the area.
- *Required Interventions*: Lists the specific actions needed based on the condition of the entity.
- Measure Surface Cracks: Quantifies the dimensions and extent of surface cracks.
- *Sign Occlusion from Vegetation*: Indicates whether vegetation obstructs road signs (Yes/No).

These fields were derived from the extensive analysis and methodologies elaborated in the previous chapters of this dissertation, reflecting both theoretical and applied components of the research. The attributes outlined are essential as they encompass the key technical and descriptive elements central to each project, ensuring that the Geographic Information System (GIS) accurately represents entities while also meeting broader informational and operational needs. By incorporating these fields into a WebGIS platform, several objectives are achieved. Each project is clearly and uniquely defined, enabling unambiguous identification and differentiation within regional and national databases. This clarity also enhances searchability, allowing users to easily locate projects within databases to extract additional information and insights. Furthermore, the system contributes valuable geographic and contextual information about interventions, reinforcing its role in spatial and informative analysis. The system ensures accessibility for both professionals and the general public, serving distinct purposes for each group. For professionals, it supports detailed queries, facilitates updates and modifications as needed, and aids in the efficient planning and maintenance of interventions. For private users, it

fosters transparency and enhances access to information, promoting public awareness and engagement with infrastructure policies and projects. By aligning these attributes with the overarching objectives of the WebGIS, the system becomes an indispensable tool for managing, analysing, and communicating data about infrastructure projects, effectively bridging the gap between technical requirements and public utility.

• The ***Logical Model***, as shown in figure 8.6, serves as a detailed framework that bridges the gap between conceptual planning and implementation. It translates the abstract elements of the conceptual design into precise attributes, data types, and logical relationships that are interpretable by GIS. This step is essential for achieving a seamless transition from theoretical planning to practical application, ensuring that the system is ready for effective use. After completing the conceptual planning phase (defining the project objectives, identifying the necessary data, and outlining the relationships among entities), the next stage involves the logical model's development. This phase is pivotal in structuring the conceptual model into a format suitable for GIS software, facilitating the system's practical implementation. The logical model is based on a structure of multiple entities, specifically multipoint, multiline, and multipolygon geometries. These entities are utilized to provide the best possible visual representation of real-world features, with their selection driven by the requirements of the intervention being depicted. Each entity is associated with an attribute table comprising a standardized set of fields to ensure consistency across the system. These attributes describe the interventions and are not logically interdependent, allowing for independent yet cohesive data representation. Given these requirements, selecting a data format with robust, scalable, and compact characteristics was crucial. Traditional formats like the Shapefile, while widely used, pose limitations in terms of data management and interoperability. Shapefiles require multiple files to represent a single entity, creating challenges in maintaining data integrity and increasing the risk of accidental data loss (Vert G., et al., 2002; Arctur D. et al., 2004). Moreover,

they lack support for multipart geometries, making them unsuitable for projects involving complex features such as non-contiguous infrastructural stretches. To address these limitations, the GeoPackage format was adopted. GeoPackage is an open, non-proprietary, and platform-independent data format developed under the standards of the Open Geospatial Consortium (Rashidan M. H. et al., 2016). Unlike Shapefiles, it consolidates all geographic and alphanumeric data into a single file with a .gpkg extension, ensuring compactness and ease of management. This format supports advanced geometric types, including points, lines, polygons, multipoint, multiline, multipolygon, and curvilinear elements, making it ideal for infrastructure monitoring and management projects. GeoPackage provides numerous advantages compared to Shapefiles, making it a superior choice for managing geospatial data. Its lightweight yet robust nature enables efficient workflows, allowing users to process and analyse data quickly without compromising reliability. Unlike Shapefiles, GeoPackage overcomes common limitations such as character restrictions and size constraints, offering greater flexibility for managing diverse datasets. Additionally, it supports multipart geometries, a critical feature for accurately describing complex infrastructural elements. By integrating metadata, tables, and various data elements into a single file, GeoPackage enhances both usability and data security, consolidating all essential components into a unified and streamlined format (Rashidan M.H. et al., 2015; Cheng Y., 2019). In this project, geometric entities are not inherently related to one another but share a logical connection with a common alphanumeric entity termed the Information Sheet. This commonality allows for relational operations within GIS software, such as table joins, enabling the transfer of attributes based on shared fields. A unique identifier, such as FID code (acronym for Feature ID number), is used to establish this connection. The FID is an integer field that ensures each feature is uniquely identified, simplifying the linkage between geographic and alphanumeric datasets. By incorporating this structured approach, the logical model facilitates the accurate representation and management of interventions. The

use of GeoPackage ensures the system is robust, compact, and adaptable to future revisions, aligning with the project's goals of creating an efficient, replicable, and open-source WebGIS for infrastructure monitoring and management.

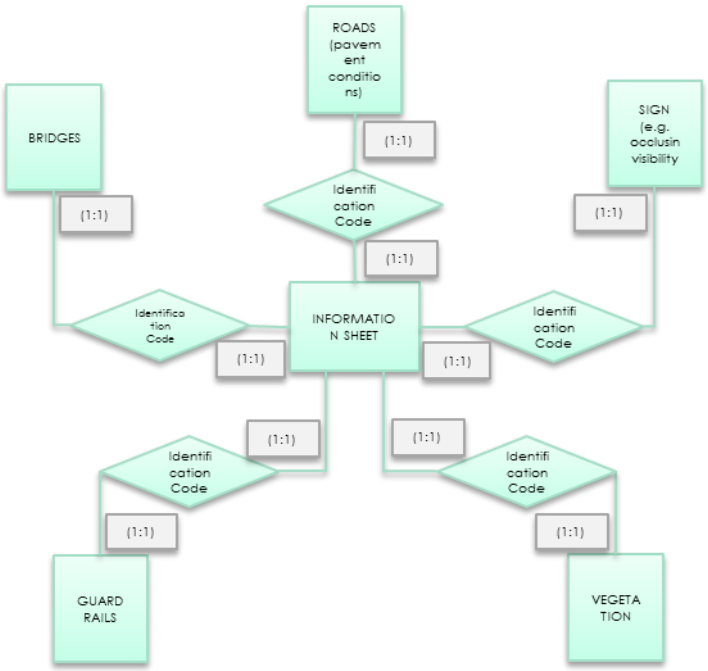


Figure 8.6: Logical scheme that enables the project's procedural process.

This approach, applied to the infrastructure systems of L'Aquila (Italy) and Indiana (USA), demonstrates its scalability and versatility for similar projects worldwide, offering a simplified yet effective framework for geographic data integration and transparency in infrastructure policies.

• After defining the conceptual and logical models, the next step is the design of the ***Physical Model***, as shown in Figure 8.7, which focuses on the actual realization of the database. This model identifies the files, data archives, and tables that will be used and loaded into the GIS for its functioning. It also establishes the relationships between these components, ensuring that they can be linked effectively within the GIS environment. The physical model involves setting up the necessary elements in a software environment, typically using GIS software such as QGIS, to incorporate both the alphanumeric and geographic data models. As outlined in the logical design phase, this includes creating an alphanumeric database

(usually in a tabular format like Microsoft Excel) and a spatial database (GeoPackage) within the GIS. The correct setup and integration of these two elements are crucial for the smooth operation of the project, as it allows for the combination of tabular and geographic data, reducing the potential for errors and facilitating quicker data integration (Breunig M. et al., 2020). The creation of the alphanumeric database is done separately from the GIS software, providing flexibility in the data entry process. This method allows for thorough analysis of the fields, comparison of data, and the use of formatting tools to ensure accuracy before importing the data into the GIS. Typically, this database is managed through spreadsheet software, such as Microsoft Excel, where attributes and fields are clearly defined in the first row. Each entry is assigned a unique identifier (ID), which links the alphanumeric data, to its corresponding geometric entity in the GIS. The alphanumeric data is organized in spreadsheets, making it easy to manipulate and check for errors before being imported into the GIS environment. Meanwhile, the geographic database is created within the GIS software using the GeoPackage format. The geographic database is populated with spatial data layers that represent various geographic entities in the project. Each layer is linked to the alphanumeric database through the ID field, ensuring the seamless connection between geographic and alphanumeric data. The first step involves creating a GeoPackage database, which does not require a predefined primary field for the FID code or any attributes. Layers are then added to the database, each containing a geometric entity such as lines, points, or polygons, depending on the project's needs. Once both the alphanumeric and geographic databases are created, they are synchronized by linking the alphanumeric fields (e.g., project identifiers) with the corresponding geometric entities in the GIS. This synchronization is crucial for integrating spatial and tabular data seamlessly. After data entry and the creation of geometric layers, the two databases are merged within the GIS software, resulting in a fully functional GIS project that is ready for use and analysis. Maintaining separate alphanumeric and geographic databases offers several advantages. By

managing the alphanumeric data externally in a spreadsheet format, the process becomes more flexible and organized. This separation allows for more detailed analysis of the data fields, making it easier to identify errors before importing into the GIS. It also enhances data management efficiency, as updates to the alphanumeric database can be made independently of the spatial data. Using Microsoft Excel for the alphanumeric database provides easy formatting, sorting, and editing capabilities, ensuring that the data is accurate. Once the alphanumeric data is ready, it can be imported into the GIS and linked to the geographic data layers, which are stored in the GeoPackage format. In conclusion, the project's physical model involves creating two separate databases: the alphanumeric database in spreadsheet format and the geographic database in GeoPackage format. These two databases are linked together within the GIS software, ensuring efficient integration of both tabular and spatial data. The proper setup and organization of these databases are essential for the smooth operation of the GIS-based application, enabling effective data analysis, visualization, and decision-making. Once the data entry process is completed, the final step is to integrate the alphanumeric and geographic data, ensuring synchronization and readiness for use in the GIS system. This model forms the foundation for creating a comprehensive GIS database that can be transferred to a public server or integrated into a WebGIS system for further use.

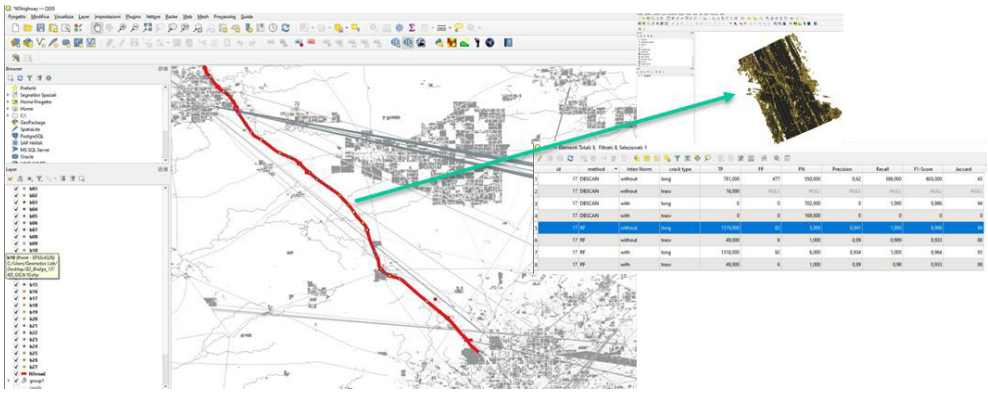


Figure 8.7: Final physical model representation zooming in on an example of a road segment and related bridge with the different criticality, analysis and intervention types in the attribute table.

These stages collectively ensure that the GIS system effectively mirrors real-world phenomena, facilitating both analysis and decision-making in a digital environment. The implementation and visualization of spatial data in a WebGIS environment represent a critical step in making infrastructure monitoring and maintenance data accessible to a wide range of users. This section focuses on the integration of the WebGIS database using QGIS and Lizmap, highlighting the system's architecture, configuration, and user interface. In this context emphasizes a structured approach to data visualization and prioritization to support decision-making processes (Vacca G. et al., 2017; Oxoli D. et al. 2019; Alicandro M. et al. 2022). Lizmap was chosen as the solution for sharing the QGIS project on the web, owing to its seamless integration with QGIS Server. The Lizmap system comprises two primary components:

- A *QGIS Plugin*: This plugin is used within QGIS to configure publishing options, including scales, base layers, metadata, and additional project-specific settings.
- A *Web Client Application*: Installed on the map server, this component provides a web interface that allows end-users to interact with the published map.

The process begins with the definition of the project settings in the Lizmap plugin. Here, layer settings, access permissions, and map themes are configured. For instance, Figure 8.8 illustrates the layer settings interface, highlighting the ease of customization.

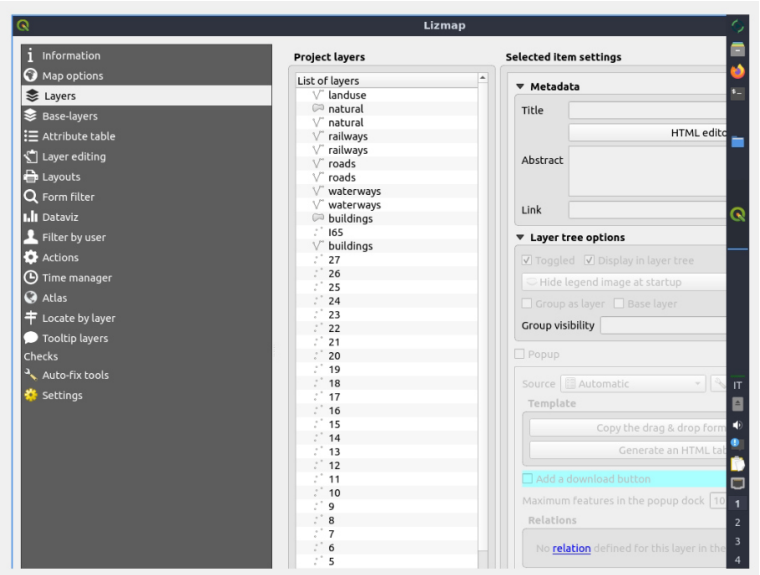


Figure 8.8: Defining layer settings in the Lizmap plugin.

Once the file configuration is complete, the working folder of the QGIS project is synchronized with QGIS Server. Upon synchronization, the QGIS project becomes accessible via the Lizmap Web Client, enabling web-based interactions. The overview WebGIS system architecture is designed to facilitate both flexibility and ease of use. The architecture, adapted from Lizmap, is depicted in Figure 8.9.

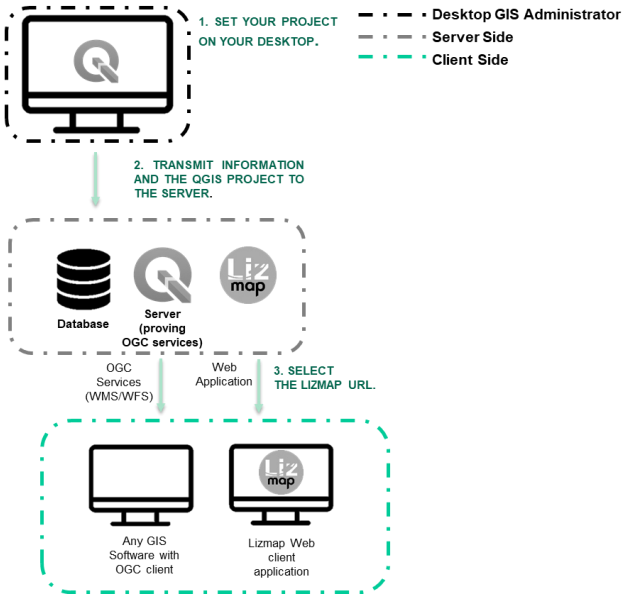


Figure 8.9: Web-GIS Architecture adapted from Lizmap.

At its core, base maps such as OpenStreetMap (in both black-and-white and colour variations) offer essential spatial context. These foundational layers support detailed geographic visualization. Complementing this, infrastructure layers depict various types of works, including transportation corridors, viaduct bridges, and signage, offering specialized insights into infrastructure networks. The system also incorporates attribute-based data visualization to enhance decision-making processes. Layers are categorized by intervention type and priority level, ranging from high to medium to low, enabling users to filter and visualize only the data most relevant to their specific needs. Designed with accessibility in mind, the architecture provides a simple, intuitive interface for interacting with the map. Basic navigation tools, efficient filtering capabilities, and scalable views further enhance the system's practicality, ensuring a seamless experience for all users, regardless of technical expertise. The flexibility of the WebGIS system is demonstrated through case studies in different geographic contexts. For example, the use of Lizmap for urban infrastructure management was highlighted for the city of L'Aquila, where layers were classified by type of intervention, a similar approach was taken for the I-65 transportation corridor that runs from Lafayette to Indianapolis, as shown in the figure 8.10. Users can view interventions along the highway, ranked by urgency.

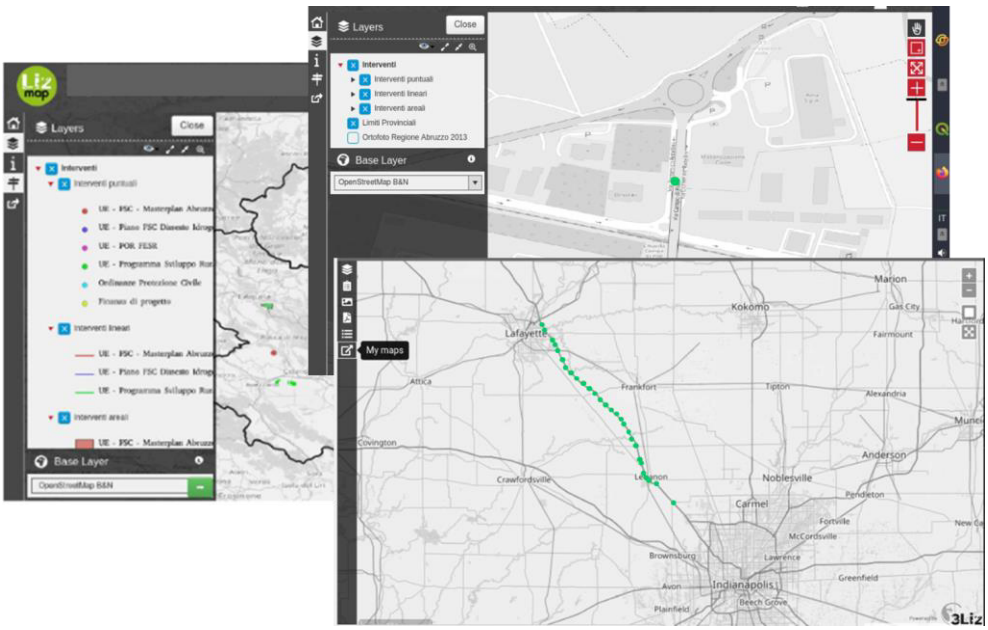


Figure 8.10: From the left the Layers panel with the type of interventions and on the right the Basemaps from OpenStreetMap (B&W/color). An example for the city of L'Aquila (up) and Lafatte to Indianapolis (Bottom).

8.4 Maintenance Recommendations Based on Database

The workflow begins with the creation of a detailed 3D model using Blender and BlenderGIS. This open-source solution allows operators to manually develop accurate infrastructure representations, enhancing spatial awareness through the integration of textures and rendered elements. The manual approach ensures high-quality results tailored to the specific requirements of the infrastructure being analyzed. The resulting 3D models provide a solid foundation for control and management tasks, supporting operators in visualizing key structural features and planning interventions effectively. Building on this, the integration of QGIS and Lizmap transforms the data into an interactive WebGIS platform. The final WebGIS configuration prioritizes usability to ensure that stakeholders can derive actionable insights. Users can select the layers and attributes they wish to visualize, tailoring the map to their specific requirements. This flexibility supports infrastructure management by providing a clear overview of

intervention needs, enabling the prioritization of resources and the planning of maintenance activities. In summary, the integration of Blender, QGIS, and Lizmap offers a comprehensive open-source pipeline that facilitates the dissemination and visualization of spatial data while ensuring accessibility and usability. While advanced predictive analytics may be considered for future iterations, the current implementation focuses on structured data visualization and 3D modelling as foundational tools for decision support and infrastructure management.

9. CONCLUSIONS

The final chapter of this thesis offers a thorough summary of the material presented in the preceding chapters and transitions into the conclusions and remarks, where the research questions and objectives outlined in Chapter 1 are revisited and addressed. This section aims to synthesize the key findings, offering a cohesive understanding of the contributions made throughout the dissertation. Following the summary, the chapter also provides recommendations grounded in the study's outcomes. These recommendations are intended to support informed decision-making in the domain of infrastructure management and highlight practical applications of the research. Moreover, this chapter explores prospective future developments, emphasizing the potential enhancements in maintenance strategies based on the models and methodologies developed. These advancements underscore the capability of such tools to facilitate data-driven decision-making, enabling more efficient infrastructure management practices. By leveraging these approaches, there is significant potential to improve preventive planning, reduce operational risks, and optimize resource allocation for timely and effective interventions. The integration of these methodologies into routine management practices has implications for advancing infrastructure safety, resilience, and sustainability in response to evolving challenges.

9.1 SUMMARY

This thesis investigates the application of advanced geomatic techniques, prioritizing NDT to acquire high-precision data for assessing risks associated with infrastructures and transportation corridors. The research leverages a combination of technologies, including LiDAR data collection

through MMS and SLAM, alongside UAV-based photogrammetry, to address key challenges in infrastructure monitoring and risk prevention. By integrating these methods, the study achieves detailed analyses of various infrastructure issues, such as road marking occlusions, road surface, and concrete cracks. The research is built upon a series of national and international case studies representing diverse, replicable contexts. These include:

• *Highway I-65 in the United States*: Evaluating road sign visibility and pavement cracking using MMS data.

• *Campo di Pile Viaduct in L'Aquila, Italy*: Assessing cracking using SLAM technologies.

• *Concrete Specimens*: Investigating crack formation and characteristics through compression cycles, demonstrating the applicability of these techniques to diverse infrastructure types.

The methodologies are evaluated through a comparative analysis of accuracy, precision, and practical applicability, using geomatic techniques. The methodologies are evaluated through a comparative analysis of precision, accuracy, and practical applicability, integrating traditional and modern geomatic techniques. Furthermore, the research incorporates machine learning and deep learning approaches, such as DBSCAN, RF, and SPG, to improve the detection and classification of infrastructure hazards. One of the key contributions of this thesis is the development of an open-source WebGIS platform designed to support infrastructure management, aligned with national and international guidelines (e.g., INDOT and MIT). This platform provides accessible, user-friendly tools for risk assessment, prevention, and maintenance planning, ensuring scalability and adaptability for infrastructure operators and stakeholders. By advancing methodologies for data acquisition, analysis, and visualization, the research not only addresses immediate challenges in infrastructure safety but also sets the stage for future developments. The proposed approaches enable data-driven decision-making, improve preventive planning, mitigate operational risks, and optimize resource allocation for timely and effective interventions.

Ultimately, this thesis contributes to the broader goal of fostering safer, more resilient, and sustainable infrastructure systems.

9.2 Conclusions and Future Developments

The methodologies outlined in previous sections were applied to four distinct case studies to evaluate their effectiveness in risk detection and their adaptability to different contexts. These case studies, conducted in the United States and Europe, aimed to address specific challenges associated with infrastructure maintenance and inspection, leveraging both automatic and semi-automatic approaches.

• *Case Study 1: Signal Occlusions in Indiana, USA*

The first case study in Indiana focused on identifying signal occlusions caused by vegetation. This challenge was addressed using MCSS and SPG classification applied to point clouds generated by a wheel-based MMS. The analysis aimed to enhance detection of occlusions and improve signal clarity. Findings revealed that the MCSS approach consistently outperformed SPG classification across datasets. However, MCSS required significant manual intervention, limiting scalability. SPG, particularly before QC, struggled with accurately classifying categories such as natural and man-made terrain. QC did not significantly enhance SPG performance, highlighting the need for improved segmentation techniques.

• *Case Study 2: Crack Detection on Bridge Pavements in Indiana, USA*

This study examined crack detection on road pavements of 27 bridges using point cloud data collected via MMS. DBSCAN and Random Forest algorithms were employed with and without normalized intensity data. The objective was to assess the impact of intensity normalization on detection accuracy. The RF algorithm demonstrated superior performance in terms of accuracy, recall, and F1-score, particularly for longitudinal cracks, which were more continuous and well defined. In contrast, DBSCAN showed

significant limitations, especially with normalized intensity, resulting in high false negatives and lower reliability for crack segmentation. These findings underscore the robustness of supervised methods like Random Forest for analyzing complex features in point cloud data.

• *Case Study 3: Crack Detection on a Viaduct in Italy*

In Italy, SLAM-derived point cloud data was analyzed to detect cracks on a viaduct using DBSCAN and Random Forest. This study compared the effectiveness of SLAM for infrastructure prevention. Results highlighted SLAM's utility for detailed 3D reconstruction but also revealed challenges in noise and data completeness. Preprocessing methods, such as intensity normalization, require refinement to enhance reliability. While both algorithms had limitations, Random Forest showed greater potential for crack detection in SLAM data, suggesting the need for integrating advanced techniques like graph-based learning or deep learning models to improve results.

• *Case Study 4: Crack Analysis of a Concrete Specimen Using UAV Photogrammetry*

The fourth case study examined cracks on a concrete specimen using photogrammetry data acquired via UAV. Advanced filters, including Enhanced Frost and Median, and OBIA techniques were applied to classify and analyze crack patterns. The methodology demonstrated several advantages, such as non-invasive inspection, rapid creation of 3D models and orthophotos, and enhanced crack detection accuracy. However, limitations included the need for further refinement of filters and classification algorithms to minimize noise and improve robustness. Future work will explore additional machine learning algorithms and testing on diverse materials.

At the same time, the increasing use of high-resolution datasets, especially from UAV photogrammetry and LiDAR-based approaches, raises critical concerns regarding data storage and management. Efficient storage

solutions, including cloud-based architectures and hybrid models, are essential for ensuring scalability and accessibility.

Moreover, the approach presented in this work aims to establish a foundation for future advancements in automatic risk detection for infrastructure, with a particular focus on the ultimate creation of an open-source WebGIS platform. This platform broadens access to data, making monitoring tools more accessible and scalable. By enabling real-time management and proactive planning, the approach aligns with international principles and standards, thereby contributing to ongoing efforts toward improved management and control practices. Across all case studies, it became evident that supervised classification methods, particularly Random Forest, consistently outperformed clustering approaches like DBSCAN. Longitudinal cracks were detected with greater accuracy than transverse cracks, highlighting the need to adapt methodologies to the specific characteristics of different crack types. In the future, research will focus on advancing risk detection and monitoring by integrating deep learning models, such as CNNs and GNNs, to better handle high-dimensional data and improve crack detection. Additionally, combining clustering methods like DBSCAN for noise reduction with supervised classification will enhance detection accuracy. Further, incorporating additional features such as surface roughness and curvature is expected to improve the robustness of the methods. Expanding validation efforts across diverse datasets and environmental conditions will ensure that these approaches can be generalized to different contexts. As infrastructure monitoring increasingly relies on large-scale data acquisition, addressing data storage challenges is critical. Optimizing workflows for high-resolution datasets through compression techniques, structured databases, and distributed storage solutions will be necessary to manage the growing volume of information effectively. Real-time systems integrated with mobile mapping platforms or UAVs will be a key focus for more efficient monitoring and decision-making. The challenges associated with SLAM-based data, such as noise and incomplete data; underline the need for targeted improvements in preprocessing techniques. Advanced learning models and refined

segmentation methods will be explored to enhance SLAM's effectiveness in crack detection. Incorporating crack characterization metrics, like surface area and depth estimation, will provide more comprehensive evaluations of infrastructure conditions. The UAV-based photogrammetry workflow has demonstrated significant potential for rapid and non-invasive infrastructure inspections. Future work should focus on incorporating UAV LiDAR alongside photogrammetry, as it could provide more accurate and detailed 3D reconstructions for infrastructure monitoring. This will involve testing additional filters and machine learning algorithms for better crack extraction, extending the methodologies to diverse structural types and materials, and optimizing processing times for large datasets. A critical aspect of future research will be the automation of reference data generation and the development of efficient data storage strategies to streamline the processing pipeline. Moreover, automating ground truth generation will help reduce manual effort and improve efficiency. In contrast, while data from wheel-based MMS provides high accuracy and reliability, it remains costly. The financial investment associated with these systems must be considered when selecting an approach for large-scale infrastructure monitoring. Nonetheless, MMS continues to offer valuable high-resolution data for precise crack detection, especially for large-scale projects. Finally, the integration of Blender, QGIS, and Lizmap has created a comprehensive, open-source pipeline for visualizing and managing spatial data. Blender enables the creation of detailed 3D models tailored to infrastructure needs, while QGIS and Lizmap transform the data into interactive WebGIS platforms. These open-source tools enhance the usability of the platform, allowing stakeholders to prioritize maintenance tasks more effectively. Future iterations of the system will explore predictive analytics to provide even more advanced decision-making capabilities. Additionally, integrating cloud-based WebGIS solutions will improve scalability, ensuring that data storage, retrieval, and processing remain efficient even as datasets grow in size and complexity.

In conclusion, the methodologies and insights gained from these case studies highlight the potential of combining automated and semi-automated

approaches with non-destructive techniques for infrastructure monitoring and maintenance. While there are still challenges to overcome, particularly in scalability, data variability, and method refinement, the integration of advanced technologies and broader validation efforts will contribute to safer, more efficient infrastructure management practices.

ADDENDUM A

In this appendix, quantitative evaluation of MCSS and SPG classification results for ROI 2 from the PWMMS-HA and PWMMS-UHA.

PWMMS-HA ROI 2 MCSS	TP (%)	FP (%)	FN (%)	Precision	Recall	F1-score
Bridge – Deck	0.000	0.000	0.000	0.000	0.000	0.000
Bridge – Beam/girder	0.000	0.000	0.000	0.000	0.000	0.000
Bridge – Abutment & wing wall	0.000	0.000	0.000	0.000	0.000	0.000
Bridge – Pier	0.000	0.000	0.000	0.000	0.000	0.000
Man-made terrain	0.940	0.000	0.059	0.999	0.941	0.969
Natural terrain	0.773	0.226	0.001	0.774	0.998	0.872
Vegetation	0.777	0.000	0.223	0.999	0.777	0.874
Buildings	0.000	0.000	0.000	0.000	0.000	0.000
Remaining hardscape	0.940	0.044	0.016	0.955	0.983	0.969
Scanning artifacts	0.983	0.010	0.007	0.989	0.993	0.991
Overall accuracy	90%					

PWMMS-HA ROI 2 SPG BEFORE QC	TP (%)	FP (%)	FN (%)	Precision	Recall	F1-score
Bridge – Deck	0.000	1.000	0.000	0.000	0.000	0.000
Bridge – Beam/girder	0.000	0.000	0.000	0.000	0.000	0.000
Bridge – Abutment & wing wall	0.000	0.000	0.000	0.000	0.000	0.000
Bridge – Pier	0.000	1.000	0.000	0.000	0.000	0.000
Man-made terrain	0.476	0.521	0.002	0.477	0.995	0.645
Natural terrain	0.258	0.027	0.714	0.903	0.265	0.410
Vegetation	0.917	0.048	0.035	0.950	0.964	0.957
Buildings	0.000	0.000	0.000	0.000	0.000	0.000
Remaining hardscape	0.705	0.271	0.024	0.723	0.967	0.827
Scanning artifacts	0.571	0.129	0.299	0.815	0.656	0.727
Overall accuracy	72%					

PWMMS-HA ROI 2 SPG AFTER QC	TP (%)	FP (%)	FN (%)	Precision	Recall	F1-score
Bridge – Deck	0.000	0.000	0.000	0.000	0.000	0.000
Bridge – Beam/girder	0.000	0.000	0.000	0.000	0.000	0.000
Bridge – Abutment & wing wall	0.000	0.000	0.000	0.000	0.000	0.000
Bridge – Pier	0.000	1.000	0.000	0.000	0.000	0.000
Man-made terrain	0.427	0.570	0.001	0.428	0.996	0.599
Natural terrain	0.207	0.031	0.761	0.868	0.214	0.344
Vegetation	0.947	0.027	0.026	0.973	0.973	0.973
Buildings	0.000	0.000	0.000	0.000	0.000	0.000
Remaining hardscape	0.634	0.350	0.016	0.644	0.974	0.776
Scanning artifacts	0.556	0.108	0.335	0.837	0.624	0.715
Overall accuracy	72%					

PWMMS-UHA ROI 2 MCSS	TP (%)	FP (%)	FN (%)	Precision	Recall	F1-score
Bridge – Deck	0.000	0.000	0.000	0.000	0.000	0.000
Bridge – Beam/girder	0.000	0.000	0.000	0.000	0.000	0.000
Bridge – Abutment & wing wall	0.000	0.000	0.000	0.000	0.000	0.000
Bridge – Pier	0.000	0.000	0.000	0.000	0.000	0.000
Man-made terrain	0.978	0.003	0.019	0.997	0.981	0.989
Natural terrain	0.842	0.145	0.013	0.853	0.985	0.914
Vegetation	0.903	0.005	0.092	0.995	0.907	0.949
Buildings	0.000	0.000	0.000	0.000	0.000	0.000
Remaining hardscape	0.879	0.113	0.008	0.886	0.991	0.936
Scanning artifacts	0.999	0.000	0.000	1.000	0.999	1.000
Overall accuracy	96%					

PWMMS-UHA ROI 2 SPG BEFORE QC	TP (%)	FP (%)	FN (%)	Precision	Recall	F1-score
Bridge – Deck	0.000	0.000	0.000	0.000	0.000	0.000
Bridge – Beam/girder	0.000	0.000	0.000	0.000	0.000	0.000
Bridge – Abutment & wing wall	0.000	0.000	0.000	0.000	0.000	0.000
Bridge – Pier	0.000	1.000	0.000	0.000	0.000	0.000
Man-made terrain	0.536	0.454	0.009	0.541	0.982	0.698
Natural terrain	0.124	0.041	0.834	0.752	0.130	0.221
Vegetation	0.944	0.031	0.024	0.968	0.975	0.971
Buildings	0.000	0.000	0.000	0.000	0.000	0.000
Remaining hardscape	0.703	0.232	0.064	0.752	0.917	0.826
Scanning artifacts	0.756	0.132	0.112	0.851	0.871	0.861
Overall accuracy	74%					

PWMMS-UHA ROI 2 SPG AFTER QC	TP (%)	FP (%)	FN (%)	Precision	Recall	F1-score
Bridge – Deck	0.000	0.000	0.000	0.000	0.000	0.000
Bridge – Beam/girder	0.000	0.000	0.000	0.000	0.000	0.000
Bridge – Abutment & wing wall	0.000	0.000	0.000	0.000	0.000	0.000
Bridge – Pier	0.000	1.000	0.000	0.000	0.000	0.000
Man-made terrain	0.546	0.444	0.010	0.552	0.982	0.706
Natural terrain	0.118	0.040	0.841	0.748	0.124	0.212
Vegetation	0.951	0.027	0.021	0.972	0.978	0.975
Buildings	0.000	0.000	0.000	0.000	0.000	0.000
Remaining hardscape	0.725	0.243	0.031	0.749	0.959	0.841
Scanning artifacts	0.823	0.097	0.080	0.895	0.911	0.903
Overall accuracy	76%					

ADDENDUM B

In this appendix, the quantitative evaluation of DBSCAN and RF with and without intensity normalization for all 27 road surface segments studied and acquired with PWMMS-UHA.

Road-Surface		Type of cracking	TP	FP	FN	Precision	Recall	F1-Score	Jaccard Index
01	DBSCAN No IN	Longitudinal	40	144	46	0.217	0.465	0.296	17%
		Transversal	0.000	8	5	0.000	0.000	NaN	0%
	DBSCAN IN	Longitudinal	0	0	83	NaN	0.000	NaN	0%
		Transversal	0	0	5	NaN	0.000	NaN	0%
	RF No IN	Longitudinal	3	139	0	0.021	1.000	0.041	2%
		Transversal	0	17	0	0.000	NaN	NaN	0%
	RF IN	Longitudinal	3	138	0	0.021	1.000	0.041	2%
		Transversal	0	17	0	0.000	NaN	NaN	0%

Road-Surface		Type of cracking	TP	FP	FN	Precision	Recall	F1-Score	Jaccard Index
02	DBSCAN No IN	Longitudinal	28	113	297	0.198	0.086	0.120	6%
		Transversal	5	55	52	0.083	0.087	0.085	4%
	DBSCAN IN	Longitudinal	0	0	414	NaN	0.000	NaN	0%
		Transversal	0	0	62	NaN	0.000	NaN	0%
	RF No IN	Longitudinal	0	688	0	0.000	NaN	NaN	0%
		Transversal	0	72	0	0.000	NaN	NaN	0%
	RF IN	Longitudinal	0	688	0	0.000	NaN	NaN	0%
		Transversal	0	72	0	0.000	NaN	NaN	0%

Road-Surface		Type of cracking	TP	FP	FN	Precision	Recall	F1-Score	Jaccard Index
03	DBSCAN No IN	Longitudinal	0	381	0	0.000	NaN	NaN	0%
		Transversal	0	22	74	0.000	0.000	NaN	0%
	DBSCAN IN	Longitudinal	0	0	716	NaN	0.000	NaN	0%
		Transversal	-	-	-	-	-	-	-
	RF No IN	Longitudinal	697	39	18	0.947	0.974	0.960	92%
		Transversal	0	84	0	0.000	NaN	NaN	0%
	RF IN	Longitudinal	697	34	18	0.953	0.974	0.964	93%
		Transversal	0	84	0	0.000	NaN	NaN	0%

Road-Surface		Type of cracking	TP	FP	FN	Precision	Recall	F1-Score	Jaccard Index
04	DBSCAN No IN	Longitudinal	0	368	0	0.000	NaN	NaN	0%
		Transversal	0	0	17	NaN	0.000	NaN	0%
	DBSCAN IN	Longitudinal	0	0	1008	NaN	0.000	NaN	0%
		Transversal	-	-	-	-	-	-	0%
	RF No IN	Longitudinal	1002	71	1	0.933	0.999	0.965	93%
		Transversal	2	16	0	0.111	0.999	0.199	11%
	RF IN	Longitudinal	1003	87	0	0.920	0.999	0.958	92%
		Transversal	2	16	0	0.111	0.999	0.199	11%

Road-Surface		Type of cracking	TP	FP	FN	Precision	Recall	F1-Score	Jaccard Index
05	DBSCAN No IN	Longitudinal	0	13	452	0.000	0.000	NaN	0%
		Transversal	0	33	6	0.000	0.000	NaN	0%
	DBSCAN IN	Longitudinal	0	0	10	NaN	0.000	NaN	0%
		Transversal	-	-	-	-	-	-	-
	RF No IN	Longitudinal	11	720	0	0.015	0.999	0.029	2%
		Transversal	0	20	0	0.000	NaN	NaN	0%
	RF IN	Longitudinal	11	717	0	0.015	0.999	0.029	2%
		Transversal	0	20	0	0.000	NaN	NaN	0%

Road-Surface		Type of cracking	TP	FP	FN	Precision	Recall	F1-Score	Jaccard Index
06	DBSCAN No IN	Longitudinal	-	-	-	-	-	-	-
		Transversal	-	-	-	-	-	-	-
	DBSCAN IN	Longitudinal	0	0	466	NaN	0.000	NaN	0%
		Transversal	-	-	-	-	-	-	-
	RF No IN	Longitudinal	1	734	0	0.001	0.999	0.002	0%
		Transversal	-	-	-	-	-	-	-
	RF IN	Longitudinal	1	734	0	0.001	0.999	0.002	0%
		Transversal	-	-	-	-	-	-	-

Road-Surface		Type of cracking	TP	FP	FN	Precision	Recall	F1-Score	Jaccard Index
07	DBSCAN No IN	Longitudinal	0	0	35	NaN	0.000	NaN	0%
		Transversal	0	0	37	NaN	0.000	NaN	0%
	DBSCAN IN	Longitudinal	-	-	-	-	-	-	-
		Transversal	-	-	-	-	-	-	-
	RF No IN	Longitudinal	0	40	0	0.000	NaN	NaN	0%
		Transversal	0	40	0	0.000	NaN	NaN	0%
	RF IN	Longitudinal	0	40	0	0.000	NaN	NaN	0%
		Transversal	0	40	0	0.000	NaN	NaN	0%

Road-Surface		Type of cracking	TP	FP	FN	Precision	Recall	F1-Score	Jaccard Index
08	DBSCAN No IN	Longitudinal	574	703	182	0.449	0.759	0.564	39%
		Transversal	81	139	157	0.368	0.340	0.353	21%
	DBSCAN IN	Longitudinal	0	0	749	NaN	0.000	NaN	0%
		Transversal	0	0	246	NaN	0.000	NaN	0%
	RF No IN	Longitudinal	472	44	277	0.914	0.630	0.746	60%
		Transversal	244	303	0	0.446	0.999	0.616	45%
	RF IN	Longitudinal	472	43	277	0.916	0.630	0.746	60%
		Transversal	244	303	0	0.446	0.999	0.616	45%

Road-Surface		Type of cracking	TP	FP	FN	Precision	Recall	F1-Score	Jaccard Index
09	DBSCAN No IN	Longitudinal	5	1465	11	0.003	0.312	0.006	0%
		Transversal	245	173	749	0.586	0.246	0.347	21%
	DBSCAN IN	Longitudinal	0	0	19	NaN	0.000	NaN	0%
		Transversal	0	0	976	NaN	0.000	NaN	0%
	RF No IN	Longitudinal	14	655	2	0.020	0.875	0.040	2%
		Transversal	1008	69	1	0.935	0.999	0.966	94%
	RF IN	Longitudinal	14	655	2	0.020	0.875	0.040	2%
		Transversal	1008	76	1	0.929	0.999	0.963	93%

Road-Surface		Type of cracking	TP	FP	FN	Precision	Recall	F1-Score	Jaccard Index
10	DBSCAN No IN	Longitudinal	399	794	137	0.334	0.744	0.461	34%
		Transversal	197	271	260	0.420	0.431	0.425	27%
	DBSCAN IN	Longitudinal	0	0	536	NaN	0.000	NaN	0%
		Transversal	0	0	457	NaN	0.000	NaN	0%
	RF No IN	Longitudinal	506	73	23	0.873	0.956	0.913	84%
		Transversal	459	57	3	0.889	0.993	0.938	88%
	RF IN	Longitudinal	506	73	23	0.873	0.956	0.913	84%
		Transversal	461	62	1	0.881	0.997	0.936	88%

Road-Surface		Type of cracking	TP	FP	FN	Precision	Recall	F1-Score	Jaccard Index
11	DBSCAN No IN	Longitudinal	179	353	446	0.336	0.286	0.309	18%
		Transversal	197	360	70	0.353	0.737	0.478	31%
	DBSCAN IN	Longitudinal	0	0	626	NaN	0.000	NaN	0%
		Transversal	0	0	288	NaN	0.000	NaN	0%
	RF No IN	Longitudinal	418	44	210	0.904	0.665	0.766	62%
		Transversal	290	237	2	0.550	0.993	0.708	55%
	RF IN	Longitudinal	418	44	210	0.904	0.665	0.766	62%
		Transversal	290	238	2	0.549	0.993	0.707	55%

Road-Surface		Type of cracking	TP	FP	FN	Precision	Recall	F1-Score	Jaccard Index
12	DBSCAN No IN	Longitudinal	437	704	177	0.382	0.711	0.498	33%
		Transversal	399	298	256	0.572	0.609	0.590	42%
	DBSCAN IN	Longitudinal	0	0	623	NaN	0.000	NaN	0%
		Transversal	0	0	673	NaN	0.000	NaN	0%
	RF No IN	Longitudinal	584	31	41	0.949	0.934	0.941	89%
		Transversal	667	75	4	0.898	0.994	0.944	89%
	RF IN	Longitudinal	584	37	41	0.940	0.934	0.937	88%
		Transversal	667	74	4	0.900	0.994	0.944	90%

Road-Surface		Type of cracking	TP	FP	FN	Precision	Recall	F1-Score	Jaccard Index
13	DBSCAN No IN	Longitudinal	466	282	233	0.622	0.666	0.644	0%
		Transversal	34	26	142	0.566	0.193	0.288	0%
	DBSCAN IN	Longitudinal	0	0	702	NaN	0.000	NaN	0%
		Transversal	0	0	169	NaN	0.000	NaN	0%
	RF No IN	Longitudinal	690	71	11	0.906	0.984	0.943	11%
		Transversal	165	17	2	0.906	0.988	0.945	0%
	RF IN	Longitudinal	692	72	9	0.905	0.987	0.944	11%
		Transversal	165	17	2	0.906	0.988	0.945	0%

Road-Surface		Type of cracking	TP	FP	FN	Precision	Recall	F1-Score	Jaccard Index
14	DBSCAN No IN	Longitudinal	1	1473	68	0.009	0.014	0.001	45%
		Transversal	0	394	4	0.000	0.000	NaN	15%
	DBSCAN IN	Longitudinal	0	0	75	NaN	0.000	NaN	0%
		Transversal	0	0	5	NaN	0.000	NaN	0%
	RF No IN	Longitudinal	73	607	0	0.107	0.999	0.193	53%
		Transversal	3	806	0	0.003	0.999	0.007	60%
	RF IN	Longitudinal	73	611	0	0.106	0.999	0.192	53%
		Transversal	3	807	0	0.003	0.999	0.007	60%

Road-Surface		Type of cracking	TP	FP	FN	Precision	Recall	F1-Score	Overall accuracy
15	DBSCAN No IN	Longitudinal	688	762	77	0.474	0.899	0.621	45%
		Transversal	105	92	487	0.532	0.177	0.266	15%
	DBSCAN IN	Longitudinal	0	0	702	NaN	0.000	NaN	0%
		Transversal	0	0	169	NaN	0.000	NaN	0%
	RF No IN	Longitudinal	421	21	346	0.952	0.548	0.696	53%
		Transversal	595	388	3	0.605	0.994	0.752	60%
	RF IN	Longitudinal	421	32	346	0.929	0.548	0.690	53%
		Transversal	595	388	3	0.605	0.994	0.752	60%

Road-Surface		Type of cracking	TP	FP	FN	Precision	Recall	F1-Score	Overall accuracy
16	DBSCAN No IN	Longitudinal	0	601	1	0.000	0.000	NaN	0%
		Transversal	78	168	43	0.317	0.644	0.425	27%
	DBSCAN IN	Longitudinal	0	0	2	NaN	0.000	NaN	0%
		Transversal	0	0	118	NaN	0.000	NaN	0%
	RF No IN	Longitudinal	4	675	0	0.005	0.999	0.011	1%
		Transversal	119	11	0	0.915	0.999	0.955	92%
	RF IN	Longitudinal	4	673	0	0.005	0.999	0.011	1%
		Transversal	119	11	0	0.915	0.999	0.955	92%

Road-Surface		Type of cracking	TP	FP	FN	Precision	Recall	F1-Score	Jaccard Index
17	DBSCAN No IN	Longitudinal	781	477	550	0.620	0.586	0.603	43%
		Transversal	16	4	33	0.800	0.326	0.463	30%
	DBSCAN IN	Longitudinal	0	0	702	NaN	0.000	NaN	0%
		Transversal	0	0	169	NaN	0.000	NaN	0%
	RF No IN	Longitudinal	1319	82	5	0.941	0.996	0.968	94%
		Transversal	49	6	1	0.890	0.989	0.933	88%
	RF IN	Longitudinal	1318	92	6	0.934	0.995	0.964	93%
		Transversal	49	6	1	0.890	0.980	0.933	88%

Road-Surface		Type of cracking	TP	FP	FN	Precision	Recall	F1-Score	Jaccard Index
18	DBSCAN No IN	Longitudinal	987	456	400	0.683	0.711	0.697	54%
		Transversal	0	35	0	0.000	0.000	NaN	0%
	DBSCAN IN	Longitudinal	0	1453	0	NaN	0.000	NaN	0%
		Transversal	-	-	-	-	-	-	-
	RF No IN	Longitudinal	1403	49	55	0.966	0.962	0.964	93%
		Transversal	0	82	0	0.000	NaN	NaN	0%
	RF IN	Longitudinal	1403	48	55	0.966	0.962	0.964	93%
		Transversal	0	82	0	0.000	NaN	NaN	0%

Road-Surface		Type of cracking	TP	FP	FN	Precision	Recall	F1-Score	Jaccard Index
19	DBSCAN No IN	Longitudinal	0	864	0	0.000	0.000	NaN	0%
		Transversal	-	-	-	-	-	-	-
	DBSCAN IN	Longitudinal	-	-	-	-	-	-	-
		Transversal	-	-	-	-	-	-	-
	RF No IN	Longitudinal	0	389	0	0.000	NaN	NaN	0%
		Transversal	0	62	0	0.000	NaN	NaN	0%
	RF IN	Longitudinal	0	389	0	0.000	NaN	NaN	0%
		Transversal	0	62	0	0.000	NaN	NaN	0%

Road-Surface		Type of cracking	TP	FP	FN	Precision	Recall	F1-Score	Jaccard Index
20	DBSCAN No IN	Longitudinal	0	927	0	NaN	0.000	NaN	0%
		Transversal	0	0	3	NaN	0.000	NaN	0%
	DBSCAN IN	Longitudinal	-	-	-	-	-	-	-
		Transversal	-	-	-	-	-	-	-
	RF No IN	Longitudinal	0	800	0	0.000	NaN	NaN	0%
		Transversal	2	69	0	0.028	0.999	0.054	3%
	RF IN	Longitudinal	919	36	57	0.962	0.941	0.951	91%
		Transversal	53	62	0	0.460	0.999	0.630	46%

Road-Surface		Type of cracking	TP	FP	FN	Precision	Recall	F1-Score	Jaccard Index
21	DBSCAN No IN	Longitudinal	726	527	247	0.579	0.746	0.652	48%
		Transversal	13	101	37	0.114	0.260	0.158	9%
	DBSCAN IN	Longitudinal	0	0	961	NaN	0.000	NaN	0%
		Transversal	0	0	51	NaN	0.000	NaN	0%
	RF No IN	Longitudinal	919	38	57	0.960	0.941	0.950	91%
		Transversal	53	62	0	0.460	0.999	0.630	46%
	RF IN	Longitudinal	919	36	57	0.962	0.941	0.951	91%
		Transversal	53	62	0	0.460	0.999	0.630	46%

Road-Surface		Type of cracking	TP	FP	FN	Precision	Recall	F1-Score	Overall accuracy
22	DBSCAN No IN	Longitudinal	60	520	8	0.103	0.882	0.185	10%
		Transversal	6	103	17	0.055	0.260	0.090	5%
	DBSCAN IN	Longitudinal	-	-	-	-	-	-	-
		Transversal	-	-	-	-	-	-	-
	RF No IN	Longitudinal	0	266	0	0.000	NaN	NaN	0%
		Transversal	0	138	0	0.000	NaN	NaN	0%
	RF IN	Longitudinal	0	266	0	0.000	NaN	NaN	0%
		Transversal	0	138	0	0.000	NaN	NaN	0%

Road-Surface		Type of cracking	TP	FP	FN	Precision	Recall	F1-Score	Overall accuracy
23	DBSCAN No IN	Longitudinal	0	32	199	0.000	0.00	NaN	0%
		Transversal	-	-	-	-	-	-	-
	DBSCAN IN	Longitudinal	0	0	195	NaN	0.000	NaN	0%
		Transversal	-	-	-	-	-	-	-
	RF No IN	Longitudinal	0	0	196	0.000	NaN	NaN	0%
		Transversal	-	-	-	-	-	-	-
	RF IN	Longitudinal	196	4	0	0.989	0.999	0.989	98%
		Transversal	-	-	-	-	-	-	-

Road-Surface		Type of cracking	TP	FP	FN	Precision	Recall	F1-Score	Overall accuracy
24	DBSCAN No IN	Longitudinal	0	344	1	0.000	0.000	NaN	0%
		Transversal	-	-	-	-	-	-	-
	DBSCAN IN	Longitudinal	-	-	-	-	-	-	-
		Transversal	-	-	-	-	-	-	-
	RF No IN	Longitudinal	0	580	0	0.000	NaN	NaN	0%
		Transversal	0	70	0	0.000	NaN	NaN	0%
	RF IN	Longitudinal	0	580	0	0.000	NaN	NaN	0%
		Transversal	0	70	0	0.000	NaN	NaN	0%

Road-Surface		Type of cracking	TP	FP	FN	Precision	Recall	F1-Score	Jaccard Index
25	DBSCAN No IN	Longitudinal	11	50	508	0.180	0.021	0.037	2%
		Transversal	-	-	-	-	-	-	-
	DBSCAN IN	Longitudinal	0	0	517	NaN	0.000	NaN	0%
		Transversal	-	-	-	-	-	-	-
	RF No IN	Longitudinal	510	30	7	0.944	0.986	0.964	93%
		Transversal	0	53	0	0.000	NaN	NaN	0%
	RF IN	Longitudinal	510	30	7	0.944	0.986	0.964	93%
		Transversal	0	53	0	0.000	NaN	NaN	0%

Road-Surface		Type of cracking	TP	FP	FN	Precision	Recall	F1-Score	Overall accuracy
26	DBSCAN No IN	Longitudinal	0	48	3	0.000	0.000	NaN	0%
		Transversal	-	-	-	-	-	-	-
	DBSCAN IN	Longitudinal	0	0	7	NaN	0.000	NaN	0%
		Transversal	-	-	-	-	-	-	-
	RF No IN	Longitudinal	6	232	0	0.025	0.999	0.049	3%
		Transversal	-	-	-	-	-	-	-
	RF IN	Longitudinal	6	229	0	0.025	0.999	0.049	3%
		Transversal	-	-	-	-	-	-	-

Road-Surface		Type of cracking	TP	FP	FN	Precision	Recall	F1-Score	Jaccard Index
27	DBSCAN No IN	Longitudinal	68	35	302	0.660	0.183	0.287	17%
		Transversal	-	-	-	-	-	-	-
	DBSCAN IN	Longitudinal	0	0	359	NaN	0.000	NaN	0%
		Transversal	-	-	-	-	-	-	-
	RF No IN	Longitudinal	357	46	0	0.885	0.999	0.939	89%
		Transversal	-	-	-	-	-	-	-
	RF IN	Longitudinal	357	46	0	0.885	0.999	0.939	89%
		Transversal	-	-	-	-	-	-	-

BIBLIOGRAPHY

Abdel-Qader, I., Abudayyeh, O., & Kelly, M. E. (2003). Analysis of edge-detection techniques for crack identification in bridges. Journal of computing in civil engineering, 17(4), 255-263. https://doi.org/10.1061/(ASCE)0887-3801(2003)17:4(255)

Abduljabbar, R., Dia, H., Liyanage, S., & Bagloee, S. A. (2019). Applications of Artificial Intelligence in Transport: An Overview. Sustainability, 11, 189. https://doi.org/10.3390/su11010189

Agnisarman, S., Lopes, S., Madathil, K. C., Piratla, K., & Gramopadhye, A. (2019). A survey of automation-enabled human-in-the-loop systems for infrastructure visual inspection. Automation in Construction, 97, 52-76. https://doi.org/10.1016/j.autcon.2018.10.019

Albeaino, G., Gheisari, M., & Franz, B. W. (2019). A systematic review of unmanned aerial vehicle application areas and technologies in the AEC domain. ITcon, 24, 381-405. https://www.itcon.org/2019/20

Al-Bayari, O. (2019). Mobile mapping systems in civil engineering projects (case studies). Applied Geomatics, 11, 1–13. https://doi.org/10.1007/s12518-018-0222-6

Alessandrini, S. (2020). Il crollo del ponte Morandi a Genova. Ingenio. Available online: https://www.ingenio-web.it/20966-il-crollo-del-ponte-

morandi-a-genova#:~:text=Alle%2011.36%20del%2014%20agosto,del%20viadotto%20sul%20Polcevera%2C%20un (accessed on 27 December 2024)

Alicandro, M., Di Angelo, L., Di Stefano, P., Dominici, D., Guardiani, E., & Zollini, S. (2022). Fast and accurate registration of terrestrial point clouds using a planar approximation of roof features. Remote Sens, 14, 2986. https://doi.org/10.3390/rs14132986

Alicandro, M., Dominici, D., Pascucci, N., Quaresima, R., & Zollini, S. (2023). Enhanced algorithms to extract decay forms of concrete infrastructures from UAV photogrammetric data. Int. Arch. Photogramm. Remote Sens. Spatial Inf. Sci., XLVIII-1/W1-2023, 9–15. https://doi.org/10.5194/isprs-archives-XLVIII-1-W1-2023-9-2023

Alicandro, M., Zollini, S., Oxoli, D., Pascucci, N., Dominici, D., & Brescia, D. (2022). Design and implementation of an open-source web-GIS to manage the public works of Abruzzo Region: An example towards the digitalization of the management process of public administrations. Int. Arch. Photogramm. Remote Sens. Spatial Inf. Sci., XLVIII-4/W1-2022, 21–26. https://doi.org/10.5194/isprs-archives-XLVIII-4-W1-2022-21-2022

Alotaibi, M., Honarvar Shakibaei Asli, B., & Khan, M. (2021). Non-Invasive Inspections: A Review on Methods and Tools. Sensors, 21(24), 8474. https://doi.org/10.3390/s21248474

Al-Sehrawy, R., Kumar, B., & Watson, R. (2021). A digital twin uses classification system for urban planning & city infrastructure management. Journal of Information Technology in Construction, 26, 832-362. Article 45. https://doi.org/10.36680/j.itcon.2021.045

Amin, M. (2000). National infrastructures as complex interactive networks. Automation, Control, and Complexity: An Integrated Approach, 3, 263-286.

Angeli, S., Lingua, A. M., Maschio, P., Piantelli, L., Dugone, D., & Giorgis, M. (2019). Dense 3D model generation of a dam surface using UAV for visual inspection. In Aspragathos, N., Koustoumpardis, P., & Moulianitis,

V. (Eds.), Advances in Service and Industrial Robotics. RAAD 2018. Mechanisms and Machine Science, vol 67. Springer, Cham. https://doi.org/10.1007/978-3-030-00232-9_16

Applanix. (2023). POSLV 220 Datasheet. Available online: https://www.applanix.com/downloads/products/specs/POS-LVDatasheet.pdf (Accessed 12 December 2024)

Arctur, D., & Zeiler, M. (2004). Designing Geodatabases: Case studies in GIS data modeling. ESRI, Inc.

Argyroudis, S. A., Mitoulis, S. A., Winter, M. G., & Kaynia, A. M. (2019). Fragility of transport assets exposed to multiple hazards: State-of-the-art review toward infrastructural resilience. Reliability Engineering & System Safety, 191, 106567. https://doi.org/10.1016/j.ress.2019.106567

Artagan, S. S., Bianchini Ciampoli, L., & D'Amico, F., et al. (2020). Non-destructive assessment and health monitoring of railway infrastructures. Survey Geophysics, 41, 447–483. https://doi.org/10.1007/s10712-019-09544-w

Avsar, Ö., Akca, D., & Altan, O. (2014). Photogrammetric deformation monitoring of the Second Bosphorus Bridge in Istanbul. Int. Arch. Photogramm. Remote Sens. Spatial Inf. Sci., XL-5, 71–76. https://doi.org/10.5194/isprsarchives-XL-5-71-2014

Bailey, T.; Durrant-Whyte, H. (2006). Simultaneous localization and mapping (SLAM): Part II. IEEE Robot. Autom. Mag., 13, 108–117. https://doi.org/10.1109/MRA.2006.1678144

Babić, D., Babić, D., Cajner, H., Sruk, A., Fiolić, M. (2020). Effect of Road Markings and Traffic Signs Presence on Young Driver Stress Level, Eye Movement and Behaviour in Night-Time Conditions: A Driving Simulator Study. Safety, 6(2), 24. https://doi.org/10.3390/safety6020024

Babić, D., Babić, D., Fiolić, M., Ferko, M. (2022). Road Markings and Signs in Road Safety. Encyclopedia, 2(4), 1738–1752. https://doi.org/10.3390/encyclopedia2040119

Balado, J., Martínez-Sánchez, J., Arias, P., Novo, A. (2019). Road Environment Semantic Segmentation with Deep Learning from MLS Point Cloud Data. Sensors, 19(16), 3466. https://doi.org/10.3390/s19163466

Bartolucci, D. (2009). Principi di laser scanning 3D. Dario Flaccovio Editore.

Belgiu, M. and Drăguţ, L., 2016. Random forest in remote sensing: A review of applications and future directions. ISPRS journal of photogrammetry and remote sensing, 114, pp.24-31. https://doi.org/10.1016/j.isprsjprs.2016.01.011

Bellino, F. (2019). "Un intervento poco risolutivo." Il Giornale dell'Ingegnere, (6), 25.

Bendib, A., Hadda, D., Mahdi, K. (2016). Application of Webgis in the development of interactive interface for urban management in Batna City. Journal of Engineering and Technology Research, 8(2), 13–20. https://academicjournals.org/journal/JETR/articleabstract/A3D58BF57892

Bernhardsen, T. (2002). Geographic information systems: an introduction. John Wiley & Sons.

Berrett, B.E., Vernon, C.A., Beckstrand, H., Pollei, M., Markert, K., Franke, K.W., Hedengren, J.D. (2021). Large-Scale Reality Modeling of a University Campus Using Combined UAV and Terrestrial Photogrammetry for Historical Preservation and Practical Use. Drones, 5, 136. https://doi.org/10.3390/drones5040136

Bertovic, M. (2015). Human factors in non-destructive testing (NDT): risks and challenges of mechanised NDT. Technische Universitaet Berlin (Germany).

Bittencourt, T.N., Frangopol, D., Beck, A. (Eds.) (2016). Maintenance, monitoring, safety, risk and resilience of bridges and bridge networks. CRC Press.

Blaschke, T. (2010). Object based image analysis for remote sensing. ISPRS Journal of Photogrammetry and Remote Sensing, 65(1), 2–16. https://doi.org/10.1016/j.isprsjprs.2009.06.004

Blazey, A., Gonguet, F., Stokoe, P. (2020). Maintaining and managing public infrastructure assets. In Schwartz G., Hansen T. S., Verdier G., Fouad M. (Eds.), Well spent: How strong infrastructure governance can end waste in public investment (p. 265). International Monetary Fund.

Bonham-Carter, G. (1994). Geographic information systems for geoscientists: modelling with GIS (No. 13). Elsevier.

Bornaz, L. (2006). Principi di funzionamento e tecniche di acquisizione. Laser scanning terrestre, Atti del corso "La tecnica del laser scanning terrestre" (Udine 2004), Udine, CISM, 1–18.

Breiman, L. (2001). Random forests. Machine Learning, 45, 5–32.

Breunig, M., Bradley, P.E., Jahn, M., Kuper, P., Mazroob, N., Rösch, N., Al-Doori, M., Stefanakis, E., Jadidi, M. (2020). Geospatial Data Management Research: Progress and Future Directions. ISPRS International Journal of Geo-Information, 9(2), 95. https://doi.org/10.3390/ijgi9020095

Brownjohn, J.M.W. (2007). Structural health monitoring of civil infrastructure. Philosophical Transactions of the Royal Society A: Mathematical, Physical and Engineering Sciences, 365(1851), 589–622. https://doi.org/10.1098/rsta.2006.1925

Burrough, P.A., McDonnell, R.A., Lloyd, C.D. (2015). Principles of geographical information systems. Oxford University Press, USA.

Cao, H., Chen, T., Zhu, H., & Ren, H. (2022). Influence of Frequent Freeze–Thaw Cycles on Performance of Asphalt Pavement in High-Cold

and High-Altitude Areas. Coatings, 12(6), 752. https://doi.org/10.3390/coatings12060752

Cantisani, G., Borrelli, C.C., Del Serrone, G., & Peluso, P. (2023). Optimizing Road Safety Inspections on Rural Roads. Infrastructures, 8, 30. https://doi.org/10.3390/infrastructures8020030

Chan, B., Guan, H., Hou, L., et al. (2016). Defining a conceptual framework for the integration of modelling and advanced imaging for improving the reliability and efficiency of bridge assessments. Journal of Civil Structural Health Monitoring, 6, 703–714. https://doi.org/10.1007/s13349-016-0191-6

Cha, Y.J., Choi, W., & Büyüköztürk, O. (2017). Deep learning-based crack damage detection using convolutional neural networks. Computer-Aided Civil and Infrastructure Engineering, 32(5), 361–378. https://doi.org/10.1111/mice.12263

Chang, C.-C., & Lin, C.-J. (2011). LIBSVM: A Library for Support Vector Machines. ACM Transactions on Intelligent Systems and Technology, 2(3), 1–27. https://doi.org/10.1145/1961189.1961199

Chang, C.M., Salinas, G.T., Gamero, T.S., Schroeder, S., Vélez Canchanya, M.A., & Mahnaz, S.L. (2023). An Infrastructure Management Humanistic Approach for Smart Cities Development, Evolution, and Sustainability. Infrastructures, 8(9), 127. https://doi.org/10.3390/infrastructures8090127

Chen, Y., 2019. Archiving Digital Maps with GeoPackage and Vector-tile Dissemination. Signature (Student).

Chen, Q., Jiang, W., Meng, X., Jiang, P., Wang, K., Xie, Y., & Ye, J. (2018). Vertical Deformation Monitoring of the Suspension Bridge Tower Using GNSS: A Case Study of the Forth Road Bridge in the UK. Remote Sensing, 10(3), 364. https://doi.org/10.3390/rs10030364

Chen, W., Zhou, C., Shang, G., Wang, X., Li, Z., Xu, C., & Hu, K. (2022). SLAM Overview: From Single Sensor to Heterogeneous Fusion. Remote Sensing, 14(23), 6033. https://doi.org/10.3390/rs14236033

Cheng, Y.-T., Lin, Y.-C., & Habib, A. (2022). Generalized LiDAR Intensity Normalization and Its Positive Impact on Geometric and Learning-Based Lane Marking Detection. Remote Sensing, 14(17), 4393. https://doi.org/10.3390/rs14174393

Chekole, S.D. (2014). Surveying with GPS, Total Station, and Terrestrial Laser Scanner: A Comparative Study.

Chiaia, B., Marasco, G., Ventura, G., et al. (2020). Customised Active Monitoring System for Structural Control and Maintenance Optimisation. Journal of Civil Structural Health Monitoring, 10, 267–282. https://doi.org/10.1007/s13349-020-00382-8

Chin, R.T., & Harlow, C.A. (1982). Automated Visual Inspection: A Survey. IEEE Transactions on Pattern Analysis and Machine Intelligence, PAMI-4(6), 557–573. https://doi.org/10.1109/TPAMI.1982.4767309

Choi, W.C., & Chong, K.S. (2022). Analysis of Road Sign-Related Factors Affecting Driving Safety with Respect to City Size. Applied Sciences, 12(19), 10163. https://doi.org/10.3390/app121910163

Cina, A. (2014). Dal GPS al GNSS (Global Navigation Satellite System). Celid, Torino.

Civera, M., Sibille, L., Fragonara, L.Z., & Ceravolo, R. (2023). A DBSCAN-Based Automated Operational Modal Analysis Algorithm for Bridge Monitoring. Measurement, 208, 112451. https://doi.org/10.1016/j.measurement.2023.112451

Coetzee, S., Ivánová, I., Mitasova, H., & Brovelli, M.A. (2020). Open Geospatial Software and Data: A Review of the Current State and a Perspective into the Future. ISPRS International Journal of Geo-Information, 9(2), 90. https://doi.org/10.3390/ijgi9020090

Corradeghini, P. (2017). Strumenti di rilievo topografico, una panoramica generale. 3DMetrica.

Cressie, N. (2015). Statistics for Spatial Data. John Wiley & Sons.

Dais, D., Bal, I.E., Smyrou, E., & Sarhosis, V. (2021). Automatic crack classification and segmentation on masonry surfaces using convolutional neural networks and transfer learning. Automation in Construction, 125, 103606. https://doi.org/10.1016/j.autcon.2021.103606

Daneshgaran, F., Marangi, A., Bruno, N., Lizzio, F., Mondin, M., & Olia, K. (2021). Visual Simultaneous Localization and Mapping with Applications to Monitoring of Underground Transportation Infrastructure. Transportation Research Record, 2675(2), 198-206. https://doi.org/10.1177/0361198120963109

Daud, M., Ugliotti, F.M., & Osello, A. (2024). Comprehensive Analysis of the Use of Web-GIS for Natural Hazard Management: A Systematic Review. Sustainability, 16(10), 4238. https://doi.org/10.3390/su16104238

Dechter, R. (1986). Learning While Searching in Constraint-Satisfaction-Problems. AAAI, 178-185.

De Flaviis, A., Alaggio, R., & Zulli, D. (2024). Generalized Beam Theory for the static and dynamic response of a bridge deck with Structural Health Monitoring purposes. Procedia Structural Integrity, 62, 871-878. https://doi.org/10.1016/j.prostr.2024.09.117

Deibe, D., Amor, M., & Doallo, R. (2020). Big Data Geospatial Processing for Massive Aerial LiDAR Datasets. Remote Sensing, 12(4), 719. https://doi.org/10.3390/rs12040719

Del Río-Barral, P., Grandío, J., Riveiro, B., & Arias, P. (2023). Identification of relevant point cloud geometric features for the detection of pavement cracks using MLS data. International Archives of Photogrammetry, Remote Sensing and Spatial Information Sciences, XLVIII-1/W1, 107–112. https://doi.org/10.5194/isprs-archives-XLVIII-1-W1-2023-107-2023

Del Río-Barral, P., Soilán, M., González-Collazo, S.M., & Arias, P. (2022). Pavement Crack Detection and Clustering via Region-Growing Algorithm from 3D MLS Point Clouds. Remote Sensing, 14, 5866. https://doi.org/10.3390/rs14225866

Demantké, J., Mallet, C., David, N., & Vallet, B. (2011). Dimensionality based scale selection in 3D LiDAR point clouds. International Archives of Photogrammetry, Remote Sensing and Spatial Information Sciences, 38(Part 5), W12. https://doi.org/10.5194/isprsarchives-XXXVIII-5-W12-97-2011

Detchev, I., Habib, A., & El-Badry, M. (2012, March). Extraction of cracks from concrete beam images. In Proceedings of ASPRS 2012 annual conference, Sacramento.

Diene, A. (2024). Infrastructure Development and Economic Development. In N. Baporikar (Ed.), Infrastructure Development Strategies for Empowerment and Inclusion (pp. 1-21). IGI Global. https://doi.org/10.4018/979-8-3693-2917-7.ch001

Di Stefano, F., Chiappini, S., Gorreja, A., Balestra, M., & Pierdicca, R. (2021). Mobile 3D scan LiDAR: a literature review. Geomatics, Natural Hazards and Risk, 12(1), 2387–2429. https://doi.org/10.1080/19475705.2021.1964617

Di Stefano, F., Pierdicca, R., Malinverni, E. S., Corneli, A., & Naticchia, B. (2023). Point cloud classification of an urban environment using a semi-automatic approach. International Archives of Photogrammetry, Remote Sensing and Spatial Information Sciences, XLVIII-1/W1, 131–138. https://doi.org/10.5194/isprs-archives-XLVIII-1-W1-2023-131-2023

Dillon, P., Aimmanee, P., Wakai, A., Sato, G., Hung, H., & Karnjana, J. (2021). A Novel Recursive Non-Parametric DBSCAN Algorithm for 3D Data Analysis with an Application in Rockfall Detection. Journal of Disaster Research, 16, 579-587. https://doi.org/10.20965/jdr.2021.p0579

DJI Matrice 200. (2020). Available online: https://www.dji.com/be/matrice-200-series (accessed on 27 December 2024).

DJI Matrice MINI 2. (2023). https://www.dji.com/it/mini-2/ (accessed 27 December 2024).

Dlesk, A., Vach, K., Šedina, J., & Pavelka, K. (2022). Comparison of Leica BLK360 and Leica BLK2GO on chosen test objects. International Archives of Photogrammetry, Remote Sensing and Spatial Information Sciences, XLVI-5/W1, 77–82. https://doi.org/10.5194/isprs-archives-XLVI-5-W1-2022-77-2022

Dorafshan, S., Thomas, R.J., & Maguire, M. (2018). Comparison of deep convolutional neural networks and edge detectors for image-based crack detection in concrete. Construction and Building Materials, 186, 1031-1045. https://doi.org/10.1016/j.conbuildmat.2018.08.011

Duarte, L., Queirós, C., & Teodoro, A.C. (2021). Comparative analysis of QGIS plugins for Web Maps creation. La Granja, 34(2), 8–26.

D'Uva, D., & Eugeni, F. (2021). DTM to NURBS—A parametric approach to landscape modeling for an environmentally-conscious design. Sustainability, 13(4), 2379. https://doi.org/10.3390/su13042379

Dung, C.V. (2019). Autonomous concrete crack detection using deep fully convolutional neural networks. Automation in Construction, 99, 52-58.

Dwivedi, S.K., Vishwakarma, M., & Soni, A. (2018). Advances and researches on non-destructive testing: A review. Materials Today: Proceedings, 5(2), 3690-3698. https://doi.org/10.1016/j.matpr.2017.11.620

El Masri, Y., & Rakha, T. (2020). A scoping review of non-destructive testing (NDT) techniques in building performance diagnostic inspections. Construction and Building Materials, 265, 120542. https://doi.org/10.1016/j.conbuildmat.2020.120542

Eugeni, F., Sacco, S., Di Ludovico, D., & D'Ovidio, G. (2024). Walkability infrastructures and urban rebalancing: The case study of L'Aquila city under post-earthquake reconstruction. Infrastructures, 9(3), 42. https://doi.org/10.3390/infrastructures9030042

Everaerts, J. (2008). The use of unmanned aerial vehicles (UAVs) for remote sensing and mapping. The International Archives of the Photogrammetry, Remote Sensing and Spatial Information Sciences, 37(2008), 1187-1192.

Elhashash, M., Albanwan, H., & Qin, R. (2022). A review of mobile mapping systems: From sensors to applications. Sensors, 22(11), 4262. https://doi.org/10.3390/s22114262

Ester, M., Kriegel, H. P., Sander, J., & Xu, X. (1996, August). A density-based algorithm for discovering clusters in large spatial databases with noise. In KDD (Vol. 96, No. 34, pp. 226-231).

European Commission. (2019). EU road safety policy framework 2021–2030—Next steps towards "Vision Zero". Retrieved from https://www.europarl.europa.eu/doceo/document/A-9-2021-0211_EN.html#_section2 (accessed 28 September 2024).

Farrar, C. R., & Worden, K. (2007). An introduction to structural health monitoring. Philosophical Transactions of the Royal Society A: Mathematical, Physical and Engineering Sciences, 365(1851), 303–315. http://doi.org/10.1098/rsta.2006.1928

Frangopol, D. M., & Tsompanakis, Y. (Eds.). (2014). Maintenance and safety of aging infrastructure (Vol. 10). Boca Raton, FL, USA: CRC Press.

Frangopol, D. M., & Liu, M. (2007). Maintenance and management of civil infrastructure based on condition, safety, optimization, and life-cycle cost. Structure and Infrastructure Engineering, 3(1), 29–41. https://doi.org/10.1080/15732470500253164

Futai, M. M., Bittencourt, T. N., Carvalho, H., & Ribeiro, D. M. (2022). Challenges in the application of digital transformation to inspection and maintenance of bridges. Structure and Infrastructure Engineering, 18(10–11), 1581–1600. https://doi.org/10.1080/15732479.2022.2063908

Fan, Y., Feng, Z., Mannan, A., Khan, T. U., Shen, C., & Saeed, S. (2018). Estimating tree position, diameter at breast height, and tree height in real-time using a mobile phone with RGB-D SLAM. Remote Sensing, 10(11), 1845. https://doi.org/10.3390/rs10111845

Feng, C. Q., Li, B. L., Liu, Y. F., Zhang, F., Yue, Y., & Fan, J. S. (2023). Crack assessment using multi-sensor fusion simultaneous localization and mapping (SLAM) and image super-resolution for bridge inspection. Automation in Construction, 155, 105047. https://doi.org/10.1016/j.autcon.2023.105047

Foody, G. M. (2002). Status of land cover classification accuracy assessment. Remote Sensing of Environment, 80(1), 185–201. https://doi.org/10.1016/S0034-4257(01)00295-4

Figueiredo, E., & Brownjohn, J. (2022). Three decades of statistical pattern recognition paradigm for SHM of bridges. Structural Health Monitoring, 21(6), 3018–3054. https://doi.org/10.1177/14759217221075241

Fernandez Galarreta, J., Kerle, N., & Gerke, M. (2015). UAV-based urban structural damage assessment using object-based image analysis and semantic reasoning. Natural Hazards and Earth System Sciences, 15(5), 1087–1101. https://doi.org/10.5194/nhess-15-1087-2015

Forman, G. (2005). Counting positives accurately despite inaccurate classification. In Gama, J., Camacho, R., Brazdil, P. B., Jorge, A. M., & Torgo, L. (Eds.), Machine Learning: ECML 2005. Lecture Notes in Computer Science (Vol. 3720, pp. 564–575). Springer, Berlin, Heidelberg. https://doi.org/10.1007/11564096_55

Gagliardi, R.M., Advanced Highway Maintenance and Construction Technology Center at UC, Davis, and by the Federal Highway Administration (FHWA).

Gaspari, F., Barbieri, F., Demnati, I., Ioli, F., Pinto, L., and Toscani, V.: MOBILE MAPPING SOLUTIONS FOR THE UPDATE AND MANAGEMENT OF TRAFFIC SIGNS IN A ROAD CADASTRE FREE

OPEN-SOURCE GIS ARCHITECTURE, Int. Arch. Photogramm. Remote Sens. Spatial Inf. Sci., XLVIII-4/W7-2023, 61–66, https://doi.org/10.5194/isprs-archives-XLVIII-4-W7-2023-61-2023, 2023.

Gaspari, F., Ioli, F., Barbieri, F., Belcore, E., and Pinto, L.: INTEGRATION OF UAV-LIDAR AND UAV-PHOTOGRAMMETRY FOR INFRASTRUCTURE MONITORING AND BRIDGE ASSESSMENT, Int. Arch. Photogramm. Remote Sens. Spatial Inf. Sci., XLIII-B2-2022, 995–1002, https://doi.org/10.5194/isprs-archives-XLIII-B2-2022-995-2022, 2022.

Gao Y, Xiong G, Hu Z, Chai C, Li H. Bridge Digital Twin for Practical Bridge Operation and Maintenance by Integrating GIS and BIM. Buildings. 2024; 14(12):3731. https://doi.org/10.3390/buildings14123731

Ghahremani, K., Khaloo, A., Mohamadi, S. and Lattanzi, D., 2018. Damage detection and finite-element model updating of structural components through point cloud analysis. Journal of Aerospace Engineering, 31(5), p.04018068. https://doi.org/10.1061/(ASCE)AS.1943-5525.0000885

Gharaibeh, N.G., Zou, Y. and Saliminejad, S., 2010. Assessing the agreement among pavement condition indexes. Journal of Transportation Engineering, 136(8), pp.765-772. https://doi.org/10.1061/(ASCE)TE.1943-5436.0000141

Gharineiat Z, Tarsha Kurdi F, Henny K, Gray H, Jamieson A, Reeves N. Assessment of NavVis VLX and BLK2GO SLAM Scanner Accuracy for Outdoor and Indoor Surveying Tasks. Remote Sensing. 2024; 16(17):3256. https://doi.org/10.3390/rs16173256

Ghose, M.K., Pradhan, R. and Ghose, S.S., 2010. Decision tree classification of remotely sensed satellite data using spec-tral separability matrix. International Journal of Advanced Computer Science and Applications, 1(5).

Giambastiani, M., & Danese, R. (2017). Quantitative Assessment of Pavement Distresses from Mobile Mapping System Data. Journal of

Infrastructure Systems, 23(3), 04017016. https://doi.org/10.1061/(ASCE)IS.1943-555X.0000395

Gkoumas, K., Marques Dos Santos, F., Van Balen, M., Tsakalidis, A., Ortega Hortelano, A., Grosso, M., Haq, A. and Pekar, F., Research and innovation in bridge maintenance, inspection and monitoring, EUR 29650 EN, Publications Office of the European Union, Luxembourg, 2019, ISBN 978-92-76-03379-0, doi:10.2760/719505, JRC115319.

Gkoumas, K., Stepniak, M., Cheimariotis, I., & Marques dos Santos, F. (2024). New technologies for bridge inspection and monitoring: a perspective from European Union research and innovation projects. Structure and Infrastructure Engineering, 20(7–8), 1120–1132. https://doi.org/10.1080/15732479.2024.2311898

Gollob C, Ritter T, Nothdurft A. Forest Inventory with Long Range and High-Speed Personal Laser Scanning (PLS) and Simultaneous Localization and Mapping (SLAM) Technology. Remote Sensing. 2020; 12(9):1509. https://doi.org/10.3390/rs12091509

Gomarasca, M. A. (2009). Basics of geomatics. Springer Science & Business Media.

Gomez, C., Purdie, H. UAV-based Photogrammetry and Geocomputing for Hazards and Disaster Risk Monitoring – A Review. Geoenviron Disasters 3, 23 (2016). https://doi.org/10.1186/s40677-016-0060-y

Gong J., Zhou H., Gordon C., and Jalayer M., "Mobile terrestrial laser scanning for highway inventory data collection," Computing in Civil Engineering, vol. 2012, pp. 545–552, 2012. https://doi.org/10.1061/9780784412343.0069

Greenwood, W. W., Lynch, J. P., & Zekkos, D. (2019). Applications of UAVs in civil infrastructure. Journal of infrastructure systems, 25(2), 04019002. https://doi.org/10.1061/(ASCE)IS.1943-555X.0000464

Grothum, O., Bienert, A., Bluemlein, M., and Eltner, A.: USING MACHINE LEARNING TECHNIQUES TO FILTER VEGETATION IN COLORIZED SFM POINT CLOUDS OF SOIL SURFACES, Int. Arch. Photogramm. Remote Sens. Spatial Inf. Sci., XLVIII-1/W2-2023, 163–170, https://doi.org/10.5194/isprs-archives-XLVIII-1-W2-2023-163-2023, 2023.

Grothum, O., Bienert, A., Bluemlein, M., and Eltner, A.: USING MACHINE LEARNING TECHNIQUES TO FILTER VEGETATION IN COLORIZED SFM POINT CLOUDS OF SOIL SURFACES, Int. Arch. Photogramm. Remote Sens. Spatial Inf. Sci., XLVIII-1/W2-2023, 163–170, https://doi.org/10.5194/isprs-archives-XLVIII-1-W2-2023-163-2023, 2023.

Guan S, Zhu Z, Wang G. A Review on UAV-Based Remote Sensing Technologies for Construction and Civil Applications. Drones. 2022; 6(5):117. https://doi.org/10.3390/drones6050117

Gui, R., Xu, X., Zhang, D., & Pu, F. (2019). Object-based crack detection and attribute extraction from laser-scanning 3D profile data. IEEE Access, 7, 172728-172743.

Guo, H.L., Li, H. and Skitmore, M., 2010. Life-cycle management of construction projects based on virtual prototyping technology. Journal of Management in Engineering, 26(1), pp.41-47. https://doi.org/10.1061/(ASCE)0742-597X(2010)26:1(41)

Gupta A, Fernando X. Simultaneous Localization and Mapping (SLAM) and Data Fusion in Unmanned Aerial Vehicles: Recent Advances and Challenges. Drones. 2022; 6(4):85. https://doi.org/10.3390/drones6040085

Haala, N., Kölle, M., Cramer, M., Laupheimer, D., Mandlburger, G., and Glira, P. (2020). HYBRID GEOREFERENCING, ENHANCEMENT AND CLASSIFICATION OF ULTRA-HIGH RESOLUTION UAV LIDAR AND IMAGE POINT CLOUDS FOR MONITORING APPLICATIONS. ISPRS Ann. Photogramm. Remote Sens. Spatial Inf. Sci., V-2-2020, 727–734. https://doi.org/10.5194/isprs-annals-V-2-2020-727-2020

Habib, A., Al-Ruzouq R., Ghanma M., and Morgan M. (2005). "Photogrammetric and LiDAR data registration using linear features". Photogrammetric Engineering & Remote Sensing, 71.6, pp. 699–707. https://doi.org/10.14358/PERS.71.6.699

Habib, A., J. Lay, and C. Wong. (2024). Specifications for the quality assurance and quality control of lidar systems. [Online]. Available: https://engineering.purdue.edu/CE/Academics/Groups/Geomatics/DPRG/files/LIDARErrorPropagation.zip

Habib, A., & Lin, Y. J. (2016). Multi-class simultaneous adaptive segmentation and quality control of point cloud data. Remote Sensing, 8(2). https://doi.org/10.3390/rs8020104

Hakimi O., Liu H., Abudayyeh O., Houshyar A., Almatared M., Alhawiti A. (2023). Data Fusion for Smart Civil Infrastructure Management: A Conceptual Digital Twin Framework. Buildings, 13(11), 2725. https://doi.org/10.3390/buildings13112725

Hassani S., Dackermann U. (2023). A Systematic Review of Advanced Sensor Technologies for Non-Destructive Testing and Structural Health Monitoring. Sensors, 23(4), 2204. https://doi.org/10.3390/s23042204

Hay, G. J., & Castilla, G. (2006, July). Object-based image analysis: strengths, weaknesses, opportunities and threats (SWOT). In Proceedings of the 1st International Conference OBIA, pp. 4-5. https://citeseerx.ist.psu.edu/document?repid=rep1&type=pdf&doi=00f56c5d2ca1389921df92d6b284f4d663d5dc25

He, Z., Li, W., Salehi, H., Zhang, H., Zhou, H., & Jiao, P. (2022). Integrated structural health monitoring in bridge engineering. Automation in Construction, 136, 104168. https://doi.org/10.1016/j.autcon.2022.104168

Hearn, G. (2016, September). Managing road transport in a world of changing climate and land use. In Proceedings of the Institution of Civil Engineers-Municipal Engineer (Vol. 169, No. 3, pp. 146-159). Thomas Telford Ltd. https://doi.org/10.1680/muen.15.00009

Heinaro, E., Tanhuanpää, T., Vastaranta, M., Yrttimaa, T., Kukko, A., Hakala, T., Mattsson, T., Holopainen, M. (2023). Evaluating Factors Impacting Fallen Tree Detection from Airborne Laser Scanning Point Clouds. Remote Sensing, 15(2), 382. https://doi.org/10.3390/rs15020382

Heipke, C., Mayer, H., Wiedemann, C., & Jamet, O. (1997). Evaluation of automatic road extraction. International Archives of Photogrammetry and Remote Sensing, 32(3 SECT 4W2), 151-160.

Hirt, P. R., Holtkamp, J., Hoegner, L., Xu, Y., & Stilla, U. (2022). Occlusion detection of traffic signs by voxel-based ray tracing using highly detailed models and MLS point clouds of vegetation. International Journal of Applied Earth Observation and Geoinformation, 114, 103017. https://doi.org/10.1016/j.jag.2022.103017

Holgado-Barco, A., Riveiro, B., González-Aguilera, D., and Arias, P. (2017). Automatic Inventory of Road Cross-Sections from Mobile Laser Scanning System. Computer-Aided Civil and Infrastructure Engineering, 32: 3-17. https://doi.org/10.1111/mice.12213

Holtz, R., Barry, C., and Berg, R. (1998). Federal Highway Administration.

Huang, P., Cheng, M., Chen, Y., Luo, H., Wang, C., & Li, J. (2017). Traffic sign occlusion detection using mobile laser scanning point clouds. IEEE Transactions on Intelligent Transportation Systems, 18(9), 2364-2376. https://doi.org/10.1109/TITS.2016.2639582

Hosseini, F., Nasimifar, M., Sivaneswaran, N., & Golalipour, A. (2024). Mutual impacts of changing climate and flexible pavement performance considering resilience and sustainable aspects. Journal of Cleaner Production, 460, 142594. https://doi.org/10.1016/j.jclepro.2024.142594

Huang T., Yang G., and Tang. G., (1979). "A fast two-dimensional median filtering algorithm," IEEE Transactions on Acoustics, Speech, and Signal Processing, vol. 27, no. 1, pp. 13-18. https://doi.org/10.1109/TASSP.1979.1163188

Indiana LTAP, "Indiana Local Road and Bridge Conditions" (2016). Indiana Local Technical Assistance Program (LTAP) Publications. Paper 111. https://docs.lib.purdue.edu/inltappubs/111

Jaccard, P. (1901). Étude comparative de la distribution florale dans une portion des Alpes et des Jura. Bulletin de la Société Vaudoise des Sciences Naturelles, 37, 547-579.

Jaccard, P. (1912). The Distribution of the Flora of the Alpine Zone. New Phytologist, 11, 37-50. https://doi.org/10.1111/j.1469-8137.1912.tb05611.x

Javanmardi, M., Javanmardi, E., Gu, Y., & Kamijo, S. (2017). Towards High-Definition 3D Urban Mapping: Road Feature-Based Registration of Mobile Mapping Systems and Aerial Imagery. Remote Sensing, 9(10):975. https://doi.org/10.3390/rs9100975

Jiang, S., Jiang, W., & Wang, L. (2022). Unmanned Aerial Vehicle-Based Photogrammetric 3D Mapping: A survey of techniques, applications, and challenges. IEEE Geoscience and Remote Sensing Magazine, 10(2), 135-171. https://doi.org/10.1109/MGRS.2021.3122248

Jin, X. (2012). Segmentation-based image processing system. U.S. patent 8,260,048, filed Nov. 14, 2007, and issued Sept. 4, 2012.

Johnson, E., Seyi-Lande, O. B., Adeleke, G. S., Amajuoyi, C. P., & Simpson, B. D. (2024). Developing scalable data solutions for small and medium enterprises: Challenges and best practices. International Journal of Management & Entrepreneurship Research, 6(6), 1910-1935. https://doi.org/10.51594/ijmer.v6i6.1206

Jordan, S., Moore, J., Hovet, S., Box, J., Perry, J., Kirsche, K., Lewis, D., & Tse, Z.T.H. (2018). State-of-the-art technologies for UAV inspections. IET Radar Sonar Navig., 12, 151-164. https://doi.org/10.1049/iet-rsn.2017.0251

Jofré-Briceño, C., Muñoz-La Rivera, F., Atencio, E., & Herrera, R.F. (2021). Implementation of Facility Management for Port Infrastructure

through the Use of UAVs, Photogrammetry, and BIM. Sensors, 21, 6686. https://doi.org/10.3390/s21196686

Jung, S., Choi, D., Song, S., & Myung, H. (2020). Bridge Inspection Using Unmanned Aerial Vehicle Based on HG-SLAM: Hierarchical Graph-Based SLAM. Remote Sensing, 12(18), 3022. https://doi.org/10.3390/rs12183022

Kaartinen, E., Dunphy, K., & Sadhu, A. (2022). LiDAR-based structural health monitoring: Applications in civil infrastructure systems. Sensors, 22(12), 4610. https://doi.org/10.3390/s22124610

Kalfarisi, R., Wu, Z.Y., & Soh, K. (2020). Crack detection and segmentation using deep learning with 3D reality mesh model for quantitative assessment and integrated visualization. Journal of Computing in Civil Engineering, 34(3), 04020010. https://doi.org/10.1061/(ASCE)CP.1943-5487.0000890

Karasiak, N., Dejoux, J.F., & Monteil, C. (2022). Spatial dependence between training and test sets: Another pitfall of classification accuracy assessment in remote sensing. Machine Learning, 111, 2715–2740. https://doi.org/10.1007/s10994-021-05972-1

Khan, A., Gupta, S., & Gupta, S.K. (2020). Multi-hazard disaster studies: Monitoring, detection, recovery, and management, based on emerging technologies and optimal techniques. International Journal of Disaster Risk Reduction, 47, 101642. https://doi.org/10.1016/j.ijdrr.2020.101642

Khan, M.W., Saad, S., Ammad, S., Rasheed, K., & Jamal, Q. (2024). Smart infrastructure and AI. In AI in Material Science (pp. 193-215). CRC Press. https://doi.org/10.1201/9781003438489

Kiker, G.A., Bridges, T.S., Varghese, A., Seager, T.P., & Linkov, I. (2005). Application of multicriteria decision analysis in environmental decision making. Integrative Environmental Assessment and Management, 1, 95-108. https://doi.org/10.1897/IEAM_2004a-015.1

Kim, B., Yuvaraj, N., Sri Preethaa, K.R., et al. (2021). Surface crack detection using deep learning with shallow CNN architecture for enhanced computation. Neural Computing and Applications, 33, 9289–9305. https://doi.org/10.1007/s00521-021-05690-8

Kim, H., Ahn, E., Shin, M., & Sim, S.-H. (2019). Crack and noncrack classification from concrete surface images using machine learning. Structural Health Monitoring, 18(3), 725–738. https://doi.org/10.1177/1475921718768747

Kim, Y.-M., Chang, A.-J., & Kim, Y.-I. (2012). Extraction of building boundary on aerial image using segmentation and overlaying algorithm. Korean Journal of Geomatics, 30(1), 49-56. https://doi.org/10.7848/ksgpc.2012.30.1.049

Koch, C., Georgieva, K., Kasireddy, V., Akinci, B., & Fieguth, P. (2015). A review on computer vision based defect detection and condition assessment of concrete and asphalt civil infrastructure. Advanced Engineering Informatics, 29(2), 196-210. https://doi.org/10.1016/j.aei.2015.01.008

Kot, P., Muradov, M., Gkantou, M., Kamaris, G.S., Hashim, K., & Yeboah, D. (2021). Recent advancements in non-destructive testing techniques for structural health monitoring. Applied Sciences, 11(6), 2750. https://doi.org/10.3390/app11062750

Kyriou, A., Mpelogianni, V., Nikolakopoulos, K., & Groumpos, P.P. (2023). Review of remote sensing approaches and soft computing for infrastructure monitoring. Geomatics, 3(3), 367-392. https://doi.org/10.3390/geomatics3030021

Laflamme, S., Ubertini, F., Di Matteo, A., Pirrotta, A., Perry, M., Fu, Y., Li, J., Wang, H., Hoang, T., Glisic, B. and Bond, L.J., 2023. Roadmap on measurement technologies for next generation structural health monitoring systems. Measurement Science and Technology, 34(9), p.093001. DOI 10.1088/1361-6501/acd135

Lachat, E., Landes, T., Grussenmeyer, P. (2017). Investigation of a Combined Surveying and Scanning Device: The Trimble SX10 Scanning Total Station. Sensors, 17(4), 730. https://doi.org/10.3390/s17040730

Landrieu, L., Obozinski G. (2017a). Cut Pursuit: fast algorithms to learn piecewise constant functions on general weighted graphs. SIAM Journal on Imaging Sciences, 10(4), 1724-1766. https://doi.org/10.1137/17M1113436

Landrieu, L.; Raguet, H.; Vallet, B.; Mallet, C.; Weinmann, M. (2017b). A structured regularization framework for spatially smoothing semantic labelings of 3D point clouds. ISPRS J. Photogramm. Remote Sens., 132, 102–118. https://doi.org/10.1016/j.isprsjprs.2017.08.010

Landrieu, L. & Simonovsky M. (2018). Large-Scale Point Cloud Semantic Segmentation with Superpoint Graphs. IEEE/CVF Conference on Computer Vision and Pattern Recognition, Salt Lake City, UT, USA, 4558-4567. https://doi.org/10.1109/CVPR.2018.00479

Leica Geosystems. Leica BLK2GO. Available online: https://shop.leica-geosystems.com/au/leica-blk/blk2go/overview?srsltid=AfmBOorBbJKRphhO93d16sn9xg910BjBxgPCZvxJWFOvJpwmuns3nNqZ (accessed on 07 December 2024).

Leica Geosystems AG - Part of Hexagon. Available online: https://leica-geosystems.com/it-it/services-and-support/leap-second-2016/page3-viva-gs

Levy, S. M. (1996). Build, operate, transfer: paving the way for tomorrow's infrastructure. John Wiley & Sons.

Li, S., Dragicevic, S., Castro, F.A., Sester, M., Winter, S., Coltekin, A., Pettit, C., Jiang, B., Haworth, J., Stein, A., and Cheng, T. (2016). Geospatial big data handling theory and methods: A review and research challenges. ISPRS Journal of Photogrammetry and Remote Sensing, 115, 119-133. https://doi.org/10.1016/j.isprsjprs.2015.10.012

Li, T., Lin, J., & Liu, J. (2022). Time-varying seismic fragility analysis of bridges under the condition of the scour and freeze–thaw cycles. European

Journal of Environmental and Civil Engineering, 27(3), 1179–1208. https://doi.org/10.1080/19648189.2022.2076746

Li, X., Shao, G. (2014). Object-based land-cover mapping with high resolution aerial photography at a county scale in midwestern USA. Remote Sens., 6, 11372–11390. https://doi.org/10.3390/rs61111372

Liang H, Lee S-C, Bae W, Kim J, Seo S. (2023). Towards UAVs in Construction: Advancements, Challenges, and Future Directions for Monitoring and Inspection. Drones, 7(3), 202. https://doi.org/10.3390/drones7030202

'LIDAR' in IUPAC Compendium of Chemical Terminology, 3rd ed. International Union of Pure and Applied Chemistry; 2006. Online version 3.0.1, 2019. https://doi.org/10.1351/goldbook.L03514

Lin, Y., & Habib, A. (2022). Semantic segmentation of bridge components and road infrastructure from mobile LiDAR data. ISPRS Journal of Photogrammetry and Remote Sensing, 6, 100023. https://doi.org/10.1016/j.ophoto.2022.100023

Lin, Y-C, Manish R, Bullock D, Habib A. (2021). Comparative Analysis of Different Mobile LiDAR Mapping Systems for Ditch Line Characterization. Remote Sensing, 13(13), 2485. https://doi.org/10.3390/rs13132485

Little, R. G. (2002). Controlling Cascading Failure: Understanding the Vulnerabilities of Interconnected Infrastructures. Journal of Urban Technology, 9(1), 109–123. https://doi.org/10.1080/106307302317379855

Loce, R., Bernal E., Wu W., & Bala, R. (2013). Computer vision in roadway transportation systems: A survey. Journal of Electronic Imaging, 22. https://doi.org/10.1117/1.JEI.22

Lopes, A., Touzi, R., Nezry, E. (1990). Adaptive speckle filters and scene heterogeneity. IEEE Transactions on Geoscience and Remote Sensing, 28(6), 992-1000. https://doi.org/10.1109/36.62623

Lopes Queiroz, G., McDermid, G.J., Castilla, G., Linke, J., Rahman, M.M. (2019). Mapping Coarse Woody Debris with Random Forest Classification of Centimetric Aerial Imagery. Forests, 10, 471. https://doi.org/10.3390/f10060471

Malihi, S., Potseluyko, L., Mathew, A., Alavi, H., Kumar Reja, V., Pan, Y., Binni, L., Wang, G., Wang, X., & Brilakis, I., 2024. Review of multimodal data and their applications for road maintenance. Smart Construction. https://doi.org/10.55092/sc20240010

Manfreda, S., McCabe, M.F., Miller, P.E., Lucas, R., Pajuelo Madrigal, V., Mallinis, G., Ben Dor, E., Helman, D., Estes, L., Ciraolo, G., and Müllerová, J., 2018. On the use of unmanned aerial systems for environmental monitoring. Remote sensing, 10(4), p.641. https://doi.org/10.3390/rs10040641

Manish, Raja, Yi-Chun Lin, Radhika Ravi, Seyyed Meghdad Hasheminasab, Tian Zhou, and Ayman Habib. 2021. "Development of a Miniaturized Mobile Mapping System for In-Row, Under-Canopy Phenotyping" Remote Sensing 13, no. 2: 276. https://doi.org/10.3390/rs13020276

Marmo, F., Demartino, C., Candela, G., Sulpizio, C., Briseghella, B., Spagnuolo, R., Xiao, Y., Vanzi, I., and Rosati, L., 2019. On the form of the Musmeci's bridge over the Basento river. Engineering Structures, 191, pp. 658-673. https://doi.org/10.1016/j.engstruct.2019.04.069

Mei, A., Zampetti, E., Di Mascio, P., Fontinovo, G., Papa, P., D'Andrea, A., 2022. ROADS—Rover for Bituminous Pavement Distress Survey: An Unmanned Ground Vehicle (UGV) Prototype for Pavement Distress Evaluation. Sensors, 22, 3414. https://doi.org/10.3390/s22093414

Mei, A., Zampetti, E., Di Mascio, P., Fontinovo, G., Papa, P., D'Andrea, A., 2022. ROADS—Rover for Bituminous Pavement Distress Survey: An Unmanned Ground Vehicle (UGV) Prototype for Pavement Distress Evaluation. Sensors, 22, 3414. https://doi.org/10.3390/s22093414

Mendoza, R.U. and Cruz, J.P., 2020. Governing the "golden age of infrastructure": assessing transparency innovations in Philippine infrastructure development. Asian Politics & Policy, 12(2), pp.175-204. https://doi.org/10.1111/aspp.12527

Meng, X., Currit, N., Zhao, K., 2010. Ground Filtering Algorithms for Airborne LiDAR Data: A Review of Critical Issues. Remote Sensing, 2(3), 833-860. https://doi.org/10.3390/rs2030833

Merritt, David K., Craig Lyon, and Bhagwant Persaud, 2015. Evaluation of pavement safety performance. No. FHWA-HRT-14-065. United States. Federal Highway Administration. https://rosap.ntl.bts.gov/view/dot/35858

Mikita, T., Krausková, D., Hrůza, P., Cibulka, M., Patočka, Z., 2022. Forest Road Wearing Course Damage Assessment Possibilities with Different Types of Laser Scanning Methods including New iPhone LiDAR Scanning Apps. Forests, 13(11), 1763. https://doi.org/10.3390/f13111763

Mishra, M., Lourenço, P. B., & Ramana, G. V., 2022. Structural health monitoring of civil engineering structures by using the internet of things: A review. Journal of Building Engineering, 48, 103954. https://doi.org/10.1016/j.jobe.2021.103954

Ministry of Infrastructure and Transport - MIT, 2020. Linee guida per la classificazione e gestione del rischio, la valutazione della sicurezza ed il monitoraggio dei ponti esistenti. https://www.mit.gov.it/sites/default/files/media/notizia/2020-05/1_Testo_Linee_Guida_ponti.pdf (accessed on 26 November 2024).

Ministry of Infrastructure and Transport - MIT, 2022. Decreto ministeriale numero 204 del 1° luglio 2022. https://www.mit.gov.it/normativa/decreto-ministeriale-numero-204-del-1-luglio-2022 (accessed on 26 November 2024).

Mishra, M., Lourenço, P. B., & Ramana, G. V., 2022. Structural health monitoring of civil engineering structures by using the internet of things: A

review. Journal of Building Engineering, 48, 103954. https://doi.org/10.1016/j.jobe.2021.103954

Mitoulis, S., 2020. Monitoring of transport infrastructure exposed to multiple hazards: a roadmap for building resilience. Science of the Total Environment. https://doi.org/10.1016/j.scitotenv.2020.141001

Mohammadi, M.E., 2019. Point cloud analysis for surface defects in civil structures (Doctoral dissertation, The University of Nebraska-Lincoln).

Mobasheri, A., Mitasova, H., Neteler, M., Singleton, A., Ledoux, H., Brovelli, M. A., 2020. Highlighting recent trends in open source geospatial science and software.

Mushonga, H. T., Banda, F., Mulolwa, A., 2017. Development of a web based GIS for health facilities mapping, monitoring and reporting: A case study of the Zambian Ministry of health. South African Journal of Geomatics, 6(3), 321.

Nagarajaiah, S., & Erazo, K. (2016). Structural monitoring and identification of civil infrastructure in the United States. Structural Monitoring and Maintenance, 3(1), 51. https://doi.org/10.12989/SMM.2016.3.1.051

Nakata Y, Hayamizu M, Ishiyama N, Torita H. Observation of Diurnal Ground Surface Changes Due to Freeze-Thaw Action by Real-Time Kinematic Unmanned Aerial Vehicle. Remote Sensing. 2021; 13(11):2167. https://doi.org/10.3390/rs13112167

Nassif A.B., Talib M.A., Nasir Q. and Dakalbab F.M., "Machine Learning for Anomaly Detection: A SystemNahiyoon SA, Ren Z, Wei P, Li X, Li X, Xu J, Yan X, Yuan H. Recent Development Trends in Plant Protection UAVs: A Journey from Conventional Practices to Cutting-Edge Technologies—A Comprehensive Review. Drones. 2024; 8(9):457. https://doi.org/10.3390/drones8090457

Nemry, F., & Demirel, H. (2012). Impacts of Climate Change on Transport: A focus on road and rail transport infrastructures. European commission, joint research centre (JRC), institute for prospective technological studies (IPTS), 89. DOI:10.1016/j.tranpol.2017.05.007

Nex, F. and Remondino, F. (2013) UAV for 3D Mapping Applications: A Review. Applied Geomatics, 6, 1-15. http://dx.doi.org/10.1007/s12518-013-0120-x

Newman, T. S., & Jain, A. K. (1995). A survey of automated visual inspection. Computer vision and image understanding, 61(2), 231-262. https://doi.org/10.1006/cviu.1995.1017

Nguyen, HN., Kam, TY. & Cheng, PY. An Automatic Approach for Accurate Edge Detection of Concrete Crack Utilizing 2D Geometric Features of Crack. J Sign Process Syst 77, 221–240 (2014). https://doi.org/10.1007/s11265-013-0813-8

Nhien Dinh Le, Daniel Tran, Mamdouh Mohammed, Development of Risk-Based Methodologies for Highway Pavement Construction Inspection, Transportation Research Record: Journal of the Transportation Research Board, 10.1177/03611981241283004, (2024).

Nooralishahi P, Ibarra-Castanedo C, Deane S, López F, Pant S, Genest M, Avdelidis NP, Maldague XPV. Drone-Based Non-Destructive Inspection of Industrial Sites: A Review and Case Studies. Drones. 2021; 5(4):106. https://doi.org/10.3390/drones5040106

Novatel, IMU-ISA-100C. Available online: https://docs.novatel.com/OEM7/Content/Technical_Specs_IMU/ISA_100C_Performance.htm. (Accessed 2 July 2023).

Novatel, IMU-ISA-100C. Available online: https://docs.novatel.com/OEM7/Content/Technical_Specs_IMU/ISA_100C_Performance.htm. (Accessed 12 July 2023).

Ogundare J. O. (2018). Understanding least squares estimation and geomatics data analysis. John Wiley & Sons.

Ong G., T. E. Nantung and K. C. Sinha. Indiana Pavement Preservation Program. Publication FHWA/IN/JTRP-2010/14. Joint Transportation Research Program, Indiana Department of Transportation and Purdue University, West Lafayette, Indiana, 2010. https://doi.org/10.5703/1288284314258

Oviedo-Trespalacios O., Truelove V., Watson B., & Hinton, J. A. (2019). The impact of road advertising signs on driver behaviour and implications for road safety: A critical systematic review. Transportation research part A: policy and practice, 122, 85-98. review,https://doi.org/10.1016/j.tra.2019.01.012

Ostadabbas H., Weippert H., Behr, F. J., 2019. Database transformation, cadastre automatic data processing in qgis and implementation in web gis. International Archives of the Photogrammetry, Remote Sensing and Spatial Information Sciences - ISPRS Archives, 42number 4/W14, 175–178.

Ouma Y. O., & Hahn M. (2017). Pothole detection on asphalt pavements from 2D-colour pothole images using fuzzy c-means clustering and morphological reconstruction. Automation in Construction, 83, 196-211. https://doi.org/10.1016/j.autcon.2017.08.017

Outay F., Mengash H.A. and Adnan, M., 2020. Applications of unmanned aerial vehicle (UAV) in road safety, traffic and highway infrastructure management: Recent advances and challenges. Transportation research part A: policy and practice, 141, pp.116-129. https://doi.org/10.1016/j.tra.2020.09.018

Oxoli D., Cannata M., Terza V., and Brovelli M. A.: NATURAL HERITAGE MANAGEMENT AND PROMOTION THROUGH FREE AND OPEN SOURCE SOFTWARE: A PRELIMINARY SYSTEM DESIGN FOR THE INSUBRIPARKS PROJECT, Int. Arch. Photogramm.

Remote Sens. Spatial Inf. Sci., XLII-4/W14, 179–183, https://doi.org/10.5194/isprs-archives-XLII-4-W14-179-2019, 2019.

Pai, S.G. and Smith, I.F., 2022. Methodology maps for model-based sensor-data interpretation to support civil-infrastructure management. Frontiers in Built Environment, 8, p.801583. doi: 10.3389/fbuil.2022.801583

Pádua, L., Vanko, J., Hruška, J., Adão, T., Sousa, J. J., Peres, E., & Morais, R. (2017). UAS, sensors, and data processing in agroforestry: a review towards practical applications. International Journal of Remote Sensing, 38(8–10), 2349–2391. https://doi.org/10.1080/01431161.2017.1297548

Parajuli, A., M. Celenk, and H.B. Riley, Robust lane detection in shadows and low illumination conditions using local gradient features. Open Journal of Applied Sciences, Vol. 3 No. 1B, 2013, pp. 68-74. doi: 10.4236/ojapps.2013.31B014.

Pascucci N., Alicandro M., Zollini S. and Dominici D., "Geomatic Techniques and CIM (City Information Modeling) to Enhance Smart Cities Management," 2024 IEEE International Workshop on Metrology for Living Environment (MetroLivEnv), Chania, Greece, 2024, pp. 51-56, doi: 10.1109/MetroLivEnv60384.2024.10615304.

Pascucci, N., Alicandro, M., Zollini, S., Dominici, D. (2024). Improving Infrastructure Monitoring: UAV-Based Photogrammetry for Crack Pattern Inspection. In: Arai, K. (eds) Proceedings of the Future Technologies Conference (FTC) 2024, Volume 1. FTC 2024. Lecture Notes in Networks and Systems, vol 1154. Springer, Cham. https://doi.org/10.1007/978-3-031-73110-5_24

Pascucci, N., Shin, S.-Y., Hodaei, M., Dominici, D., and Habib, A.: COMPARATIVE ANALYSIS OF MORPHOLOGICAL (MCSS) AND LEARNING-BASED (SPG) STRATEGIES FOR DETECTING SIGNAGE OCCLUSIONS ALONG TRANSPORTATION CORRIDORS, Int. Arch. Photogramm. Remote Sens. Spatial Inf. Sci., XLVIII-1/W2-2023, 1651–

1658, https://doi.org/10.5194/isprs-archives-XLVIII-1-W2-2023-1651-2023, 2023.

Pérez-Ruiz, M., Prior, A., Martínez-Guanter, J., Apolo-Apolo, O.E., Andrade-Sanchez, P. and Egea, G., 2020. Development and evaluation of a self-propelled electric platform for high-throughput field phenotyping in wheat breeding trials. Computers and Electronics in Agriculture, 169, p.105237. https://doi.org/10.1016/j.compag.2020.105237

Persia, L., Usami, D. S., De Simone, F., De La Beaumelle, V. F., Yannis, G., Laiou, A., ... & Salathè, M. (2016). Management of road infrastructure safety. Transportation research procedia, 14, 3436-3445. https://doi.org/10.1016/j.trpro.2016.05.303

Plevris V, Papazafeiropoulos G. AI in Structural Health Monitoring for Infrastructure Maintenance and Safety. Infrastructures. 2024; 9(12):225. https://doi.org/10.3390/infrastructures9120225

Priemus, H., & Zonneveld, W. (2003). What are corridors and what are the issues? Introduction to special issue: the governance of corridors. Journal of transport geography, 11(3), 167-177. https://doi.org/10.1016/S0966-6923(03)00028-0

Powers, D.M. (2008). Evaluation: From Precision, Recall and F-Factor to ROC, Informedness, Markedness & Correlation.

Powers, D. M. (2020). Evaluation: from precision, recall and F-measure to ROC, informedness, markedness and correlation. arXiv preprint arXiv:2010.16061. https://doi.org/10.48550/arXiv.2010.16061

Qi, C. R., Su, H., Mo, K., & Guibas, L. J. (2017). Pointnet: Deep learning on point sets for 3d classification and segmentation. In Proceedings of the IEEE conference on computer vision and pattern recognition (pp. 652-660). https://doi.org/10.48550/arXiv.1612.00593

Raja Permaisuri Bainun.Int. J. Softw. Eng. Comput. Syst. 9(1), 10–26 (2023). https://doi.org/10.15282/ijsecs.9.1.2023.2.0106

Rane, Nitin and Choudhary, Saurabh and Rane, Jayesh, Leading-edge Technologies for Architectural Design: A Comprehensive Review (November 19, 2023). Available at SSRN: https://ssrn.com/abstract=4637891 or http://dx.doi.org/10.2139/ssrn.4637891

Rashdi R., Garrido I., Balado J., Del Río-Barral P., Rodríguez-Somoza J. L., & Martínez-Sánchez J. (2024). Comparative Evaluation of LiDAR systems for transport infrastructure: case studies and performance analysis. European Journal of Remote Sensing, 57(1). https://doi.org/10.1080/22797254.2024.2316304

Rashidan, M. H., Musliman, I. A., and Rahman, A. A.: GEOPACKAGE DATA FORMAT FOR COLLABORATIVEMAPPING OF GEOSPATIAL DATAIN LIMITED NETWORKENVIRONMENTS, Int. Arch. Photogramm. Remote Sens. Spatial Inf. Sci., XLII-4/W1, 15–21, https://doi.org/10.5194/isprs-archives-XLII-4-W1-15-2016, 2016.

Rashidan, M.H. and Musliman, I.A., 2015. GeoPackage as future ubiquitous GIS data format: a review. Jurnal Teknologi, 73(5). https://doi.org/10.11113/jt.v73.4319

Rashidi M, Mohammadi M, Sadeghlou Kivi S, Abdolvand MM, Truong-Hong L, Samali B. A Decade of Modern Bridge Monitoring Using Terrestrial Laser Scanning: Review and Future Directions. Remote Sensing. 2020; 12(22):3796. https://doi.org/10.3390/rs12223796

Rathod, H., & Gupta, R. (2019). Sub-surface simulated damage detection using Non-Destructive Testing Techniques in reinforced-concrete slabs. Construction and Building Materials, 215, 754-764. https://doi.org/10.1016/j.conbuildmat.2019.04.223

Rattanachot, W., Wang, Y., Chong, D., & Suwansawas, S. (2015). Adaptation strategies of transport infrastructures to global climate change. Transport Policy, 41, 159-166. https://doi.org/10.1016/j.tranpol.2015.03.001

Rau, J. Y., Hsiao, K. W., Jhan, J. P., Wang, S. H., Fang, W. C., and Wang, J. L.: BRIDGE CRACK DETECTION USING MULTI-ROTARY UAV AND OBJECT-BASE IMAGE ANALYSIS, Int. Arch. Photogramm. Remote Sens. Spatial Inf. Sci., XLII-2/W6, 311–318, https://doi.org/10.5194/isprs-archives-XLII-2-W6-311-2017, 2017.

Ravi R., Habib A., & BullockD. (2020). Pothole Mapping and Patching Quantity Estimates using LiDAR-Based Mobile Mapping Systems. Transportation Research Record, 2674(9), 124–134. https://doi.org/10.1177/0361198120927006

Ravi R., Lin Y.-J., Elbahnasawy M., Shamseldin T., and Habib A., "Simultaneous system calibration of a multi-lidar multicamera mobile mapping platform," IEEE Journal ofSelected Topics in Applied Earth Observations and Remote Sensing, vol. 11, no. 5, pp. 16941714, 2018. doi:10.1109/JSTARS.2018.2812796

Ray R, Das A, Hasan MSU, Aldrees A, Islam S, Khan MA, Lama GFC. Quantitative Analysis of Land Use and Land Cover Dynamics using Geoinformatics Techniques: A Case Study on Kolkata Metropolitan Development Authority (KMDA) in West Bengal, India. Remote Sensing. 2023; 15(4):959. https://doi.org/10.3390/rs15040959

Reddy G.O., Singh S.K. (eds.) Geospatial Technologies in Land Resources Mapping, Monitoring and Management. Springer International Publishing, Berlin/Heidelberg, Germany (2018). https://doi.org/10.1007/978-3-319-78711-4

Reiterer A., Wäschle K., Störk D., Leydecker A., & Gitzen N. (2020). Fully automated segmentation of 2D and 3D mobile mapping data for reliable modeling of surface structures using deep learning. Remote Sensing, 12(16). https://doi.org/10.3390/RS12162530

Remondino F. Heritage Recording and 3D Modeling with Photogrammetry and 3D Scanning. Remote Sensing. 2011; 3(6):1104-1138. https://doi.org/10.3390/rs3061104

Rezaee A. (2021). Partition Fuzzy Median Filter for Image Restoration. Fuzzy Information and Engineering, 13(2), 199–210. https://doi.org/10.1080/16168658.2021.1921377

Riegl, VUX-1HA Datasheet. Available online: http://www.riegl.com/uploads/tx_pxpriegldownloads/DataSheet_VUX-1HA__2015-10-06.pdf (Accessed 12 July 2023).

Riveiro B., & Solla M. (Eds.). (2016). Non-destructive techniques for the evaluation of structures and infrastructure (Vol. 11). Boca Raton, FL, USA:: CRC Press.

Rodríguez M., González-Prida V., Sánchez A., & Crespo A. (2024). Application of Degradation and Optimization Models for digitization of Maintenance Management in Railway Infrastructures. IFAC-PapersOnLine, 58(8), 115-120. https://doi.org/10.1016/j.ifacol.2024.08.059

Roerdink, J.B.T.M., Meijster, A.: The watershed transform: definitions, algorithms and parallelization strategies. Fundamenta Informaticae 41(1,2), 187–228 (2000). https://doi.org/10. 3233/FI-2000-411207

Sairam N, Nagarajan S, Ornitz S. Development of Mobile Mapping System for 3D Road Asset Inventory. Sensors. 2016; 16(3):367. https://doi.org/10.3390/s16030367

Samuel, Arthur L(1959). “Some studies in machine learning using the game of checkers”.In: IBM Journal of researchand development 3.3, pp. 210–229.

Sari, I. L., Weston, C. J., Newnham, G. J., & Volkova, L. (2021, November). Estimating land cover map accuracy and area uncertainty using a confusion matrix: A case study in Kalimantan, Indonesia. In IOP Conference Series: Earth and Environmental Science (Vol. 914, No. 1, p. 012025). IOP Publishing. DOI 10.1088/1755-1315/914/1/012025

Schnebele, E., Tanyu, B.F., Cervone, G. et al. Review of remote sensing methodologies for pavement management and as-sessment. Eur. Transp. Res. Rev. 7, 7 (2015). https://doi.org/10.1007/s12544-015-0156-6

Schubert, E., Sander, J., Ester, M., Kriegel, H.P., Xu, X., 2017. DBSCAN Revisited, Revisited: Why and How You Should (Still) Use DBSCAN. ACM Trans. Database Syst. 42, 1–21. https://doi.org/10.1145/3068335

Schwilch, G., Bestelmeyer, B., Bunning, S., Critchley, W., Herrick, J., Kellner, K., Liniger, H.P., Nachtergaele, F., Ritsema, C.J., Schuster, B., Tabo, R., van Lynden, G. and Winslow, M. (2011), Experiences in monitoring and assessment of sustainable land management. Land Degrad. Dev., 22: 214-225. https://doi.org/10.1002/ldr.1040

Secco, P. (2022). Point cloud based improvement of the trajectory of a Railway Mobile Mapping System.

Selim, G.E.I., Hemdan, E.ED., Shehata, A.M. et al. Anomaly events classification and detection system in critical industrial internet of things infrastructure using machine learning algorithms. Multimed Tools Appl 80, 12619–12640 (2021). https://doi.org/10.1007/s11042-020-10354-1

Shakhatreh, H., Sawalmeh, A.H., Al-Fuqaha, A., Dou, Z., Almaita, E., Khalil, I., Othman, N.S., Khreishah, A. and Guizani, M., 2019. Unmanned aerial vehicles (UAVs): A survey on civil applications and key research challenges. Ieee Access, 7, pp.48572-48634. doi: 10.1109/ACCESS.2019.2909530.

Shao, J., Lin, Y.C., Wingren, C., Shin, S.Y., Fei, W., Carpenter, J., Habib, A. and Fei, S., 2024. Large-scale inventory in natural forests with mobile LiDAR point clouds. Science of Remote Sensing, 10, p.100168. https://doi.org/10.1016/j.srs.2024.100168

Shapiro, V.B., Hawkins, J.D. & Oesterle, S. Building Local Infrastructure for Community Adoption of Science-Based Prevention: The Role of Coalition Functioning. Prev Sci 16, 1136–1146 (2015). https://doi.org/10.1007/s11121-015-0562-y

Sharifisoraki, Z., Dey, A., Selzler, R., Amini, M., Green, J. R., Rajan, S., & Kwamena, F. A. (2022). Monitoring critical infrastructure using 3d lidar

point clouds. IEEE Access, 11, 314-336. doi: 10.1109/ACCESS.2022.3232338.

Sheng, G.W., Din, W.I.S.B.W., Quadri, W., Zabidi, A.B.: Investigation and analysis of crack detection using UAV and CNN:a case study of hospital

Shokirov, S., Schaefer, M., Levick, S.R., Jucker, T., Borevitz, J., Abdurahmanov, I., Youngentob, K., 2021. Multi-platform LiDAR approach for detecting coarse woody debris in a landscape with varied ground cover. International Journal of Remote Sensing 42, 93249350. https://doi.org/10.1080/01431161.2021.1995072

Skinner R.E. (2012). Building thesecond mind: 1956and theoriginsofartificial intelligence computing.

Singh, H., Gambhir, D., 2014. An open source approach to build a web GIS application. International Journal of Computer Science and Technology (IJCST), 3.

Sinha, K. C., Labi, S., & Agbelie, B. R. D. K. (2017). Transportation infrastructure asset management in the new millennium: continuing issues, and emerging challenges and opportunities. Transportmetrica A: Transport Science, 13(7), 591–606. https://doi.org/10.1080/23249935.2017.1308977

Smith, B. W. (2016). Automated driving policy. Road Vehicle Automation 3, 53-58.

Smith L.I., (2002). A tutorial on Principal Components Analysis.

Sohn, H., Farrar, C. R., Hemez, F. M., Shunk, D. D., Stinemates, D. W., Nadler, B. R., & Czarnecki, J. J. (2003). A review of structural health monitoring literature: 1996–2001. Los Alamos National Laboratory, USA, 1, 16.

Spencer Jr, B. F., Hoskere, V., & Narazaki, Y. (2019). Advances in computer vision-based civil infrastructure inspection and monitoring. Engineering, 5(2), 199-222. https://doi.org/10.1016/j.eng.2018.11.030

Stefanov, S., 2021. Visualization of Meteorological Data Sets With Open Source GIS. International Journal of Computer Trends and Technology, 69(4), 15–17. https://www.researchgate.net/publication/350877893.

Stehman, S. V. (1997). Selecting and interpreting measures of thematic classification accuracy. Remote sensing of Environment, 62(1), 77-89. https://doi.org/10.1016/S0034-4257(97)00083-7

Steyerberg, Ewout W.a; Vickers, Andrew J.b; Cook, Nancy R.c; Gerds, Thomasd; Gonen, Mithatb; Obuchowski, Nancye; Pencina, Michael J.f; Kattan, Michael W.e. Assessing the Performance of Prediction Models: A Framework for Traditional and Novel Measures. Epidemiology 21(1):p 128-138, January 2010. | DOI: 10.1097/EDE.0b013e3181c30fb2

Sun, A. Y., & Scanlon, B. R. (2019). How can Big Data and machine learning benefit environment and water management: a survey of methods, applications, and future directions. Environmental Research Letters, 14(7), 073001. DOI 10.1088/1748-9326/ab1b7d

Sun S, Li C, Paterson AH, Jiang Y, Xu R, Robertson JS, Snider JL and Chee PW (2018) In-field High Throughput Phenotyping and Cotton Plant Growth Analysis Using LiDAR. Front. Plant Sci. 9:16. doi: 10.3389/fpls.2018.00016

Sun Z, Jayasinghe S, Sidiq A, Shahrivar F, Mahmoodian M, Setunge S. Approach Towards the Development of Digital Twin for Structural Health Monitoring of Civil Infrastructure: A Comprehensive Review. Sensors. 2024; 25(1):59. https://doi.org/10.3390/s25010059

Taheri H, Gonzalez Bocanegra M, Taheri M. Artificial Intelligence, Machine Learning and Smart Technologies for Nondestructive Evaluation. Sensors. 2022; 22(11):4055. https://doi.org/10.3390/s22114055

Tang P., Akinci B., & Garrett J. H. (2007, January). Laser scanning for bridge inspection and management. In IABSE Symposium Report (Vol. 93, No. 18, pp. 17-24). International Association for Bridge and Structural Engineering.

Teo T.-A. and H.-L. Yu, Empirical radiometric normalization of road points from terrestrial mobile LiDAR system. Remote Sensing, 2015. 7(5): p. 6336-6357.

Teza G., Galgaro A., & Moro F. (2009). Contactless recognition of concrete surface damage from laser scanning and curvature computation. Ndt & E International, 42(4), 240-249. https://doi.org/10.1016/j.ndteint.2008.10.009

Tiwari A., Jain D. K., 2013. Geospatial framework for dengue using open source web gis technology. Joint International Workshop of ISPRS WG VIII/1 and WG IV/4 on Geospatial Data for Disaster and Risk Reduction Nov21-22, Hyderabad, India.

Tonhauser, M.; Ristvej, J. Implementation of New Technologies to Improve Safety of Road Transport. Transp. Res. Procedia 2021, 55, 1599–1604. https://doi.org/10.1016/j.trpro.2021.07.149

Transportation Research Part A: Policy and Practice,Volume 122, 2019. https://doi.org/10.1016/j.tra.2019.01.012

Trybała P, Szrek J, Dębogórski B, Ziętek B, Blachowski J, Wodecki J, Zimroz R. Analysis of Lidar Actuator System Influence on the Quality of Dense 3D Point Cloud Obtained with SLAM. Sensors. 2023; 23(2):721. https://doi.org/10.3390/s23020721

Urban R, Štroner M, Braun J, Suk T, Kovanič Ľ, Blistan P. Determination of Accuracy and Usability of a SLAM Scanner GeoSLAM Zeb Horizon: A Bridge Structure Case Study. Applied Sciences. 2024; 14(12):5258. https://doi.org/10.3390/app14125258

US Department of Transportation, Federal Highway Administration (FHWA). (2008). Publication No. FHWA-SA-07-018: Office of Safety. Washington, DC.

Vacca, G., Fiorino, D. R., and Pili, D.: A WEBGIS FOR THE KNOWLEDGE AND CONSERVATION OF THE HISTORICAL BUILDINGS IN SARDINIA (ITALY), Int. Arch. Photogramm. Remote

Sens. Spatial Inf. Sci., XLII-4/W2, 171–178, https://doi.org/10.5194/isprs-archives-XLII-4-W2-171-2017, 2017.

van der Horst, B. B., Lindenbergh, R. C., and Puister, S. W. J.: MOBILE LASER SCAN DATA FOR ROAD SURFACE DAMAGE DETECTION, Int. Arch. Photogramm. Remote Sens. Spatial Inf. Sci., XLII-2/W13, 1141–1148, https://doi.org/10.5194/isprs-archives-XLII-2-W13-1141-2019, 2019.

Velodyne, HDL32E Datasheet. Available online: https://pdf.directindustry.com/pdf/velodynelidar/hdl-32e-datasheet/182407-676098.html (Accessed 12 July 2023a).

Velodyne, Puck Hi-Res Datasheet. Available online: https://velodynelidar.com/products/puck-hi-res/ (Accessed 12 July 2023b).

Verma, Sanjeev Kumar, Bhadauria, Sudhir Singh, Akhtar, Saleem, Review of Nondestructive Testing Methods for Condition Monitoring of Concrete Structures, Journal of Construction Engineering, 2013, 834572, 11 pages, 2013. https://doi.org/10.1155/2013/834572

Vert, G., Stock, M., Jankowski, P. and Gessler, P., 2002. An architecture for the management of GIS data files. Transactions in GIS, 6(3), pp.259-275. https://doi.org/10.1111/1467-9671.00110

Vierhub-Lorenz, V., Kellner, M., Zipfel, O., Reiterer, A. (2022) A Study on the Effect of Multispectral LiDAR Data on Automated Semantic Segmentation of 3D-Point Clouds. Remote Sens. 2022, 14(24), 6349; https://doi.org/10.3390/rs14246349

Volk, R., Stengel, J. and Schultmann, F., 2014. Building Information Modeling (BIM) for existing buildings—Literature review and future needs. Automation in construction, 38, pp.109-127.https://doi.org/10.1016/j.autcon.2013.10.023

Vyas, V. (2020). Development of Data-Driven Decision Support Approaches Using Non-Destructive Testing for Enhancing Pavement Management Systems (Doctoral dissertation, BITS Pilani).

Wang, H., Barone, G., & Smith, A. (2023). Current and future role of data fusion and machine learning in infrastructure health monitoring. Structure and Infrastructure Engineering, 20(12), 1853–1882. https://doi.org/10.1080/15732479.2023.2165118

Wang, X., Mazumder, R.K., Salarieh, B., Salman, A.M., Shafieezadeh, A. and Li, Y., 2022. Machine learning for risk and resilience assessment in structural engineering: Progress and future trends. Journal of Structural Engineering, 148(8), p.03122003. https://doi.org/10.1061/(ASCE)ST.1943-541X.0003392

Xia Y, Jian X, Yan B, Su D. Infrastructure Safety Oriented Traffic Load Monitoring Using Multi-Sensor and Single Camera for Short and Medium Span Bridges. Remote Sensing. 2019; 11(22):2651. https://doi.org/10.3390/rs11222651

Xu, L., Feng, C., Kamat, V.R. and Menassa, C.C., 2019. An occupancy grid mapping enhanced visual SLAM for real-time locating applications in indoor GPS-denied environments. Automation in Construction, 104, pp.230-245.https://doi.org/10.1016/j.autcon.2019.04.011

Yamaguchi, T., Nakamura, S., Saegusa, R., & Hashimoto, S. (2008). Image-based crack detection for real concrete surfaces. IEEJ Transactions on Electrical and Electronic Engineering, 3(1), 128-135. https://doi.org/10.1002/tee.20244

Yang, B., Liu, Y., Dong, Z., Liang, F., Li, B. and Peng, X., 2017. 3D local feature BKD to extract road information from mobile laser scanning point clouds. ISPRS Journal of Photogrammetry and Remote Sensing, 130, pp.329-343. https://doi.org/10.1016/j.isprsjprs.2017.06.007.

Yang, D. Y., & Frangopol, D. M. (2019). Life-cycle management of deteriorating civil infrastructure considering resilience to lifetime hazards: A general approach based on renewal-reward processes. Reliability Engineering & System Safety, 183, 197-212. https://doi.org/10.1016/j.ress.2018.11.016

Yang, G., Liu, K., Zhang, J., Zhao, B., Zhao, Z., Chen, X., & Chen, B. M. (2022). Datasets and processing methods for boosting visual inspection of civil infrastructure: A comprehensive review and algorithm comparison for crack classification, segmentation, and detection. Construction and Building Materials, 356, 129226. https://doi.org/10.1016/j.conbuildmat.2022.129226

Z+F, Profiler 9012. Available online:https://www.zofre.de/en/laser-scanners/2d-laser-scanner/z-fprofilerr-9012 (Accessed 12 December 2024)

ZEB Horizon—GeoSLAM. Available online: https://geoslam.com/solutions/zeb-horizon/ (accessed on 13 January 2020). Oggi funzionava01/01

Zhang L. and Zhang L., "Artificial Intelligence for Remote Sensing Data Analysis: A review of challenges and opportunities," in IEEE Geoscience and Remote Sensing Magazine, vol. 10, no. 2, pp. 270-294, June 2022, doi: 10.1109/MGRS.2022.3145854.

Zhang, W., Qi, J., Wan, P., Wang, H., Xie, D., Wang, X., & Yan, G. (2016). An easy-to-use airborne LiDAR data filtering method based on cloth simulation. Remote sensing, 8(6), 501.

Zhang W, Liu C, Chang F, Song Y. Multi-Scale and Occlusion Aware Network for Vehicle Detection and Segmentation on UAV Aerial Images. Remote Sensing. 2020; 12(11):1760. https://doi.org/10.3390/rs12111760

Zhang, J., Zhao, X., Chen, Z., & Lu, Z. (2019). A review of deep learning-based semantic segmentation for point cloud. IEEE access, 7, 179118-179133. DOI:10.1109/ACCESS.2019.2958671

Zhang S., Wang C., Li L., Wen C., Yang C., Zhang Z., Li J. (2019), Automated Visual Recognizability Evaluation of Traffic Sign Based on 3D LiDAR Point Clouds. Remote Sens. 2019, 11(12), 1453; https://doi.org/10.3390/rs11121453

Zhang Y, Dou X, Zhao H, Xue Y, Liang J. Safety Risk Assessment of Low-Volume Road Segments on the Tibetan Plateau Using UAV LiDAR Data. Sustainability. 2023; 15(14):11443. https://doi.org/10.3390/su151411443

Zhao, C., Zhou, T., Fei, S., and Habib, A.: FOREST FEATURE LIDAR SLAM (F2-LSLAM) AND INTEGRATED SCAN SIMULTANEOUS TRAJECTORY ENHANCEMENT AND MAPPING (IS2-TEAM) FOR ACCURATE FOREST INVENTORY USING BACKPACK SYSTEMS, Int. Arch. Photogramm. Remote Sens. Spatial Inf. Sci., XLVIII-1/W2-2023, 1823–1830, https://doi.org/10.5194/isprs-archives-XLVIII-1-W2-2023-1823-2023, 2023.

Zhou H, Xu C, Tang X, Wang S, Zhang Z. A Review of Vision-Laser-Based Civil Infrastructure Inspection and Monitoring. Sensors. 2022; 22(15):5882. https://doi.org/10.3390/s22155882

Zhou T, dos Santos RC, Liu J, Lin Y-C, Fei WC, Fei S, Habib A. Comparative Evaluation of a Newly Developed Trunk-Based Tree Detection/Localization Strategy on Leaf-Off LiDAR Point Clouds with Varying Characteristics. Remote Sensing. 2022; 14(15):3738. https://doi.org/10.3390/rs14153738

Zhou, T., Zhao, C., Wingren, C.P., Fei, S. and Habib, A., 2024. Forest feature LiDAR SLAM (F2-LSLAM) for backpack systems. ISPRS Journal of Photogrammetry and Remote Sensing, 212, pp.96-121. https://doi.org/10.1016/j.isprsjprs.2024.04.025

Zhou, Y.; Guo, X.; Hou, F.; Wu, J. Review of Intelligent Road Defects Detection Technology. Sustainability 2022, 14, 6306. https://doi.org/10.3390/su14106306

Zhu, X. X., Tuia, D., Mou, L., Xia, G. S., Zhang, L., Xu, F., & Fraundorfer, F. (2017). Deep learning in remote sensing: A comprehensive review and list of resources. IEEE geoscience and remote sensing magazine, 5(4), 8-36. doi: 10.1109/MGRS.2017.2762307.

Zollini, S., Alicandro, M., Dominici, D., Quaresima, R., & Giallonardo, M. (2020). UAV photogrammetry for concrete bridge inspection using object-based image analysis (OBIA). Remote Sensing, 12(19), 3180, https://doi.org/10.3390/rs12193180.

Zou, Q., Cao, Y., Li, Q., Mao, Q., & Wang, S. (2012). CrackTree: Automatic crack detection from pavement images. Pattern Recognition Letters, 33(3), 227-238. https://doi.org/10.1016/j.patrec.2011.11.004

Župan R, Vinković A, Nikçi R, Pinjatela B. Automatic 3D Building Model Generation from Airborne LiDAR Data and OpenStreetMap Using Procedural Modeling. Information. 2023; 14(7):394. https://doi.org/10.3390/info14070394

ACKNOWLEDGEMENTS

After a little more than three years, I find myself facing the most difficult blank page to write: the acknowledgments. Difficult because, as Fabrizio De André once said, "*Try to have a world in your heart and not be able to express it in words*" and for that, I apologize in advance. A simple "*Thank you*" is not enough to express my gratitude for these years, filled with challenges, growth, and meaningful encounters, leading me to explore and literally live on new continents.

My first thank you goes to my Professor, Donatella Dominici. When we embarked on this journey, I was enthusiastic, ready to embrace a new adventure, with a curious heart and an empty suitcase, eager to be filled with knowledge and experiences. I am grateful to her for always being by my side, both here and across the ocean. Her patience, trust, and guidance have helped me navigate even the most confusing moments, allowing me to grow both professionally and personally.

My second thank you goes to Professor Ayman Habib. Attending his lectures and collaborating with him has been a privilege. The months spent at the DPRG Group were intense but incredibly rewarding. I have learned that research requires time, patience, and determination, especially in an era where everything seems to need to happen quickly.

Their guidance made me understand, as Carl Friedrich Gauss once said: "*It is not knowledge, but the act of learning; not possession, but the act of*

getting there, which grants the greatest enjoyment." And this thought perfectly reflects how both of them have accompanied and encouraged me along my journey.

RINGRAZIAMENTI

Dopo poco più di tre anni, mi ritrovo di fronte alla pagina bianca più difficile da scrivere: i ringraziamenti. Più difficile perché, come diceva Fabrizio De André, "*tu prova ad avere un mondo nel cuore e non riesci ad esprimerlo con le parole*" e per questo mi scuso anticipatamente. Un semplice "*Grazie*" non è sufficiente per esprimere la mia gratitudine per questi anni, che sono stati ricchi di sfide, crescita e incontri significativi, portandomi a vivere ed esplorare letteralmente nuovi continenti.

Un primo grazie va alla mia Professoressa Donatella Dominici. Quando abbiamo iniziato questo percorso, ero entusiasta, con un cuore curioso e un bagaglio vuoto, pronto a essere riempito di conoscenze ed esperienze. La ringrazio per essermi stata accanto, sia qui che oltre oceano. La sua pazienza, fiducia e guida mi hanno permesso di affrontare anche i momenti più confusi, portandomi a crescere tanto, sia a livello professionale che personale. Un secondo ringraziamento va al Professore Ayman Habib. Poter seguire le sue lezioni e collaborare con lui è stato un privilegio. I mesi passati nel DPRG Group sono stati intensi ma richissimi, ho imparato che la ricerca richiede tempo, pazienza e determinazione, soprattutto in un'epoca in cui tutto sembra dover accadere in fretta.

La loro guida mi ha fatto capire, come diceva Carl Friedrich Gauss: "*Non è la conoscenza, ma l'atto di imparare; non il possesso, ma l'atto di arrivarci,*

che dà la gioia maggiore". E questo pensiero riflette il modo in cui entrambi mi hanno accompagnato e incoraggiato nel mio percorso.